THE STRUCTURAL BASIS OF THE DISABLING OF THE ACTIN POLYMERIZATION MACHINERY BY *YERSINIA*



Wei Lin Lee

Nuffield Department of Clinical Medicine
Merton College
Oxford University

A thesis submitted in partial fulfilment of the requirements for the degree of *Doctor of Philosophy* at the University of Oxford

Trinity Term 2013

The Structural Basis of the Disabling of the Actin Polymerization Machinery by *Yersinia*

Wei Lin Lee, Merton College, University of Oxford
D.Phil, Nuffield Department of Clinical Medicine
Trinity term 2013

ABSTRACT

Yersinia pestis is a human pathogen and the causative agent of bubonic plague, responsible for causing three massive pandemics, resulting in hundreds of millions of deaths in the 14th century alone. *Yersinia*'s virulence stems from its ability to overcome host immune defences by the injection of six *Yersinia* outer proteins (Yops) into the host cells via its Type III secretion system. One of these Yops, YopO specifically disables the actin polymerization machinery, leading to the crippling of phagocytosis. YopO consists of a GDI domain which sequesters Rac and Rho, and a kinase domain, the activity of which is dependent on host actin. Little is known about the targets of the kinase domain and the mechanism of function of YopO remains incomplete.

In this work, YopO was crystallized in complex with actin, revealing that YopO binds to actin on subdomain 4, away from the 'hotspot' between subdomains 1 and 3 which is involved in binding most actin-binding proteins. The structure reveals how recruitment of YopO-bound actin monomers stalls actin polymerization by steric hindrance. The structure also demonstrates how YopO uses actin for self-activation and suggests that actin is being used by YopO as bait for recruitment into actin machineries. Using SILAC mass spectrometry, actin cytoskeletal machineries within macrophages that recruit YopO are identified and these include, amongst others: VASP family proteins, gelsolin family proteins, formins and WASP. Of these, VASP, EVL, diaphanous1, WASP and gelsolin have been identified to be phosphorylated by YopO and were validated by *in vitro* phosphorylation. This work demonstrates that YopO uses actin as a scaffold for selection of kinase substrates, enabling targeted phosphorylation of the actin machinery and provides insight into the regulation of the actin cytoskeleton by phosphorylation under non-pathogenic conditions.

DECLARATION

The work described in this thesis was performed in collaboration between The Division of Structural Biology, University of Oxford and the Institute of Molecular and Cell Biology, A*STAR, Singapore.

Wei Lin Lee
Merton College, University of Oxford

ACKNOWLEDGEMENTS

The course of my PhD was a fulfilling experience, no doubt very difficult and trying at times, and I owe my gratitude to all the people who have made the completion of this journey possible.

I am indebted to Dr Jonathan Grimes and Dr Robert Robinson, my co-supervisors. To Jon, thank you for the opportunity to join STRUBI in Oxford University, which was an eye-opening experience; and for your care and guidance. To Bob, thank you for igniting the flame in me and giving me the conviction to start my graduate studies; and for the constant encouragement that kept me going.

I would like thank the Agency for Science, Technology and Research (A*STAR), Singapore, for funding my PhD, without which, none of this would have been possible.

I am very grateful to Dr Karl Halos, Dr Thomas Walter, Dr Geoff Sutton, Dr Guido Paesen, Dr Mohammad Bahar, Margaret Jones and Lu Weixian, who were great help for my experiments in Oxford University.

I owe my sincere thanks to the current and ex-members of the BR lab for a cheerful and supportive research environment: Albert, with special thanks, for guidance on experiments; Widya, for informative discussions on protein kinases; Khay chun, Jantana, Lin Jie, Bala, Marten, Shiming, Kriss, Pavithra, Liling, Diyva, Daavid, Letian and David for helping me in one way or another.

I would also like to thank Dr Yao Shao Qin, of National University of Singapore, for getting me started on my journey in science and for the foundation he established in me during my undergraduate studies.

To my friend Yongli, thank you for being with me through the difficult times.

And my deepest gratitude to my family: my brother, for being an exceptional role model; my parents for their unconditional love; and my husband Keith, for supporting me in all of my endeavours.

ABBREVIATIONS

1D LC/MS-MS	one dimensional liquid chromatography coupled tandem mass spectrometry
A	acidic region
Å	Angstrom
ABC	Dimethylamine-borane complex
Abi1	Abelson interactor 1
Abl	Abelson kinase
Abp1	actin-binding protein-1
ACK1	activated CDC42 kinase 1
Actn1	alpha-actinin-1
ADF	actin-depolymerizing factor
ADF-H	actin-depolymerizing factor homology domain
ADP	Adenosine diphosphate
Adrbk1	beta-adrenergic receptor kinase 1
Aip	actin-interacting protein
Ala	alanine
Aldh18a1	delta-1-pyrroline-5-carboxylate synthase
AMPK	AMP-activated protein kinase
Amu	atomic mass unit
Apbb1ip	amyloid beta A4 precursor protein-binding family B member 1-interacting protein
APE	Asp-Pro-Glu motif
Arg	arginine
Arhgap9	Rho GTPase activating protein 9
Arhgap27	Rho GTPase-activating protein 27
Arp	actin-related protein
Arp2	actin-related protein 2
Arp3	actin-related protein 3
Asn	Asparagine
Asp	aspartic acid
ATP	adenosine-5'-triphosphate
BLAST	Basic Local Alignment Search Tool
Brk1	BRICK1 Protein
Bt2cAMP	dibutyryl cAMP kinase
Btk	Bruton's tyrosine kinase
C domain	central domain
$CaCl_2$	calcium chloride
CapG	macrophage capping protein
CapZ	F-actin-capping protein
Capzα1	F-actin-capping protein subunit alpha-1
Capzα2	F-actin-capping protein subunit alpha-2
Car3	carbonic anhydrase 3
CARMIL	leucine-rich repeat-containing protein 16A
CC	cyclase adenylase interaction domain
CCD	charge-coupled device
Cdc42	cell division control protein 42 homolog

Cdk1	cyclin-dependent kinase 1
Cdk5	Cyclin-dependent kinase 5
Chrng	acetylcholine receptor subunit gamma
CK2	casein kinase 2
CLIP-170	Cytoplasmic linker protein CLIP-170
C-lobe	C-terminus lobe
Cobl	Cordon bleu
CR16	WAS/WASL-interacting protein family member 3
CR3	complement receptor 3
CrkL	Crk-like protein
C-terminal	carboxy terminal
Cyfip1	cytoplasmic FMR1-interacting protein 1
Cys	cysteine
DAAM	disheveled-associated activator of morphogenesis
DAD	diaphanous-autoregulatory domain
DFG	Asp-Phe-Gly motif
Dia	diaphanous
DID	diaphanous inhibitory domain
D-loop	DNase I-binding loop
DNA	Deoxyribonucleic acid
DNase1	Deoxyribonuclease 1
DRF	diaphanous-related formin
DTT	Dithiothreitol
E.coli	*Escherichia coli*
EGTA	ethylene glycol tetraacetic acid
Eif4e2	Eukaryotic translation initiation factor 4E type 2
Ena/VASP	Enabled/Vasodilator-stimulated phosphoprotein family
Ergic1	Endoplasmic reticulum-Golgi intermediate compartment protein 1
ERK	Extracellular signal-regulated kinase
EVH1	Ena/VASP homology domain 1, also known as WH1
EVH2	Ena/VASP homology domain 2
EVL	Ena/VASP-like protein
F-actin	filamentous actin
FAK	focal adhesion kinase
Fasn	Fatty acid synthase
FcγR	Fc-gamma receptor
FFAS	Fold and Function Assignment System server
FH1	formin homology domain 1
FH1-FH2	formin homology domains 1 and 2
FH2	formin homology domain 2
FH3	formin homology domain 3
FHOD	FH1/FH2 domain-containing protein
Fhod1	FH1-FH2 domain-containing protein 1
Flii	Protein flightless-1
FMN	formin
FMN1	formin-1
FMNL	formin-like protein
FMNL1	formin-like protein 1
Fnbp1	formin-binding protein 1

Fyb	FYN-binding protein
G1	Gelsolin domain 1
G1-3	gelsolin domains 1-3
G4-6	gelsolin domains 4-6
G-actin	globular actin
GBD	GTPase-binding domain
GDI	guanine nucleotide dissociation inhibitor
GEF	guanine nucleotide exchange factor
Gigyf2	PERQ amino acid-rich with GYF domain-containing protein 2
Gln	glutamine
Glu	glutamic acid
Gly	glycine
GMF	glia maturation factor
Golga4	golgin subfamily A member 4
Grb2	growth factor receptor-bound protein 2
GST	glutathione S-transferase
GTP	guanosine-5'-triphosphate
Gαq	G-protein αq
H28	Interferon-induced protein 44-like
Hars2	histidyl-tRNA synthetase
HFD	helical folded domain
His	histidine
IcsA	outer membrane protein IcsA autotransporter
Ifit1	interferon-induced protein with tetratricopeptide repeats 1
IFNγ	interferon-gamma
IKKβ	inhibitor κB kinase β
Ile	Isoleucine
INF2	Inverted formin 2
IPTG	isopropyl β-D-1-thiogalactopyranoside
IQGAP1	Ras GTPase-activating-like protein 1
IRSp53	insulin receptor substrate p53
JMY	junction-mediating and regulatory protein
JNK	Stress-activated protein kinase
JNKb	JNK-binding domain
KCl	potassium chloride
K_d	dissociation constant
kDa	kilo daltons
KIND	kinase non-catalytic C-lobe domain
Klf16	Krueppel-like factor 16
KMEI	actin polymerization buffer containing 50 mM KCl, 1 mM $MgCl_2$, 1 mM EGTA and 10 mM Imidazole HCl (pH 7.0)
LAT	linker for activation of T-cells family member 1
Lck	leukocyte C-terminal Src kinase
Leu	leucine
LIMK	LIM kinase
Lpxn	leupaxin
Lrrc20	leucine-rich repeat-containing protein 20
Lys	lysine
M	molar
MAL	megakaryocytic acute leukemia protein

MAP	mitogen-activated protein
MAPK	mitogen-activated protein kinase
Mat2a	S-adenosylmethionine synthase isoform type-2
mDia1	mouse diaphanous 1
Me2	NAD-dependent malic enzyme
Mena	Protein enabled homolog
MES	2-ethanesulfonic acid
Met	methionine
mFYVE	modified FYVE zinc-finger domain
Mg	magnesium
$MgCl_2$	magnesium chloride
Mk	molecular size marker
MKK	mitogen-activated protein kinase kinase
MKL1	MKL/myocardin-like protein 1
MLC	myosin light chain
mM	millimolar
$MnCl_2$	manganese chloride
MST3	Mammalian STE20-like protein kinase 3 also known as Serine/threonine-protein kinase 24
Na	sodium
NaCl	sodium chloride
NADPH	nicotinamide adenine dinucleotide phosphate
Nampt	Nicotinamide phosphoribosyltransferase
Nap1	Nck-associated protein 1
Nck	NCK adaptor protein 1
Nfs1	cysteine desulfurase
NFκB	nuclear factor kappa-B
Ni	nickel
Ni-NTA	nickel- nitrilotriacetic acid
NK	natural killer cells
nl	nano litre
N-lobe	N-terminus lobe
nm	nano metre
NPF	nucleation promoting factor
NPI-1	nucleoprotein interactor 1
NSRRC	National Synchrotron Radiation Research Center
N-terminal	amino-terminal
NTF2	nuclear transport factor 2
NWASP	neural Wiskott Aldrich syndrome protein
Oas1	oligoadenylate synthetase 1
^oC	degree Celsius
P	proline-rich motifs
p130Cas	Breast cancer anti-estrogen resistance protein 1 (Bcar1)
p67(Phox)	Neutrophil cytosol factor 2
PAK	p21-activated kinase
PDB	Protein Data Bank
Pdia4	protein disulfide-isomerase A4
PEG	polyethylene glycol
Phe	phenyalanine
Pi	inorganic phosphate

PICK1	protein interacting with C kinase 1
PIP	phosphatidylinositol
PIP_2	phosphatidylinositol-4,5-bisphosphate
PIP_3	Phosphatidylinositol (3,4,5)-trisphosphate
PKA	cAMP-dependent protein kinase
PKC	protein kinase C
PKCdelta	protein kinase C delta
PKD1	protein kinase D1
PKG	cGMP-dependent protein kinase
PLC	Phospholipase C
P-loop	Loop within protein kinases that is involved in binding phosphates of ATP
PRK2	protein kinase C-like 2
Prkag1	AMP-activated protein kinase subunit gamma-1
Pro	proline
Psph	phosphoserine phosphatase
PWA	proline-rich and VCA domains
PyK	pyruvate kinase
PYK2	proline-rich tyrosine kinase 2
Rac	Ras-related C3 botulinum toxin substrate
Ran	GTP-binding nuclear protein
Rbm33	RNA-binding protein 33
RhoA	Transforming protein RhoA
RhoC	Rho-related GTP-binding protein RhoC
RhoG	Rho-related GTP-binding protein RhoG
RickA	Arp2/3 complex-activating protein rickA
RMSD	root-mean-square deviation
Robo	Roundabout homolog
ROCK	Rho-kinase
Rpl7	60S ribosomal protein L7
Rplp0	60S acidic ribosomal protein P0
Rraga	Ras-related GTP-binding protein A
RSK1	ribosomal S6 protein kinase 1
SDS-PAGE	sodium dodecyl sulphate Polyacrylamide gel electrophoresis
Ser	serine
SER	surface entropy reduction
SERp	surface Entropy Reduction prediction server
Sf	*Spodoptera frugipera*
Sf1	Splicing factor 1
SH3	SRC Homology 3 Domain
SHD	SCAR homology domain
SILAC	stable isotope labeling by amino acids in cell culture
SipA	salmonella invasion protein A
SipC	salmonella invasion protein C
SKAP-HOM	Src kinase-associated phosphoprotein
SLAP	SLP-76-associated phosphoprotein
SLP-76	lymphocyte cytosolic protein 2 or SLP-76 tyrosine phosphoprotein
Spec	spectral
SRC	Proto-oncogene tyrosine-protein kinase Src

SRF	serum response factor
srv2/CAP	cyclase adenylase associated protein
Stoml2	stomatin-like protein 2
Tes	testin
Tet	tetramerization domain
TFZ	translation function Z-score
Thr	threonine
Tir	translocated intimin receptor
TMR	tetramethylrhodamine-5-maleimide
TNF-α	tumor necrosis factor-α
TOCA-1	transducer of Cdc42-dependent actin assembly protein 1 also known as formin-binding protein 1-like (Fbp1l)
Tpp2	tripeptidyl-peptidase 2
TRAF	TNF receptor-associated factor
Tris	trisaminomethane
Trp	Tryptophan
Ttc35	tetratricopeptide repeat protein 35
Twf1	twinfilin1
Twf2	twinfilin2
Txnrd2	Thioredoxin reductase 2
Tyr	tyrosine
Tβ	β-thymosin
Tβ4	β-thymosin 4
Usp4	Ubiquitin carboxyl-terminal hydrolase 4
V domain	verprolin homology domain
Val	Valine
VASP	Vasodilator-stimulated phosphoprotein
Vav	Proto-oncogene vav
VCA	verprolin-central-acidic domain
VopF	Vibrio outer protein F
VopL	Vibrio outer protein L
Wars2	Tryptophanyl tRNA synthetase 2
WAS	Wiskott-Aldrich syndrome
WASH	WASP and SCAR homologue
WASP PWA	WASP construct contain poly-proline region and VCA domains
WASP	Wiskott Aldrich syndrome protein
WAVE	WASP family verprolin-homologous protein
WAVE2	Wiskott-Aldrich syndrome protein family member 2
WH1	WASP homology domain 1
WH2	Wiskott-Aldrich syndrome homology region 2 domain
WHD	WAVE homology domain
WHIF1	WH2 domain-containing formin 1, also known as Inverted formin 2 (INF2)
WIP	WAS/WASL-interacting protein
WW	protein domain that contains two highly conserved tryptophans
X	any residue
x-ray	x-radiation
Yop	Yersinia outer protein
YopO 1YY	YopO (89-729) surface entropy reduction mutant (K205Y, E206Y, E207Y, K440Y, K441Y)

YopO K245M	YopO (89-729) K245M mutant
YopO KD	YopO (89-729) kinase dead mutant (D267A, K269A)
YopO nAct	YopO (89-729) non-actin-binding mutant (V374D,T376D, R723A, E727A)
YopO nRac	YopO (89-729) non-Rac binding mutant (Y588A, N592A, E596A)
YopO nRacKD	YopO (89-729) non-Rac binding, kinase dead mutant (D267A, K269A, Y588A, N592A, E596A)
YopO WT	YopO wild type
YpkA	Yersinia protein kinase A
α	alpha
β	beta
µl	micro litre
µM	micromolar
φ	either tyrosine or phenylalanine

LIST OF TABLES

Table 2.1	Table of constructs used for recombinant expression of proteins…	69
Table 3.1	Cluster candidates proposed by Surface Entropy Reduction prediction (SERp) server……..……..……..……...	106
Table 3.2	Design, expression, purification and crystallization of surface entropy mutation constructs…….……..……...	109
Table 3.3	Unit cell and space group of YopO 1YY-actin crystals…...……	111
Table 3.4	Map correlations against final map phases after accounting for origin shifts calculated with Phenix…….……..…….…….	115
Table 3.5	Data collection, processing and refinement statistics for YopO 1YY-actin complex…….……...…..…….	115
Table 3.6	Hydrogen bonds and electrostatic interactions between YopO and actin……..	119
Table 3.7	Contacts between YopO and actin with bond lengths at 3.5 Å and below, obtained from PDBePISA…….……..……...…..…….…….	131
Table 4.1	Proteins that were identified to be enriched via pull down with His-tagged YopO as bait in SILAC mass spectrometry…….….....	148
Table 4.2	Proteins that were identified to be enriched via pull down with His-tagged profilin as bait in SILAC mass spectrometry…...…..….	159
Table 4.3	Proteins that were identified to be enriched via pull down with His-tagged YopO nRac as bait in SILAC mass spectrometry...…...	166
Table A.1	Vectors used in protein production…….……..……..……	256

LIST OF FIGURES

Figure 1.1	Structure of actin as a monomer and as a subunit of F-actin……..	6
Figure 1.2	Schematic representation of nucleation and filament elongation by Arp2/3, formin and tandem WH2 nucleator cordon bleu……	9
Figure 1.3	Schematic representation of monomer sequestration, capping, severing and cross-linking of actin by various actin-binding proteins…….	10
Figure 1.4	Crystal structures showing the interaction of Tβ with actin……	12
Figure 1.5	Crystal structures of the complex of profilin and β-actin…….	14
Figure 1.6	Model of the Arp2/3 actin filament branch junction……	16
Figure 1.7	Schematic of WASP and WAVE2 domain organizations……	20
Figure 1.8	Crystal structures of ternary complexes of the WH2 domains with actin-DNase1……	21
Figure 1.9	Schematic of WIP domain organization……	26
Figure 1.10	Schematic of domain organization for formin Diaphanous (Dia), inverted formin 2 (INF2) and formin-like protein (FMNL)…….	28
Figure 1.11	Crystal structure of FMNL3 FH2 domain bound to tetra-rhodamine- conjugated actin……	28
Figure 1.12	Schematic of domain organization for tandem WH2 nucleators including human spire, human cordon bleu, Vibrio outer proteins VopF and VopL….	32
Figure 1.13	Schematic of domain organization for vasodilator-stimulated phosphoprotein VASP and Ena/VASP-like (EVL) protein…….	37
Figure 1.14	Crystal structure of complex of profilin, actin with a construct of VASP containing a part of the proline-rich region and G-actin-binding site…….	37
Figure 1.15	Schematic of domain organization for gelsolin and CapG……..	42
Figure 1.16	The interaction of active gelsolin N-and C-terminal halves with monomeric actin..…….	44
Figure 1.17	Crystal structure of the interaction of ADF-H from twinfilin with G-actin…….	47
Figure 1.18	Schematic of Srv2/CAP domain organization……	50
Figure 1.19	Regulation of cytoskeletal dynamics by Rho GTPases……	54
Figure 1.20	Structure of GDI domain of YpkA……	64
Figure 1.21	Sequence alignment of the kinase domains of YopO with top hits identified with FFAS (Fold Function Assignment Server) against Protein Data Bank (PDB)…….	68
Figure 1.22	Structure of protein kinases in the active and inactive states……..	69
Figure 3.1	Preparation of complexes of YopO-actin and YopO-actin-profilin complexes.....	99
Figure 3.2	YopO-actin crystals……	101
Figure 3.3	Example of YopO-actin-profilin crystals……	102
Figure 3.4	Attempts at improving resolution of diffraction of YopO-actin crystals……..	105
Figure 3.5	Sites most suitable for mutation proposed by Surface Entropy Reduction prediction (SERp) server…….	107
Figure 3.6	Candidate SER mutations Lys440 and Lys441 in the GDI domain.	109
Figure 3.7	Example of YopO SER mutant 1YY-actin crystals grown……..	110

Figure 3.8	Electron densities at different stages of phase refinement for residues 261 - 265 of actin…….....	114
Figure 3.9	Structure of the YopO-actin complex…….....….	117
Figure 3.10	Sequence-structural analysis of YopO (89-729) …….……	118
Figure 3.11	The surface area of actin that is occluded by YopO…….……	120
Figure 3.12	The surface area of YopO that is occluded by actin and Rac1…….	120
Figure 3.13	Interaction of the GDI domain with actin……	121
Figure 3.14	Conformational changes to the GDI domain on actin-binding….....	122
Figure 3.15	Conformational changes to GDI domain. …….…….……	123
Figure 3.16	Superimposition of the GDI domain in complex with Rac1 on YopO-actin…….……	124
Figure 3.17	Structural elements of the kinase domain of YopO…….……	126
Figure 3.18	Mutations to disrupt the actin-binding interface of YopO……..….	128
Figure 3.19	Monomer sequestration activity of YopO and YopO nAct mutant..	128
Figure 3.20	The involvement of surface entropy reduction mutations (K205Y, E206Y, E207Y) in YopO-actin crystal contacts……..……	129
Figure 3.21	Sequence alignment of actin protein sequences……	132
Figure 3.22	Structural basis of differential actin isoform preference of YopO...	133
Figure 3.23	Actin monomer sequestration activities of YopO and the K245M mutant towards different actin …….	134
Figure 3.24	Autophosphorylation of YopO WT and YopO K245M in the presence of various ratios of Sf9, cytoplasmic and skeletal α-actin	134
Figure 3.25	Actin monomer sequestration of YopO WT…….……...	135
Figure 3.26	Kinase substrate binding groove on YopO……..……..…….....	136
Figure 3.27	Interaction of the kinase domain of YopO with actin…….….	138
Figure 3.28	Conformations of the nucleotide-binding cleft of actin……....	139
Figure 4.1	Flowchart describing the steps in identification of proteins that interact with either YopO, profilin or YopO nRac mutant…….	145
Figure 4.2	Gel of pull down with YopO as bait submitted for analysis by mass spectrometry…….…….……..	146
Figure 4.3	Chart showing distribution of proteins identified by mass spectrometry upon pull down using His-tagged YopO as heavy to light ratio against spectrometry count (logarithmic scale) ……..	147
Figure 4.4	Superimposition of selected actin-binding proteins on YopO-actin	152
Figure 4.5	Superimposition of gelsolin-actin structures on YopO-actin……....	154
Figure 4.6	Superimposition of WH2 domains from WASP and WIP on YopO-actin……..	154
Figure 4.7	Superimposition of YopO-actin on two actin protomers in the F-actin conformation…….……..……..……..……	155
Figure 4.8	Gel of pull down with profilin as bait submitted for analysis by mass spectrometry…….…….…….……	156
Figure 4.9	Chart showing distribution of proteins identified by mass spectrometry upon pull down using His-tagged profilin as heavy to light ratio against spectrometry count (logarithmic scale) …..…	158
Figure 4.10	Actin monomer sequestration activity of YopO and YopO nRac mutant towards Sf9 actin…….……..…...	162
Figure 4.11	Gel of pull down with YopO nRac as bait submitted for analysis by mass spectrometry…….…….……	164

Figure 4.12 Chart showing distribution of proteins identified by mass spectrometry upon pull down using His-tagged YopO nRac as heavy to light ratio against spectrometry count (logarithmic scale) 165
Figure 4.13 Venn diagram showing the overlap of and exclusive targets enriched within the datasets obtained with YopO WT and YopO nRac…… 169
Figure 4.14 Venn diagram showing a comparison of common targets between YopO WT and YopO nRac against targets identified with profilin 170
Figure 4.15 Superimposition of RPEL domain 1 from MKL1 on YopO-actin 173
Figure 4.16 *In vitro* phosphorylation assay of YopO WT and mutants……..… 174
Figure 4.17 Actin monomer sequestration activity of YopO WT and YopO KD mutant towards Sf9 actin…….. 175
Figure 4.18 *In vitro* phosphorylation assays for potential substrates of YopO 177
Figure 4.19 The phosphorylation of WASP PWA by YopO…….. 179
Figure 4.20 Effect of YopO-phosphorylated VASP on rate of actin polymerization…….. 180
Figure 4.21 Schematic representation of steric hindrance of YopO towards filament elongation by various actin polymerization machineries... 182
Figure 4.22 Schematic representation of binding of actin-binding proteins for phosphorylation by YopO…….…… 184
Figure 5.1 The mode of binding of substrates for phosphorylation…….. 191
Figure 5.2 Approximation of putative phosphorylation sites on VASP by sequence alignment with WH2 from WIP……...…… 193
Figure 5.3 The interference of actin turnover by inhibition of nucleotide exchange of profilin-actin by YopO…….……...… 195
Figure 5.4 The effects of Rac, RhoA and RhoG sequestration……..…… 198
Figure 5.51 The effects of YopO on actin polymerization……..…… 199
Figure 5.6 Effectors involved in FcγR- and CR3-mediated phagocytosis…… 202
Figure 5.7 Actin cytoskeletal disruption by YopO…… 204
Figure 5.8 Domain movements of YopO as predicted by HingeProt…… 209
Figure 5.9 Normal mode analysis of YopO using Elnemo…… 210
Figure 5.10 Overlay of all frames within the trajectories of four of the lowest frequency modes derived from Elnemo……... 210
Figure 5.11 The distance between the catalytic cleft and the first ordered residue of YopO.....……...…….…… 211
Figure 5.12 Hypothetical models of inactive YopO and conformational changes upon binding actin…….……...……. 214

TABLE OF CONTENTS

Chapter 1 Introduction..... 1
1.1 The eukaryotic cytoskeleton..... 1
1.2 Protrusive structures of the actin cytoskeleton..... 3
1.3 The actin molecule..... 5
1.4 The actin filament..... 7
1.5 Modulation of the actin cytoskeleton by actin-binding proteins..... 8
1.6 Actin monomer-binding proteins..... 11
1.6.1 β-thymosins..... 11
1.6.2 Profilin..... 13
1.7 Actin nucleators 15
1.7.1 Arp2/3 15
1.7.1.1 Regulation of Arp2/3..... 18
1.7.1.2 Type I nucleation promoting factor WASP..... 19
1.7.1.3 Regulation of WASP by phosphorylation..... 22
1.7.1.4 Type I nucleation promoting factor WAVE..... 23
1.7.1.5 Regulation of WAVE by phosphorylation..... 23
1.7.1.6 WASP interacting protein WIP..... 25
1.7.2 Formins..... 27
1.7.2.1 Regulation of formins by phosphorylation..... 31
1.7.3 Tandem WH2 nucleators..... 32
1.8 Filament elongators..... 35
1.8.1 Ena/VASP proteins..... 35
1.8.2 Regulation of Ena/VASP proteins by phosphorylation..... 38
1.9 Capping proteins..... 39
1.9.1 CapZ..... 39
1.10 Severing and depolymerizing proteins..... 41
1.10.1 Gelsolin family of proteins 41
1.10.2 Gelsolin..... 42
1.10.3 Regulation of gelsolin by phosphorylation..... 44
1.10.4 CapG..... 45
1.10.5 ADF/cofilin..... 46
1.10.6 Twinfilin..... 48
1.10.7 Srv2/CAP..... 49
1.11 Regulation of actin cytoskeletal dynamics by Rho GTPases..... 51
1.12 Molecular mechanisms of actin dynamics in phagocytic uptake..... 55
1.13 Pathogenic manipulation of the actin cytoskeleton..... 58
1.14 The pathogenicity of *Yersinia* bacteria..... 60
1.14.1 *Yersinia* protein kinase A YpkA/YopO..... 63
1.14.2 Kinase structure and function..... 67
1.15 Rationale and significance of work..... 72

Chapter 2 Experimental procedures ……..……..…… 73
2.1 Molecular biology methods……..…… 73
2.2 Constructs, vectors and *E.coli* strains……...…… 74
2.3 Transformation and plasmid selection……...……... 77
2.4 Recombinant expression of mouse β-actin from baculovirus infection of Sf9 cells…… 78
2.4.1 Transfection of Sf9 cells with recombinant bacmid DNA…….…. 78
2.4.2 Baculovirus amplification and infection of Sf9 cells for expression of recombinant protein……..... 79
2.5 Purification of recombinant mouse β-actin from insect cells……...…… 80
2.6 Purification of native Sf9 actin from insect cells……..….... 81
2.7 Expression and purification of YopO constructs…….. 81
2.8 Preparation of YopO-actin and YopO-actin-profilin complexes……..… 82
2.9 Crystallization trials for YopO-actin and YopO-actin-profilin complexes 82
2.9.1 Crystallization hits of YopO-actin…...…….…… 83
2.9.2 Crystallization hits of YopO-actin-profilin…….. 83
2.10 Methylation of YopO and preparation of complexes with methylated YopO…… 84
2.11 Dehydration and in loop annealing of YopO-actin crystals…..…… 84
2.12 Data collection and processing for YopO-actin crystals……..…… 85
2.13 Crystallization of YopO SER mutants-actin……...…… 86
2.14 Data collection and processing for YopO 1YY-actin crystals……. 86
2.15 Crystallographic software…….…… 87
2.16 Homologous sequence alignment and structural analysis…… 87
2.17 Biochemical studies……..…...……. 89
2.17.1 Actin polymerization assay using pyrene-labelled actin…….. 89
2.17.2 *In vitro* kinase assays…….……..……. 89
2.18 SILAC (Stable isotope labelling by amino acids in cell culture) …… 91
2.18.1 Metabolic labeling of RAW264.7 cells and lysate preparation…… 91
2.18.2 Identification of proteins that bind to YopO, profilin and YopO nRac mutant…….…… 91
2.18.3 Mass Spectrometry ……..…… 92
2.18.4 1D LC/MS/MS protein identification…….…… 92
2.18.5 Analysis of spectra using database searches…… 93
2.19 Expression and purification of kinase substrates (VASP, EVL, CapG, gelsolin, twinfilin, Dia1 FH1-FH2 and WASP PWA) …… 94

Chapter 3 Structure of the Yopo-actin complex……..... 97
3.1 Preparation of YopO, β-actin, profilin and their complexes…… 97
3.2 Crystallization trials of YopO-actin and YopO-actin-profilin complexes 100
3.3 Crystallization trials of YopO-actin and YopO-actin-profilin complexes with methylated YopO……...……...…… 103
3.4 Post-crystallization treatment of YopO-actin crystals……..…… 104
3.5 Surface entropy reduction mutagenesis of YopO…….…… 105
3.6 Crystallization of YopO 1YY-actin…….……..……. 110
3.7 Data collection and processing…….……..…. 111
3.8 Structure determination, model building and refinement……..…. 111
3.9 The structure of YopO 1YY-actin…….……..… 116
3.10 Conformational changes of the GDI domain upon binding actin……..... 122
3.11 Interaction of the kinase domain of YopO with actin…….……. 125
3.12 Validation of YopO 1YY-actin crystal structure……. 127
3.13 Crystal packing of YopO-actin…….……...…. 129
3.14 Structural basis of differential actin isoform preference of YopO……..… 130
3.15 Discussion……...…….. 135
3.15.1 Insights into the mechanism of actin sequestration by YopO..…..... 135
3.15.2 Insights into the kinase domain of YopO……..... 136
3.15.3 Interference of YopO with nucleotide-exchange of profilin-actin... 137
3.16 Conclusions…….. 140

Chapter 4 Identifying novel kinase substrates of YopO ……..……..… 143
4.1 Stable isotope labelling with amino acids in cell culture……..……..…… 143
4.2 Identification of proteins that interact with YopO…….…..…… 144
4.3 Identification of proteins that interact with profilin…….…….……..…… 156
4.4 Identification of proteins that interact with YopO nRac mutant……..…… 163
4.5 Mechanism of actin recruitment of actin machinery of YopO……..… 168
4.6 Implications of recruitment of actin-binding proteins by YopO……..…… 171
4.6.1 Implications of recruitment of MKL1 by YopO……..…… 172
4.7 Determining the kinase activity of different YopO mutants…….…... 174
4.8 Validation of phosphorylation targets via *in vitro* autoradiography assays. 176
4.9 Effect of phosphorylation on activity of VASP……..……..… 180
4.10 Discussion……..……..…… 181
4.10.1 Modulation of the actin cytoskeleton by steric hindrance…… 181
4.10.2 Mechanism of kinase substrate selection of YopO……..… 183
4.10.3 Modulation of the actin cytoskeleton by phosphorylation……..… 185
4.11 Conclusions……..… 185

Chapter 5 Establishing an integrated model for mechanism of action of YopO……..…. 189
5.1 The proposed mechanism of substrate selection YopO……..…… 190
5.1.1 Model of binding and phosphorylation of VASP by YopO……... 192
5.2 Multi-faceted interference of the actin polymerization machinery by YopO…… 194
5.2.1 Interference with nucleotide exchange of profilin-actin……..…… 194
5.2.2 Implications of sequestration of Rho GTPases on actin dynamics 196
5.2.3 Actin monomer sequestration and inhibition to actin filament formation…….. 199
5.2.4 Implications of phosphorylation of actin machinery by YopO…… 200
5.3 Mechanism of disruption of phagocytosis by YopO……..……..… 200
5.4 Overview of actin cytoskeletal disruption by YopO……..…..……. 203
5.5 Reconciling the activity of YopO with activities of other Yops…..…… 205
5.6 Mechanism of activation of YopO……..…..…… 208
5.7 Hypothetical models of inactive YopO…….……..……. 211

Chapter 6 Conclusions and future research…….…. 215
6.1 Conclusions…….…… 215
6.2 Future work……. 220
6.2.1 Identification of other novel substrates…… 220
6.2.2 Determining the effect of phosphorylation on substrate protein function……. 220
6.2.3 Validation of the interaction between YopO and RhoG……..…… 221
6.2.4 Determining if YopO blocks pointed end depolymerisation……..... 221
6.2.5 Validation of the inhibition of nucleotide exchange of actin by YopO…… 222
6.2.6 Validation of the hypothesis of autoinhibition……..….. 223

References…….……..… 225

Appendix…….……..……..…… 255
.
A1. Vectors…….. 255

Chapter 1

Introduction

1.1 The eukaryotic cytoskeleton

The eukaryotic cytoskeleton is responsible for providing the cell with shape and structure and is made up of three main kinds of cytoskeletal filaments, the microfilament, microtubule and intermediate filament systems.

Microtubules are hollow cylinders about 25 nm in diameter, made up of polymerized α and β tubulin dimers. Microtubules perform many functions: providing structural support and motility in eukaryotic cilia and flagella; cellular organization and force generation in chromosome segregation in the form of the mitotic spindle; and intracellular transport of organelles including vesicles or mitochondria, in association with motor proteins like dyneins and kinesins.

Intermediate filaments have an average diameter of 10 nm, which is between that of microfilaments and microtubules. These filaments serve to organise the internal structure of the cell and provide mechanical strength, which unlike actin filaments and microtubules, are not involved in the generation of movement. Intermediate filaments are heterogeneously composed of a family of related proteins sharing similar structure and sequence. Many intermediate filament proteins are differentially expressed in different types of cells, *i.e.* keratins are expressed in epithelial cells, neurofilament proteins in neurons, desmin in muscle cells, nestin in stem cells of the central nervous system, and vimentin in cell types including

fibroblasts and white blood cells. Some intermediate filament proteins are more ubiquitous, such as nuclear lamins, which make up the nuclear lamina of all cell types.

Microfilaments, also known as actin filaments, are the thinnest filaments of the cytoskeleton, at about 7 nm and are made up of polymers of actin. Actin filaments are involved in a range of cellular functions: providing mechanical forces for cell locomotion, phagocytosis and cell division; providing tracks for vesicular trafficking in endo- and exocytosis; maintenance of cell morphology and polarity; and establishing cell junctions. Via interactions with muscle myosins, actin is also involved in muscle contraction. Actin, actin filaments and the actin cytoskeleton will be the focus in this thesis and will be described in greater detail in subsequent sections.

1.2 Protrusive structures of the actin cytoskeleton

Actin filaments, together with cross-linking proteins form a mesh-like structure that makes up the actin cortex which lies immediately beneath the plasma membrane of animal cells. This provides mechanical support to the plasma membrane, conferring mechanical rigidity for maintenance of cell shape and establishment of specialized cell morphologies like in neurons and activated platelets. Actin filaments are also dynamically plastic and allow remodelling for the formation of a number of higher order cellular architectures including lamellipodia/lamella, filopodia and ruffles which are important in cell locomotion and phagocytic uptake (Small et al. 2002).

During cell crawling, locomotion and spreading, surface-attached sheet-like protrusions of membrane-enclosed cytoplasm known as lamellipodia and lamella are formed at the cell front (Chhabra & Higgs 2007). Lamellipodia and lamella are actin-rich structures in which the actin filaments are oriented with their barbed end pointed towards the plasma membrane at the leading edge (T M Svitkina et al. 1997). The region immediately behind the leading edge and extending for several micrometers into the cell is the lamellipodium. The lamellum extends from the lamellipodia to the cell body. The lamellipodium is thinner (< 200 nm) and is only weakly adherent to the substratum and is dominated by short dendritically branched filaments that disassemble abruptly in the transition into the lamella (Svitkina & Borisy 1999; Ponti et al. 2004). The ARP2/3 complex is the primary actin nucleator in the assembly of the lamellipodia (Svitkina & Borisy 1999). At the lamellum, actin filaments are less dense with most filaments being longer and less dendritically branched, with stronger adhesion to the substratum than observed for the lamellipodium (Ponti et al. 2004). Ruffles are transient structures containing

dendritically branched filaments which do not attach to the substratum (Borm et al. 2005). Membrane ruffles promote binding of immune opsonized particles which is required for efficient phagocytosis (Patel & Harrison 2008).

Filopodia are dynamic finger-like protrusions comprised of bundled, parallel F-actin filaments. Filopodia dynamically extend and retract, functioning as directional sensors for navigation of migration in cell locomotion, chemotaxis, neuronal growth cone path finding, pathogen-sensing and the formation of adherens junctions between epithelial cells (Vasioukhin et al. 2000). They contain parallel bundles of actin filaments that run the length of the protrusion with the actin barbed ends oriented towards the tip (Oldenbourg et al. 2000). Filopodia arise from a lamellipodial/lamellar sheet via elongation of actin filaments at filopodial tips by proteins like Ena/VASP (Lebrand et al. 2004) or formins (Mellor 2005) which protect actin barbed ends from capping proteins. The resultant actin filaments are shaped into parallel bundles by the F-actin-bundling protein fascin (Yang et al. 2013). Retraction of filopodia occurs by retrograde flow of the actin filament bundle (Oldenbourg et al. 2000). Thus actin is a major force provider and dynamic structural element of structures that are involved in cellular remodelling and movement.

1.3 The actin molecule

The actin molecule is the most abundant protein in most eukaryotic cell types. Actin is present at about 0.5 mM in the cytosol of non-muscle cells, while it makes up almost 20% of total protein mass in muscle cells. Actin is about 42 kDa in size and exists as six isoforms, two of which are ubiquitously expressed (β-cytoplasmic, γ-cytoplasmic) while the rest are found in muscle (α-skeletal, α-cardiac, α-smooth, γ-smooth). They are extremely conserved with 93% amino acid sequence identity between the most distant isoforms (Perrin & Ervasti 2010), with the greatest differences observed at the highly acidic N-termini. Actin can exist as a monomer (known as globular or G-actin), or upon polymerization, in the form of a filament (known as F-actin).

Structurally, G-actin consists of four subdomains, subdomains one and two form a lobe while subdomains three and four form the other lobe (**Fig. 1.1**). At the upper cleft between the two lobes, each G-actin binds one Mg^{2+} complexed with an ATP or ADP. Mg^{2+} is the predominant cation *in vivo*, but can be substituted for Ca^{2+} to reduce polymerization *in vitro* (Selden et al. 1986). The lower cleft between subdomains one and three is predominantly hydrophobic and is important for interaction with many actin-binding proteins and for mediating longitudinal contacts between actin subunits within the filament (Dominguez 2004). The upper and lower clefts are closely associated in which changes at the lower cleft are transmitted to the upper cleft and vice versa, such that differences in nucleotide binding gives rise to conformational changes that modulate the strength of intersubunit contacts within the filament and binding affinities of actin-binding proteins (Fujii et al. 2010; Oda et al. 2009). The top of subdomain 2, residues 39-51, is known as the DNase1-binding

loop (or D-loop) due to its interaction with DNase1 (Kabsch et al. 1990). The D-loop plays an important role in longitudinal intersubunit contacts in the filament (Oda et al. 2009) and is disordered in most G-actin-ATP structures but adopts a helical conformation in one G-actin-ADP structure (Otterbein et al. 2001).

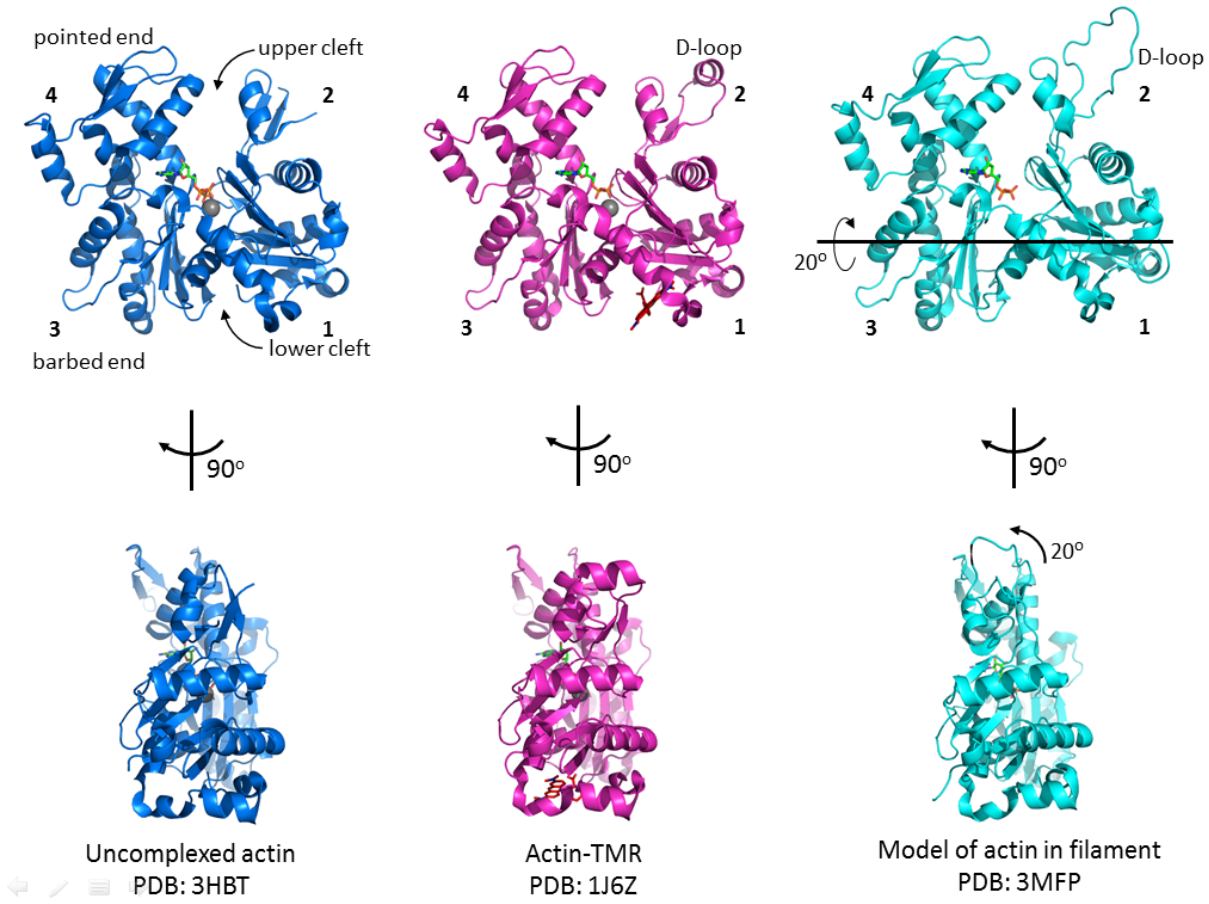


Figure 1.1 Structure of actin as a monomer and as a subunit of F-actin. Actin subdomains are labelled 1, 2, 3 and 4, with pointed and barbed ends as indicated. ATP is shown as a stick representation and calcium ions as grey spheres. (A) Structure of calcium-ATP-bound G-actin. D-loop residues His40 to Gly48 in subdomain 2 are disordered. (PDB: 3HBT (H Wang et al. 2010)) (B) Structure of calcium-ADP-bound tetramethylrhodamine-actin (PDB: 1J6Z (Otterbein et al. 2001)). (C) Model of an actin subunit in the filament (PDB: 3MFP (Fujii et al. 2010)).

1.4 The actin filament

ATP-bound G-actin is preferentially incorporated into the actin filament over ADP-bound G-actin. G-actin is a poor ATPase but its ATPase activity is greatly enhanced upon polymerization. When G-actin is incorporated into a filament, it undergoes a structural transition whereby the D-loop extends into the cleft beneath subdomains 1 and 3 of its neighbour along the long pitch helix and the two lobes undergo a rotation of 20° relative to each other, which results in the flattening of the actin molecule (**Fig. 1.1**). This moves the catalytic water bound to Gln137 closer to the β- and γ-phosphate groups of the ATP molecule, turning on the ATPase activity of F-actin (Oda et al. 2009; Fujii et al. 2010). ATP hydrolysis is not important for polymerization, but rather acts as an indication for the age of the filament. The ATP in actin hydrolyzes to ADP and inorganic phosphate with a half-life of about two seconds upon incorporation into a filament, while the release of the inorganic phosphate has a half-life of 350 seconds (Pollard et al. 2003). The ATP hydrolysis during actin assembly gives rise to conformational differences which translate to different dynamics of actin at opposite ends of a filament. The end corresponding to exposed subdomains one and three is termed the barbed end while that of subdomains 2 and 4 is termed the pointed end. Addition of G-actin is faster at the barbed end and disassembly occurs faster at the pointed end (Pollard & Cooper 2009), conferring structural and dynamical polarity to the filament.

The crystal structure of G-actin has been solved many times, and requires modification or sequestration by small molecules or actin-binding proteins to maintain it in the monomeric state for crystallization. For example, the structure determination of G-actin was made possible by the conjugation of

tetramethylrhodamine-5-maleimide at Cys374 of actin, causing steric hindrance to incorporation into a filament (Otterbein et al. 2001); or with small molecule inhibitors of polymerization Latrunculin A (Yarmola et al. 2000). The only structure of uncomplexed G-actin was obtained in the presence of heat shock protein hsp27, in which hsp27 dissociated, leaving only actin in the crystal (Wang et al. 2010). The structure of F-actin has been studied with electron microscopy (Murakami et al. 2010) and by fibre diffraction (Fujii et al. 2010; Oda et al. 2009). F-actin is helical, with 13 actin molecules per 6 turns, giving rise to 2.17 subunits per turn of a helix (Holmes et al. 1990). The prerequisite for formation of crystals requires the number of subunits per turn to be an integer, as such F-actin is incompatible with crystallization.

1.5 Modulation of the actin cytoskeleton by actin-binding proteins

Following stimuli, cytoskeletal dynamics are orchestrated by a plethora of actin-binding proteins. Actin, existing either in the form of G-actin or F-actin, possibly participates in more protein–protein interactions than any other known protein. As last tabulated in 2003, actin-binding proteins without including synonyms or isoforms were at 162 (Dos Remedios et al. 2003). Due to the huge number of actin-binding proteins, only actin-binding proteins that are of relevance to this work will be described here, with particular focus on those involved in the process of phagocytosis in haematopoietic cells. The fundamental roles performed by actin-binding proteins include monomer sequestration, filament nucleation and elongation, filament end capping, filament cross-linking, filament severing and depolymerisation (Pollard & Cooper 2009; Dos Remedios et al. 2003) (**Fig. 1.2 & 1.3**).

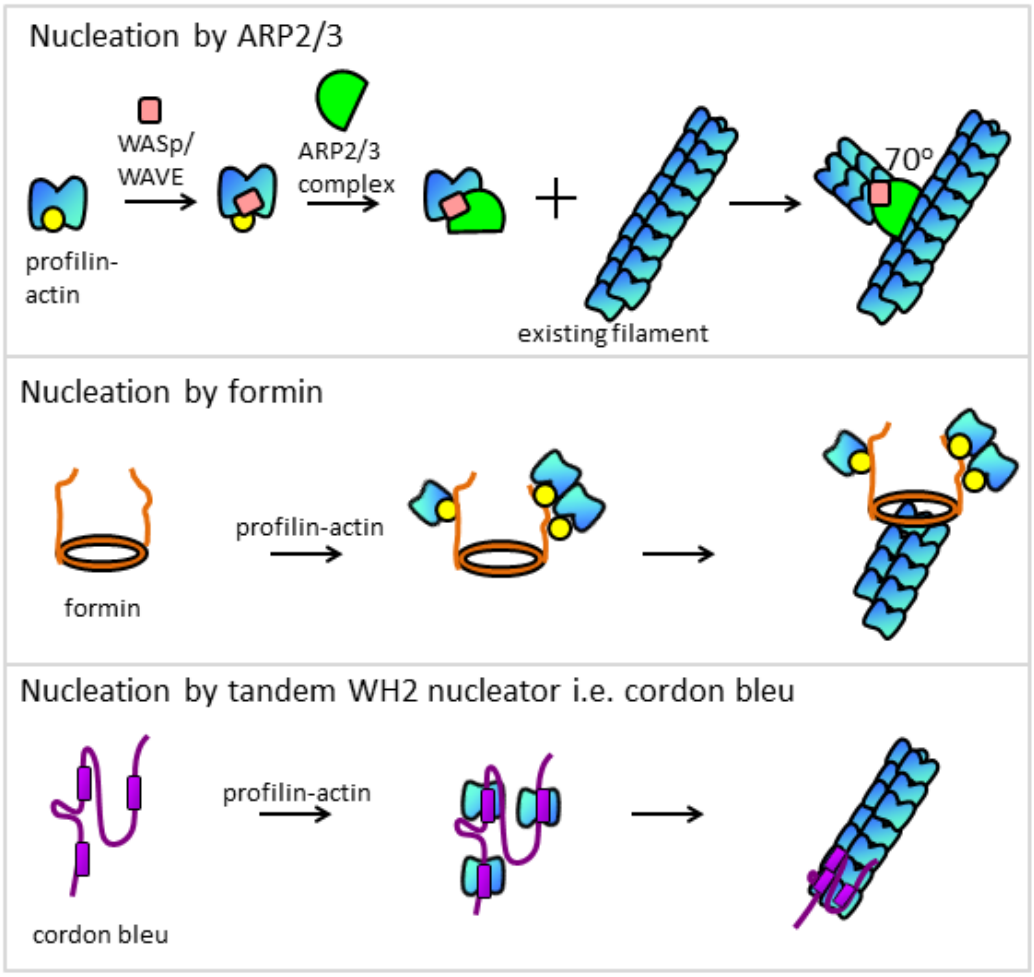


Figure 1.2 Schematic representation of nucleation and filament elongation by ARP2/3, formin and tandem WH2 nucleator cordon bleu. These proteins recruit actin-profilin and feed them onto the barbed end of existing filaments. Diagram adapted from (Pollard & Cooper 2009)

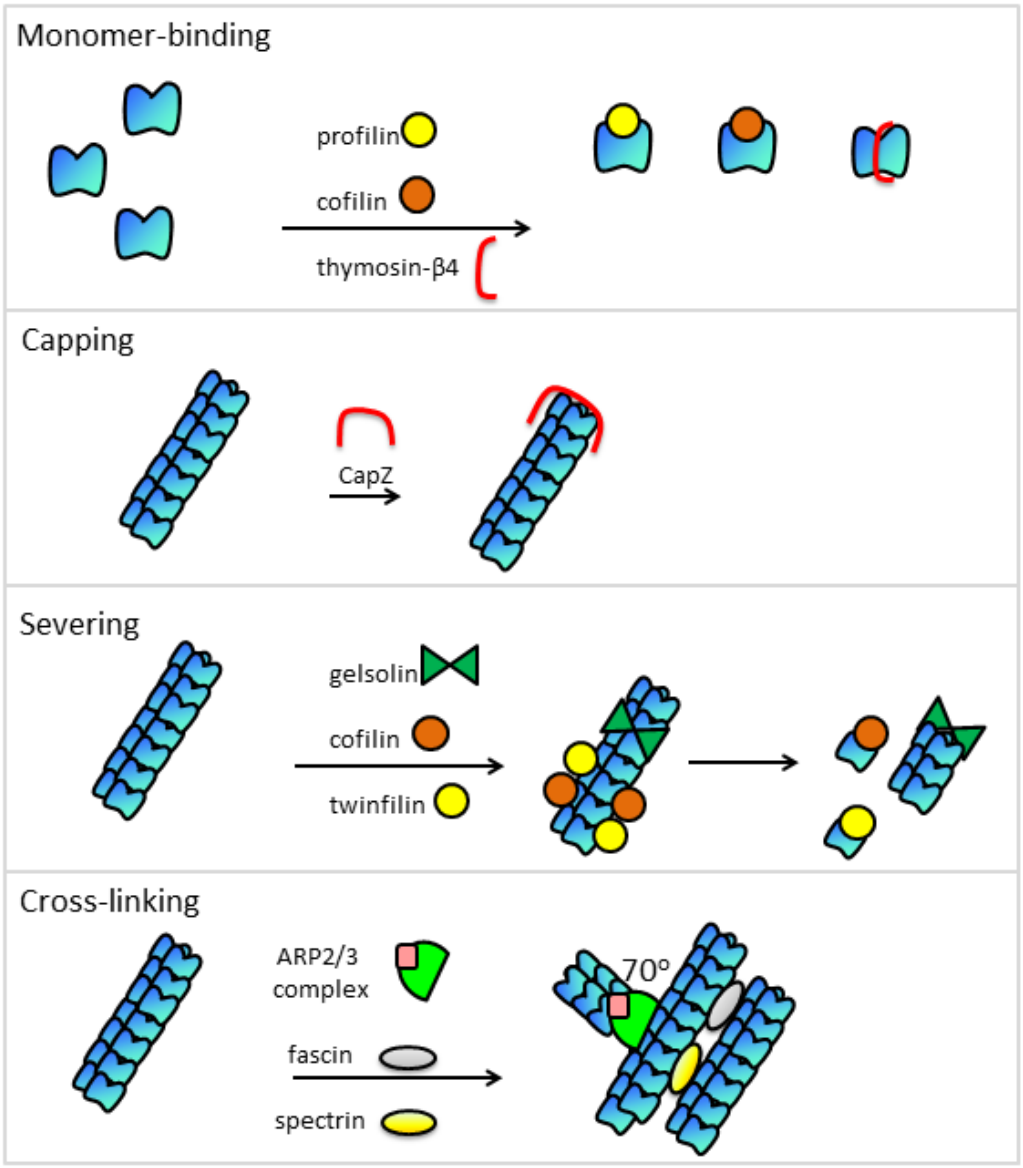


Figure 1.3 Schematic representation of monomer sequestration, capping, severing and cross-linking of actin by various actin-binding proteins. Diagram adapted from (Pollard & Cooper 2009).

1.6 Actin monomer-binding proteins

Under resting conditions, most of the G-actin in the cell is sequestered in the monomeric form in complex with actin monomer-binding proteins like profilin and β-thymosins (Tβ) (Weber et al. 1992). Actin monomer-binding proteins prevent spontaneous nucleation and polymerization.

1.6.1 β-thymosins

β-thymosins (Tβ), approximately 43 amino acids, are the most abundant actin monomer binding proteins in mammals. In certain cell types, like platelets that respond to external signals with increased motility, Tβ is present in concentrations greater than 300 μM (Safer et al. 1990). Tβ is often present at concentrations in excess of actin monomers (Weber et al. 1992). Tβ sequesters monomeric actin-ATP by preventing its addition to actin filaments through steric hindrance (Carlier et al. 1996), controlling the availability of actin monomers for incorporation into filaments. There are 15 highly homologous β-thymosin variants of which Tβ4 is ubiquitous and present in highest concentrations and is most studied. Tβ4 has a preferential affinity for ATP-actin and binds ATP actin (K_d = 0.5 μM) with a 50 fold higher affinity over ADP-actin (Carlier et al. 1993). Nucleotide exchange on G-actin is blocked by Tβ4 (Goldschmidt-Clermont et al. 1992) as Tβ4 binding closes the nucleotide-binding cleft of actin (De La Cruz et al. 2000). The crystal structure of a Tβ domain from Ciboulot in complex with actin and small molecule inhibitor Latrunculin A reveals that the N-terminal half of Tβ forms an amphipathic α-helix which binds to actin in the hydrophobic cleft between subdomains 1 and 3 (Hertzog et al. 2004) (**Fig. 1.4A**). The interaction of the C-terminal half of Tβ with actin is

revealed in the crystal structure of actin in complex with a hybrid protein made up of gelsolin domain 1 and the C-terminal half of Tβ4 (**Fig. 1.4B**). The C-terminal half of Tβ forms a capping helix which binds between actin subdomains 2 and 4 preventing the dynamic opening and closing of the two halves of actin, thus inhibiting nucleotide exchange (Irobi et al. 2004).

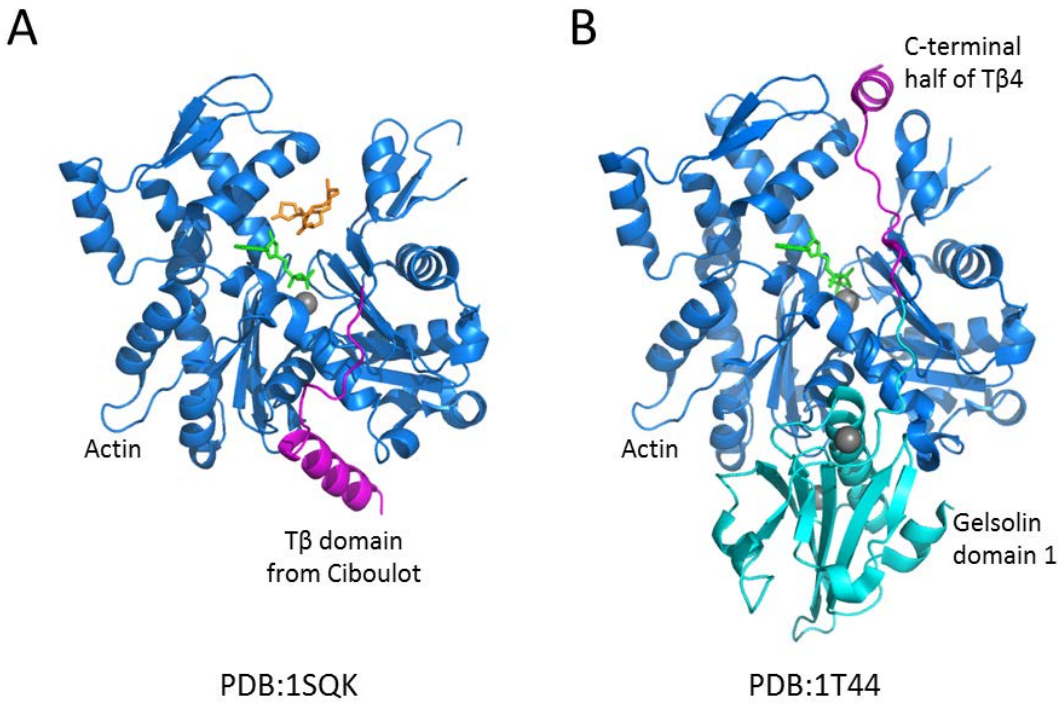


Figure 1.4 Crystal structures showing the interaction of Tβ with actin. (A) Crystal structure of Tβ domain from Ciboulot in complex with actin and small molecule inhibitor Latrunculin A. No density was observed for the C-terminal half of Tβ domain. Magnesium is shown as grey spheres, ADP as green sticks and Latrunculin A as orange sticks. (PDB: 1SQK (Hertzog et al. 2004) (B) Crystal structure of actin in complex with a hybrid protein between gelsolin domain 1 and the C-terminal half of Tβ4. Gelsolin domain 1 is shown in cyan, C-terminal half of Tβ4 shown in magenta, calcium shown as grey spheres and ATP as green sticks (PDB: 1T44 (Irobi et al. 2004)).

1.6.2 Profilin

Actin monomers arising from the disassembly of the pointed end of filaments are ADP-bound. However, ATP-bound G-actin is preferentially incorporated into the actin filament over ADP-bound G-actin. Profilin binds to actin and catalyzes the exchange of ADP for ATP, thus maintaining the pool of ATP-bound actin monomers (Perelroizen et al. 1996). The actin within profilin-actin crystal structures has been identified to adopt two different conformations: a closed conformation (Schutt et al. 1993) and an open conformation which promotes the exchange of the bound nucleotide (Chik et al. 1996) (**Fig. 1.5**). Profilin binds to and exchanges actin with Tβ, as such, Tβ together with profilin provide a reservoir of unpolymerized ATP-actin that can be readily de-sequestered for explosive filament growth following cell stimulus (Pantaloni & Carlier 1993). Profilin binds to the barbed end of actin monomers, inhibiting pointed end polymerization but can be added to barbed ends for filament elongation (Pollard & Cooper 1984; Chik et al. 1996). In fact, profilin serves as an adapter for recruitment by actin-binding proteins, like Ena/VASP and formins which contain proline-rich regions for recruiting profilin-actin which feeds the bound actin to the barbed ends for growth of filaments. The binding of phosphatidylinositol-4,5-bisphosphate (PIP_2) to profilin-actin results in the dissociation of the profilin-actin complex and polymerization of the actin monomers (Lassing & Lindberg 1985). Profilin serves as a negative regulator of the phosphoinositide-signaling pathway by binding to PIP_2 and inhibiting its hydrolysis by phospholipase C (PLC) (Goldschmidt-Clermont et al. 1990).

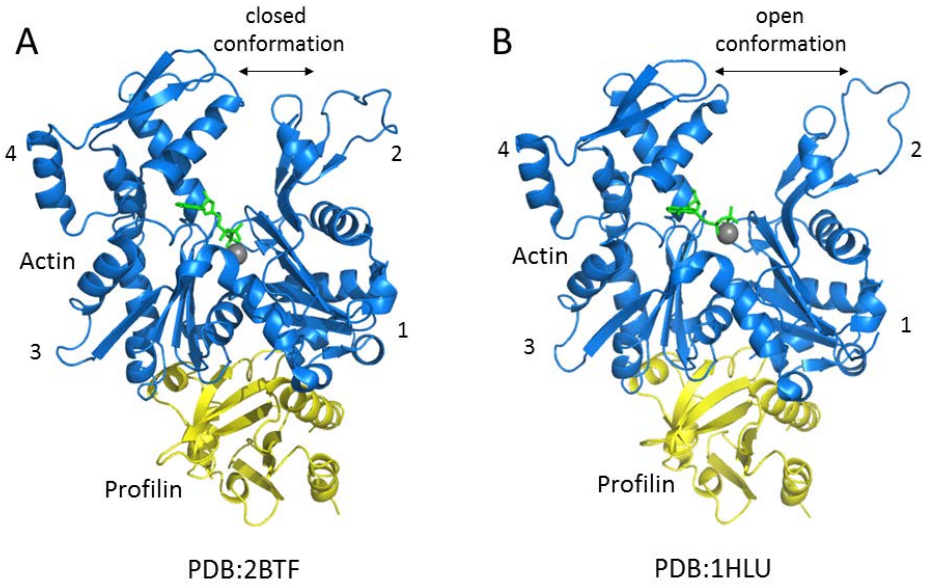


Figure 1.5 Crystal structures of the complex of profilin and β-actin. (A) Actin in the closed conformation (PDB: 2BTF (Schutt et al. 1993)). (B) Actin in the open conformation (Chik et al. 1996). Actin is shown in marine, profilin in yellow, calcium as grey spheres and ATP as green sticks.

1.7 Actin nucleators

The formation of a new filament from actin monomers requires the formation of an actin multimer via a process called nucleation. Spontaneous nucleation is kinetically unfavourable due to instability of the actin multimer intermediate, also known as the actin nucleus, as such nucleation forms the rate-limiting step in polymerization. *De novo* nucleation requires catalysis by actin nucleators which help to overcome inhibition to nucleation by profilin and β-thymosins, providing spatial and temporal control to polymerization, as well as influence the architecture of the actin networks that they generate. There are three main types of actin nucleators: the ARP2/3 complex, formins and WH2 domain-containing actin nucleators.

1.7.1 ARP2/3

ARP2/3 is a 220 kDa protein complex consisting of seven protein subunits - Actin-Related Protein ARP2, ARP3 and five additional subunits, ARPC1-5. It is the only known protein complex that performs nucleation and formation of Y-branched actin filament networks. ARP2/3 binds to a pre-existing actin filament and initiates the assembly of a new filament at a 70° angle from the side of the pre-existing filament and stays bound at the pointed end of the nascent filament (Mullins et al. 1998). By itself, the ARP2/3 complex has weak nucleating activity (Higgs 1999) and requires binding of ATP and nucleation promoting factors for activation (Goley et al. 2004). The crystal structure of inactive bovine ARP2/3 complex has been solved and ARP2 and ARP3 are similar in structure to the actin monomer (Robinson et al. 2001). The structure of the active complex has been studied with electron microscopy (Egile et al. 2005) and electron tomography (Rouiller et al. 2008) (**Fig.**

1.6). Together these reconstructions lead to the proposal that in the active structure, ARPC2 and ARPC4 mediate contacts with the parental filament and the barbed ends of ARP2 and ARP3 interact with the pointed end of the nascent filament (Gournier et al. 2001). As ARP2 and ARP3 are too distant to mimic a short pitch actin dimer in the inactive structure (Robinson et al. 2001), it is proposed that conformational change in the complex occurs upon activation. The conformational change would bring ARP2 and ARP3 subunits into a configuration that mimics the barbed end of an actin filament, and together with a G-actin bound to the verprolin (V) domain of nucleation promoting factors, form a trimeric template for the nucleation of a nascent filament branch that is at a 70° angle from the side of a pre-existing filament (Rouiller et al. 2008; Egile et al. 2005). Actin assembly of the ARP2/3 complex is greatly enhanced upon oligomerization of nucleation promoting factors (Padrick et al. 2008) and it has been shown that the ARP2/3 complex simultaneously binds two VCA (Verprolin-central-acidic domain) peptides in which each delivers an actin monomer (Padrick et al. 2011).

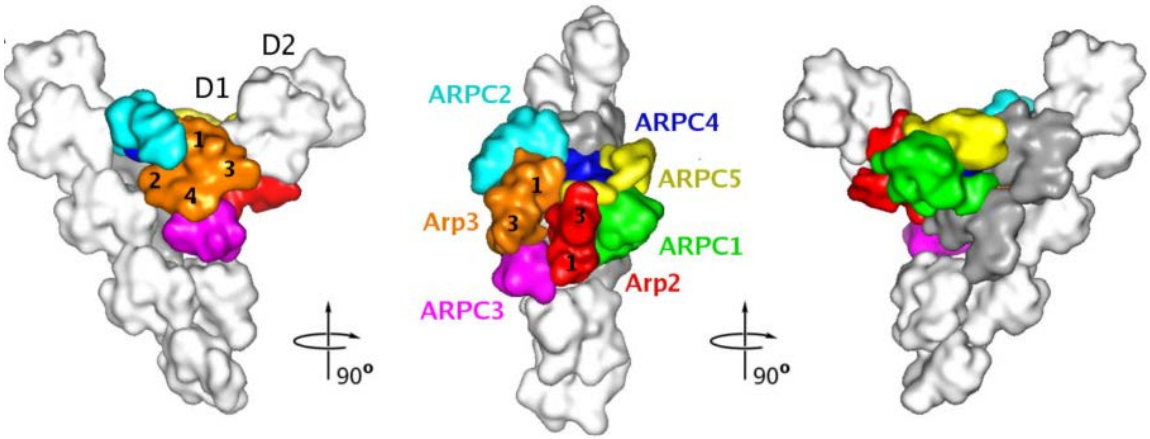


Figure 1.6 Model of the ARP2/3 actin filament branch junction. Model rotated by 90° clockwise for three different views. The first two actin subunits in the daughter filament are denoted D1 and D2. The subdomains 1 and 3 of ARP2 and ARP3 are indicated. Figure reproduced from (Isabelle Rouiller et al. 2008)

The ARP2/3 is localized to structures like lamellipodia and pseudopodia within several micrometers to the leading edge but is not observed in filopodia (Machesky et al. 1997). ARP2/3 functions as the dominant nucleator in driving leading-edge protrusion, in the formation of structures such as lamellipodia which predominantly contains branched actin networks (Svitkina & Borisy 1999). ARP2/3 localization within lamellopodia is closely correlated with lamellopodial dynamics. ARPC3 double knockout fibroblasts had a strong defect in persistent directional migration and exhibited loss of lamellipodia at leading edges which were instead dominated with filopodia, suggesting a role of ARP2/3 in lamellipodia assembly and directional migration (Suraneni et al. 2012). ARP2/3 is also important in mediating the actin polymerization needed for phagocytic cup formation and particle engulfment in both Fc-gamma receptor (FcγR) -mediated and complement receptor 3 (CR3) -mediated phagocytosis. ARP2/3 localizes to phagosomes in both phagocytic pathways (May et al. 2000).

1.7.1.1 Regulation of ARP2/3

ARP2/3 is activated by nucleation promoting factors (NPFs), which can be categorised into two subclasses. Type I NPFs possess a VCA domain which consists of a verprolin homology (V) domain, also known as a Wiskott-Aldrich syndrome homology region 2 domain (WH2), the central (C) domain and the acidic (A) region. The WH2 motif binds G-actin while the A region binds and activates ARP2/3. Type I NPFs include Wiskott-Aldrich syndrome protein (WASP), WASP family verprolin-homologous protein (WAVE, also known as SCAR), neural WASP (NWASP), WASP and SCAR homologue (WASH) and junction-mediating and regulatory protein (JMY). Type II NPFs contain acidic domains that bind the ARP2/3 complex but do not contain a G-actin-binding region, and bind to F-actin instead, via tandem repeat domains. Type II NPFs include metazoan cortactin (Uruno et al. 2001), *S. cerevisiae* actin-binding protein-1 (Abp1) (Goode et al. 2001) and Pan1 (Duncan et al. 2001). Recently, negative regulators of ARP2/3 have been discovered, including glia maturation factor (GMF) (Nakano et al. 2010), coronin 1B (Cai et al. 2008), gadkin (Maritzen et al. 2012) and protein interacting with C kinase 1 (PICK1) (Rocca et al. 2008). *In vitro*, GMF directly interacts with ARP2/3 and reduces its actin nucleation activity in a dose-dependent manner (Nakano et al. 2010), and has been found to bind the barbed end of ARP2, overlapping with the binding site of NPFs (Luan & Nolen 2013). PICK1 and Gadkin both contain acidic regions, competing for the same site on ARP2/3 that binds to the acidic region of NPFs but do not activate the nucleation activity of ARP2/3. Coronin 1B induces dissociation of ARP2/3 from actin filament branches, causing the disassembly of branches, driving the turnover of branched actin networks (Cai et al. 2008).

1.7.1.2 Type I nucleation promoting factor WASP

NWASP is ubiquitously expressed although first discovered to be expressed predominantly in the brain (Miki & Miura 1996) while WASP is expressed only in haematopoietic cells (Stewart et al. 1996). Mutations in WASP are associated with two diseases which are associated with severe congenital immune defects: the Wiskott-Aldrich syndrome and X-linked neutropenia. The former results from loss-of-function mutations of the WASP gene (Imai et al. 2004) while the latter results from mutations that confer constitutive activation of WASP (Devriendt et al. 2001). WASP-deficient peripheral blood monocytes exhibit impaired FcγR-mediated phagocytosis (Lorenzi et al. 2000). These suggest the importance of WASP in cytoskeletal regulation in haematopoietic cells.

WASP and NWASP possess an N-terminal WASP homology domain 1 (WH1), also called an Ena-VASP homology domain 1 (EVH1), a central GTPase-binding domain (GBD), a poly-proline region and a C-terminal VCA (verprolin-central-acidic) domain (**Fig. 1.7**). The interaction of the verprolin domain, also known as the WH2 domain, with actin has been elucidated for WASP and WAVE. The WH2 domains bind actin on the hydrophobic cleft between subdomains 1 and 3 (Chereau et al. 2005) (**Fig. 1.8**). WASP and NWASP exist as a complex with WASP-interacting protein (WIP) family proteins via the interaction of the C- terminus of WIP with the WH1 domain (Ramesh et al. 1997). WASP and NWASP are autoinhibited, in which the VCA domain for binding ARP2/3 is masked (Rohatgi et al. 2000). Autoinhibition is released by Cdc42 and/or PIP_2 binding (Prehoda 2000). Via the proline-rich regions, WASP and NWASP interact with profilin-actin and SH3 domain containing adaptor proteins like Grb2 (Carlier et al. 2000) and Nck

(Rohatgi et al. 2001).

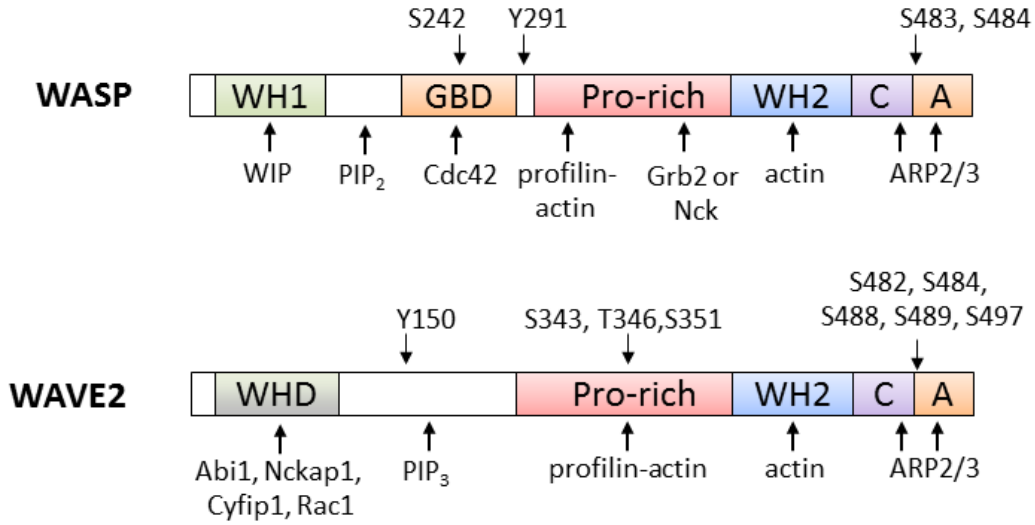


Figure 1.7 Schematics of WASP and WAVE2 domain organization. The domain nomenclature denotes WASP homology domain 1 (WH1), GTPase-binding domain (GBD), proline-rich region (Pro-rich), WASP homology domain 2 (WH2), central domain (C), acidic domain (A) and WAVE homology domain (WHD). Relevant binding partners are shown below each domain. Reported phosphorylation sites are indicated. The schematics are not drawn to scale.

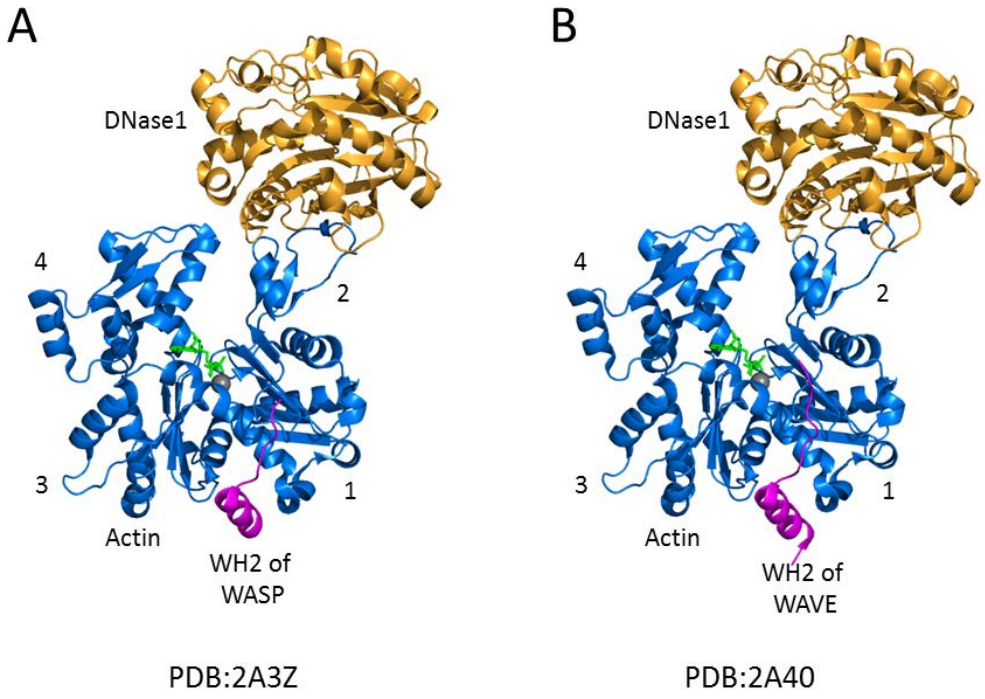


Figure 1.8 Crystal structures of ternary complexes of the WH2 domains with actin-DNase1. (A) WH2 domain from WASP. (PDB: 2A3Z (Chereau et al. 2005)) (B) WH2 domain from WAVE (PDB: 2A40 (Chereau et al. 2005). Actin is shown in marine, DNase1 in orange, WH2 domains in magenta, calcium as grey spheres and ATP as green sticks.

1.7.1.3 Regulation of WASP by phosphorylation

Endogenous WASP and NWASP are found to be phosphorylated (Cory et al. 2003). WASP and NWASP are regulated by phosphorylation by a number of kinases: tyrosine kinases Btk and FAK, serine/threonine kinase CK2 and dual specificity kinase ACK1. Phosphorylation by these kinases activates WASP and NWASP and influences their subcellular localization. Phosphorylation also enhances association with ARP2/3 and/or the ability to activate the ARP2/3 complex. Bruton's tyrosine kinase Btk transiently phosphorylates WASP on Tyr291 during B-lymphocyte development (Baba et al. 1999). Casein kinase 2 (CK2) phosphorylates WASP in its VCA domain, between the V and A regions on Ser483 and Ser484. The resultant CK2-phosphorylated VCA domain has an increased affinity for the ARP2/3 complex and enhances actin polymerization (Cory et al. 2003). Cdc42-associated kinase ACK1 activates WASP via phosphorylation on Ser242 and Tyr256, of which phosphorylation of Ser242 has been confirmed to enhance ability to activate the ARP2/3 (Yokoyama et al. 2005). NWASP is phosphorylated by focal adhesion kinase FAK Tyr256. Phosphorylation at Tyr256 slightly enhances the ability of NWASP to activate the ARP2/3 and inhibits nuclear translocation of NWASP by reducing its interaction with nuclear importin NPI-1 (Wu et al. 2004).

1.7.1.4 Type I nucleation promoting factor WAVE

WAVE does not contain a WH1 domain but instead contains a WAVE homology domain (WHD), also known as a SCAR homology domain (SHD). WAVE exists in a pentameric complex with Cyfip1, Nap, Abi1 and Brk1. The WAVE complex is autoinhibited with the VCA domain masked by the Cyfip1/Nap subcomplex (Ismail et al. 2009). WAVE1 is predominantly expressed in the brain, while WAVE2 is ubiquitously expressed (Suetsugu et al. 1999). The WAVE complex is regulated by Rac which binds to the Cyfip1 subunit of WAVE (Kobayashi et al. 1998). IRSp53, through its SH3 domain, forms a complex with WAVE2 and recruits it to the membrane, and mediates the interaction of WAVE2 with PIP_3 (Oikawa et al. 2004; Suetsugu et al. 2006; Takahashi & Suzuki 2010).

1.7.1.5 Regulation of WAVE by phosphorylation

Endogenous WAVE is reported to be constitutively phosphorylated in fibroblasts (Pocha & Cory 2009) and has been reported to be regulated by multiple kinases in a variety of cell lines. Abl and Src directly phosphorylate WAVE, promoting the activation of the WAVE complex leading to recruitment to the cell membrane and activation of the ARP2/3 complex, while MAP kinase ERK, cyclin-dependent kinase 5 (Cdk5) and casein kinase 2 (CK2) phosphorylate and inhibit the activation of the WAVE complex. Phosphorylation of WAVE2 by Abl promotes localization to the cell edge and specifically, the phosphorylation on Tyr150 increases the ability of the VCA region to activate ARP2/3 (Leng et al. 2005). Phosphorylation of WAVE1 at Tyr125 within the WAVE/Scar homology domain (WHD) by Src results in increased affinity for the ARP2/3 complex (Ardern et al.

2006). WAVE2 can be phosphorylated by MAP kinases ERK and JNK (Danson et al. 2007). ERK phosphorylates Ser482 and Ser484 within the VCA region, resulting in higher affinity for the ARP2/3 complex but exhibits reduced induction of ARP2/3-mediated actin polymerization *in vitro* (Nakanishi et al. 2007). JNK phosphorylates WAVE2 on Ser343, Thr346 and Ser351 (Danson et al. 2007). Phosphorylation at these sites has no effect on the ability of WAVE2 to activate ARP2/3 but leads to faster cell migration speeds of fibroblasts, with a decrease in persistence of direction of migration (Danson et al. 2007). In mouse neurons, cyclin-dependent kinase 5 (Cdk5) phosphorylates WAVE1 at three sites (Ser310, Ser397 and Ser441) and inhibits WAVE1 from activating ARP2/3-dependent actin polymerization (Kim et al. 2006). The phosphorylation of WAVE1 by Cdk5 is in turn regulated by Cdk1. Cdk1 phosphorylates Abi1 resulting in the attenuation of phosphorylation of WAVE within the WAVE complex (Zhuang et al. 2011). CK2 phosphorylates WAVE2 at five sites (serines 482, 484, 488, 489, and 497) within the VCA domain, causing an increase in affinity for ARP2/3 of which phosphorylation of Ser482 and 484 inhibits the activation of ARP2/3 by WAVE (Pocha & Cory 2009).

1.7.1.6 WASP interacting protein WIP

WASP and NWASP exist as a complex with WASP-interacting protein (WIP) family proteins, which includes WIP, CR16 and WICH/WIRE. WIP is ubiquitously expressed but is more abundant in hematopoietic tissues (Ramesh et al. 1997), while CR16 and WICH/WIRE are predominantly brain-expressed (Ho et al. 2001). WIP family proteins contain an N-terminal verprolin domain which contains two WH2 domains which bind actin directly and a WASP binding site at the C-terminus (**Fig. 1.9**). Exclusively to WIP, the central region contains multiple proline-rich sequences which have been shown to interact with cortactin or actin-binding protein (Abp1) at one site and the adaptors Nck or CrkL at another site. WIP is the most studied member and is found to localize in actin-rich structures like lamellipodia, stress fibres and at the base of filopodia (Martinez-quiles et al. 2001; Vetterkind et al. 2002). WIP exists as a complex with WASP by binding to the WH1 domain of WASP. The interaction of WIP with cortactin is involved in the regulation of activity of ARP2/3 (Kinley et al. 2003). WIP binding promotes WASP stability and confers protection from degradation (De la Fuente et al. 2007). WIP regulates WASP activity, promotes its inactive conformation, inhibiting Cdc42-induced activation of WASP (Martinez-quiles et al. 2001) and is involved in WASP recruitment to specific subcellular locations (Chou et al. 2006). Overexpression of WIP in fibroblasts increases the amount of polymerized actin and filopodial projections on the cell surface (Martinez-quiles et al. 2001). The WIP-WASP complex is released by TOCA-1 (also known as formin-binding protein 1-like, Fnbp1l) which binds both Cdc42 and WASP (Ho et al. 2004). WIP is phosphorylated by PKCdelta at Ser488, near the C-terminal end of WIP (Sasahara et al. 2002).

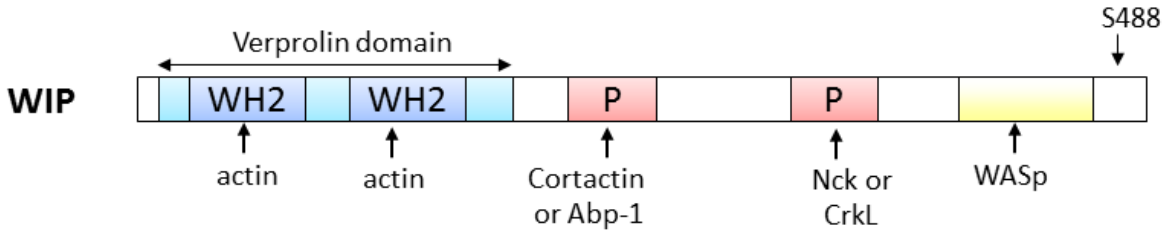


Figure 1.9 Schematic of WIP domain organization. The verprolin homology domain includes two WASP homology 2 (WH2) domains. P denotes proline-rich region. Relevant binding partners are shown above each domain. The reported phosphorylation site is indicated. The schematic is not drawn to scale.

1.7.2 Formins

Formins perform *de novo* nucleation of actin filaments as well as elongation of existing filaments, assembling unbranched actin filaments. Formins are characterised by the presence of three formin homology FH domains (FH1, FH2 and FH3) (**Fig. 1.10**). FH1 is proline-rich and its predominant function is to bind profilin. The FH2 domain exists as a donut-shaped homodimer as revealed in the crystal structure of FH2 domain and actin (Otomo et al. 2005) (**Fig. 1.11**) and catalyzes actin filament nucleation by stabilizing actin dimers (Pring et al. 2003). The FH2 dimer stays attached to the barbed end of an actin filament, processively executing a stair-stepping mechanism as the filament elongates and preventing barbed end capping (Zigmond et al. 2003) while the adjacent FH1 domain delivers profilin-actin to the barbed end (Romero et al. 2004). The FH3 domain located N-terminal to the catalytic FH1–FH2 is less well conserved and functions to bind the C-terminal diaphanous-autoregulatory domain (DAD) in the autoinhibited state (Li & Higgs 2005; Alberts 2001). Binding of GTP-bound Rho GTPases to the GTPase-binding site regulates membrane localization of formins (Seth et al. 2006) and releases the formin from its autoinhibited state to turn on the actin assembly activity (Watanabe et al. 1997).

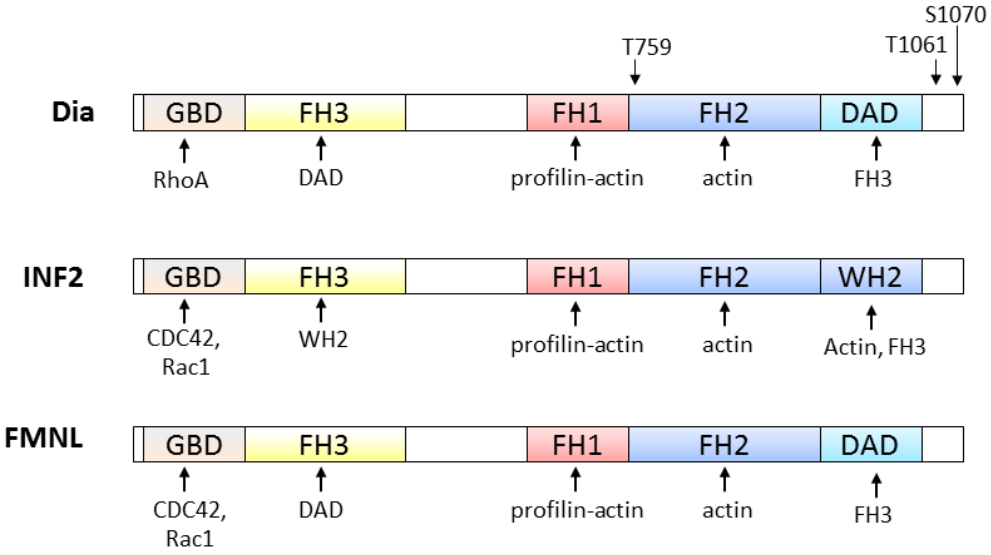


Figure 1.10 Schematics of domain organization for formin diaphanous (Dia), inverted formin 2 (INF2) and formin-like protein (FMNL). The domain nomenclature denotes the formin homology 1 (FH1), 2 (FH2) and 3 (FH3) domains, the GTPase-binding domain (GBD), the C-terminal diaphanous autoregulatory domain (DAD), WASP homology 2 (WH2) actin-binding domain. Relevant binding partners are shown below each domain. Reported phosphorylation sites for Dia (as a compilation of Dia1 and Dia2) are indicated. The schematics are not drawn to scale. Figure adapted from (Schönichen & Geyer 2010).

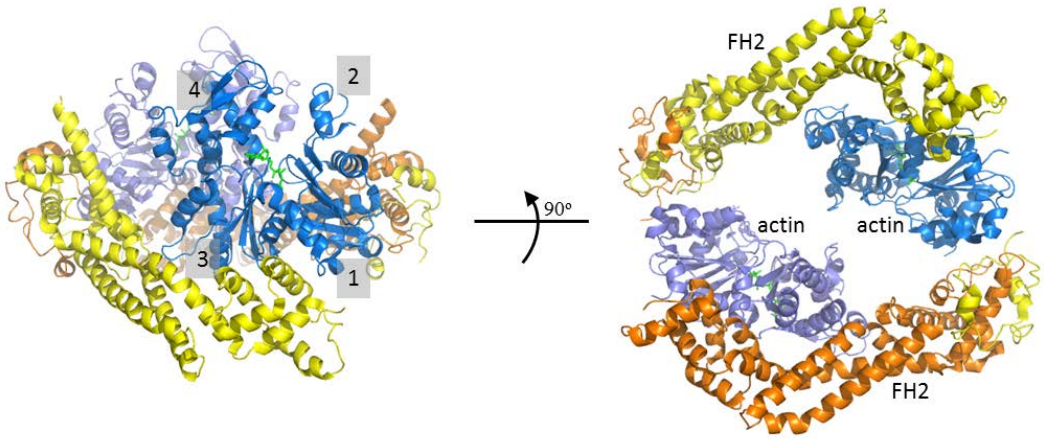


Figure 1.11 Crystal structure of FMNL3 FH2 domain bound to tetra-rhodamine- conjugated actin. FMNL3 FH2–actin with an FH2 dimer (yellow and orange) bound to two actin subunits (marine and light blue). Left panel, actin subdomains are numbered. Right panel, barbed end of actin points out of paper. (PDB: 4EAH (Thompson et al. 2013))

To date, fifteen formins have been identified in *homo sapiens* and they can be grouped into eight different families – diaphanous (Dia), disheveled-associated activator of morphogenesis (DAAM), formin-like protein (FMNL), WH2 domain-containing formin 1 (WHIF1/INF2), Inverted formin (INF1), FH1/FH2 domain-containing protein (FHOD), delphilin and formin (FMN).

Dia was the first formin to be discovered, and had been most extensively studied. Mouse diaphanous mDia links actin polymerization to transcriptional activation of serum response factor. mDia induced actin assembly promotes the release of actin from megakaryocytic acute leukemia protein (MAL) leading to nuclear accumulation of MAL which in turn activates transcriptional activity of serum response factor (SRF) (Baarlink et al. 2013). Cytoskeletal scaffold protein IQGAP1 directly binds and recruits Rho-activated mDia1 via the DAD domain to phagocytic cups during phagocytosis (Brandt et al. 2007). Microtubule-binding protein CLIP-170 appears to be implicated in the recruitment of formin mDia1 to phagocytic cups during CR3-mediated phagocytosis (Lewkowicz et al. 2008). Rho-activated mDia2 has been found to co-localize with microtubules when overexpressed (Palazzo et al. 2001) and *in vitro*, can stabilize microtubules independently of its ability to nucleate actin or dimerize (Bartolini et al. 2008), suggesting its role in regulating the dynamics of microtubule ends.

INF2 is localized at the cytoplasmic face of the endoplasmic reticulum (Chhabra et al. 2009). INF2 associates with Cdc42 and Rac1 and is involved in vesicular transport (Madrid et al. 2010). Unlike other formins, it contains a WH2 domain in place of the DAD domain (Chhabra & Higgs 2006). The WH2 domain

binds to actin monomers and also binds the FH3 domain like DAD. *In vitro*, an INF2 construct containing the FH2 and WH2 domain has a biphasic effect on actin polymerization, in which INF2 induced accelerated polymerization is followed by accelerated depolymerisation. Accelerated depolymerisation is not observed in constructs of INF2 that lack the WH2 domain (Chhabra & Higgs 2006).

FMNL previously known as formin-related gene in leukocytes (FRL) is strongly expressed in spleen, lymph node and haematopoietic cells (Yayoshi-Yamamoto et al. 2000). It is activated from the autoinhibited state by Cdc42 (Seth et al. 2006) and Rac (Yayoshi-Yamamoto et al. 2000). FMNL2 accumulates at lamellipodia and filopodia tips and influences the rate of lamellipodia protrusion (Block et al. 2012).

1.7.2.1 Regulation of formins by phosphorylation

Dia1 is phosphorylated at Thr759 following Dibutyryl cAMP stimulation, via an ERK-dependent pathway. Thr759 lies in the FH2 domain and non-phosphorylatable mutant T759A is more stable with attenuated interaction with actin (Li et al. 2013). Thr759 is also identified to be phosphorylated by Cdk1 in the corresponding position (Thr747) in diaphanous-related formins (DRF) (Blethrow et al. 2008). Dia2 is phosphorylated by ROCK (Rho-kinase) at two conserved residues (Thr1061 and Ser1070) which lie C-terminal to the DAD region. Phosphomimetic mutations inhibited the ability of DAD to interact with diaphanous inhibitory domain DID, enhancing Dia2 activation by RhoA, leading to increased actin polymerization and SRF-dependent gene transcription (Staus et al. 2011). ROCK phosphorylates formin homology domain protein 1 (FHOD1) on residues Ser1131, Ser1137 and Thr1141 in the poly-basic region within the DAD domain, leading to the disruption of autoinhibition and inducing actin stress fibre formation (Takeya et al. 2008).

1.7.3 Tandem WH2 nucleators

Tandem WH2 nucleators form the largest group of actin filament nucleators. These contain two or more WH2 domains in tandem, each binding a G-actin, bringing together monomers to form a nucleus for polymerization (**Fig. 1.12**). Tandem WH2 proteins like Spire, Vibrio outer proteins VopF and VopL stabilize actin monomers aligned along the longitudinal axis of an actin filament to form a single stranded long pitch multimer nucleus (Quinlan et al. 2005; Zuchero et al. 2009) while other proteins like cordon bleu stabilize cross-filament interactions to form a short pitch trimer nucleus (Ahuja et al. 2007; Namgoong et al. 2011). Like formins, tandem WH2 nucleators nucleate unbranched filaments, but stay bound at the pointed end of nascent filaments like the ARP2/3 complex. Many of these tandem WH2 nucleators are aided by additional actin-binding elements.

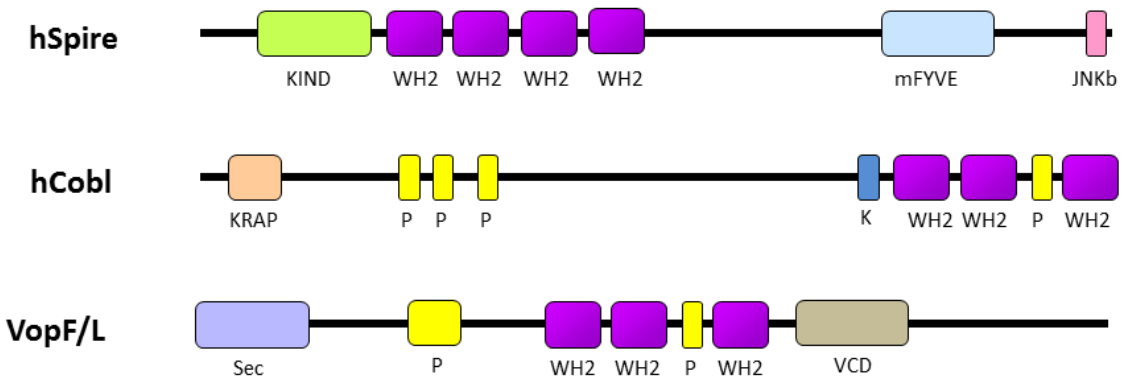


Figure 1.12 Schematics of domain organization for tandem WH2 nucleators including human spire, human cordon bleu, Vibrio outer proteins VopF and VopL. The domain nomenclature denotes kinase noncatalytic C-lobe domain (KIND), Wiskott-Aldrich-homology 2 domain (WH2), modified FYVE zinc-finger domain (mFYVE), JNK-binding domain (JNKb), lysine-, arginine-, and proline-rich (KRAP) motifs, proline-rich motif (P), lysine-rich region (K), type II secretion/translocation signal (Sec), Vop C-terminal dimerization domain (VCD). The schematics are not drawn to scale.

Spire exists in two isoforms in mammals - Spire1 and Spire2 are expressed only in the developing nervous system and the adult brain (Schumacher et al. 2004) in mice. Spire contains a kinase non-catalytic C-lobe domain (KIND) N-terminal of its four tandem WH2 domains followed by a modified FYVE zinc-finger (mFYVE) domain and a JNK-binding domain (JNKb). The KIND domain mediates interaction with the formin cappuccino (drosophila homolog of human FMN2). Each of the four WH2 domains binds to one actin monomer (Quinlan et al. 2005). The four WH2 domains of Spire are only weakly nucleating and requires interaction of the KIND domain with the FH2 domain of formin cappucino for enhanced actin nucleation (Quinlan et al. 2007). Spire binds to the pointed end of the filament and protects it from depolymerization (Quinlan et al., 2005). While Spire has been confirmed to contribute to actin nucleation, there is debate on how this is achieved (Carlier et al. 2011).

Cordon bleu (Cobl) is a brain-enriched actin nucleator containing three tandem WH2 domains (Ahuja et al. 2007). Cobl accumulates largely in axonal and dendritic growth cones that are also enriched with F-actin (Ahuja et al. 2007). Overexpression of Cobl or the WH2 containing C-terminus induces increased neurite formation and branching suggesting a role of Cobl in modulating cell morphology of neurons via effects on actin polymerization. The C-terminus of Cobl contains three WH2 domains which are arranged such that the first two WH2 domains are closely spaced while the second and the third WH2 are considerably further apart, giving rise to the hypothesis that Cobl assembles a trimeric cross-filament nucleus (Ahuja et al. 2007). Immediately N-terminal to the first WH2 domain, is a 14 residue highly

conserved lysine-rich sequence termed the K region, without which, the nucleation activity of the three WH2 domains is lost (Husson et al. 2011).

1.8 Filament elongators

Formins and Ena/VASP proteins are the only proteins discovered to date that interact with growing filament barbed ends and recruit monomeric actin for directly enhancing filament elongation, yet are not nucleators.

1.8.1 Ena/VASP proteins

Members of Ena/VASP proteins include vasodilator-stimulated phosphoprotein VASP, drosophila protein enabled (Ena), its mammalian orthologue Mena, and the Ena/VASP-like protein EVL. VASP is expressed in a wide variety of cells, with the highest levels of expression in platelets (Reinhard et al. 1992). Mena is abundantly expressed in the brain while EVL is highly expressed in haematopoietic cells (Gambaryan et al. 2001). Ena/VASP family members are concentrated at focal adhesions (Reinhard et al. 1992), actin stress fibres (Bachmann et al. 1999), the distal rim of the lamellipodial leading edge and the tips of filopodia in migratory cells (Applewhite et al. 2007). Ena/VASP proteins contain an N-terminal Ena/VASP homology domain 1 (EVH1, also known as WH1), a central proline-rich region and a C-terminal EVH2 domain (**Fig. 1.13**). The EVH1 domain binds to proline-rich ligands (Carl et al. 1999) such as lamellipodia/filopodia protein lamellipodin (Krause et al. 2004), axon guidance receptor Robo (Bashaw et al. 2000), semaphorin 6A-1 (Klostermann et al. 2000), focal adhesion proteins zyxin and vinculin and *Listeria* surface protein ActA (Niebuhr et al. 1997). The proline-rich region binds to profilin, as well as to SH3- and WW-domain-containing proteins (Lambrechts et al. 2000). The EVH2 domain contains a G-actin-binding site, an F-actin-binding site and a coiled-coil region that mediates the tetramerization of Ena/VASP (Bachmann et al.

1999). Ena/VASP binds G-actin via two interfaces, using its proline-rich region to recruit profilin-actin, and using EVH2 to bind G-actin directly. The crystal structure of the ternary complex of proline-rich region and the G-actin-binding region of VASP in interaction with actin and profilin has been solved (**Fig. 1.14**). The G-actin-binding region of VASP interacts with actin similarly to WH2 domains, binding on the hydrophobic cleft between subdomains 1 and 3. Ena/VASP associates with barbed ends of actin filaments and prevents filament capping by capping protein (Applewhite et al. 2007). Ena/VASP promotes clustering of filaments at their polymerizing ends and performs filament elongation for the formation and assembly of long filaments for structures such as filopodia (Bear et al. 2002). Ena/VASP has been demonstrated to be important for formation and elongation of filopodia for neuritogenesis (Lebrand et al. 2004). Ena/VASP reduces filament branching possibly by protecting the sides of the growing ends of filaments from interaction with the ARP2/3 complex (Boujemaa-Paterski et al. 2001). Ena/VASP is not a *bona fide* nucleator. It displays nucleation activity only at low salt concentrations but at physiological salt conditions, nucleation activity becomes negligible, leading to the conclusion that its nucleation activity has no relevance *in vivo* (Barzik et al. 2005). VASP is hijacked for actin-based motility of pathogen *Listeria monocytogenes* along with ARP2/3 (Skoble et al. 2001).

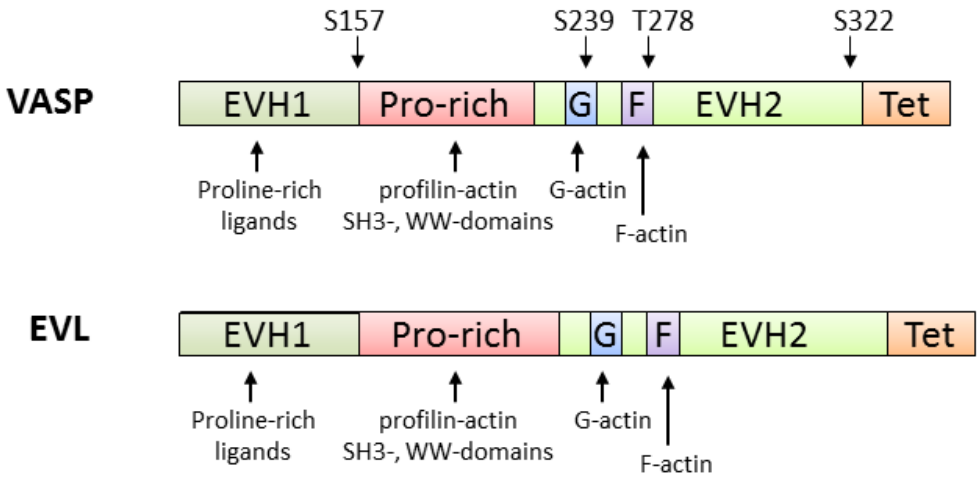


Figure 1.13 Schematics of domain organization for vasodilator-stimulated phosphoprotein VASP and Ena/VASP-like (EVL) protein. The domain nomenclature denotes Ena/VASP homology domain 1 (EVH1 also known as WH1), proline-rich region (Pro-rich) and a Ena/VASP homology domain 2 (EVH2) that contains a G-actin-binding site (G), an F-actin-binding site (F) and a tetramerization (Tet) domain. Relevant binding partners are shown below each domain and reported phosphorylation sites are indicated. The schematics are not drawn to scale.

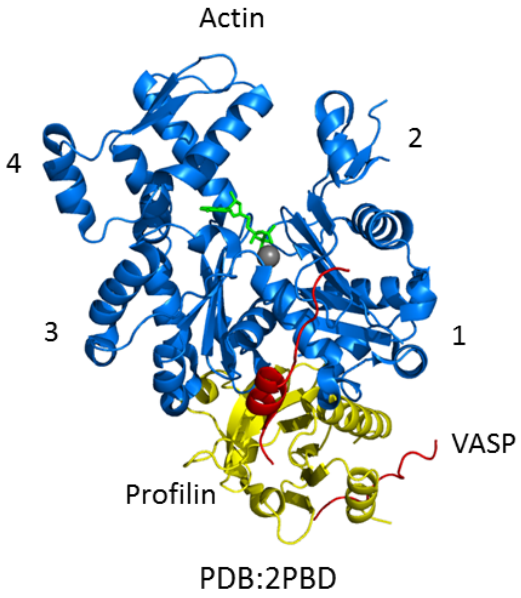


Figure 1.14 Crystal structure of complex of profilin, actin with a construct of VASP containing a part of the proline-rich region and G-actin-binding site. Actin is shown in marine, profilin in yellow, VASP in red, calcium as grey spheres and ATP as green sticks. PDB: 2PBD (Ferron et al. 2007)

1.8.2 Regulation of Ena/VASP proteins by phosphorylation

Ena/VASP is regulated by a number of kinases which include cAMP-dependent protein kinase (PKA), cGMP-dependent protein kinase (PKG), protein kinase C (PKC), AMP-activated protein kinase (AMPK) and protein kinase D1 (PKD1). Known phosphorylation sites in VASP are residues Ser157, Ser239, Thr278 and Ser322. PKA and PKG mediate phosphorylation of Ser157, Ser239 and Thr278 (Butt et al. 1994); AMPK phosphorylates Thr278 (Blume et al. 2007); PKC phosphorylates Ser157 (Wentworth et al. 2006) and PKD1 mediates phosphorylation of Ser157 and Ser322. Collectively, phosphorylation at Ser157, Ser239 and Thr278 reduces VASP's ability to enhance the rate of actin polymerization compared to wild type VASP (Harbeck et al. 2000; Doeppler et al. 2013). Ser157 within the PRD domain of VASP is a common phosphorylation site for PKA, PKG, PKC and PKD. Ser157 phosphorylation abolishes the interaction of VASP with actin and the SH3 domains of Abl, Src and spectrin and promotes localization of VASP to focal adhesions and the plasma membrane (Benz et al. 2008). PKD1 directly phosphorylates VASP at two serine residues, Ser157 and Ser322, and mediates VASP re-localization from focal adhesions to the leading edge, inducing an increase in F-actin polymerization, lamellipodia and filopodia formation (Doeppler et al. 2013). Ena/VASP family protein EVL is also a substrate of PKA. Similar to VASP, phosphorylation by PKA on Ser156 within the proline-rich region resulted in a decrease of actin nucleating activity and abolished the binding of SH3 domains from Abl and Src (Lambrechts et al. 2000).

1.9 Capping proteins

Upon filament nucleation and elongation, each filament grows until capping proteins (such as CapZ) bind and terminate growth, regulating filament length for optimal force generation (Wear & Cooper 2004).

1.9.1 CapZ

CapZ, also known as heterodimeric capping protein, is a heterodimer consisting of α- and β- subunits. In yeast, the CapZ protein colocalizes with cortical actin at the site of budding and at the tips of growing buds and does not colocalize with actin cables or actin rings at cytokinesis sites (Amatruda & Cooper 1992). In chicken epithelial cells, CapZ localizes at cell-cell junctional complexes (Schafer et al. 1992). CapZ binds to the barbed end of an actin filament, preventing the addition or loss of actin monomers at that end (Wear et al. 2003). The crystal structure (Yamashita et al. 2003) together with biochemical data suggest that CapZ adopts a mushroom-shaped structure with the C-termini of both the α- and β- subunits as extended amphipathic α-helices. These are termed the α- and β- tentacles respectively and are key to binding actin (Kim et al. 2004). These mask the barbed ends of both of the terminal actin protomers when CapZ is bound to the filament, blocking barbed end polymerization (Yamashita et al. 2003). The activity of CapZ is regulated by PIP_2, myotrophin (V-1) and CARMIL. PIP_2 inhibits free CapZ's ability to affect actin polymerization (Heiss & Cooper 1999) and dissociates CapZ bound to actin barbed ends *in vitro* (Schafer et al. 1996). Upon signal transduction, PIP_2 removes CapZ from filaments, resulting in localized regions with increased numbers of free barbed ends, allowing for a sudden surge in localized actin polymerization. V-

1 prevents free CapZ from interacting with the barbed end (Taoka et al. 2003), while CARMIL proteins act on the barbed end-bound CapZ and facilitate its dissociation from the filament (Jung et al. 2001). CapZ interacts with twinfilin, regulating twinfilin's localization to actin patches and inhibits the severing activity of twinfilin (Palmgren et al. 2001; Moseley et al. 2006).

1.10 Severing and depolymerising proteins

As G-actin is incorporated into a filament, the bound ATP undergoes hydrolysis into ADP and inorganic phosphate (Pi) (Belmont et al. 1999; Sablin et al. 2002). The release of Pi from filaments after ATP hydrolysis favours depolymerization and severing by proteins like gelsolin, cofilin and twinfilin. They serve to take apart filaments, and together with proteins like cyclase adenylase associated protein (srv2/CAP), recycle actin subunits during cell movement (Dos Remedios et al. 2003; Paavilainen et al. 2004). Actin turnover is essential in persistent cell migration.

1.10.1 Gelsolin family of proteins

The gelsolin superfamily of proteins include gelsolin, CapG, adseverin, flightless 1, advillin, villin, villin-like protein and supervillin. Gelsolin is the most studied member of this superfamily and is composed of six repeating homologous domains named G1-6 (**Fig. 1.15**). All members of this superfamily contain three or more of gelsolin homology domains. Gelsolin binds actin directly and has been shown *in vitro* to sever, cap, uncap, and nucleate actin filaments contributing to actin assembly and filament remodelling (Janmey et al. 1985).

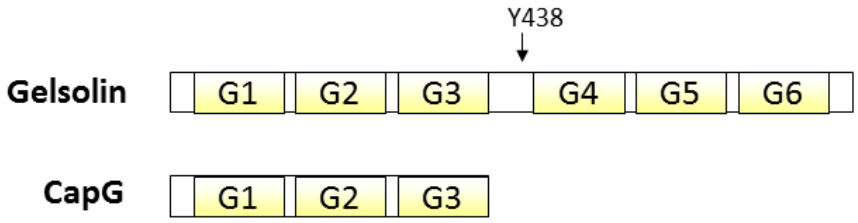


Figure 1.15 Schematics of domain organization for gelsolin and CapG. The domain nomenclature denotes gelsolin domains 1 (G1), 2 (G2), 3(G3), 4(G4), 5(G5) and 6(G6). The reported phosphorylation site on gelsolin is indicated. The schematics are not drawn to scale.

1.10.2 Gelsolin

Gelsolin exists in the blood plasma and in the cytoplasm. Plasma (85kDa) and cytoplasmic gelsolin (80 kDa) are identical in amino acid sequence, except that plasma gelsolin contains a 51-residue N-terminal extension, of which the first 27 residues constitute a signal peptide (Kwiatkowski et al. 1986). Cytoplasmic gelsolin is ubiquitiously expressed (Lueck et al. 1998; Yin et al. 1981) but expression levels vary during cell differentiation (Kwiatkowski 1988) and in carcinogenesis (Tanaka et al. 1995). Gelsolin-null mice have multiple defects in morphology and motility in various cell types including neutrophils, platelets, osteoclasts, and dermal fibroblasts (Witke et al. 1995). Gelsolin is involved in Fc-gamma receptor (FcγR) and integrin-mediated phagocytosis, but not in complement-mediated phagocytosis (Serrander et al. 2000). Gelsolin-null neutrophils are impaired in FcγR-mediated phagocytosis while gelsolin-null fibroblasts exhibit defective binding and phagocytosis (Serrander et al. 2000).

In the absence of calcium, gelsolin is inactive, and exists as a globular protein with six gelsolin domains in a compact arrangement (Burtnick et al. 1997). In the

presence of micromolar concentrations of calcium, gelsolin undergoes activation to adopt an extended structure exposing actin-binding surfaces on G1, G2 and G6 (Robinson et al. 1999; Choe et al. 2002). As identified by protein crystallography, each gelsolin domain binds a calcium ion and binding of the six calcium ions serves to disrupt the structure of calcium-free gelsolin and stabilize the activated form. Calcium also modulates the affinity of activated gelsolin for actin, as seen by the involvement of a calcium ion each at the interfaces of G1:actin and G4:actin (Robinson et al. 1999; Choe et al. 2002). Gelsolin in the activated form binds to the side of actin filaments and severs them into two smaller polymers. Gelsolin remains attached and caps the barbed end of the actin filament. The cap can be dissociated by interaction with PIP_2 (Janmey & Stossel 1987). PIP_2 can also inhibit the interaction between free gelsolin and actin (Janmey & Stossel 1987). Gelsolin-capped filaments are marked for rapid depolymerization by cofilin, possibly due to the change of twist of the filaments (Ressad et al. 1998). The crystal structure of gelsolin in complex with monomeric actin has been solved in two parts, G1-3 in complex with actin and G4-6 in complex with actin (**Fig. 1.16**).

1.10.3 Regulation of gelsolin by phosphorylation

Gelsolin can be negatively regulated by phosphorylation. Gelsolin is phosphorylated by tyrosine kinase c-Src primarily at Tyr438 in the linker between gelsolin domains G3 and G4. *In vitro*, this phosphorylation is inhibited when gelsolin is bound to actin and greatly enhanced in the presence of PIP_2 (De Corte et al. 1999; De Corte et al. 1997). In osteoclasts, proline-rich tyrosine kinase 2 (PYK2) directly interacts with gelsolin, phosphorylating gelsolin at tyrosine residues, reducing gelsolin-actin interaction and increasing the association of gelsolin with PIP_2 (Wang et al. 2003).

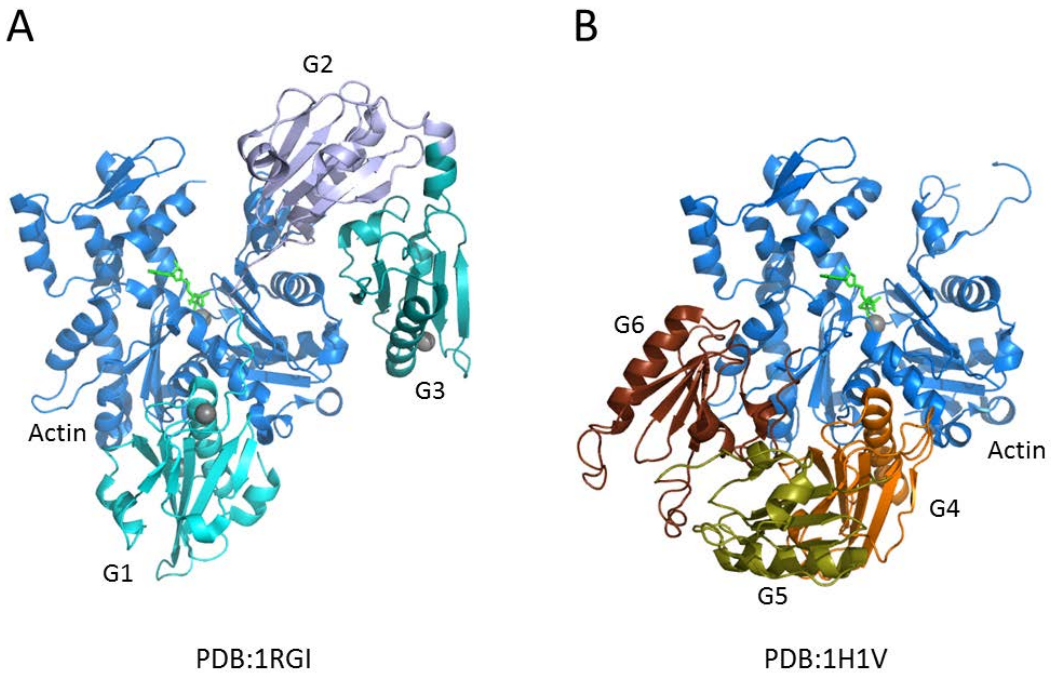


Figure 1.16 The interaction of active gelsolin N-and C-terminal halves with monomeric actin. (A) Crystal structure of complex of gelsolin domains 1-3 with G-actin (PDB: 1RGI (Burtnick et al. 2004)) (B) Crystal structure of complex of gelsolin domains 4-6 with G-actin (PDB: 1H1V (Choe et al. 2002)). Actin is shown in marine, calcium as grey spheres, ATP as green sticks and gelsolin domain 1-6 are as indicated.

1.10.4 CapG

CapG (also known as macrophage capping protein) is a three-domain member of the mammalian gelsolin clan (**Fig. 1.15**). CapG binds actin directly and caps the barbed ends of actin filaments, but it appears to lack severing activity unlike other gelsolin family members (Southwick 1995). While gelsolin is present in most cell types, CapG is detected primarily in neutrophils, macrophages and dendritic cells (Dabiri et al. 1992; Parikh et al. 2003). CapG is present in both the cytoplasm and nucleus, whereby nuclear import of CapG is controlled by nuclear transport factor 2 (NTF2) and GTP-binding nuclear protein Ran (Van Impe et al. 2008). Actin-binding activity of CapG is regulated by calcium and PIP_2 (Yu et al. 1990). The efficiency of FcγR- and complement-mediated phagocytosis is halved in CapG-null macrophages (Witke et al. 2001). CapG-null macrophages display decreased spontaneous ruffling. Membrane ruffles promote binding of opsonized particles required for efficient phagocytosis (Patel & Harrison 2008). CapG-null macrophages but not gelsolin-null macrophages display decreased membrane ruffling suggesting that CapG and gelsolin serve distinct, non-overlapping functions in macrophages (Witke et al. 2001). CapG is discovered to be phosphorylated at multiple sites on serine and threonine residues in macrophages by an unknown kinase and phosphorylated CapG exists predominantly in the nucleus (Onoda 1993). CapG has been discovered to be highly overexpressed in several metastatic cancers, suggesting its involvement in cell invasion and metastasis (Renz et al. 2008; Morofuji et al. 2012; Kimura et al. 2013).

1.10.5 ADF/cofilin

ADF/cofilins consist of one actin-depolymerizing factor homology (ADF-H) domain and are 13-19 kDa in size. ADF/cofilins consist of three isoforms, cofilin-1 which is ubiquitously expressed, cofilin-2 which is expressed predominantly in muscle and ADF (also known as destrin) which is expressed in non-muscle cells. ADF/cofilins bind both monomeric and filamentous actin through distinct binding sites (Lappalainen et al. 1997). ADF/cofilins primarily serve to depolymerize mature actin filaments for actin filament turnover (Carlier et al. 1997). ADF/cofilins bind ADP-actin preferentially over ATP-actin (Carlier et al. 1997). Pi-bound actin filaments inhibit binding of ADF/cofilins (Muhlrad et al. 2006), suggesting that ADF/cofilins specifically recognise mature filaments containing ADP with dissociated gamma-phosphate (Blanchoin 1999). ADF/cofilins increase the rate of phosphate release from actin filaments by more than 10-fold and induce a twisted conformation that destabilizes F-actin and drives the disassembly of such filaments (Orlova et al. 2004). ADF/cofilins bind F-actin in a cooperative manner which leads to the allosteric destabilization of actin protomers in the cofilin-free parts of F-actin (Bobkov et al. 2006). In addition to depolymerization, ADF/cofilins also sever actin filaments, predominantly at boundaries between bare and cofilin cooperatively decorated regions (Suarez et al. 2011), contributing to increased number of barbed ends used for actin polymerization (Ichetovkin et al. 2002). By electron cryo-microscropy and helical reconstruction, cofilin has been determined to bind F-actin by bridging two longitudinally associated actin subunits, between subdomain 2 of the lower actin subunit and the cleft between subdomains 1 and 3 of the upper actin subunit, resulting in a change in filament twist (McGough et al. 1997). The crystal structure of the complex of an ADF-H with G-actin suggests that ADF/cofilin binds

to actin at the hydrophobic cleft between subdomains 1 and 3 (Paavilainen et al. 2008) (**Fig. 1.17**).

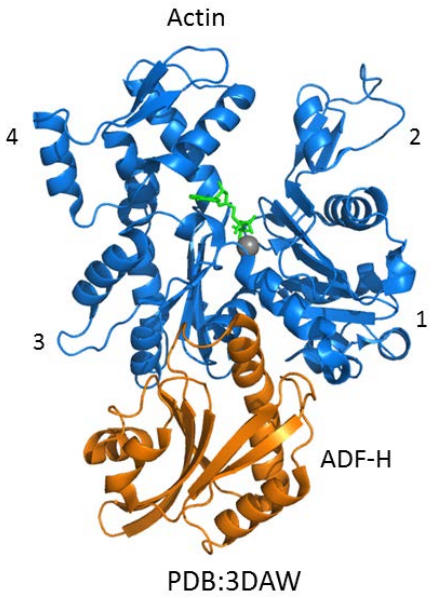


Figure 1.17 Crystal structure of the interaction of ADF-H from twinfilin with G-actin. Actin is shown in marine, ADF-H domain in orange, calcium as grey sphere, and ATP as green sticks. (PDB: 3DAW (Paavilainen et al. 2008))

Cofilin can be regulated by phosphorylation. Phosphorylation at Ser3 blocks cofilin's ability to bind to actin. This phosphorylation is performed by Lim family kinases (Lim 1 and 2) (Arber et al. 1998) and the Tes family kinases (Tes 1 and Tes 2) (Toshima et al. 2001) and can be by dephosphorylated by phosphatases slingshot (Ohta et al. 2003) and chronophin (Gohla et al. 2005). The direct binding of PIP_2 (Gorbatyuk et al. 2006) or cortactin (Oser et al. 2009) to cofilin blocks cofilin activity. The activity of cofilin, on the other hand, is enhanced by scaffolding activators including cyclase-associated protein (Srv2/CAP), Aip1 (Balcer et al. 2003), β-arrestin (Zoudilova et al. 2007), Memo (Meira et al. 2009) and coronin (Cai et al. 2008).

1.10.6 Twinfilin

Twinfilin contains two ADF-H domains separated by a short linker and a short but conserved C-terminal tail region. In budding yeast, twinfilin localizes primarily to the cytoplasm, but is also found in cortical actin patches (Goode et al. 1998). In mouse neuroblastoma cells, twinfilin localizes to cortical actin structures (Vartiainen et al. 2000). Twinfilin serves as a barbed end capper (Paavilainen et al. 2007) with severing activity (Moseley et al. 2006). Twinfilin forms a 1:1 complex with G-actin, inhibiting their nucleotide exchange (Vartiainen et al. 2000; Vartiainen et al. 2003). Similar to ADF/cofilins, twinfilins bind to ADP-G-actin with higher affinity (K_d = 0.05 μM) than ATP–G-actin (K_d = 0.5–2.0 μM) (Vartiainen et al. 2003), however unlike ADF/cofilin, twinfilin does not promote filament depolymerization (Ojala et al. 2002). Twinfilin prevents actin filament polymerization *in vitro* and binds filament barbed ends (Helfer et al. 2006). The two ADF-H domains of twinfilin are involved in binding actin. Individually both domains bind the same site on actin, however the two ADF-H domains are not functionally equivalent. The C-terminal ADF-H domain binds G-actin with higher affinity than the N-terminal ADF-H domain (Ojala et al. 2002). During filament barbed end capping, the N-terminal ADF-H domain interacts with the terminal actin subunit and the C-terminal ADF-H domain binds between two adjacent subunits at the side of the filament similar to the interaction of ADF/cofilin with F-actin (Paavilainen et al. 2008). Via the C-terminal tail region, twinfilin directly interacts with CapZ, regulating twinfilin's localization to cortical actin patches, resulting in the inhibition of severing activity of twinfilin (Falck et al. 2004; Moseley et al. 2006). Twinfilin is regulated by PIP_2 (Palmgren et al. 2001) which inhibits filament-severing activity of twinfilin (Moseley et al. 2006).

1.10.7 Srv2/CAP

Srv2/cyclase-associated protein (CAP) is a 55 kDa actin monomer binding protein. CAP binds actin at a 1:1 ratio and exists as a hexamer, forming a 600 kDa Srv2/CAP-actin complex (Balcer et al. 2003; Quintero-Monzon et al. 2009). CAP1 colocalizes with cofilin to dynamic regions of the actin cortex (Bertling et al. 2004). Depletion of CAP results in similar cytoskeletal defects observed in cofilin-1 knockdown cells and decreased actin-filament depolymerization and polymerization rates (Bertling et al. 2004). CAP functions to recycle depolymerized actin monomers from ADF/cofilin for actin filament turnover (Balcer et al. 2003). The N-terminal half of CAP contains a cyclase adenylase interaction domain, followed by a helical folded domain (HFD), while the C-terminal half contains a WH2 domain sandwiched between two proline-rich motifs, followed by a domain rich in β-sheets (Gerst et al. 1991; Vojtek et al. 1991) (**Fig. 1.18**). The HFD consists of antiparallel helices with a 14-3-3–like fold (Ksiazek et al. 2003) and is responsible for organising into Srv2/CAP into hexamers (Chaudhry et al. 2013). The two proline-rich motifs interact with profilin and SH3 domains respectively and the WH2 and β-sheet domain each interact with G-actin (Mattila et al. 2004). CAP recycles cofilin-bound ADP-actin monomers and catalyzes nucleotide exchange (ATP for ADP) on cofilin-bound ADP actin monomers. CAP preferentially binds ADP-G-actin (K_d = 0.02 μM) over ATP-G-actin (K_d = 1.9 M) and competitively displaces cofilin from ADP-G-actin (Mattila et al. 2004). CAP serves as a scaffold for coordinating the transfer of ADP-G-actin from cofilin to binding partner profilin which catalyzes any further needed nucleotide exchange (Bertling et al. 2007). The WH2 domain is involved in this process as mutations that impair actin-binding of WH2 domain disrupt the catalysis of nucleotide exchange on ADF/cofilin-bound actin monomers (Chaudhry et al. 2010).

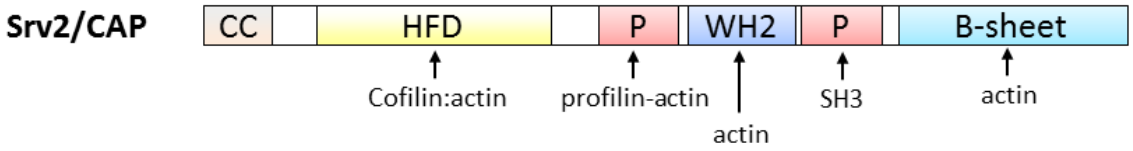


Figure 1.18 Schematic of Srv2/CAP domain organization. The domain nomenclature denotes cyclase adenylase interaction domain (CC), helical folded domain (HFD), proline-rich motifs (P), Wiskott-Aldrich-homology 2 domain (WH2). Relevant binding partners are shown above each domain. The schematic is not drawn to scale.

1.11 Regulation of actin cytoskeletal dynamics by Rho GTPases

Various signalling pathways regulate the activities of actin-binding proteins. Rho GTPase family members Cdc42, Rac, RhoA and RhoG are key regulators in the dynamics of the actin cytoskeleton, enabling spatial and temporal control of actin dynamics. Rho GTPases are binary switches existing in either an inactive, GDP-bound state or an active GTP-bound state. The activation of Rho GTPases via exchange of GDP to GTP is catalyzed by guanine nucleotide exchange factors (GEFs). GEFs act downstream of integrins, cadherins, growth factor receptors and cytokine receptors, converging different extracellular signals and coupling them to the activity of Rho GTPases. In turn, GTP-bound active GTPases interact with a plethora of different effectors mediating different cellular functions.

Rac exists in three isoforms, Rac1 is ubiquitously expressed, Rac2 is only expressed in haematopoietic cells, while Rac3 is highly expressed in brain (Didsbury et al. 1989). Rac in general is involved in the organisation of actin polymerization while Rac2 in particular, is essential for the activation of NADPH oxidase and generation of reactive oxygen species (ROS) in hematopoietic cells (Ambruso et al. 2000; Williams et al. 2013). Individuals with a dominant-negative mutation in Rac2 are associated with phagocyte and neutrophil immunodeficiencies (Ambruso et al. 2000; Williams et al. 2013). Rac stimulates actin polymerization by the formins INF2, FMNL and diaphanous 2 and 3 and by the ARP2/3 complex, while diaphanous 1 is activated only by RhoA (Lammers et al. 2008). Rac acts on the ARP2/3 complex via IRSp53 or via direct activation of the WAVE complex. Rac binds to the Cyfip1 subunit of WAVE complex, to release the WAVE complex from its autoinhibited state (Kobayashi et al. 1998; Ismail et al. 2009). IRSp53, through its SH3 domain,

forms a complex with WAVE2 and recruits it to the membrane for the activation of WAVE2 by PIP_3 (Oikawa et al. 2004; Suetsugu et al. 2006; Takahashi & Suzuki 2010). The activated WAVE complex then in turn activates ARP2/3 (**Fig. 1.19**).

RhoG is relatively newly discovered. It is most closely related to Rac2 and Rac1, at 74% and 73% amino acid sequence identity respectively and is placed in the same Rho GTPase subfamily as Rac1, 2 and 3. It is more closely related to Cdc42 than RhoA, with 62% and 55% amino acid sequence identity respectively (Vincent et al. 1992). RhoG was identified as a growth factor response gene (Vincent et al. 1992) and found to be involved in a variety of cellular processes, which include cell migration (Katoh et al. 2006); FcγR- and CR3- mediated phagocytosis (Tzircotis et al. 2011); the regulation of membrane dynamics in macropinocytosis (Ellerbroek et al. 2004); in neurite outgrowth (H. Katoh et al. 2000); in the engulfment of apoptotic bodies (DeBakker et al. 2004); in NADPH oxidase activation (Condliffe et al. 2006); and in transendothelial cell migration by leukocytes (Van Buul et al. 2007). Trans-endothelial migration is an important aspect of host defence and involves the movement of leukocytes across vascular walls into underlying tissues. RhoG-null mice have no major growth abnormalities suggesting a functional redundancy of RhoG with other Rac proteins (Vigorito et al., 2004). Neutrophils from RhoG-null mice display marked impairment in NADPH oxidase activation (Condliffe et al. 2006). RhoG acts upstream of Rac1 and Cdc42, regulating the activation of Rac1 and Cdc42 (Katoh et al. 2000). RhoG interacts with Elmo and forms a ternary complex with Dock180 to induce activation of Rac1 (Katoh & Negishi 2003). RhoG is required for both FcγR- and CR3-mediated phagocytosis and is recruited and activated at phagocytic cups in both FcγR- and CR3-mediated pathways (Tzircotis et

al. 2011).

Cdc42 functions similarly to Rac and stimulates actin polymerization via the formins INF2, FMNL and diaphanous 2 and 3 and via the ARP2/3 complex. Cdc42's effect on the ARP2/3 complex is mediated by IRSp53 but instead of the WAVE complex, Cdc42 activates WASP (Prehoda 2000). Rac and Cdc42 also mediate activation of the Ser/Thr kinase PAK (p21-activated kinase) which phosphorylates LIM kinase (LIMK), which in turn phosphorylates and inhibits cofilin, leading to regulation of actin-filament turnover (Edwards et al. 1999).

RhoA stimulates actin polymerization by the formin diaphanous 1 (Watanabe et al. 1997). RhoA activates ROCK (Rho-associated protein kinase) which phosphorylates MLC (myosin light chain). This leads to the formation of stress fibres and focal adhesions (Leung et al. 1996). In its active form, RhoA-GTP binds to and activates ROCK, leading to phosphorylation of LIMK by ROCK and activated LIMK in turn phosphorylates and inhibits cofilin, exerting similar downstream effects to the phosphorylation of LIMK by PAK, which is mediated by Rac and Cdc42 (Maekawa 1999) (**Fig. 1.19**).

Thus Rho GTPases RhoA, Rac and Cdc42 either directly affect polymerization through activation of nucleators or elongators or indirectly through activation of kinases while RhoG affects polymerization through the activation of Rac and Cdc42.

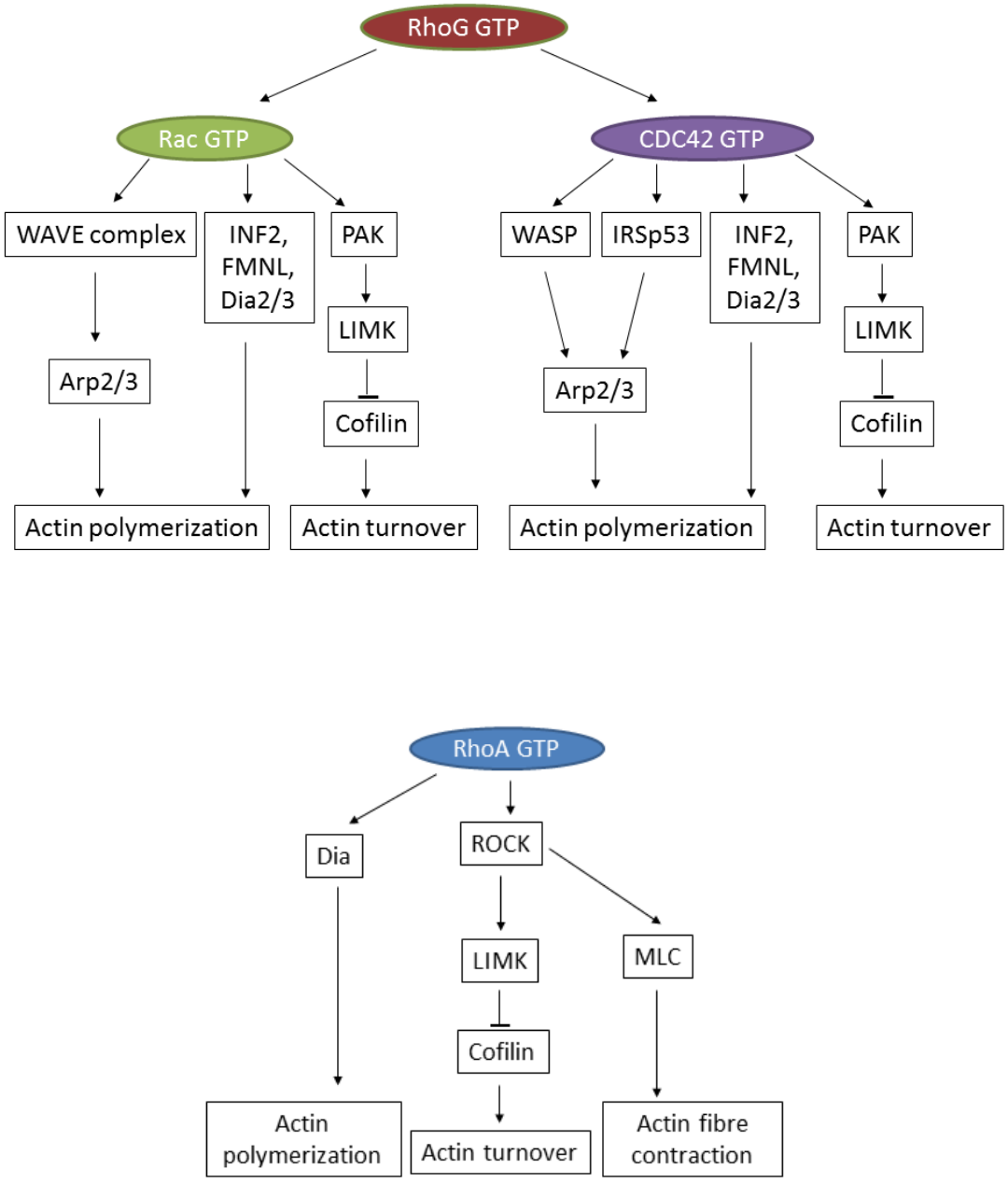


Figure 1.19 Regulation of cytoskeletal dynamics by selected Rho GTPases. Adapted from (Heasman & Ridley 2008)

1.12 Molecular mechanisms of actin dynamics in phagocytic uptake

Phagocytosis is a receptor-mediated, actin-driven process, classically defined as the process for recognising and engulfing particles greater than 0.5 μm in size. The engulfment of particles is initiated by the interaction of specific receptors on the surface of the phagocyte with ligands on the surface of the particle (Aderem & Underhill 1999). Phagocytes have many types of receptors, necessitated by the variety of microbes for recognition. They include opsonin receptors, scavenger receptors, Toll-like receptors and integrins (Aderem & Underhill 1999). Scavenger receptors, Toll-like receptors and integrins are non-opsono receptors. They recognize surface components including lipopolysaccharide or glycoproteins on particles instead of opsonisation. The major phagocytic receptors involved during infection are opsonin receptors Fcγ receptors (FcγR) and complement receptors (CR3), which recognise particles that have been opsonized with IgG and complement proteins C3bi respectively.

Following recognition mediated by the interaction of the phagocyte receptor with ligands on the particle to be phagocytosed, internalization of the particle takes place via an actin-based mechanism. Actin polymerization provides the driving force for macrophage phagocytosis and reorganization of filamentous actin is observed in phagocytic uptake. Particle internalization via FcγR- and CR3-mediated phagocytosis evoke different membrane morphologies and involve different pathways (Aderem & Underhill 1999). In FcγR-mediated phagocytosis, macrophage membrane protrusions in the form of pseudopod extensions and membrane ruffling are observed. The membrane protrusions fuse around the particle to be phagocytosed, drawing the particle into the macrophage (Kaplan 1977). In CR3-mediated

phagocytosis, the particle sinks into the macrophage, producing minor membrane protrusions (Kaplan 1977). Only FcγR-mediated uptake results in the activation of the respiratory burst and an inflammatory response in the form of production of arachidonic acid metabolites and cytokines, such as tumor necrosis factor-α. CR3-mediated uptake does not result in any of these inflammatory signals. FcγR-mediated phagocytosis and CR3 mediated uptake are controlled by different signalling pathways. The rearrangements of the actin cytoskeleton necessary for FcγR-mediated phagocytosis is mediated by Cdc42 and Rac while in contrast, CR3-mediated uptake is mediated by RhoA (Caron & Hall 1998). RhoG is implicated in both FcγR- and CR3-mediated phagocytosis (Tzircotis et al. 2011). During FcγR-mediated internalization, active Cdc42 accumulates early to the forming phagosomes and is restricted to the tips of extending pseudopodia while active Rac1 localizes throughout the phagocytic cup. Activation of Rac1 and Rac2 increases during phagosome closure (Hoppe & Swanson 2004). The knockout of Rac1 and Cdc42 in macrophages inhibits phagocytosis by preventing the accumulation of F-actin in the phagocytic cup (Cox et al. 1997). PIP_2 is an important regulator of actin dynamics around the nascent phagosomes. Disassembly of actin from the phagosomal membrane is closely correlated to the disappearance of PIP_2 while inhibition of PIP_2 hydrolysis prevented actin disassembly around the phagosome (Scott et al. 2005).

It has been clearly established that WASP and WASP activation by Cdc42 are of central importance in FcγR-mediated phagocytosis (Park & Cox 2009). In macrophages, WASP localizes to the actin cup. Formation of the actin cup is significantly attenuated in WASP deficient macrophages (Lorenzi et al. 2000). Phosphorylation of WASP on Tyr291 and the formation of a complex between

WASP and WIP are important for the assembly of a phagocytic cup in FcγR-mediated phagocytosis (Tsuboi & Meerloo 2007).

Actin polymerizing machineries implicated in the phagocytic processes include WASP, ARP2/3 and VASP. ARP2/3 is important in mediating actin polymerization for phagocytic cup formation and particle engulfment in both FcγR-mediated and CR3-mediated phagocytosis, localizing to phagosomes in both phagocytic pathways (May et al. 2000), while VASP is linked to FcγR-mediated phagocytosis. VASP accumulates with F-actin at nascent FcγR-induced phagosomes together with other proteins including Fyb/SLAP, Nck, Vav, SLP-76 and WASP (Coppolino & Krause 2001). Diaphanous is recruited at the start of CR3-mediated phagocytosis and colocalizes with actin in the phagocytic cup. Reduction of Dia activity significantly reduces CR3-mediated phagocytosis with no effect on FcγR-mediated phagocytosis (Colucci-Guyon et al. 2005). Cytoskeletal scaffold protein IQGAP1 is involved in recruiting Rho-activated mDia1 via the DAD domain to phagocytic cups (Brandt et al. 2007).

Severing proteins implicated in the phagocytic process include gelsolin and CapG. Gelsolin is enriched at phagosomes and gelsolin-null neutrophils are impaired in FcγR-mediated phagocytosis but not in complement-mediated phagocytosis (Serrander et al. 2000). In contrast, CapG-null macrophages are impaired in both FcγR and CR3 phagocytosis (Witke et al. 2001). Thus the regulation of actin dynamics by Cdc42, Rac, RhoA, RhoG and PIP_2 and effectors WASP, ARP2/3, VASP, gelsolin and CapG are integral to phagocytosis.

1.13 Pathogenic manipulation of the actin cytoskeleton

Diverse intracellular microorganisms, including both viral and bacterial pathogens, manipulate or disrupt the actin cytoskeleton during their life cycle. Pathogenic manipulation of the actin cytoskeleton takes many forms. Some pathogens hijack the actin polymerization machinery for motility within the host cell and for propulsion into neighboring mammalian host cells to achieve rapid dissemination, while avoiding immune survelliance. The protein ActA from *Listeria monocytogenes* has similar domains as host nucleation promoting factor WASP and stimulates actin polymerization by directly activating the ARP2/3 complex (Boujemaa-Paterski et al. 2001) and interacting with the EVH1 domain of VASP via its proline-rich sequence (Geese et al. 2002), utilizing both ARP2/3 and VASP for accelerated motility. RickA of *Rickettsia conorii/rickettsia* functions in a similar manner, as a WASP mimic (Gouin et al. 2004). Protein IcsA of *Shigella flexneri* hijacks host nucleation promoting factors by acting as a Cdc42 mimic, activating and recruiting WASP family proteins, which in turn, activates ARP2/3 for actin polymerization (Gouin et al. 2004). *Vaccinia* virus protein A36R gets phosphorylated by host Src tyrosine kinase and recruits adaptor proteins Nck and Grb2 which in turn recruit and activate WASP (Frischknecht et al. 1999). Enteropathogenic *Escherichia coli* (*E.coli*) and enterohaemorrhagic *E. coli* can induce actin rich pedestals on intestinal epithelia to propel the bacteria across the epithelial surface to facilitate colonization of other parts of the intestine without having to enter the host cell. These pathogenic *E.coli* inject translocated intimin receptor (Tir) into host cells via a type III secretion system. After phosphorylation by host Src tyrosine kinase, Tir recruits host-cell adaptor protein Nck, which in turn recruits N-WASP, activating actin polymerization by ARP2/3 (Gruenheid et al. 2001). *Salmonella* bacteria encodes two

actin-binding proteins SipA and SipC, which nucleate actin polymerization and stabilizes actin filaments, inducing membrane ruffling that promote uptake of the bacteria into intestinal epithelial cells (Ginocchio et al. 1994).

The actin cytoskeleton is crucial to the function of phagocytosis in phagocytes (*i.e.* macrophages, dendritic cells and neutrophils), which play crucial roles in innate immunity (Aderem & Underhill 1999). Many intracellular pathogens have evolved mechanisms to impair phagocytosis of phagocytes by directly modifying the actin in host cell cytosol (Stevens et al. 2006). There are three categories of toxins that bacterial pathogens secrete into host cells – *Salmonella enterica, Bacillus cereus, Photorhabdus luminescens, Aeromonas salmonicida/hydrophila,* and *Clostridium botulinum* secrete effectors that ADP-ribosylate actin at Arg177 rendering the actin incapable of forming filaments (Schleberger et al. 2006; Aktories et al. 2011); Tc toxin from *Photorhabdus luminescens* ADP-ribosylates actin at threonine-148 promoting extensive actin polymerization and aggregation (Lang et al. 2010) and lastly, *Vibrio cholera* secretes *cholera* toxin that catalyzes chemical crosslinking of actin into oligomers, preventing the formation of functional filaments (Kudryashov et al. 2008). Thus many pathogens have developed ways to manipulate the actin polymerization machinery to aid their lifecycles and evade the immune system.

1.14 The pathogenicity of *Yersinia* bacteria

There are three pathogenic species within the genus *Yersinia*: *Yersinia enterocolitica* causes gastrointestinal syndromes, *Yersinia pseudotuberculosis* causes Far East scarlet-like fever; and the most notorious is *Yersinia pestis*, being the causative agent of plague (Cornelis et al. 1998). *Yersinia pestis* is responsible for killing many millions of people through the 14th up to the 19th century. There are still cases reported in the 21st century. While all infection can now be treated with antibiotics, the discovery of strains that have acquired a self-transmissible plasmid conferring antibiotic resistance, has fuelled concerns of re-emergence (Galimand et al. 2006). The plague is highly infectious through airborne transmission and is highly lethal. It has been developed into biological weapons by the United States and Soviet Union and constitutes a significant terror concern (Pohanka & Skladal 2009).

The pathogenicity of *Yersinia* bacteria is conferred by a virulence plasmid pYV which encodes for the type III secretion system apparatus (Cornelis & Wolf-Watz 1997; Galán 1999; Cornelis 2000; Cornelis 2002; Cornelis 2006) which allows the bacteria to secrete and translocate a cocktail of six effector proteins YpkA/YopO, YopH, YopM, YopT, YopP/J, and YopE into the cytosol of host cells (Viboud & Bliska 2005; Aepfelbacher et al. 2007; Trosky et al. 2008). These effector proteins collectively inhibit the phagocytosis machinery and modulate host signalling to reorient the innate immune response of the host (Viboud & Bliska 2005).

YopM and YopP/J do not contribute to resistance to phagocytosis but affects apoptosis and immune signalling. **YopM** functions as a scaffold, forming a complex with host kinases ribosomal S6 protein kinase 1 (RSK1) and protein kinase C-like 2

(PRK2), leading to activation of both kinases of which cellular targets are involved in proliferation, apoptosis and translation pathways (McDonald et al. 2003). **YopP/J** inhibits the NF-κB and MAP kinase signal transduction pathways, leading to: reduction in production of pro-inflammatory cytokines tumor necrosis factor alpha (TNF-α) (Ruckdeschel et al. 1998; Ruckdeschel et al. 1997) and interferon-gamma (IFNγ) (Sweet et al. 2007); and rapid apoptosis in infected macrophage and dendritic cells, attenuating antigen presentation (Monack et al. 1997; Ruckdeschel et al. 1998; Zhang et al. 2013). YopP/J functions as a serine/threonine acetyl-transferase, targeting various mitogen-activated protein kinase kinases (MKKs) and the inhibitor κB kinase β (IKKβ) (Mittal et al. 2006). The acetylations blocks the phosphorylation and activation of these target proteins (Mukherjee et al. 2006; Mittal et al. 2006). YopP/J is also reported to deubiquitinate TRAF proteins, inhibiting their proteasomal degradation contributing to the inhibition of the NF-κB innate immune signalling pathway (Zhou et al. 2005; Sweet et al. 2007).

Resistance to phagocytosis is conferred in particular, by effectors YopH, YopT, YopO and YopE. As compared to wild type *Yersinia* bacteria, mutants lacking these effectors were more prone to phagocytosis by macrophages in both opsonin receptor-dependent and -independent pathways (Grosdent et al. 2002). In leukocytes, YopH, YopT and YopO confer resistance to phagocytosis but not YopE (Grosdent et al. 2002).

YopH is a tyrosine phosphatase targeting tyrosine kinases and adaptors in a number of cell types. In epithelial cells, YopH dephosphorylates tyrosine kinase FAK, adaptor proteins p130Cas and paxilin resulting in the disruption of focal

adhesion complexes (Hamid et al. 1999). In macrophages, YopH dephosphorylates p130Cas, Fyb, SKAP-HOM, and FAK homolog tyrosine kinase PyK resulting in the inhibition of the β1 integrin phagocytic pathway (Black et al. 2000) and the attenuation of oxidative burst in macrophages and neutrophils (Bliska & Black 1995). In T-cells, YopH dephosphorylates Lck, LAT and SLP-76, resulting in the inhibition of T cell antigen receptor signalling (De la Puerta et al. 2009). Collectively, YopH results in the inhibition of the β1 integrin phagocytic pathway and the activation of signal transduction in early stages of the immune response.

YopO, **YopT** and **YopE** target Rho GTPases, with observed phenotypes of disruption of stress fibres and cell rounding, accompanied by inhibition to phagocytosis. YopT is a cysteine protease that cleaves the lipid modification from Rho GTPases RhoA, Rac and Cdc42, resulting in the release of the Rho GTPase from the membrane (Shao et al. 2003). YopE, a GTPase-activating protein, binds to RhoA, Rac1 and Cdc42 *in vitro*, stimulating their GTPase activity, terminating their capacity for signalling (Black & Bliska 2000). YopO contains a serine/threonine kinase domain and a GDI domain. The GDI domain inhibits nucleotide exchange in Rac1 and RhoA (Galyov et al. 1993; Prehna et al. 2006). YopE causes morphological changes that are similar but distinct from those mediated by YopO. Cells overexpressing YopE round up and detach from the substratum, while YopO-overexpressing cells only round up but maintain focal adhesions (Håkansson et al. 1996). YopO will be described in greater detail in the next section.

1.14.1 *Yersinia* protein kinase A YpkA/YopO

Yersinia protein kinase A, known as YopO in *enterocolitca* and YpkA in *pestis* and *pseudotuberculosis*, is a critical virulence determinant (Galyov et al. 1993; Wiley et al. 2006). The primary sequence identity is greater than 96% amongst these homologs. In mouse models, pathogenic *Yersinia* strains that have deletion mutations in the YpkA gene are no longer lethal (Galyov et al. 1993). YpkA expression enhances resistance to killing by macrophages (Wiley et al. 2006). In HeLa cells, when overexpressed with YpkA, or subjected to infection with YpkA over-producing strain, extensive actin cytoskeletal disruption takes place, with loss of actin stress fibres (Juris et al. 2000) and cells are observed to retract around their edges but maintain focal adhesions (Håkansson et al. 1996; Juris et al. 2000). In yeast, YpkA expression disrupts the normal distribution of actin (Straley & Bowmer 1986; Nejedlik et al. 2004). YopO significantly inhibits the uptake of both IgG-opsonised and C3bi-opsonised particles, which take place via Fcγ-mediated and CR3-mediated phagocytosis respectively, with a greater inhibitory effect on the FcγR pathway (Groves et al. 2010).

YpkA is a multi-domain protein that has an N-terminal membrane localization domain (Letzelter et al. 2006), which binds to its type III secretion effector chaperone SycO (Letzelter et al. 2006) and targets YpkA to the inner surface of the host cell membrane (Håkansson et al. 1996). The membrane localization domain is followed by a region homologous to eukaryotic serine/threonine kinases and a Rho-GTPase-binding domain (Galyov et al. 1993; Håkansson et al. 1996; Barz et al. 2000; Dukuzumuremyi et al. 2000; Juris et al. 2000). The structure of the GTPase-binding domain has been solved alone and in complex with Rac1 (**Fig. 1.20**). The

structure reveals it to be a guanine nucleotide dissociation inhibitor (GDI) mimic (Prehna et al. 2006). The GDI domain of YpkA inhibits nucleotide exchange of bound Rho-GTPases, similar to eukaryotic Rho GDIs. At the C-terminal end of YpkA is a stretch of amino acids (710-729) that has homology to the coiled-coil domain of actin-bundling protein coronin (Juris et al. 2000). Deletion of 20 amino acids at the C-terminus results in a complete loss of kinase activity, and abolishes the interaction between YpkA and actin (Juris et al. 2000).

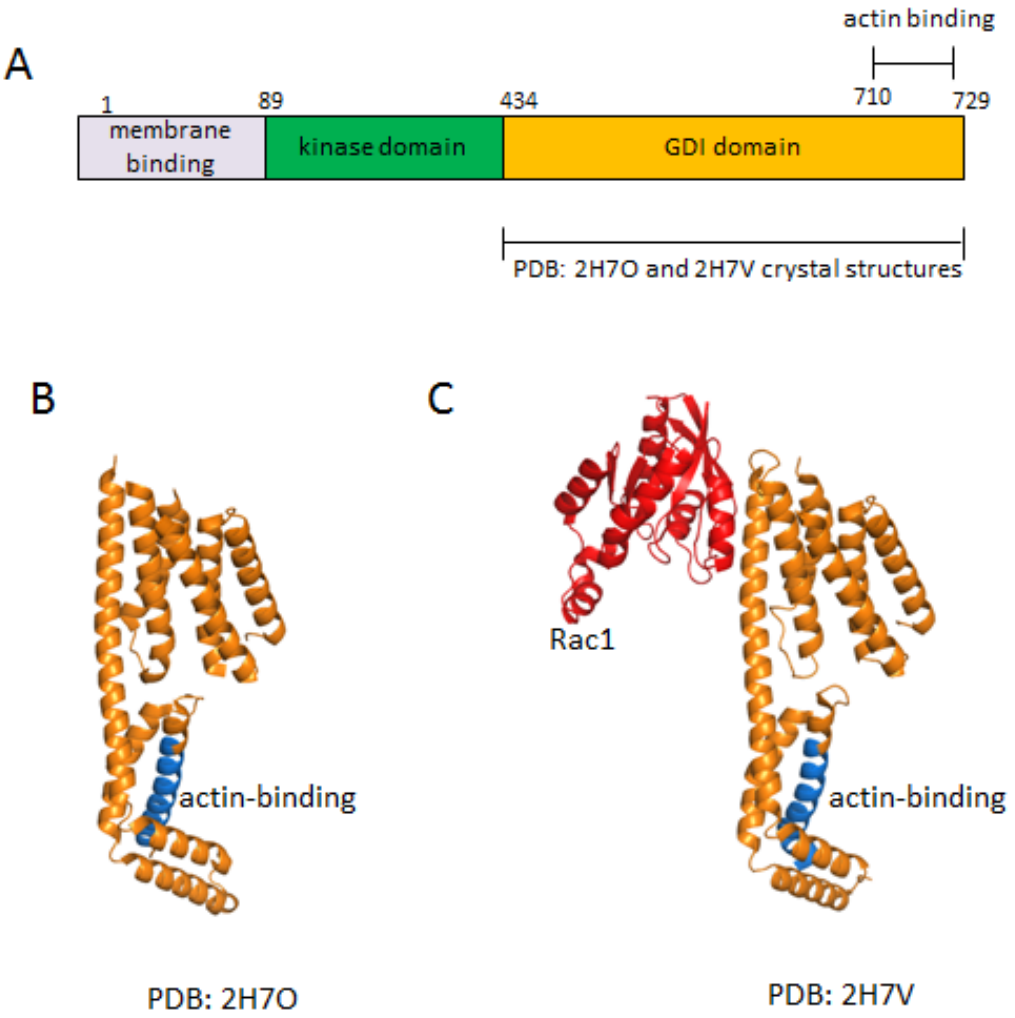


Figure 1.20 Structure of GDI domain of YpkA (Prehna et al. 2006). (A) Schematic representation of domain structure of YpkA; (B) structure of the GDI domain crystallized on its own, PDB: 2H7O; (C) structure of the GDI domain crystallized in complex with RacI, PDB: 2H7V with YpkA. Rac1 is shown in red, the GDI domain

is shown in orange and the actin-binding region is shown in blue.

Via yeast two-hybrid and co-immunoprecipitation, YpkA has been identified to bind RhoA and Rac1 but not Cdc42 (Barz et al. 2000; Dukuzumuremyi et al. 2000; Groves et al. 2010), though YpkA is suggested to selectively interact with Rac due their collective localization at the plasma membrane (Groves et al. 2010). YpkA recombinantly-purified from bacteria and *Yersinia* secreted YpkA are inactive and not autophosphorylated (Barz et al. 2000; Dukuzumuremyi et al. 2000; Juris et al. 2000) and its activity is dependent on a eukaryotic host factor, identified to be actin (Juris et al. 2000; Trasak et al. 2007). YopO binds to actin with an affinity of K_d= 1.9 μM (Trasak et al. 2007). Two separate actin-binding sites have been identified within YopO, one within the kinase domain (89-440) and one within the GDI-domain (441-729) (Trasak et al. 2007). YopO is activated by G-actin binding and this brings about autophosphorylation on Ser90 and Ser95 of YopO (Trasak et al. 2007). Autophosphorylation occurs by an intramolecular process and trans-phosphorylation of neighbouring YopO molecules do not take place (Trasak et al. 2007). YopO forms a 1:1 complex with G-actin and prevents its polymerization (Trasak et al. 2007). YopO is differentially activated by actin of different isoforms, with the muscle isoform about ten-fold weaker in activating the autophosphorylation of YpkA compared to non-muscle isoforms (Trasak et al. 2007).

Various studies have failed to gain a consensus on the precise contribution of the GDI domain and the kinase domain to the disruption of the actin cytoskeleton (Dukuzumuremyi et al. 2000; Juris et al. 2000; Groves et al. 2010). Expression of full length wild type YpkA results in a pronounced phenotype with cell rounding

(retraction of cell edges) and obliteration of actin stress fibres. Full length YpkA with mutations to the kinase active site generated a phenotype that either appeared indistinguishable to wild type YpkA (Dukuzumuremyi et al. 2000), or had an intermediate level of cytoskeletal disruption (Juris et al. 2000; Prehna et al. 2006). Deletion of the kinase domain results in an intermediate phenotype (Juris et al. 2000; Dukuzumuremyi et al. 2000; Prehna et al. 2006), while deletion of the GDI domain results in complete abolishment of cytoskeletal disruption (Groves et al. 2010). These led to the conclusion that the GDI domain is the main contributor to cytoskeletal disruption. Intriguingly, when both the kinase active site and the GDI domain are mutated, cytoskeletal effects are not completely abolished and a low level of cytoskeletal disruption persists (Dukuzumuremyi et al. 2000; Juris et al. 2000; Prehna et al. 2006).

YpkA has been found to inhibit Gαq signalling pathways through its kinase activity (Navarro et al. 2007), though there seems to be no direct implications on observed phenotypes of disruption of the actin cytoskeleton. As such, the major substrates of the kinase domain of YpkA, pertaining to its effects on actin cytoskeletal disruption, remain elusive.

1.14.2 Kinase structure and function

A protein kinase is an enzyme that covalently transfers a phosphate group from a phosphate donor ATP molecule onto amino acids with a free hydroxyl group, namely serine, threonine or tyrosine, in a process termed phosphorylation. Phosphorylation usually results in changes in enzyme activity, subcellular location, or protein-protein interactions, of the target protein (substrate), contributing to a functional change (Johnson & Barford 1993). Despite low sequence homology, the structure of the catalytic domain of kinases are strongly conserved across kingdoms (Hanks & Hunter 1995; Young et al. 2003; Pereira et al. 2011). Specific motifs and residues which are involved in the catalysis or positioning of the phosphate donor ATP molecule and the protein substrate are highly conserved (Hanks & Hunter 1995) (**Fig. 1.21**).

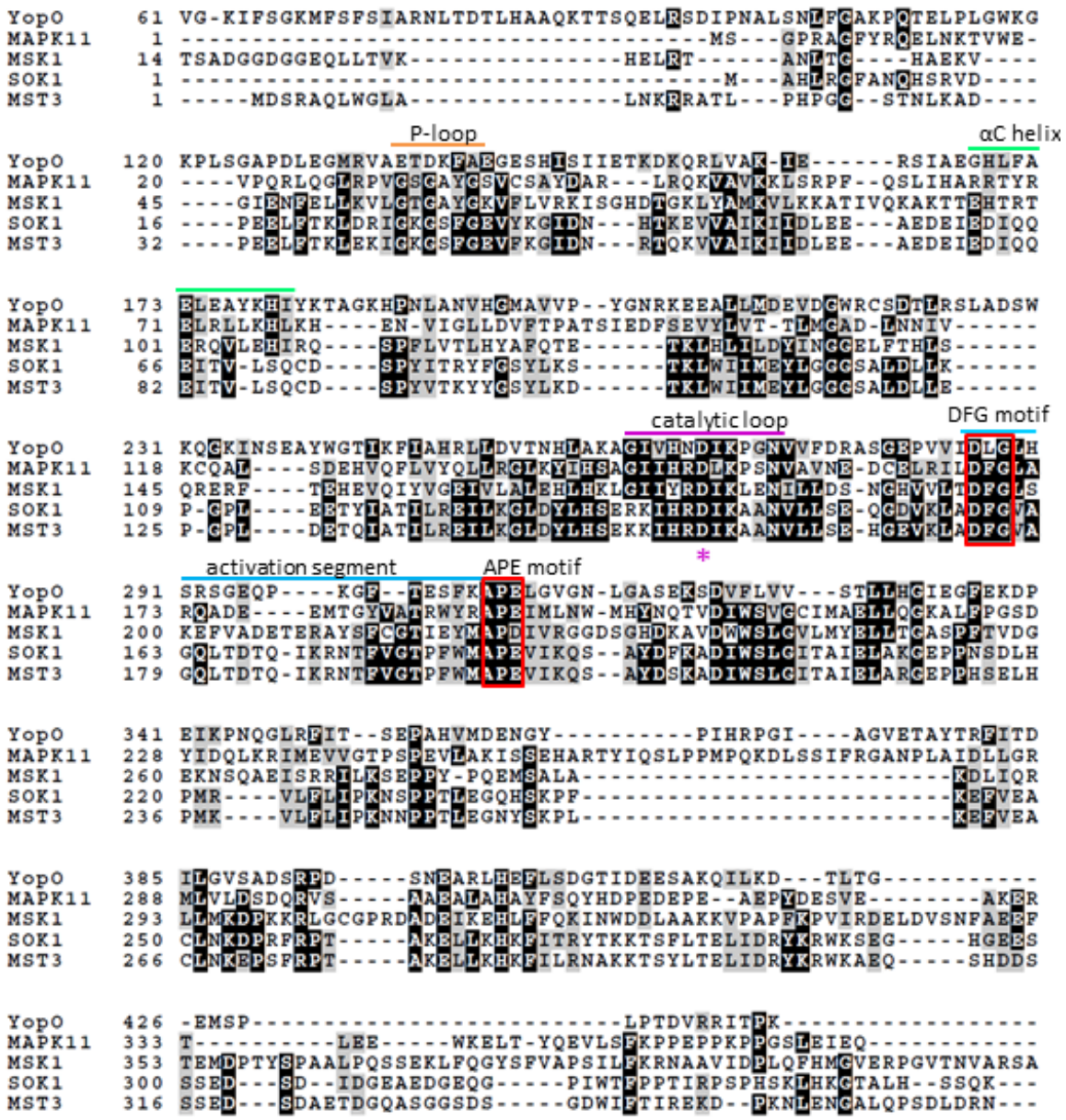


Figure 1.21 Sequence alignment of the kinase domains of YopO with top hits identified with FFAS (Fold Function Assignment Server) against Protein Data Bank (PDB). Mitogen-activated protein kinase 11 (MAPK11, human), Ribosomal protein S6 kinase alpha-5 (S6Kα5/MSK1), Ste20/oxidant stress response kinase 1 (SOK1, human) and Mammalian STE20-like protein kinase 3 (MST3/STK24, human). Several conserved and functionally important motifs are indicated. The levels of sequence identity with the YopO kinase domain (89–440) are 21% for MAPK11, 22% for MSK1, 18% for MST3 and 18% for SOK1. The asterisk marks the catalytic aspartate. The diagram is made using BOXSHADE (http://www.ch.embnet.org/software/BOX_form.html).

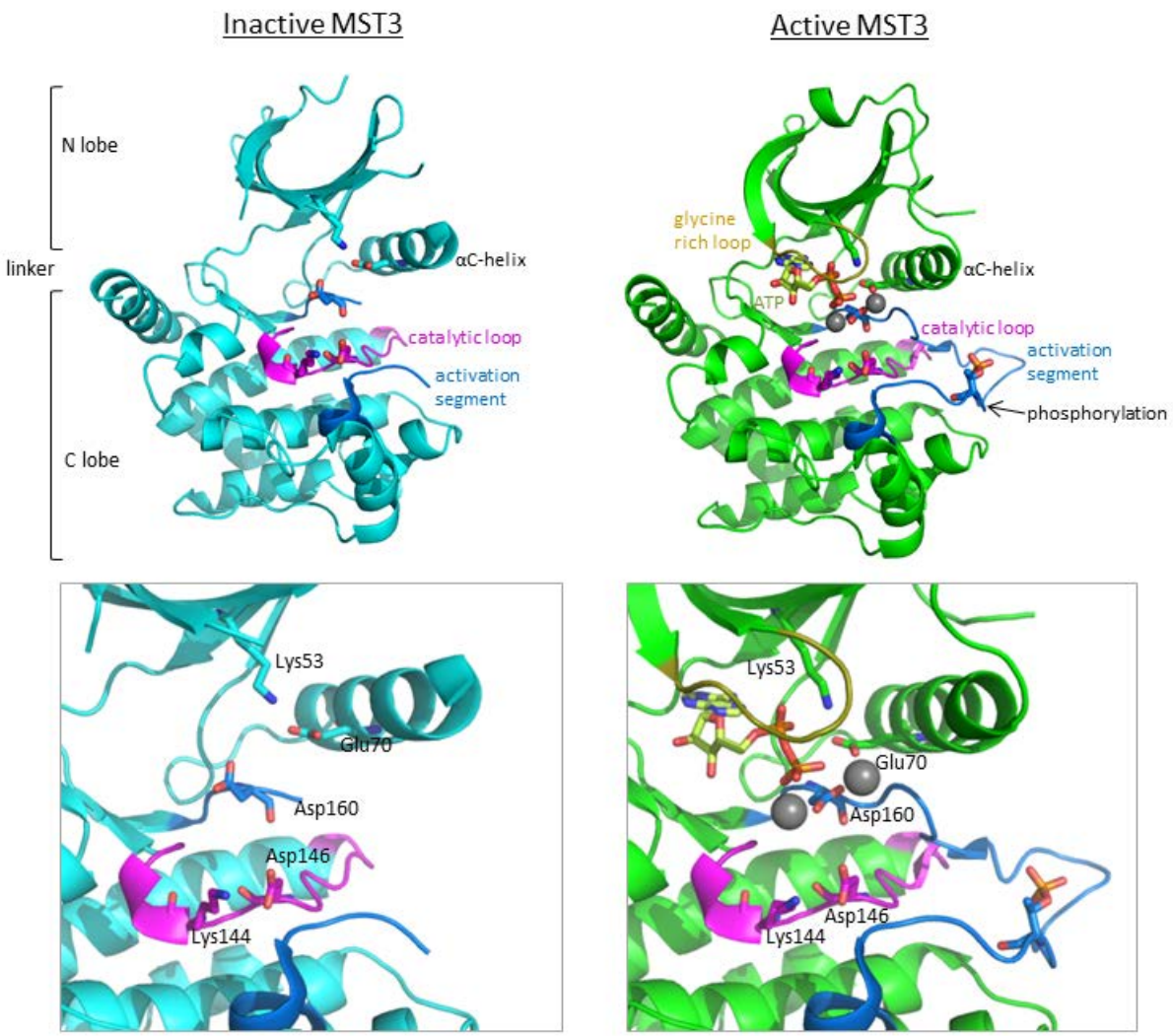


Figure 1.22 Structure of protein kinases in the active and inactive states. Mammalian STE20-like protein kinase 3 (MST3/STK24) inactive (cyan, PDB: 3CKW) and active (green, PDB: 3A7H (Ko et al. 2010)) structures. The catalytic loop (magenta) contains catalytic residues Asp-X-Lys of which Asp144 and Lys146 are shown in sticks. Conserved residues Lys53, Glu70 and Asp160 that coordinate ATP (yellow and orange sticks) and Mg^{2+} (grey spheres) are shown. Activation segment (blue) is partially disordered in the inactive structure but fully ordered in the active structure. The glycine rich loop (olive) coordinates the phosphates of ATP. Phosphorylated threonine on the activation segment of active MST3 shown in sticks. An enlarged view of the catalytic cleft is shown in the lower panel.

The catalytic domain of kinases (**Fig. 1.22**) consists of an N-terminal lobe made up of a β-sheet and a single α-helix (αC helix) which is connected by a linker to a larger C-terminal lobe which is predominantly α-helical in nature (Hanks & Hunter 1995; Huse & Kuriyan 2002). The N-terminal lobe contains a P-loop normally consisting of a conserved glycine-rich sequence motif GXGXφG (where φ is usually tyrosine or phenylalanine) of which the glycines coordinate the phosphates of ATP via backbone interactions. The C-terminal lobe contains the activation segment of about 20–35 residues demarcated by a conserved Asp-Phe-Gly (DFG) motif and an Ala-Pro-Glu (APE) motif; and the catalytic loop which contains the Asp-X-Lys residues in which Asp is directly involved in catalysis (Hanks & Hunter 1995; Huse & Kuriyan 2002) and Lys binds to the phosphate before and after transfer. The region between the N- and C-terminal lobe forms an ATP-binding cleft that constitutes the catalytic cleft, also known as the active site.

Ser/Thr and Tyr kinases have similar catalytic domain structures, but protein Tyr kinases have a deeper catalytic cleft such that a Tyr residue can reach the catalytic residues while the smaller side chains of Ser and Thr cannot approach (Ubersax & Ferrell 2007). Kinases are molecular switches that exist in either an active or inactive state. Structural transition to an activated state involves extensive conformational changes whereby the glycine-rich P-loop and αC helix in the N-terminal lobe move towards the activation loop, allowing multiple interactions between the two lobes, leading to the correct positioning of phosphate donor ATP, catalytic aspartate and protein substrate within the catalytic cleft for transfer of the γ-phoshoryl group of ATP (Endicott et al. 2012; Kornev et al. 2006; Eswaran et al. 2008). The activation segment is partially disordered in inactive kinases. Activation

leads to stabilization of the activation segment which is a crucial constituent of the substrate-binding site (**Fig. 1.22**).

The activation of kinases is tightly controlled, with many kinases being maintained in the inactive state via autoinhibition (Chen et al. 2009; Endicott et al. 2012; Ha et al. 2012). Mechanisms of activation are highly diverse and include binding of allosteric effectors (Sharrocks et al. 2000), activation segment exchange (Pike et al. 2008) and phosphorylation on the activation segment (Bayliss et al. 2003). Protein kinases are further regulated by subcellular localization which limits the availability of substrates, activators and inactivators (Ubersax & Ferrell 2007). Specificity of phosphorylation is determined by two factors: peptide specificity of the kinase for the substrate, and the frequency of encounter between the kinase and substrate, the recruitment (Zhu et al. 2005). Peptide specificity is conferred by the structure of the catalytic site, as well as local and distal interactions between the kinase and substrate, while recruitment can be controlled via complex formation with scaffolding or adaptor proteins that regulate the kinase (Reményi et al. 2006; Ubersax & Ferrell 2007; M. Good et al. 2011).

1.15 Rationale and significance of work

YpkA/YopO is the only instance, discovered so far, in which the kinase activity of a protein is dependent on actin. It is intriguing mechanistically to understand how interaction with actin could lead to the activation of a kinase. The structure of the kinase domain of YpkA/YopO has not been solved and a BLAST (Basic Local Alignment Search Tool) search with the kinase domain of YpkA/YopO against PDB (Protein Data Bank) yielded structures of at best 22% sequence identity, with top hits being eukaryotic kinases (**Fig. 22**). Of the hundreds of actin-binding proteins discovered so far, YpkA/YopO is one of the few actin-binding proteins that display a preference between different actin isoforms (Trasak et al. 2007). YpkA/YopO is a virulence determinant in the pathogenesis of *Yersinia*, which is responsible for causing several diseases in humans, including the plague (Cornelis et al. 1998). The goal of this work is: (1) to understand how interaction with actin leads to the activation of kinase activity of YpkA/YopO; (2) to determine the mechanism behind actin isoform-specific preference of YpkA/YopO; (3) to identify major substrates of the kinase activity of YpkA/YopO; (4) to determine the relative contributions of the GDI domain and the kinase domain on the disruption of the actin cytoskeleton; and (5) to reconcile the mechanism of action of YpkA/YopO in the larger context of *Yersinia* pathogenesis.

Chapter 2

Experimental procedures

2.1 Molecular biology methods

Ligation-independent cloning (Aslanidis & De Jong 1990) was used for cloning into the pSY5 vector, refer to **Table 2.1** for list of genes. The insert and vector were amplified via the polymerase chain reaction (PCR) using primers designed with specific extensions to generate complementary overhangs between the inserts and vectors. KOD Hot Start DNA Polymerase (Merck) was used to amplify both the insert and vector. Following PCR amplification, the products were analysed by agarose gel electrophoresis and confirmed to have successful amplification of the desired product. The PCR products were then purified using a PCR purification kit (Qiagen). Both the purified insert and vector were then treated with T4 DNA polymerase in NEB buffer 2 (New England Biolabs) (10mM Tris-HCl (pH 7.9), 50mM NaCl, 10mM $MgCl_2$, 1mM DTT). The 3'->5' exonuclease activity of the T4 DNA polymerase enables the generation of single strand overhangs in both the insert and vector. The T4 DNA polymerase treatment was supplemented with a specific nucleotide to cause the exonuclease to stall at the first base that the enzyme encounters that is the same as the supplemented nucleotide, thus conferring control over the length of the single strand overhang. The T4 DNA polymerase-digested insert and vector with complementary overhangs were mixed and allowed to anneal for a couple of minutes. The resultant mix of vector and insert was then transformed into *Escherichia coli* (*E.coli*) DH5α bacterial cells. For cloning into pOPIN vectors, In-Fusion^{TM} cloning (Clontech) was used following the published protocol (Berrow

et al. 2007). Multiple mutations to YopO constructs were generated using overlap extension ligation-independent cloning (Higuchi et al. 1988). YopO constructs containing single and double mutations were created using Quikchange™ site directed mutagenesis (Agilent technologies), following the manufacturer's recommendations.

2.2 Constructs, vectors and *E.coli* strains

Most genes were cloned into N-terminal His tag vectors pOPINF and pSY5. pSY5 was derived from pET-21d (Novagen) while pOPINF was derived from pTriEx2. Both vectors contain an N-terminal His-tag followed by a human rhinovirus 3C protease cleavage site. Other vectors included: pOPINE which contains a non-cleavable C-terminal His-tag; a modified pGEX-4T1 which contains an N-terminal GST tag cleavable by thrombin, with a non-cleavable C-terminal His-tag; and pToomy, modified from pGEX-6P1 to contain an N-terminal GST followed by a human rhinovirus 3C protease cleavage site, and a His-tag followed by a thrombin cleavage site N-terminal to the protein of interest (Narayan et al. 2003). *E.coli* strain DH5α was used for plasmid selection and propagation following molecular cloning. *E.coli* strain BL21*star* (DE3) was used for recombinant expression of proteins in bacteria.

Table 2.1 Table of constructs used for recombinant expression of proteins

Accession number	Constructs	Construct demarcations	Mutations	Vector	*E.coli* strain
NP_783721	YopO wild type	89-729		pOPINF	BL21*star*
	YopO kinase dead mutant (YopO KD)	89-729	D267A, K269A	pSY5	BL21*star*
	YopO non-actin-binding mutant (YopO nAct)	89-729	V374D, T376D, R723A, E727A	pSY5	BL21*star*
	YopO K245M	89-729	K245M	pSY5	BL21*star*
	YopO non-Rac binding mutant (YopO nRac)	89-729	Y588A, N592A, E596A	pSY5	BL21*star*
	YopO non-Rac binding, kinase dead mutant (YopO nRacKD)	89-729	D267A, K269A, Y588A, N592A, E596A	pSY5	BL21*star*
	YopO SER mutant 2AA	89-729	K152A, K154A, Q155A, K440A, K441A	pOPINF	BL21*star*
	YopO SER mutant 2AY	89-729	K152A, K154A, Q155A, K440Y, K441Y	pOPINF	BL21*star*
	YopO SER mutant 1AA	89-729	K205A, E206A, E207A, K440A, K441A	pOPINF	BL21*star*
	YopO SER mutant 1AY	89-729	K205A, E206A, E207A, K440Y, K441Y	pOPINF	BL21*star*
	YopO SER mutant 2YA	89-729	K152Y, K154Y, Q155Y, K440A, K441A	pOPINF	BL21*star*
	YopO SER mutant 2YY	89-729	K152Y, K154Y,	pOPINF	BL21*star*

			Q155Y, K440Y, K441Y		
	YopO SER mutant 1YA	89-729	K205Y, E206Y, E207Y, K440A, K441A	pOPINF	BL21*star*
	YopO SER mutant 1YY (YopO 1YY)	89-729	K205Y, E206Y, E207Y, K440Y, K441Y	pOPINF	BL21*star*
AAA37164	mouse β-actin	1-377		pOPINF and pOPINE	Sf9 cells
AAA36486	Profilin	1-140		pSY5	BL21*star*
NP_003361	VASP	1-380		pSY5	BL21*star*
NP_057421	EVL	1-416		pSY5	BL21*star*
P06396.1	gelsolin	1-782		pSY5	*Rosetta*
P06396.1	gelsolin G4-6	412-745		pToomy (modified pGEX-6P1#)	BL21*star*
NP_031884.1	diaphanous 1 domains FH1-FH2	586-1154		Modified pGEX-4T1^	*Rosetta*
P42768.4	WASP PWA	160-502		Modified pGEX-4T1^	*Rosetta*
NP_001243068	CapG	1-348		pSY5	BL21*star*
NP_032997.3	twinfilin1	1-349		pSY5	BL21*star*

The vector was modified to include an eight-histidine tag followed by a thrombin-cleavage site upstream of the gene of interest.

^ The vector was modified to include a six-histidine tag at the C-terminus of gene of interest to complement the GST-tag at the N-terminus of the gene of interest.

2.3 Transformation and plasmid selection

Products from ligation-independent cloning, In-Fusion™ cloning and overlap extension ligation-independent cloning were introduced into DH5α bacteria cells by chemical transformation. 5 μl or 20 – 50 ng of DNA was added to 50 μl of chemically competent DH5α bacteria which has been pre-thawed on ice. The DNA-competent cell mix was allowed to incubate on ice for 30 mins in a polypropylene round-bottom culture tube and then heat-shocked in a 42 ^{o}C water bath for 45 seconds, and returned to ice for 2 minutes. 500 μl of Luria-Bertani (LB) media was added and the cells were allowed to recover for 1 hour at 37 ^{o}C. 150 μl of the bacteria-media mix was plated on LB agar supplemented with antibiotics (100 μg/ml ampicillin for plasmids pSY5, pGEX-4T1 and pToomy; and 50 μg/ml ampicillin for pOPINF). Plates were inverted and incubated overnight at 37 ^{o}C.

Successful cloning generates at least 30 colonies per LB agar plate. A few colonies were randomly picked and used to inoculate 5 ml of LB media with antibiotics. The cultures were allowed to propagate with vigorous agitation overnight at 37 ^{o}C and used for miniprep (Qiagen) following manufacturer's recommendations. The purified DNA is subjected to sequencing analysis to verify the DNA sequence.

2.4 Recombinant expression of mouse β-actin from baculovirus infection of Sf9 cells

Gene coding for mouse β-actin was cloned into N-terminal His tag vector pOPINF and C-terminal His tag vector pOPINE via In-Fusion^{TM} (Clontech). A stop codon was inserted at the end of the gene to terminate translation before the C-terminal His-tag in pOPINE so that β-actin would be untagged. Constructs were verified via DNA sequencing. Sf9 cells were then transfected with the recombinant bacmid DNA using Cellfectin reagent (Invitrogen) following **section 2.4.1**. The resultant baculovirus stocks were amplified to required volume and titer and added to Sf9 cells at a multiplicity of infection of 2 following **section 2.4.2**. Infected Sf9 cells were harvested after 3 days and the expression of mouse β-actin was confirmed by analysis with SDS-PAGE.

2.4.1 Transfection of Sf9 cells with recombinant bacmid DNA

1 x 10^6 Sf9 cells in 2ml of SF900II SFM (Invitrogen) were seeded onto each well of a 6-well flat bottom cell culture plate and allowed to attach for 30 minutes at 28 ^oC. In a 1.5ml tube, 100 µl of SF900II SFM without antibiotics was added to 2 µg of plasmid DNA containing the gene of interest and 2ul of baculovirus DNA (Sapphire^{TM}). In a separate tube, 100 µl SF900II SFM without antibiotics was added to 6 µl of Cellfectin reagent (Invitrogen). The two mixtures were combined and mixed to form lipid-DNA complexes and allowed to incubate for 30 minutes at room temperature. The seeded Sf9 cells were washed once with 2ml of SF900II SFM without antibiotics and the media was removed. The mixture containing lipid-DNA complexes were diluted in 800 µl of SF900II SFM and then added to the seeded Sf9

cells. The cells were incubated at 28 ^{o}C overnight and the transfection mixture was removed and 2 ml of SF900II SFM containing penicillin/streptomycin (30µg/ml sodium benzylpenicillin, 50µg/ml streptomycin sulphate) was added. The cells were incubated at 28 °C for 72 hours. The cell culture medium was harvested and typically contained baculovirus of titer 1 x 10^6 to 1 x 10^7 pfu/ml.

2.4.2 Baculovirus amplification and infection of Sf9 cells for expression of recombinant protein

For amplification, 1 ml of the viral stock from **Section 2.5** was added to 50ml of SF900II SFM (with penicillin/streptomycin) containing 2 x 10^6 cells/ml, in a 1 L flask and incubated at 28°C, with shaking at 150 rpm. The medium is harvested after 72 hours and typically contained baculovirus of titer about 1 x 10^9 pfu/ml.

For production of recombinant protein, baculovirus is added to Sf9 cells at a density of 2 x 10^6 cells/ml with a multiplicity of infection of 2 and incubated at 28°C with shaking at 150rpm. After 3 days, cells were harvested by centrifugation for 5 mins at 1000 x *g*. The expression of recombinant protein was confirmed by analysis with SDS-PAGE.

2.5 Purification of recombinant mouse β-actin from Sf9 cells

Expression of N-terminal His-tagged β-actin in pOPINF was very poor as compared to untagged β-actin in pOPINE. As such, untagged β-actin was expressed and purified following the established protocol (Ohki et al. 2009). GST-His-gelsolin domains 4-6 in the modified pGEX-6P1 vector (includes an eight-histidine tag followed by a thrombin-cleavage site upstream of the gene of interest) was expressed in *E.coli* strain BL21*star* (Invitrogen) and purified via Ni^{2+} affinity and size exclusion chromatography (Superdex 200, GE Healthcare) in the presence of 2 mM $CaCl_2$ for stability and frozen in aliquots. Sf9 cells expressing β-actin were resuspended in 10 mM Hepes, 5 mM $CaCl_2$, 1 mM ATP, 50 mM KCl and protease inhibitors (1 tablet per 50 ml) and lyzed using a Potter-Elvehjem homogenizer. Purified G4-6 was added to Sf9 cell lysate and allowed to incubate overnight. The lysate was then clarified via centrifugation at 30,000 x *g* for 1 hour. Imidazole was added to the lysate to a final concentration of 20 mM prior to applying the lysate to equilibrated Ni^{2+} sepharose beads. After incubation for 1 hour at 4^oC, beads were then washed with 10 mM Hepes (pH 7.6), 50 mM KCl, 1 mM ATP, 20 mM Imidazole followed by 10 mM Hepes (pH 7.6), 50 mM KCl, 1 mM ATP. Actin was eluted from G4-6 via the chelation of $CaCl_2$, using buffer 50 mM KCl, 10 mM Hepes (pH 7.6), 0.1 mM EGTA, 7 mM β-mercaptoethanol. The purified actin was then polymerized by the addition of 2 mM $MgCl_2$ and 0.2 mM ATP and incubated for 2 hours at 4^oC. The polymerized actin was pelleted via centrifugation at 80,000 x *g* for 2 hours at 4^oC. The actin pellet was then allowed to depolymerize via dialysis into 2 mM Tris (pH 7.6), 0.2 mM ATP, 0.5 mM DTT, 0.2 mM $CaCl_2$ over three days with daily buffer changes. The protein solution was then clarified via centrifugation for 2 hours at 16,000 x *g* at 4^oC. The yield of actin is approximately 8 mg/L of media.

2.6 Purification of native Sf9 actin from insect cells

Native Sf9 actin was purified from Sf9 cells similarly to purification of recombinant mouse β-actin from Sf9 cells, except that Sf9 cells were not infected with baculovirus and were allowed to grow to a higher cell density of 0.8 – $1x10^7$ cells per ml prior to harvesting. Approximately 4 mg of actin can be purified from each litre of media.

2.7 Expression and purification of YopO constructs

The following protocol was used for expression and purification of all YopO constructs. Cells were induced for recombinant protein expression at mid log phase of OD_{600} 0.4-0.8 with 0.2 mM IPTG at 15^oC for 16 hours and harvested via centrifugation at 4000 x *g* at 4°C for 40 min. YopO was poorly soluble and induction with low concentrations of IPTG at low temperatures improved the yield of soluble protein. The cell pellet was then resuspended in 50 mM Tris (pH 7.6), 500 mM NaCl, 20 mM Imidazole, 5% glycerol, 0.1% Triton-X, 0.5 mg/ml lysozyme, protease inhibitor tablets (1 per 50 ml). The cells were lyzed via sonication with 30 bursts of 10 seconds on ice, with 20 seconds intervals in between, at an amplitude of 35% using a Vibra-Cell™ ultrasonic processor (Sonics & Materials Inc). The cell lysate was clarified via centrifugation at 30,000 x *g* for 30 min and passed through a 0.45 μm syringe filter. The filtered supernatant was loaded on a HisTrap FF 1 ml (GE healthcare) equilibrated with 50 mM Tris (pH 7.6), 500 mM NaCl, 20 mM Imidazole and then cleaved on-column with human rhinovirus 3C protease overnight. The protein was then subjected to size exclusion chromatography (Superdex 200pg, GE Healthcare) equilibrated in 10 mM Hepes (pH 7.6), 100 mM NaCl.

2.8 Preparation of YopO-actin and YopO-actin-profilin complexes

YopO was mixed with actin at a molar ratio of 1:1.5 then purified by size exclusion chromatography (Superdex 200pg) at 4^{o}C in 10 mM Hepes (pH 7.6), 50 mM NaCl. Column fractions containing YopO-actin complex as analyzed by SDS-PAGE were pooled and dialyzed into 2 mM Tris (pH 7.6), 0.2 mM ATP, 0.5 mM DTT, 0.2 mM $CaCl_2$ at 4^{o}C overnight and then concentrated to approximately 10 mg/ml. Similarly YopO was mixed with actin and profilin at a molar ratio of 1:1.5:2 then purified by size exclusion chromatography Superdex 16/60 200pg at 4^{o}C in 10 mM Hepes (pH 7.6), 50 mM NaCl. Column fractions containing the complex of YopO-actin-profilin, as analyzed by SDS-PAGE, were pooled and dialyzed into 2 mM Tris (pH 7.6), 0.2 mM ATP, 0.5 mM DTT, 0.2 mM $CaCl_2$ at 4^{o}C overnight and then concentrated to approximately 10 mg/ml.

2.9 Crystallization trials for YopO-actin and YopO-actin-profilin complexes

The Pre-Crystallization Test (PCT, Hampton Research) was used to determine appropriate protein concentrations for crystallization. Crystallization conditions screening experiments were carried in 96-well Greiner plates using the sitting drop vapour diffusion method as described (Walter et al. 2005). A number of commercially available crystallization screens were used for the initial screening trials. The drops were set by dispensing either 200 nl or 100 nl of mother liquor on top of 100 nl of protein sample on the crystallization platform in each well using a Cartesian robot (Genomic Solutions) and sealed and left to equilibrate against 100 µl of mother liquor. Plates were stored at either 21 ^{o}C or 6 ^{o}C in the plate storage vaults

where images of the crystallization experiments were taken automatically following a schedule defined by the Oxford Protein Production Facility UK, University of Oxford (OPPF).

2.9.1 Crystallization hits of YopO-actin

Crystal hits were observed in a number of conditions after five to eight days, in 10% PEG 10,000, 0.1 M BIS-TRIS (pH 6.5), 0.2 M Na/K tartrate tetrahydrate; 12% PEG 8000, 0.1 M Na phosphate (pH 6.5); and 15% ethanol, 0.1 M trisaminomethane-chloride (TRIS-HCl) (pH 8) at 6^{o}C. Additive screening (Hampton Research) and microseeding against varying concentrations of PEG and pH were used to improve crystal morphology (Benvenuti & Mangani 2007).

2.9.2 Crystallization hits of YopO-actin-profilin

Crystal hits were obtained in one condition after five days, in 0.02 M Na formate, 0.02 M NH_4 acetate, 0.02 M Na citrate, 0.02 M Na/K tartrate, 0.02 M Na oxamate; 0.1 M Imidazole-MES (acid) (pH 6.5), 10% PEG 4000, 20% glycerol at 6^{o}C. Varying concentrations of PEG and pH were used to improve crystal morphology (Benvenuti & Mangani 2007).

2.10 Methylation of YopO and preparation of complexes with methylated YopO

YopO was subjected to reductive methylation of lysines (Walter et al. 2006). Briefly, 100 µl of freshly prepared 1 M dimethylamine-borane complex (ABC) and 200 µl of 1M formaldehyde were added to 5 ml of YopO at 1 mg/ml in 50mM Hepes (pH7.5), 250mM NaCl and allowed to incubate at 4 ^{o}C. After 2 hours, a further 100 µl of 1 M ABC and 200 µl of 1M formaldehyde were added and the incubation was continued for 2 hours. Thereafter, a final of 50 µl of ABC was added and the reaction was allowed to incubate overnight at 4 ^{o}C. The mixture was filtered through a 0.2 µm syringe filter (Sartorius) and purified by size exclusion chromatography. Methylated YopO was used to prepare YopO-actin and YopO-actin-profilin complexes and set up for crystallization similarly to wild type YopO. Complexes with methylated YopO eluted at similar elution volume as complexes containing the unmethylated versions.

2.11 Dehydration and in loop annealing of YopO-actin crystals

The YopO-actin crystals were subjected to dehydration via sequential addition to the crystal droplet of a stronger dehydrating solution followed by a 16 hour equilibration against the same dehydrating solution. The same protocol was repeated over a few days until the concentration of PEG has been doubled or tripled. For instance, crystals in 8% PEG 10,000 0.2 M Na/K phosphate (pH 6.9) were sequentially dehydrated to 25% PEG 10,000, 0.2 M Na/K phosphate (pH 6.9) over five days and crystals in 10% PEG 10,000, 0.1 M BIS-TRIS (pH 6.5), 0.2 M Na/K tartrate tetrahydrate were dehydrated to 25% PEG 10,000, 0.1 M BIS-TRIS (pH 6.5),

0.2 M Na/K tartrate tetrahydrate over three days. In loop annealing was performed at the synchrotron while the crystal was mounted and involved blocking the cryostream for a few seconds, allowing the solution containing the crystal to thaw, followed by refreezing in the cryostream.

2.12 Data collection and processing for YopO-actin crystals

Crystals were cryo-protected by passing them through reservoir solution doped with 25% glycerol before flash freezing in liquid nitrogen. YopO-actin crystals were tested at the Diamond Light Source, Oxfordshire, UK at beamline IO3. Due to poor crystal diffraction, data sets were not collected.

2.13 Crystallization of YopO SER mutants-actin

YopO-actin complexes with YopO SER mutants 2AA (K152A, K154A, Q155A, K440A, K441A) and 1YY (K205Y, E206Y, E207Y, K440Y, K441Y) were prepared and crystallized similarly to YopO WT except that actin of the Sf9 isoform was used instead of mouse β-actin, since the native Sf9 actin preparation is isoform-homogenous. Crystal hits were obtained for YopO 1YY-actin in a number of conditions, including 30% PEG 400, 0.2 M sodium chloride, 0.1 M Hepes (pH 7.5); 0.1 M Tris pH 8.0, 30% PEG 400; 0.8 M ammonium sulphate, 0.1 M Hepes (pH 7.0) after five to seven days at 6^{o}C. Additive screen (Hampton Research) and microseeding against varying concentrations of PEG and pH were used to improve crystal morphology (Benvenuti & Mangani 2007).

2.14 Data collection and processing for YopO 1YY-actin crystals

Crystals grown in 0.1 M Hepes (pH 7.5), 30% PEG 400, 0.2 M NaCl were subjected to data collection. Crystals were cryo-protected by passing them through reservoir solution doped with 25% glycerol before flash freezing in liquid nitrogen. Initial X-ray diffraction data for YopO 1YY-actin crystals that diffracted to 2.9 Å were collected on beamline I04 at Diamond Light Source, Oxfordshire, UK. A subsequent dataset from crystals optimized with seeding, with improved resolution of 2.65 Å were collected at the National Synchrotron Radiation Research Center, Taiwan (NSRRC). At the NSRRC, data were collected using an Area Detection Systems Corporation Quantum 315 CCD detector ADSC Q315 3x3 CCD detector on beamline BL13B1. The wavelength was set to 1 Å and the data collected at 105 Kelvin. Each image covered an oscillation of 1^{o} and exposure times were about 45-

60 seconds.

2.15 Crystallographic software

Crystallographic data were indexed, integrated and scaled using HKL-2000 suite of software (Otwinowski & Minor 1997) at the NSRRC and using Xia2 (Winter et al. 2013; Kabsch 1993) at Diamond Light Source. Molecular replacement was performed using Phaser as part of the PHENIX suite of crystallographic programs (Zwart et al. 2008). Autobuilding of the model was performed with Mr_Rosetta (Terwilliger et al. 2012). Density modification was performed using Parrot (Cowtan 2010). Restrained positional and B-factor refinement were performed using Phenix.refine (Afonine et al. 2012). Manual building was performed using graphics program COOT (Emsley et al. 2010). The MolProbity server (http://molprobity.biochem.duke.edu/) and validation tools present in COOT were used to assess the quality of the model in the refinement of the structure.

2.16 Homologous sequence alignment and structural analysis

Protein-protein interfaces within the crystal structures were analyzed by PDBePISA (http://www.ebi.ac.uk/msd-srv/prot_int/). Images of protein models were generated by PYMOL (http://pymol.sourceforge.net). Amino acid sequence analysis between homologous proteins performed using using FFAS (Fold function assignment server) (Jaroszewski et al. 2011) and Clustal Omega (www.ebi.ac.uk/Tools/msa/clustalo/). Surface entropy mutations designed using the Surface Entropy Reduction prediction (SERp) server (http://services.mbi.ucla.edu/SER/). Selected sequence alignments were presented

using BOXSHADE (http://www.ch.embnet.org/software/BOX_form.html). Figures from normal mode analysis of YopO were generated using Visual Molecular Dynamics (VMD) (www.ks.uiuc.edu/Research/vmd/). To predict flexible hinges in YopO, programs HingeProt (http://www.prc.boun.edu.tr/appserv/prc/hingeprot/) and Elnemo (http://www.igs.cnrs-mrs.fr/elnemo/) were used.

2.17 Biochemical studies

2.17.1 Actin polymerization assay using pyrene-labelled actin

Rabbit muscle α-actin was prepared from rabbit skeletal acetone powder following (Spudich & Watt 1971). Pyrene-labelled G-actin was prepared (Kouyama & Mihasi 1981), through conjugating purified rabbit muscle α-actin with N-(1-pyrene) iodoacetamide at Cys-374. Upon polymerization, pyrene-labelled actin's fluorescence intensity is enhanced by about 25 times at 407 nm (excitation at 365 nm), providing real time readout for kinetics of polymerization. Where indicated, 1.8 μM human cytoplasmic G-actin, Sf9 G-actin, or rabbit skeletal muscle G-actin were mixed with 0.2 μM pyrene-labelled actin in buffer A (2 mM Hepes (pH7.6), 0.2 mM ATP, 0.5 mM DTT, 0.1 mM $CaCl_2$, 1 mM Na azide). YopO or YopO mutants were added at indicated ratios and reactions were equilibrated for 10 minutes prior to inducing polymerization with the addition of 10 μl of 10 times KMEI polymerization buffer (500 mM KCl, 10 mM $MgCl_2$, 10 mM EGTA, 100 mM Imidazole-HCl (pH 7.0)). The reactions were incubated in 96-well, black, flat-bottomed plates (Corning, NUNC), with total volume in each well of 100 μl and the fluorescence intensities were measured kinetically at wavelength 407 nm after excitation at 365 nm using a Safire2 fluorimeter (Tecan).

2.17.2 *In vitro* kinase assays

3 - 10 μg of YopO, or YopO mutants, were mixed with an equimolar ratio of G-actin in the presence or absence of an equimolar ratio of substrates and/or three molar ratio of gelsolin G1 or profilin, the volume was adjusted to 10 μl with buffer A

(2 mM Hepes, 0.2 mM ATP, 0.5 mM DTT, 0.1 mM $CaCl_2$, 1 mM Na azide). An equal volume of kinase buffer containing 20 mM Hepes (pH 7.6), 1.0 mM ATP, 1 mM DTT, 10 mM $MgCl_2$, 2 mM $MnCl_2$ was added and supplemented with 5 μCi of [γ-^{32}P]ATP (Perkin Elmer). The phosphorylation reactions were allowed to take place for 30 min at 30 °C. Where indicated, human cytoplasmic G-actin, Sf9 G-actin, or rabbit skeletal muscle G-actin were used. As WASP PWA migrated at the same rate on SDS-PAGE as YopO, WASP PWA was subjected to cleavage with thrombin (GE Healthcare) overnight at 4^{o}C. The reactions were terminated by the addition of SDS-PAGE sample buffer and heating for 5 min at 95 °C. Radioactivity in dried SDS-PAGE gels was visualized by exposure to X-ray film.

2.18 SILAC (Stable isotope labelling by amino acids in cell culture)

2.18.1 Metabolic labeling of Raw264.7 cells and lysate preparation

Macrophages have been characterised as a key target of *Yersinia* so the Raw264.7 mouse leukemic monocyte macrophage cell line was selected. All isotopically-labelled amino acids were from Cambridge Isotope Laboratories. Raw264.7 cells were grown in SILAC Dulbecco's Modified Eagle's Medium (DMEM) (Thermo Scientific) supplemented with 10% fetal calf serum, 1% penicillin and streptomycin and either heavy isotopic ^{13}C-arginine and ^{13}C-lysine or normal isotopic ^{12}C-arginine and ^{12}C-lysine. Both cell populations are passaged for at least five cell doublings to allow full isotope incorporation and then expanded to the required cell numbers. In each pull down setup, about $1x10^8$ cells were used. Cells were lyzed in 50 mM Hepes (pH 7.6), 150 mM NaCl, 1% NP40, 5% glycerol, protease inhibitor cocktail (Roche, 1 tablet per 50ml), phosphatase inhibitor tablets (Pierce, 1 tablet per 10 ml). Lysate was clarified by centrifugation at 30,000 x *g* for 30 mins at 4^{o}C. Approximately 12 mg of total protein in the lysate was used in each heavy or light setup as determined by bicinchoninic acid protein assay (Pierce).

2.18.2 Identification of proteins that bind to YopO, profilin and YopO nRac mutant

The pull down experimental conditions were as follows: YopO (heavy) against empty beads (light) (**Section 4.1.1**); profilin (heavy) against empty beads (light) (**Section 4.1.2**); and YopO non-Rac binding mutant (YopO nRac) (heavy) against empty beads (light) (**Section 4.1.3**). 80 µl of Ni-NTA agarose beads (Qiagen)

was incubated with the respective bait (3 mg) for 1 hour at 4^{o}C and then washed to remove the unbound bait. Agarose beads saturated with the baits were incubated with heavy lysate (~12 mg) for 4 hours at 6^{o}C, and in parallel, an equal volume of empty beads were incubated with light lysate (~12 mg) and then subjected to several washes with 50 mM Hepes (pH 7.6), 150 mM NaCl, 1% NP40, 5% glycerol. Elution of the bait and bound proteins was performed by overnight cleavage by 3C protease at 4^{o}C. Samples eluted from both heavy and light setups were then mixed in an equal ratio, ran on the SDS-PAGE and submitted for mass spectrometry.

2.18.3 Mass Spectrometry

All trypsin digests, mass spectrometry and peptide/protein/phosphorylation searches were carried out by the Sanford-Burnham Proteomics Facility (La Jolla, California). Samples were submitted to the facility either as SDS-PAGE gels or in solution shipped on dry ice.

2.18.4 1D LC/MS/MS protein identification

SDS-PAGE gels were stained with Coomassie blue and the gel lanes were divided into five or three slices, as indicated, and subjected to complete destaining and then were dried down. Protein samples were subjected to reduction, alkylation and trypsin digestion in the gel. Peptides were extracted and desalted using ZipTip pipette tips (Millipore) and then run on the Thermo LTQ OrbiTrap XL (Thermo Scientific).

2.18.5 Analysis of spectra using protein database searches

Protein identification was achieved by searching the tandem mass spectrometry spectral data against the mouse non-redundant protein database using SEQUEST. In parallel, the mass spectrometry spectral data was used to search against a decoy database (*i.e.* database of sequences known to be incorrect), which gave an estimated false positive rate of about 1.3% average across the datasets. Heavy and light peptides were differentiated using their isotropic differences, heavy Lys has a differential atomic mass unit (amu) of 8 and heavy Arg of 10. Heavy over light ratios were then calculated by averaging its associated peptide ratios. Searches were also performed to identify post-translational modifications such as phosphorylation, which has a differential amu of 80.

2.19 Expression and purification of kinase substrates (VASP, EVL, CapG, gelsolin, twinfilin1, Dia1 FH1-FH2 and WASP PWA)

The following protocol was used for the expression and purification of VASP, EVL, CapG and gelsolin. These constructs are in the pSY5 vector, which includes an N-terminal His-tag followed by a 3C protease cleavage site. Cells were induced for recombinant protein expression at mid log phase of OD_{600} 0.4-0.8 with 0.2 mM IPTG at 15 ^{o}C for 16 hours for VASP; 1 mM IPTG at 15 ^{o}C for 16 hours for EVL and 1 mM IPTG at 25 ^{o}C for 16 hours for gelsolin and CapG. Cells were then harvested via centrifugation at 4000 x *g* at 4 °C for 40 min. Cell pellets were then resuspended in 50 mM Tris (pH 7.6), 500 mM NaCl, 20 mM Imidazole, 5% glycerol, 0.1% Triton-X, 0.5 mg/ml lysozyme, protease inhibitor tablets (1 per 50 ml). The cells were lyzed via sonication with 30 bursts of 10 seconds on ice, with 20 seconds intervals in between, at amplitude of 35% using a Vibra-Cell^{TM} ultrasonic processor (Sonics & Materials Inc). The cell lysate was clarified via centrifugation at 30,000 x *g* for 30 min and passed through a 0.45 μm syringe filter. The filtered supernatant was loaded on a HisTrap FF 1 ml (GE healthcare) equilibrated with 50 mM Tris (pH 7.6), 500 mM NaCl, 20 mM Imidazole and then cleaved on-column with 3C protease overnight. The protein was then subjected to size exclusion chromatography (Superdex 200pg, GE Healthcare) using 10 mM Hepes (pH 7.6), 100 mM NaCl for VASP, EVL and CapG, and supplemented with 1 mM EGTA for gelsolin.

Dia1 FH1-FH2 and WASP PWCA were encoded in the pGEX4T1 vector, which includes an N-terminal GST-tag followed by a thrombin cleavage site. The vector was modified to include a His-tag at the C-terminus of the protein of interest.

These constructs were gifts (Maiti et al. 2012). The following protocol was used for expression and purification of Dia1 FH1-FH2 and WASP PWCA. Cells were induced for recombinant protein expression at mid log phase of OD_{600} 0.4-0.8 with 0.2 mM IPTG at 15^{o}C for 16 hours and harvested via centrifugation at 4000 x *g* at 4°C for 40 min. Cell pellet was then resuspended in 50 mM Tris (pH 7.6), 200 mM NaCl, 5% glycerol, 0.1% Triton-X, 0.5mg/ml lysozyme, protease inhibitor tablets (1 per 50 ml). The cells were lyzed via sonication with 30 bursts of 10 seconds on ice, with 20 seconds intervals in between, at amplitude of 35% using a Vibra-Cell^{TM} ultrasonic processor (Sonics & Materials Inc). The cell lysate was clarified via centrifugation at 30,000 x *g* for 30 min and passed through a 0.45 μm syringe filter. The filtered supernatant was loaded on a GSTrap FF 5 ml (GE healthcare) equilibrated with 50 mM Tris (pH 7.6), 200 mM NaCl, and then eluted with 50 mM Tris (pH 7.6), 200 mM NaCl, 100 mM reduced glutathione and then dialyzed into 50 mM Tris (pH 7.6), 200 mM NaCl overnight. The protein was then applied to HisTrap FF 1 ml (GE healthcare) equilibrated with 50 mM Tris (pH 7.6), 500 mM NaCl, 20 mM Imidazole and eluted with 50 mM Tris (pH 7.6), 500 mM NaCl, 500 mM Imidazole and then dialyzed into 10 mM Hepes (pH 7.6), 100 mM NaCl overnight. The proteins were kept with their GST tags intact as cleavage removal of the GST tags prompted precipitation of Dia1 FH1-FH2 and WASP PWA.

Chapter 3

Structure of the YopO-actin complex

3.1 Preparation of YopO, β-actin, profilin and their complexes

Regions of YpkA/YopO that are involved in the interaction with actin have been reported in literature (Trasak et al. 2007). There are two separate actin-binding sites on YpkA/YopO, one in the kinase (89-440) domain and one in the GDI (441-729) domain. Constructs are more soluble in the absence of the membrane localization domain (1-88) (Trasak et al. 2007). In this work, YopO from *Yersinia enterocolitica*, residues 89-729, encompassing the kinase domain and the GDI domain represents the standard construct.

YopO (89-729) was recombinantly expressed with an N-terminal His-tag in *E.coli* and purified via Ni^{2+} affinity resin with on-column tag cleavage by 3C protease, followed by size exclusion chromatography, as described in **section 2.7**. Mouse β-actin was recombinantly expressed in Sf9 cells and purified using gelsolin domains 4-6 following a published protocol (Ohki et al. 2009), briefly described in **sections 2.4**. The complex of YopO and actin was prepared by mixing YopO with mouse β-actin at a molar ratio of 1:1.5 followed by purification using size exclusion chromatography, as described in **section 2.8** (**Fig. 3.1 A & B**). When actin was initially identified as the eukaryotic host factor that activates the kinase activity of YpkA/YopO, profilin was heavily enriched in the same fractions as YpkA/YopO and actin (Juris et al. 2000). Given the possibility that profilin might stabilize YopO-actin interactions, a ternary complex with profilin was also formed. Profilin was

recombinantly expressed with an N-terminal His-tag in *E.coli* and purified similarly to YopO (89-729). The complex of YopO, actin and profilin was prepared by mixing YopO with actin and profilin at molar ratios of 1:1.5:2 followed by purification by size exclusion chromatography (**Fig. 3.1 C & D**). Detailed descriptions of the methods can be found in **sections 2.4-2.8**.

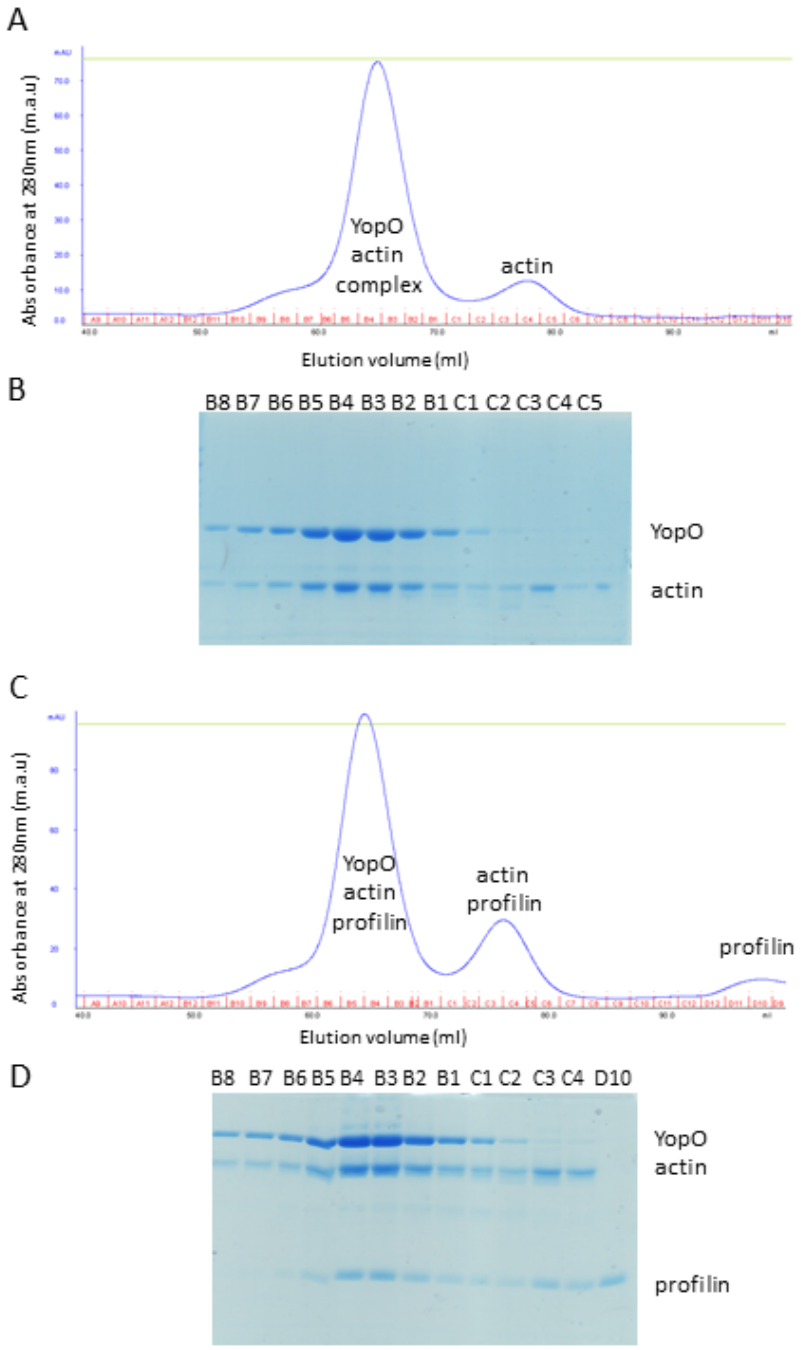
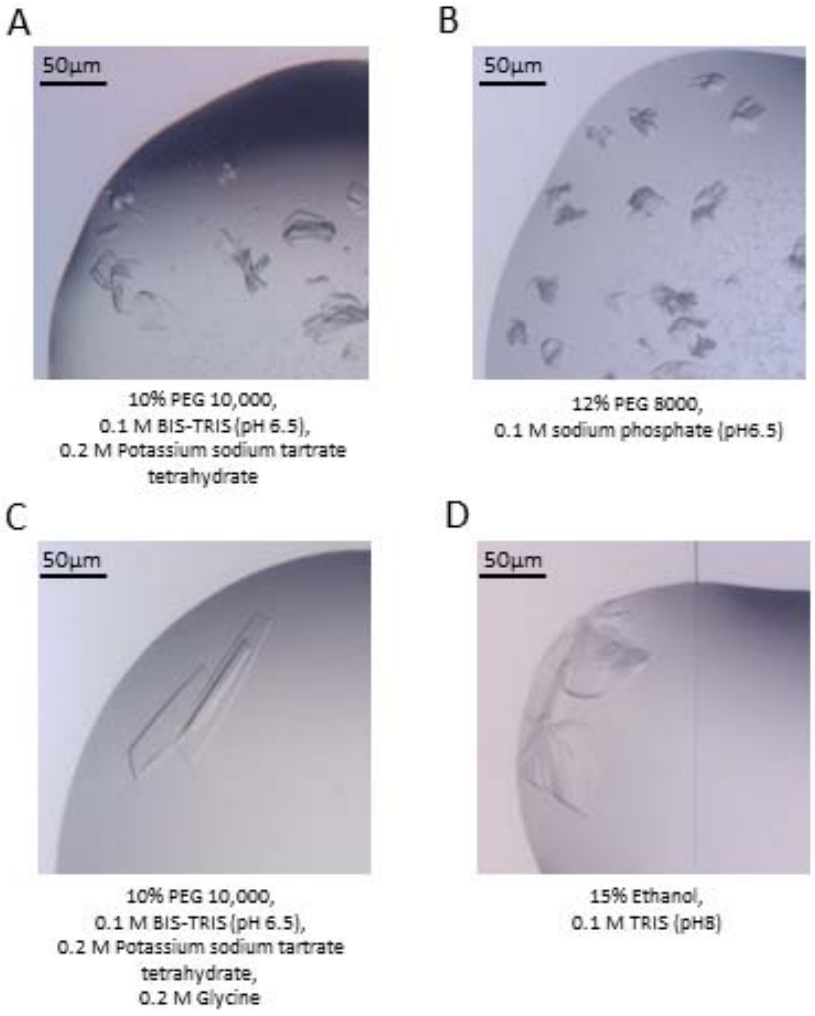


Figure 3.1 Preparation of complexes of YopO-actin and YopO-actin-profilin complexes. (A) The elution profile (A_{280}) from size exclusion chromatography using Superdex 200pg with peaks corresponding to fractions containing YopO-actin complex and excess actin. Fractions are lettered in red at the bottom. (B) SDS-PAGE gel of fractions with fractions named in accordance to elution profile in (A). (C) The elution profile (A_{280}) from size exclusion chromatography using Superdex 200pg with peaks corresponding to fractions containing YopO-actin-profilin complex, actin-profilin complex and excess profilin. Fractions are lettered in red at the bottom. (D) SDS-PAGE gel of fractions with fractions named in accordance to elution profile in (C).

3.2 Crystallization trials of YopO-actin and YopO-actin-profilin complexes

YopO-actin and YopO-actin-profilin were subjected to crystallization trials as described in **section 2.9**. Crystal hits were observed for both YopO-actin and YopO-actin-profilin complexes. YopO-actin crystallized in a number of conditions and crystal hits were optimized via additive screening and microseeding to obtain larger crystals which were analyzed in a synchrotron X-ray beam (**Fig. 3.2**). YopO-actin-profilin crystallized in only one condition and crystals were poorly reproducible. Despite optimization attempts, crystals of sufficient quality for high resolution analysis at a synchrotron were not obtained (**Fig. 3.3**). YopO-actin crystals diffract maximally to 6 to 7 Å. In a bid to improve diffraction quality of these crystals, lysine methylation of YopO and post-crystallization treatments were attempted.



E

	Crystal (C)	Crystal (D)
Space group	C2	P222
Unit cell dimensions (a, b, c) (Å) (α, β, γ) (°)	a=232.24, b=95.56, c=144 α=90, b=101.8, ɣ=90	a=95.325, b=147.90, c=215.99 α=90, b=90, ɣ=90
Resolution	~6Å	~7Å
Solvent content	2 complexes: 64.23% 3 complexes: 46.34%	2 complexes: 62.76% 3 complexes: 44%

Figure 3.2 YopO-actin crystals. The crystal conditions are indicated below each image and a scale bar shown to indicate size. (A) and (B) are crystals obtained from initial screening, which appeared after five days. (C) Crystals obtained from additive screening, with the presence of 0.2 M glycine as an additive. (D) Crystals obtained from initial screening, which appeared after eight days. (C) and (D) were analyzed at the synchrotron. (E) Crystallographic details for YopO-actin crystals from (C) and (D).

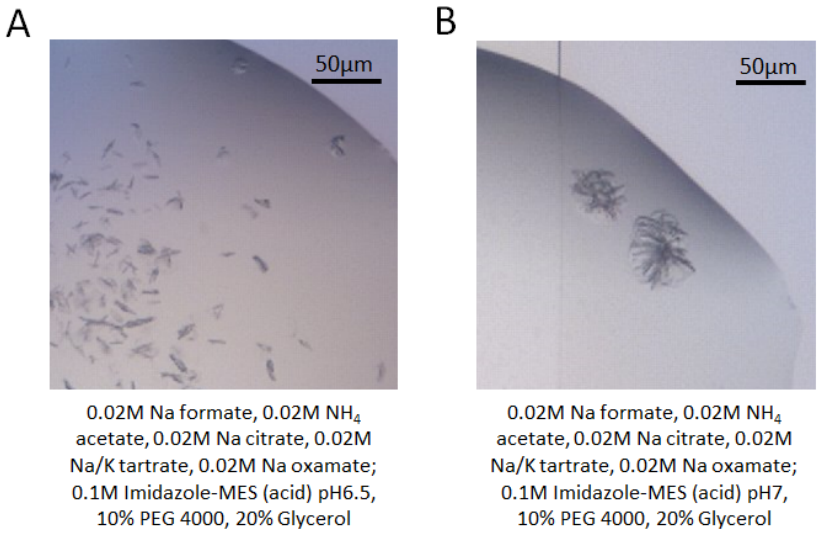


Figure 3.3 Example of YopO-actin-profilin crystals. The crystal conditions are indicated below each image and a scale bar shown to indicate size. (A) Initial crystals obtained (B) Crystals obtained after optimization screening.

3.3 Crystallization trials of YopO-actin and YopO-actin-profilin complexes with methylated YopO

The GDI domain of YopO had been subjected to reductive methylation for successful crystallization (Prehna et al. 2006). Given the possibility that reductive methylation of YopO might improve crystal diffraction, YopO was subjected to reductive methylation and the methylated YopO-actin and methylated YopO-actin-profilin complexes were set up for crystallization. While methylated YopO forms YopO-actin and YopO-actin-profilin complexes similarly to unmethylated versions as observed from the size exclusion chromatography profiles, no crystal hits were obtained for either methylated-YopO-actin or methylated-YopO-actin-profilin. Reductive methylation involves the modification of surface exposed primary amines (lysines and the N-terminus) to tertiary amines. Reductive methylation might have changed surface charges required for stable interaction between YopO and actin. To get around this problem, the YopO-actin complex was subjected to methylation after complex formation. However, the methylation reaction caused actin within the YopO-actin complex to polymerize or precipitate as observed by elution of actin at the void volume during size exclusion chromatography of the methylated complex.

3.4 Post-crystallization treatment of YopO-actin crystals

The Matthews Coefficient suggests that the solvent content of the unit cell of YopO-actin crystals is greater than 60%. Reduction of solvent content has been reported to produce more closely packed and better ordered protein crystals in some cases, improving the resolution of X-ray diffraction patterns (Esnouf et al. 1998; Heras et al. 2003; Heras & Martin 2005). Crystals were subjected to dehydration following the protocol described in **section 2.11** (**Fig. 3.4**). Unfortunately, dehydration did not yield any improvement in resolution of diffraction of the crystals. In addition, crystal annealing was also attempted (Heras & Martin 2005), following the protocol described in **section 2.11**. Annealing for approximately three to five seconds degraded the internal order of the crystals and only very low resolution diffraction (~20 Å) was subsequently observed. The poor ordering of the crystals could be due to the presence of a mixture of actin isoforms within the YopO-actin complex. The actin was derived from recombinant expression of mouse β-actin in Sf9 cells and purified using gelsolin domains 4-6 (G4-6) (Ohki et al. 2009). Sf9 cells contain native Sf9 actin, which would be copurified with the recombinantly expressed mouse β-actin during the interaction with G4-6. To rule out that actin isoform heterogeneity within the crystal is the cause for poor diffraction, native Sf9 actin was purified from Sf9 cells without recombinant expression of exogenous actin genes. Since Sf9 cells contain actin of a single isoform, actin preparation was homogenous within this respect. However, YopO-actin crystals prepared with Sf9 actin had no changes to unit cell, space group or improved diffraction.

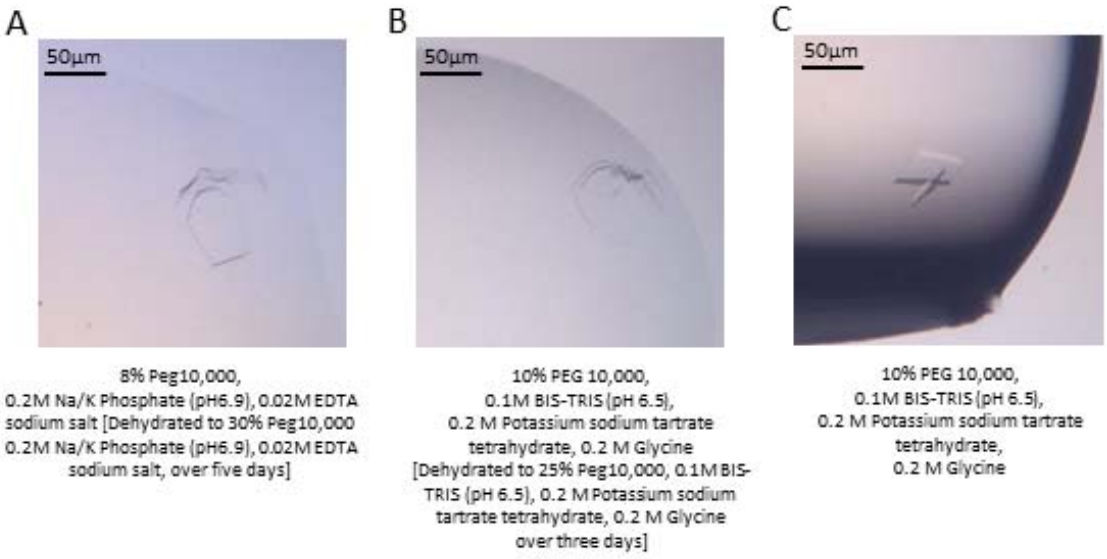


Figure 3.4 Attempts at improving resolution of diffraction of YopO-actin crystals. A scale bar is shown to indicate size. (A) and (B) YopO-actin crystals that have been subjected to dehydration. Images are taken post-dehydration. (C) YopO-actin crystals from native Sf9 actin. The respective crystallization conditions are indicated below each image.

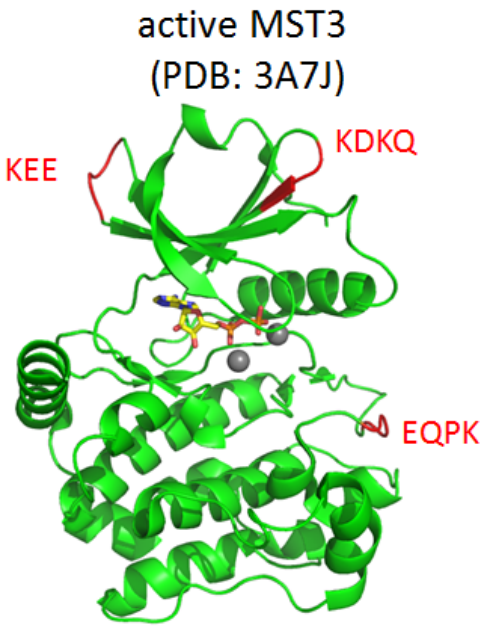
3.5 Surface entropy reduction mutagenesis of YopO

Based on the structure of the GDI domain (434-729) (Prehna et al. 2006) and the demarcation of the kinase domain (102-425) obtained by alignment to homologous serine/threonine kinases, it appears that the two domains are discrete and bound by a linker region. As such, the flexibility of YopO could be the reason for poor ordering of the crystals. Several reports (Bauman et al. 2008; Yip et al. 2005) have shown that new crystal contacts that lead to new crystal forms that have improved crystal diffraction, can be obtained with the replacement of highly entropic (flexible side chains) residues (e.g. lysines and glutamic acids) with residues with low surface entropy (e.g. alanines, serines, tyrosines). Thus 'surface entropy reduction' (Longenecker et al. 2001; Price et al. 2009) was attempted on YopO. The sequence of YopO (89-729) was submitted to the Surface Entropy Reduction

prediction (SERp) server (Goldschmidt et al. 2007) and the software proposed three clusters of favourable mutations, all within the kinase region (**Table 3.1**). The clusters are ranked according to scores which indicate the predicted success. Clusters with scores of 3.0 and above are considered good candidates for mutation. The highest ranking cluster containing three adjacent residues K205, E206, E207 score 7.49, followed by the second and third ranking clusters K152A, K154A, Q155A and E119, Q120, K122 with similar SERp scores of 5.34 and 5.06 respectively. These proposed mutations were modelled onto the structure of MST3 (PDB: 3A7J as aligned by Fold and Function Assignment System server FFAS (Jaroszewski et al. 2011), which confirmed that these residues are found on surface exposed loops (**Fig. 3.5**). One of the clusters (E119, Q120, K122) is on the activation segment of the kinase domain and thus was not selected. Mutations were performed on the other two proposed clusters.

Table 3.1 Cluster candidates proposed by Surface Entropy Reduction prediction (SERp) server. Scores are indicated for residues suitable for mutation.

Cluster #1 K205 => A E206 => A E207 => A	Residues 205-207: KEEA SERp score 7.49
Cluster #2 K152 => A K154 => A Q155 => A	Residues 152-155: KDKQ SERp score 5.34
Cluster #3 E295 => A Q296 => A K298 => A	Residues 295-298: EQPK SERp score 5.06




```
YopO 126 PDLEGMRVAETDKFAEGESHISIIE--TKDKQRLVAKIERSIAEGHLFAELEAYKHIYKT 183
MST3  29 SLDPEELFTKLEKIGKGSFGEVFKGIDNRTQKVVAIKIIDLEEAEDEIEDIQQEITVLSQ  88

YopO 184 AGKHPNLANVHGMAVVPYGNRKEEALLMDEVDGWRCSDTLRSLADSWKQGKINSEAYWGT 243
MST3  89 C-DSPYVTKYYGSYL----KDTKLWIIMEYLGGGSALDLLE-----------PGPLDETQ 132

YopO 244 IKFIAHRLLDVTNHLAKAGIVHNDIKPGNVVFDRASGEPVVIDLGLHSRS-----GEQPK 298
MST3 133 IATILREILKGLDYLHSEKKIHRDIKAANVLLSE-HGEVKLADFGVAGQLTDTQIKRNTF 191

YopO 299 GFTESFKAPELGVGNLGASEKSDVFLVVSTLLHGIEGFEKDPEIKPNQGLRFITSEPAHV 358
MST3 192 VGTPFWMAPEVIK-QSAYDSKADIWSLGITAIELARGEPPHSELHPMKVLFLIPKNNPPT 250

YopO 359 MDENGYPIHRPGIAGVETAYTRFITDILGVSADSRPDSNEARLHEFLSDGTIDEESAKQI 418
MST3 251 LE-----------GNYSKPLKEFVEACLNKEPSFRPTAKELLKHKFILRNAKKTSYLTEL 299

YopO 331 LKDTLTGEMSP 429
MST3 273 IDRYKRWKAEQ 310
```

Figure 3.5 Sites most suitable for mutation proposed by Surface Entropy Reduction prediction (SERp) server. Proposed mutations mapped onto the homologous kinase MST3 (PDB: 3A7J) using the sequence alignment of kinase domain of YopO against MST3 kinase using FFAS. Proposed mutations on the model are displayed in red. Residues within the catalytic loop are displayed in magenta, the activation segment in blue and proposed mutations are shown in red.

Then SER mutations were engineered into the GDI domain. Inspection of the crystal structure of the GDI domain of YopO (Prehna et al. 2006) revealed that Lys440 and Lys441 were surface exposed and could be targeted for surface entropy reduction (**Fig. 3.6**). Previous studies have demonstrated that high-quality crystals could be obtained when mutating surface residues to specific residues with more crystallization-friendly side chains (Cooper et al. 2007). Mutation to alanines removes impediment to crystallization but does not necessarily improve crystal contacts by creating 'sticky patches' (Cooper et al. 2007). On the other hand, tyrosines which play predominant roles in antigen-antibody interfaces (Fellouse et al. 2004) can dramatically enhance the formation of improved crystal contacts. The selected mutagenesis sites were substituted with either alanines or tyrosines, resulting in eight sets of mutants (**Table 3.2**). The mutants were cloned via overlap extension polymerase chain reaction. Upon expression tests, two of the mutants expressed poorly. Three of the remaining mutants were selected for purification and complexed with Sf9 actin following the protocol for wild type YopO as described in **section 2.8**. Sf9 actin was used instead of mouse β-actin, since the Sf9 actin preparation is isoform-homogenous. During size exclusion chromatography of the respective complexes, one of the mutants aggregated, eluting in the void volume. The remaining two mutants form complexes which migrate similarly to the wild type complex on size exclusion chromatography.

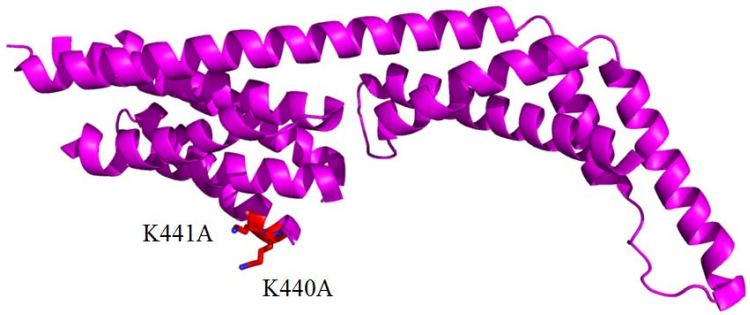


Figure 3.6 Candidate SER mutations Lys440 and Lys441 in the GDI domain (PDB: 2H7O (Prehna et al. 2006)).

Table 3.2 Design, expression, purification and crystallization of surface entropy mutation constructs.

Mutant	Mutations	Expression levels	Selected for purification	Complex survives size exclusion chromatography	Crystal hits
1AA	K205A, E206A, E207A, K440A, K441A	Very good	Yes	Mutant 'aggregates'	-
1AY	K205A, E206A, E207A, K440Y, K441Y	Very good	-	-	-
2AA	K152A, K154A, Q155A, K440A, K441A	Very good	Yes	Yes	No
2AY	K152A, K154A, Q155A, K440Y, K441Y	Good	-	-	-
1YA	K205Y, E206Y, E207Y, K440A, K441A	Good	-	-	-
1YY	K205Y, E206Y, E207Y, K440Y, K441Y	Good	Yes	Yes	Yes
2YA	K152Y, K154Y, Q155Y, K440A, K441A	Poor	-	-	-
2YY	K152Y, K154Y, Q155Y, K440Y, K441Y	Poor	-	-	-

3.6 Crystallization of YopO 1YY-actin

Crystal hits were observed for only one of the mutants YopO 1YY (K205Y, E206Y, E207Y, K440Y, K441Y) with crystals obtained in crystallization conditions that were different to those obtained for the wild type (WT) complex. Crystals formed included thin plates and irregular chunks morphologically similar to those observed for YopO WT-actin as well as a new crystal morphology, cuboid crystals which formed with ammonium sulphate as the precipitant (**Fig. 3.7**). Analysis of the crystals in a synchrotron X-ray beam revealed that the thin plates and irregular chunks diffracted to about 2.9 Å, while the cuboid crystals diffracted at best to 8 Å. As compared to WT YopO-actin crystals, these crystals with improved resolution of 2.9 Å were of a different space group and unit cell and consist of only one complex in each asymmetric unit. From their Matthews Coefficients, the solvent content remains greater than 60%. The unit cell and space group of YopO 1YY-actin crystals can be found in **Table 3.3**.

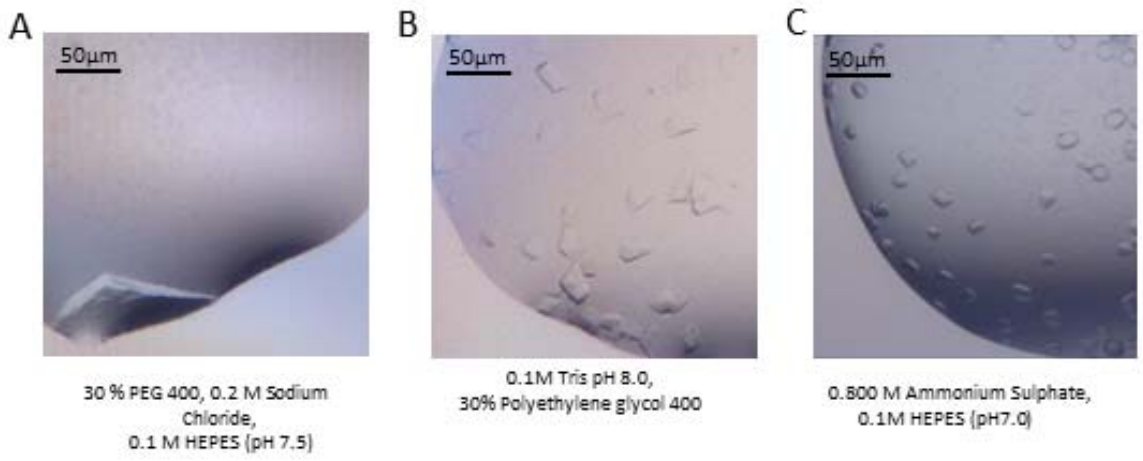


Figure 3.7 Example of YopO SER mutant 1YY-actin crystals. The crystal conditions are indicated below each image and scale bar shown to indicate size. (A) Irregular chunks. (B) Thin plates. (C) Cuboid crystals.

Table 3.3 Unit cell and space group of YopO 1YY-actin crystals.

	YopO 1YY-actin
Space group	$P2_1$
Unit cell	a=70.77, b=121.95, c=89.16, α=90.00, β=94.74, γ=90
Resolution (Å)	2.65 Å
Solvent content	1 complex with 64.0% solvent

3.7 Data collection and processing

The datasets were obtained from crystals grown in 0.1 M Hepes (pH 7.5), 30% PEG 400, 0.2 M NaCl. Initial X-ray diffraction data for YopO 1YY-actin crystals that diffracted to 2.9 Å were collected on beamline I04 at Diamond Light Source, Oxfordshire, UK. A subsequent dataset from optimized crystals, with improved resolution of 2.65 Å was collected at the National Synchrotron Radiation Research Center, Taiwan (NSRRC).

3.8 Structure determination, model building and refinement

The crystal structure of YopO 1YY-actin, using data to 2.65 Å, was solved by molecular replacement using Phaser (McCoy 2007). First, the atomic model of actin (PDB: 3HBT) (Wang et al. 2010) was used as a search model. The obtained solution was subjected to a single cycle of restrained refinement using Phenix.refine and yielded an R_{free} of 0.50. This solution was used for subsequent placement of YopO.

YopO consists of a GDI domain and a kinase domain. The crystal structure of the GDI domain has been solved (PDB: 2H7O (Prehna et al. 2006)). The kinase domain is homologous to a number of eukaryotic kinases that have been structurally

elucidated, though sequence identities as calculated by Clustal Omega are below 25%. The PDB file from the earlier molecular replacement solution with actin placed was used as a partial solution for the molecular replacement of the GDI domain. However, Phaser was unable to find solutions with translation function Z-score (TFZ) of greater than eight. The molecular replacement possibly failed due to the search model being dissimilar to the structure of the GDI domain in the crystal. The GDI domain could have undergone conformational changes upon binding to actin. Normal mode analysis within the CCP4 suite was used to perturb the coordinates of search model PDB: 2H7O to derive different conformations of the search model. With these normal modes as search models, phaser was able to successfully place the GDI domain. The obtained solution was subjected to a few cycles of restrained refinement using Phenix.refine and yielded an R_{free} of 0.48. This solution was used for subsequent placement of the kinase domain.

Using UniProt (www.uniprot.org/) to BLAST search sequences in the PDB (Protein Data Bank), kinase MSK1 (PDB: 3KN6) gave the highest hit with a sequence identity of 0.19. The structure of the kinase MSK1 (PDB: 3KN6) was pruned by CHAINSAW (Stein 2008) and was used as a search model for the kinase domain. After successful placement of the kinase domain, the obtained solution was subjected to a few cycles of restrained refinement using Phenix.refine and yielded an R_{free} of 0.45. Subsequently, density modification was performed using Parrot (Cowtan 2010) and automated model building was carried out using Phenix Mr_Rosetta (Terwilliger et al. 2012). Autobuilding resulted with 1014 residues out of 1262 placed automatically in three chains with an improved electron density map and an R_{free} of 0.43. Some residues had not been built correctly at this stage but visually,

the kinase domain appeared to be appropriately built and the C-terminal 100 residues of the GDI domain fitted the electron density better than the search model of PDB: 2H7O.

The working model was then assembled from coordinates of actin from PDB: 3HBT; coordinates of the GDI domain from PDB: 2H7O (excluding the C-terminal 100 residues); and from autobuilding, the coordinates of the kinase domain and the C-terminal 100 residues of the GDI domain. Chains belonging to the kinase domain and the GDI domain were combined with the correct sequence numbering. Differences in side chains between search models and the structure were corrected. The search model used for actin is the rabbit skeletal α-actin (PDB: 3HBT) while the actin in the crystal is Sf9 actin, and they have a sequence identity of 92.3%. The search model used for the GDI domain is from *Yersinia pseudotuberculosis* while that in the crystal is from *Yersinia enterocolitica* and they have a sequence identity of 97%.

Several rounds of manual model rebuilding using the graphics program COOT (Emsley et al. 2010) were performed, making corrections predominantly on the kinase domain. Subsequently, restrained positional and B-factor refinement were performed using Phenix (Afonine et al. 2012). A composit omit map (Terwilliger et al. 2008) was calculated to reduce the effects of model bias, and used to check against the structure during refinement. The electron densities obtained at various stages of phase refinement are shown in **Fig. 3.8**. Phases obtained at various stages of structure determination, model building and refinement as compared to final map phases could be found in **Table 3.4**. The structure was refined to an overall R_{work} of

0.20 and R_{free} value of 0.25 and detailed data collection and refinement statistics for YopO 1YY-actin can be found in **Table 3.5**.

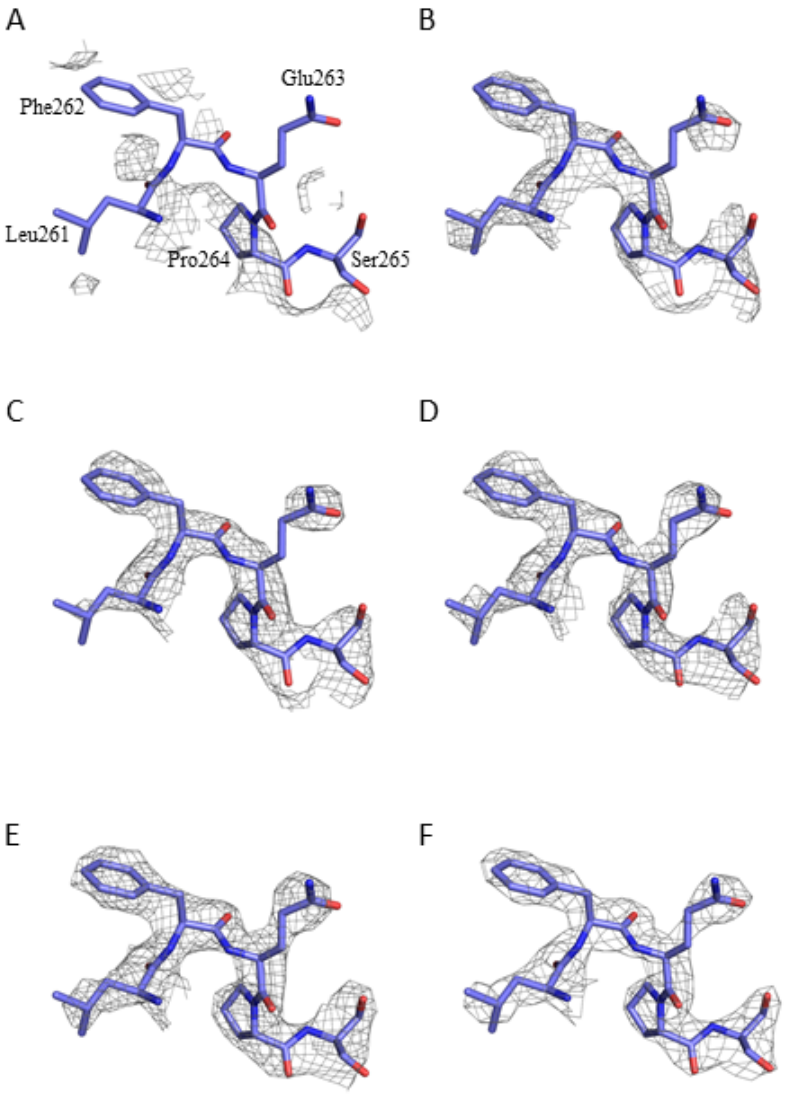


Figure 3.8 Electron densities at different stages of phase refinement for residues 261 - 265 of actin. (A) After molecular replacement with actin (B) After molecular replacement of the GDI domain and actin. (C) After successful molecular replacement of the kinase domain, actin and the GDI domain. (D) After density modification with Parrot (E) After automated model building with Phenix Mr_Rosetta (F) Map obtained after a number of rounds of restrained refinement

Table 3.4 Map correlations against final map phases after accounting for origin shifts calculated with Phenix

		Correlation coefficient
A	After molecular replacement with actin and the GDI domain.	0.37
B	After successful molecular replacement of kinase domain on top of actin and the GDI domain.	0.60
C	After density modification with Parrot	0.64
D	After autobuilding with Mr_Rosetta	0.74
E	After a number of rounds of restrained refinement	0.79

Table 3.5 Data collection, processing and refinement statistics for YopO 1YY-actin complex

Data collection statistics	
Synchrotron	Taiwan NSRRC
Beamline	BL13B1
Wavelength (Å)	1
Space group	$P2_1$
Unit cell dimensions (a, b, c) (Å) (α, β, γ) (°)	a=70.77, b=121.95, c= 89.16, α=90.00, β=94.74, γ=90.00
Resolution range (Å)[a]	20.0-2.65 (2.70-2.65)
Observations	151226
Unique reflections	41770
Redundancy	3.6 (3.2)
Completeness (%)[a]	95.9 (75.1)
Average I/Iσ (%)[a]	12.75 (2.65)
R_{merge} (%)[b]	0.10 (0.44)
$CC_{1/2}$	0.99 (0.90)
Model refinement statistics	
Resolution range (Å)	20.0-2.65
No. of reflections (working/test)	41,770/2,107
R_{work} [c] /R_{free} [d]	0.2042/0.2465
No. of atoms: (protein/ligand/water)	7357/32/333
RMSD bond length (Å)	0.009
RMSD bond angle (°)	1.194
Mean B-factor (Å^2) (actin/YopO)	43.9/54.0
Ramachandran favoured (disallowed) (%)	95.9 (0.2)

a Values in parenthesis refer to the highest resolution shell.

b R_{merge}= Σ*i* Σ*h*(|I*j*,*h* -<I*h*>|) / Σ*j*Σ*h*(<I*h*>), where h are unique reflections indices, *i*, *j*,*h* are intensities of symmetry related reflections and <I*h*> is the mean intensity

c R_{work} and d R_{free} are defined by R= Σ *hkl*||F_{obs}|- |F_{calc}|| / Σ *hkl* |F_{obs}|, where *h,k,l* are the indices of the reflections (used in refinement for R_{work}; 5%, not used in refinement, for R_{free}), F_{obs} and F_{calc} are the structure factors, deduced from measured intensities and calculated from the model, respectively.

3.9 The structure of YopO 1YY-actin

The YopO-actin structure was refined to an overall R_{free} value of 24.7. For YopO, there is no interpretable electron density for residues 89-107, which contains the putative phosphorylation sites Ser90 and Ser95 (Trasak et al. 2007); 135-142, the ATP-binding P-loop; residues 150-154 and 163-167 within the N-lobe of the kinase domain, and 510-532 which is involved in interaction with Rac1 (**Fig. 3.10**). The GDI domain and the kinase domain are individual domains connected by a 14 residue linker (424-437) (**Fig. 3.9**). The GDI domain and the kinase domain sandwich subdomain 4 and part of subdomain 2 of actin, with the GDI domain contacting the front face, and the kinase domain contacting the back face, of actin. The catalytic cleft is flanked between the kinase domain and the GDI domain. Residues involved in the interaction between YopO and actin are listed in **Table 3.6**. The total surface area occluded on YopO-actin complex formation is 2030.2 $Å^2$, of which 811.8 $Å^2$ is in the interface with the GDI domain and 1218.4 $Å^2$ is in the interface with the kinase domain as calculated using PDBePISA. YopO sterically blocks the pointed end of the actin monomer, providing structural basis for the sequestration of actin monomers and the inhibition of actin polymerization by YopO (Trasak et al. 2007). The binding of YopO leaves the barbed end of actin free, agreeing with previous studies that the barbed end binder profilin co-elutes in the same fractions as YpkA/YopO and actin (Juris et al. 2000). Actin adopts a typical actin-ATP monomer structure with no electron density observed for the DNase1 binding loop (residues 40-51).

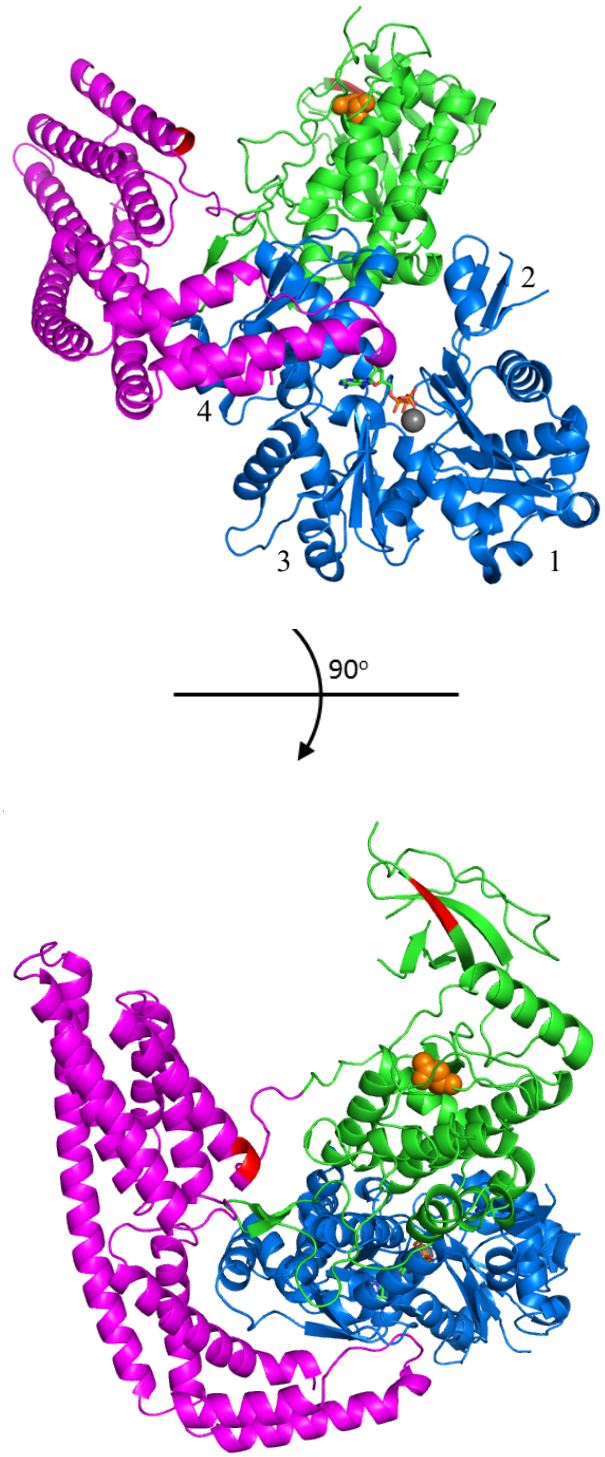


Figure 3.9 Structure of the YopO-actin complex. (A) Overview of the YopO (89-729)-actin structure. Actin is shown in blue, the kinase domain in green and the GDI domain in magenta. Calcium is shown as a grey sphere and ATP as green sticks. The subdomains of actin are labelled 1-4. The catalytic residue Asp267 within the catalytic cleft of kinase domain is shown as orange spheres. YopO 1YY SER mutations (K205Y, E206Y, E207Y, K440Y, K441Y) are shown in red.



Figure 3.10 Sequence-structural analysis of YopO (89-729). The secondary structure for given residues is indicated below the sequence. The kinase domain is shown in green, the GDI domain in magenta and disordered regions are shown in grey. The surface entropy reduction mutations are shown in red and are marked with red asterisks. Residues that form hydrogen bonds or electrostatic interactions with actin, with bond lengths of 3.5 Å or less, as determined by PDBePISA, are shown in black.

Table 3.6 Hydrogen bonds and electrostatic interactions between YopO and actin. Data generated from PDBePISA (http://www.ebi.ac.uk/msd-srv/prot_int/), showing only bond lengths at 3.5 Å and below.

Interacting residue on YopO	Bond length (Å)	Interacting residue on actin
B:TRP 230[O]	3.15	A:LYS 192[NZ]
B:LYS 231[O]	3.29	A:LYS 192[NZ]
B:LYS 231[NZ]	3.29	A:THR 195[OG1]
B:LYS 231[NZ]	2.60	A:GLU 196[OE2]
B:ASN 236[ND2]	3.32	A:ASP 188[OD2]
B:SER 237[N]	2.58	A:ASP 188[OD1]
B:SER 237[OG]	2.91	A:ASP 188[O]
B:GLU 238[N]	3.09	A:ASP 188[OD2]
B:LYS 245[NZ]	2.90	A:THR 202[OG1]
B:HIS 367[ND1]	2.82	A:THR 195[O]
B:HIS 367[N]	2.83	A:GLU 196[OE1]
B:GLY 373[N]	2.64	A:GLY 198[O]
B:GLU 375[N]	2.75	A:GLN 247[OE1]
B:GLU 375[O]	2.75	A:GLN 247[NE2]
B:THR 376[OG1]	2.80	A:SER 200[O]
B:ALA 377[N]	3.02	A:GLU 206[OE2]
B:ASP 407[OD2]	2.74	A:ARG 63[NE]
B:ASP 407[OD1]	2.50	A:THR 204[OG1]
B:ASP 407[OD1]	3.07	A:THR 204[N]
B:VAL 647[N]	2.87	A:SER 240[O]
B:VAL 647[O]	2.85	A:GLU 242[N]
B:LYS 648[NZ]	2.44	A:GLU 242[OE2]
B:LYS 648[O]	3.12	A:LYS 216[NZ]
B:PHE 649[N]	3.46	A:GLU 242[O]
B:GLY 650[O]	2.83	A:LYS 216[NZ]
B:ARG 696[NE]	2.89	A:ALA 232[O]
B:ARG 696[NH2]	3.14	A:ALA 232[O]
B:ARG 712[NE]	2.88	A:ALA 232[O]
B:ARG 723[NH2]	2.61	A:GLU 227[OE2]
B:GLU 727[OE2]	3.03	A:LYS 239[NZ]
B:GLU 727[O]	2.76	A:LYS 239[NZ]
B:GLU 727[OE2]	3.26	A:ARG 255[NH1]
B:GLU 727[OE2]	2.88	A:ARG 255[NH2]
B:GLU 727[OE1]	2.93	A:ARG 255[NH1]

The interaction of YopO with actin is limited to subdomains 2 and 4 of actin, with binding predominantly on subdomain 4 (**Fig. 3.11**). Both the GDI domain and the kinase domain are involved in binding actin. The binding of Rac1, actin and kinase substrates involve entirely different interfaces (**Fig. 3.12**).

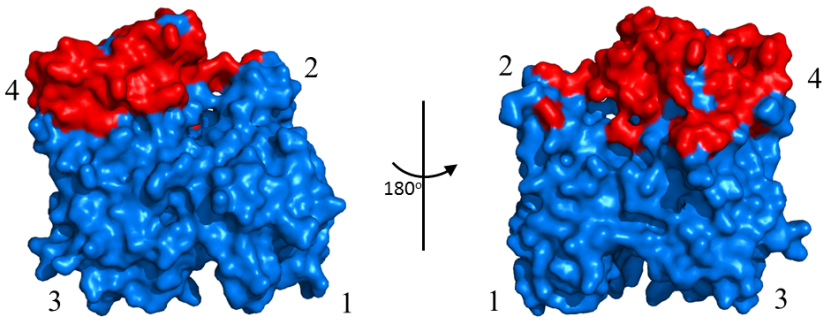


Figure 3.11 The surface area of actin that is occluded by YopO. Left panel, front face of actin; right panel, back face of actin. Actin is shown in blue and the surface occluded by YopO is shown in red. The subdomains of actin are as indicated.

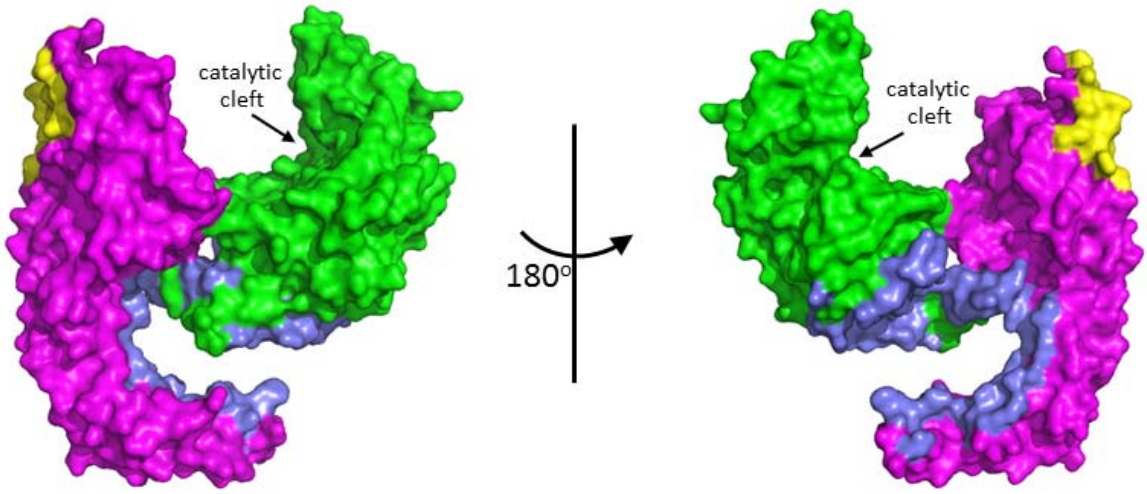


Figure 3.12 The surface area of YopO that is occluded by actin and Rac1. The GDI domain is shown in magenta and the kinase domain in green. The surface occluded by actin is shown in light blue, and by Rac1 in yellow.

The interaction of the GDI domain with actin is separate and distinct from the Rac1-interaction site and involves only the C-terminal bundle of four helices α15-18 and their connecting loops. The loop between helices α15 and α16, residues 646-649 (in β7), make extensive contact with actin via backbone-backbone hydrogen bonding to give rise to β-sheet interactions with residues 240-242 of actin (**Fig. 3.13**). The penultimate 20 residues within helix α18 form multiple salt bridges with actin via Arg723 and Glu727, agreeing with literature that the C-terminal 20 residues of YopO are important for binding actin (Juris et al. 2000; Trasak et al. 2007). The interaction is further stabilized by hydrogen bonding of Arg696 of YopO to the backbone carbonyl of Ala232 of actin.

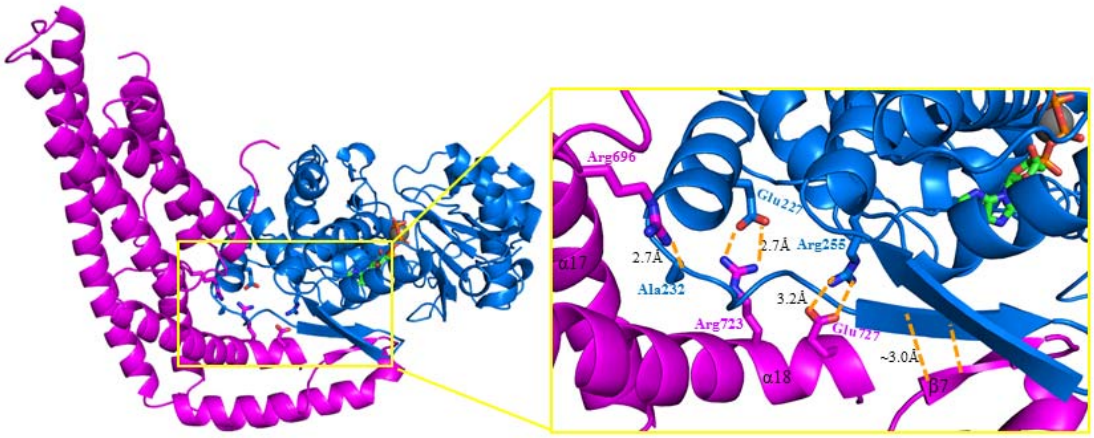


Figure 3.13 Interaction of the GDI domain with actin. For simplicity, the kinase domain is not shown. The GDI domain is shown in magenta and actin is shown in marine.

3.10 Conformational changes of the GDI domain upon binding actin

The domain structure of the GDI domain is similar to the previously reported structures of GDI domain in isolation (PDB: 2H7O) and in complex with Rac1 (PDB: 2H7V), except that upon binding actin, the backbone helix α14 undergoes a 30^{o} bending and helices α14-18 translocate towards actin (**Fig. 3.14 & 3.15**). The binding of Rac1 does not sterically hinder access to the catalytic cleft of the kinase domain (**Fig. 3.16**).

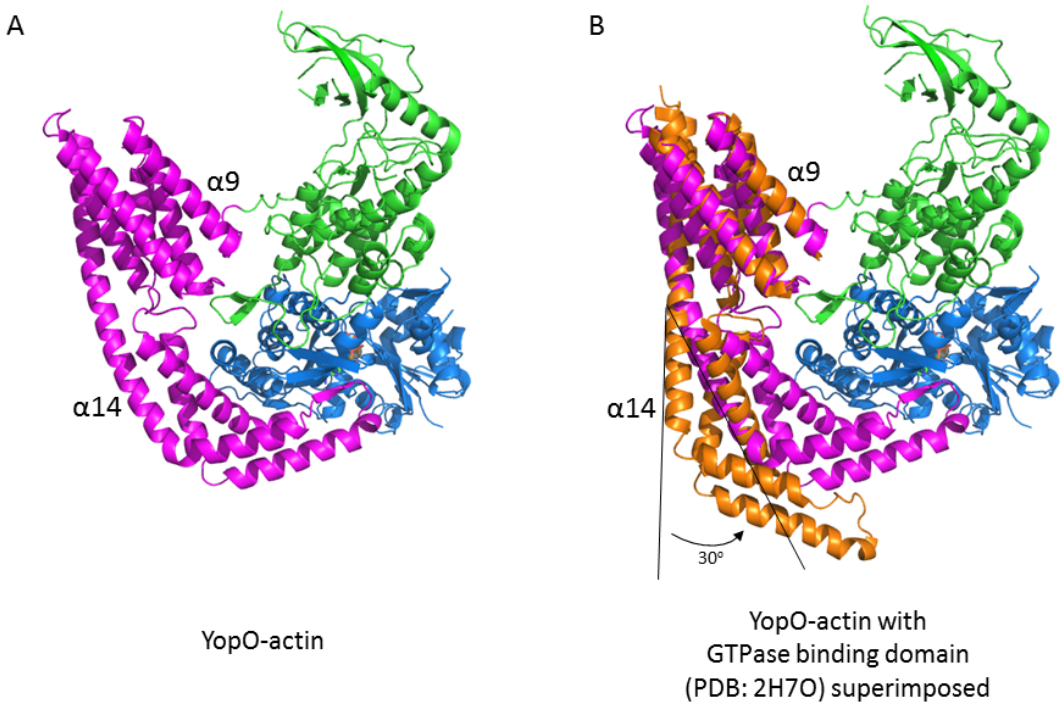


Figure 3.14 Conformational changes to the GDI domain on actin-binding. (A) The structure of YopO-actin. The GTPase domain, the kinase domain and actin of YopO-actin are shown in magenta, forest green and marine respectively. (B) The structure of YopO-actin with the superimposition of the GDI domain alone is shown in orange (PDB: 2H7O (Prehna et al. 2006)). The alignment was based on helix α9 (residues 440-458) of YopO. The conformational change consists of a 30° bending of backbone helix α14 towards actin.

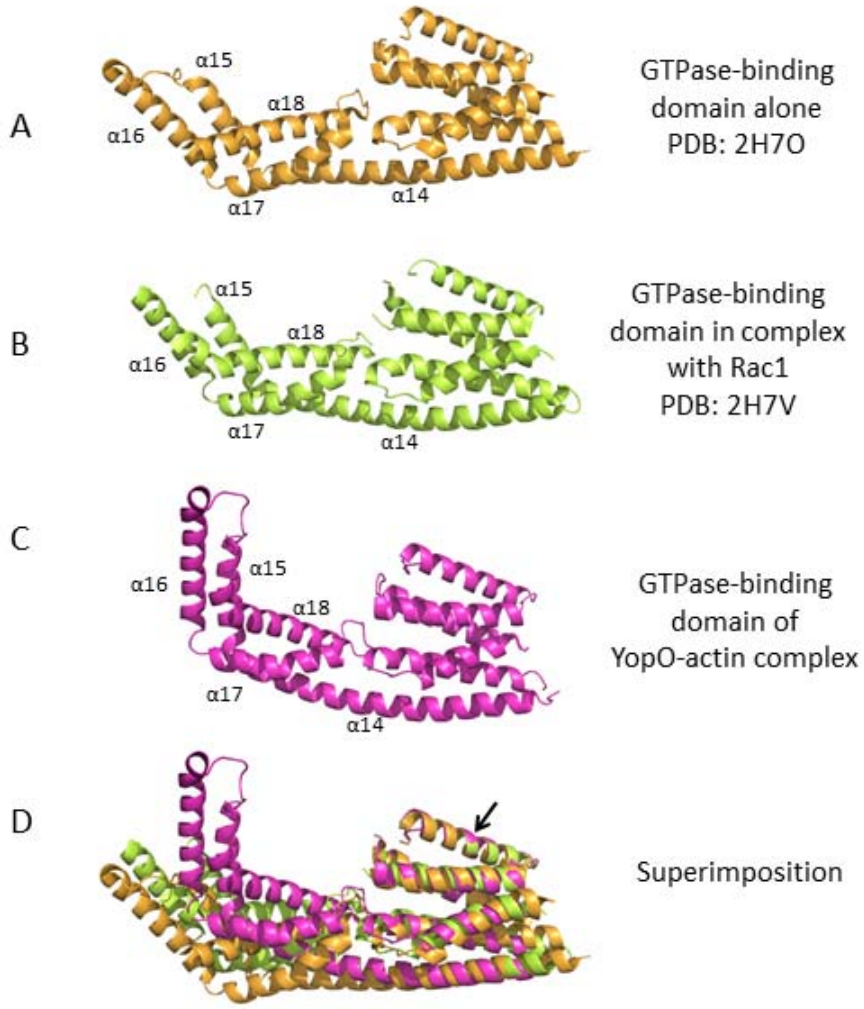


Figure 3.15 Conformational changes to the GDI domain. (A) The GDI domain alone is shown in orange (PDB: 2H7O (Prehna et al. 2006)). (B) The GDI domain in complex with Rac1 (PDB: 2H7V) is shown in lime, with Rac1 not shown. (C) The GDI domain of YopO-actin complex is shown in magenta, with actin and the kinase domain not shown. (D) Superimposition of all three GDI domain structures showing the conformational differences. Structures were aligned on helix α9 (residues 440-458), marked with a black arrow. Helices α14-18 are labelled.

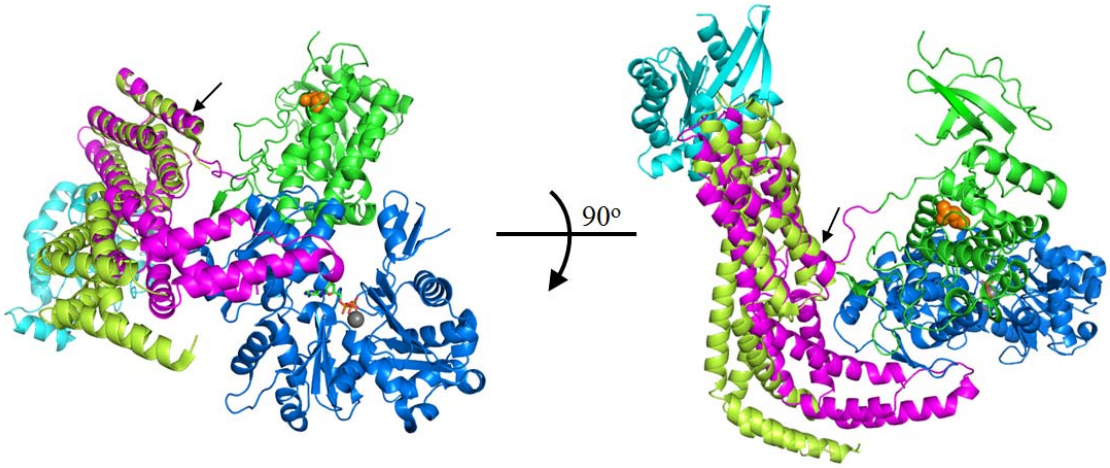


Figure 3.16 Superimposition of the GDI domain in complex with Rac1 on YopO-actin. The GDI domain, kinase domain and actin of the YopO-actin structure are shown magenta, green and marine respectively. The catalytic Asp267 is shown as orange spheres. The GDI domain in complex with Rac1 (PDB: 2H7V) are shown in lime and cyan respectively. Structures were aligned on helix α9 (residues 440-458), which is marked with a black arrow.

3.11 Interaction of the kinase domain of YopO with actin

The kinase domain adopts largely the structure of a typical kinase, with an N-lobe consisting of β-sheets and one single α-helix (αC helix) and a C lobe comprising an α-helical bundle (**Fig 3.17**). In addition, the C lobe contains a series of loops between helices α4 and α5, which were unique to YopO, and seemed to be an adaptation for interaction with actin . The kinase domain adopts the active structure, with a well-defined activation segment. The kinase domain interacts extensively with actin through the C-lobe of the kinase domain while the N-lobe and the catalytic cleft do not interact with actin. The interaction of the C-lobe with actin is mediated by residues at the base of helices α2 and α3 as well as via the loops between helices α4 and α5. The interaction of the helices of the C-lobe appears to be important for the allosteric positioning and stabilization of the activation segment and the catalytic loop, which are essential structural elements for the activation of kinase activity. There is poor density for the P-loop which requires MgATP binding for stabilization. Ser90 and Ser95, which are putative phosphorylation sites (Trasak et al. 2007), are disordered and there is no sign of phosphorylation on the activation segment or on other ordered parts of the structure. The location of phosphorylation sites outside of the catalytic centre suggests that YopO is auto-inhibited in the inactive state. There is a glycine-rich sequence immediately C-terminal to the APE motif which is partially disordered and is a candidate region to be involved in substrate binding.

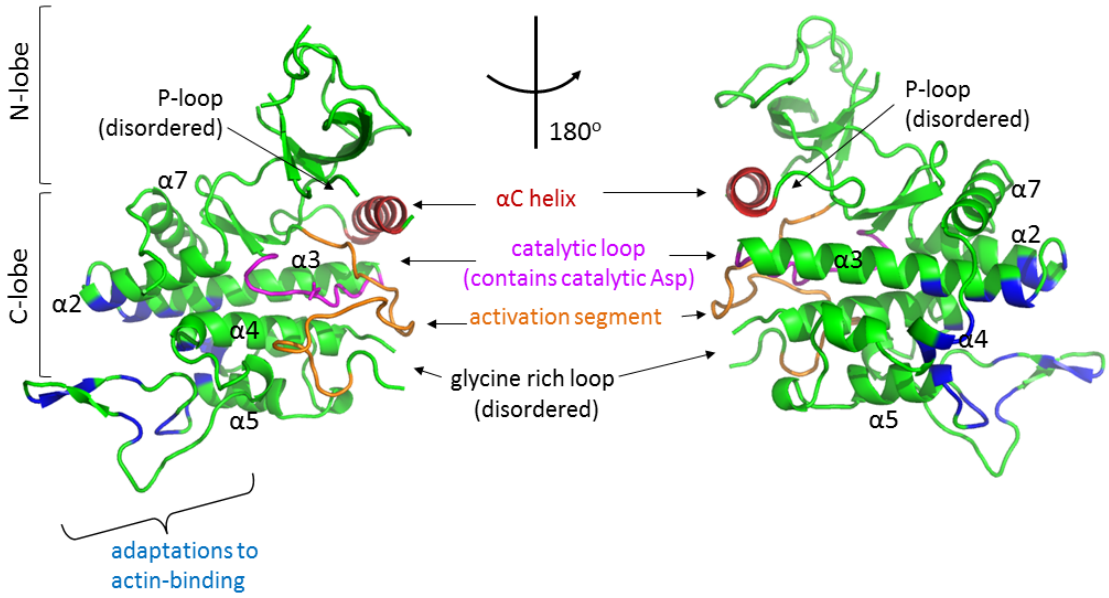


Figure 3.17 Structural elements of the kinase domain of YopO and interaction of the kinase domain of YopO with actin. The GDI domain is not shown. The αC helix is shown in red, the catalytic loop in magenta, with the catalytic Asp267 shown as sticks and the activation segment is shown in orange. The P-loop and glycine rich loop are disordered. Residues involved, or are occluded, in the interaction with actin are shown in blue.

3.12 Validation of YopO 1YY-actin crystal structure

To validate the crystal structure, a YopO non-actin-binding mutant (YopO nAct- V374D, T376D, R723A, E727A) was designed to abolish interaction with actin. Val 374 and Thr 376 of YopO lie in a hydrophobic region on actin in the vicinity of hydrophobic residues Tyr 199, Phe 201 and Ile 249 (**Fig. 3.18**). Mutations of Val 374 and Thr 376 to aspartic acid aim to introduce large charged groups to disrupt this hydrophobic interface. Arg 723 and Glu 727 of YopO form salt bridges with Glu 227 and Arg 255 of actin respectively. Mutations of Glu 227 and Arg 255 to alanine abrogate these electrostatic interactions. As tested in the pyrene actin polymerization assay (as described in **section 2.17.1**), YopO nAct mutant has no effect on the increase in fluorescence of pyrene actin on polymerization, in contrast to YopO WT, suggesting that YopO nAct does not sequester actin, and confirming the functional validity of the crystal structure (**Fig. 3.19**).

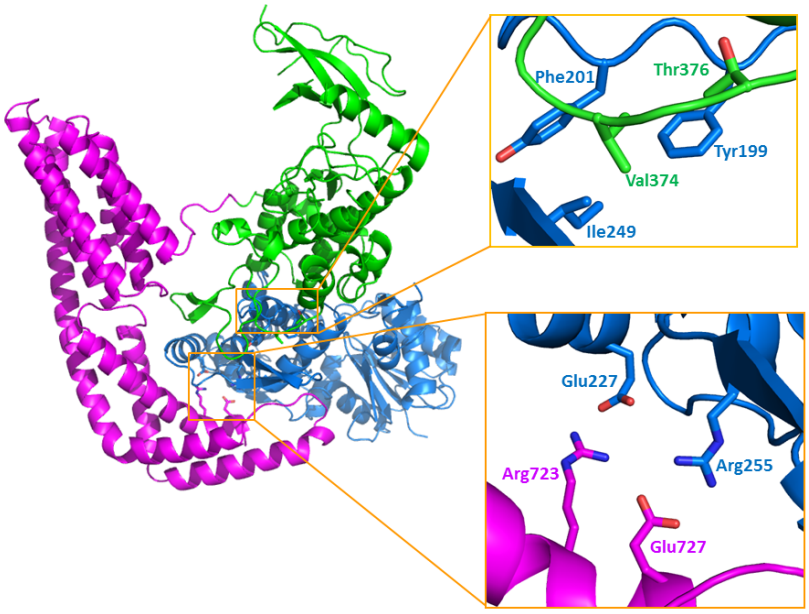


Figure 3.18 Mutations to disrupt the actin-binding interface of YopO. The GTPase domain, the kinase domain and actin of the YopO-actin structure are shown in magenta, green and marine respectively. Right panels show close up of the interfaces between YopO and actin at the proposed mutation sites.

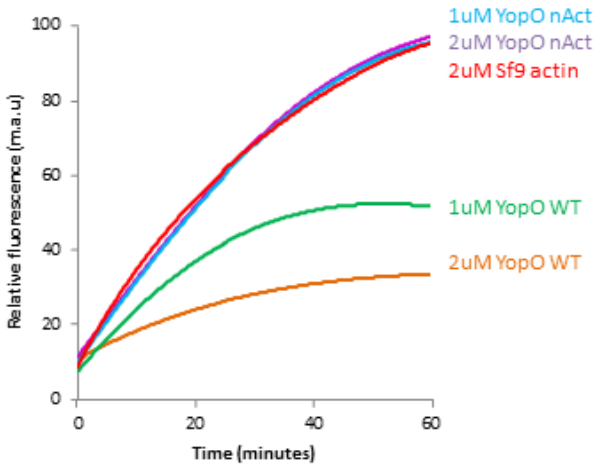


Figure 3.19 Monomer sequestration activity of YopO and YopO nAct mutant. Red – 2 µM Sf9 actin. Green – 1 µM YopO WT added to 2µM Sf9 actin. Orange – 2 µM YopO WT added to 2 µM Sf9 actin. Blue – 1 µM YopO nAct added to 2µM Sf9 actin. Magenta – 2 µM YopO nAct added to 2 µM Sf9 actin. Polymerization was initiated with the addition of KMEI buffer.

3.13 Crystal packing of YopO 1YY-actin

The site of one SER mutation cluster was found at a crystal contact (**Fig. 3.20**). Tyr mutation (Tyr207) mediates a Pi-stacking interaction with Tyr588 on helix α14 of YopO, stabilizing the kinase domain against the GDI domain of another YopO. This could have been the determining factor for crystal packing and the improved crystal order in crystals of YopO 1YY-actin over YopO WT-actin. The SER mutation cluster consisting of K440Y and K441Y was not involved in crystal contact. We suspect that YopO is a flexible structure and poor crystal diffraction of YopO WT-actin crystals were a result of relative mobility within crystals.

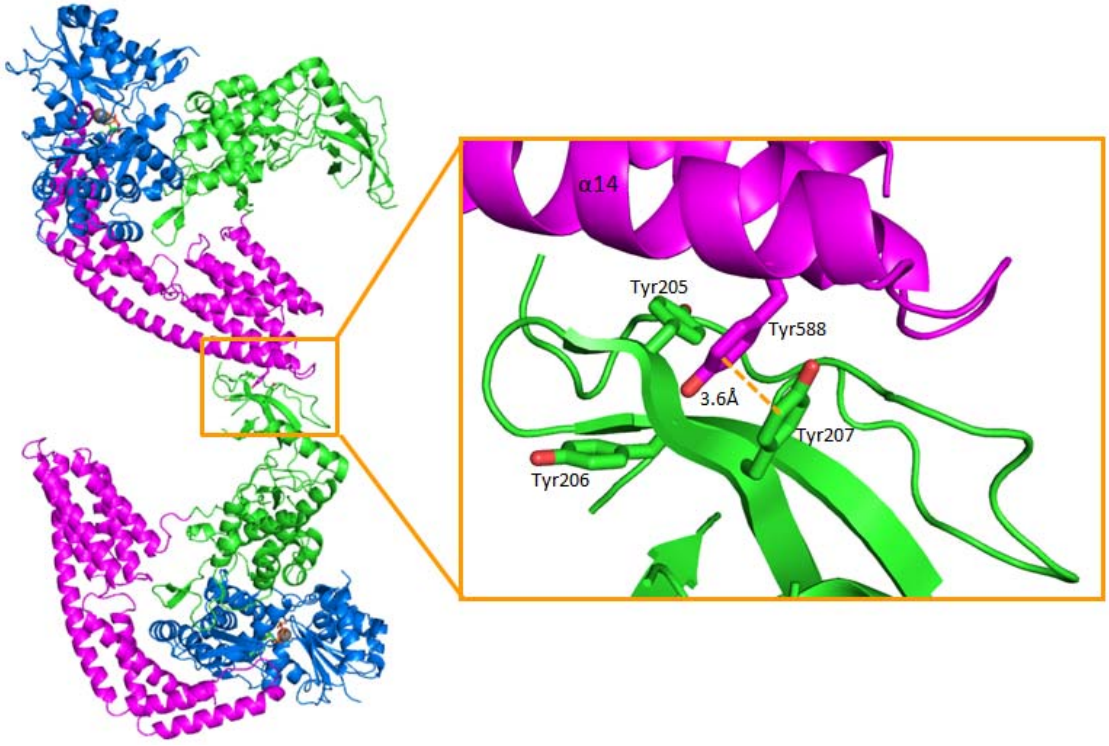


Figure 3.20 The involvement of surface entropy reduction mutations (K205Y, E206Y, E207Y) in YopO-actin crystal contacts. Actin is shown in marine, the GDI domain in magenta and the kinase domain in green. Mutated residues on YopO (K205Y, E206Y, E207Y) and the interacting residue on actin (Tyr588) are shown in stick representation.

3.14 Structural basis of differential actin isoform preference of YopO

Rabbit skeletal α-actin is much weaker in activating the autophosphorylation of YpkA compared to *Dictyostelium discoideum* (*D. discoideum*) or platelet actin (mixture of β and γ isoforms) (Trasak et al. 2007). The YopO-actin structure provides structural insight into understanding the differential activation of YopO by non-muscle versus muscle isoforms. A sequence alignment of homologous actins - cytoplasmic isoforms (human β-actin, mouse β-actin, *S.frugipera, D.discoideum)* and a muscle isoform (rabbit skeletal α-actin) yielded a number of candidate residues which were conserved amongst cytoplasmic isoforms but were different in the muscle isoform (**Fig. 3.21**). Only one of these residues was observed to be involved in the interaction with YopO (**Table 3.7**). Thr202 is conserved in *S.frugipera*, *D.discoideum*, and in the corresponding position, Thr201 in human and Thr201 in mouse β-actin. In the YopO-actin structure, actin Thr202 forms a hydrogen bond with Lys245 of YopO with a bond length of 2.9 Å (**Fig. 3.22**). Lys245 lies on helix α3 of YopO, which is immediately N-terminal of the catalytic loop that contains the catalytic aspartate (Asp267). Thus, this hydrogen bond might be important for positioning helix α4 for stabilizing the catalytic loop. The corresponding residue is Val203 in rabbit α-actin, which unlike threonine, valine cannot form a hydrogen bond with lysine.

Table 3.7 Contacts between YopO and actin with bond lengths at 3.5 Å and below, obtained from PDBePISA (http://www.ebi.ac.uk/msd-srv/prot_int/). The level of conservation of residues involved between human β-actin, mouse β-actin, *S. frugiperda* actin and rabbit α-actin is indicated.

Interacting residue on YopO	Bond length (Å)	Interacting residue on actin	Sequence conservation
B:ASP 407[OD2]	2.74	A:ARG 63[NE]	Conserved
B:ASN 236[ND2]	3.32	A:ASP 188[OD2]	Conserved
B:SER 237[N]	2.58	A:ASP 188[OD1]	
B:SER 237[OG]	2.91	A:ASP 188[O]	
B:GLU 238[N]	3.09	A:ASP 188[OD2]	
B:TRP 230[O]	3.15	A:LYS 192[NZ]	Conserved
B:LYS 231[O]	3.29	A:LYS 192[NZ]	
B:LYS 231[NZ]	3.29	A:THR 195[OG1]	Conserved
B:HIS 367[ND1]	2.82	A:THR 195[O]	
B:LYS 231[NZ]	2.60	A:GLU 196[OE2]	Conserved
B:HIS 367[N]	2.83	A:GLU 196[OE1]	
B:GLY 373[N]	2.64	A:GLY 198[O]	Conserved
B:THR 376[OG1]	2.80	A:SER 200[O]	Conserved
B:LYS 245[NZ]	2.90	A:THR 202[OG1]	Valine in rabbit α-actin. Conserved in all others
B:ASP 407[OD1]	2.50	A:THR 204[OG1]	Conserved
B:ASP 407[OD1]	3.07	A:THR 204[N]	
B:ALA 377[N]	3.02	A:GLU 206[OE2]	Conserved
B:LYS 648[O]	3.12	A:LYS 216[NZ]	Conserved
B:GLY 650[O]	2.83	A:LYS 216[NZ]	
B:ARG 723[NH2]	2.61	A:GLU 227[OE2]	Conserved
B:ARG 696[NE]	2.89	A:ALA 232[O]	Conserved
B:ARG 696[NH2]	3.14	A:ALA 233[O]	Conserved
B:ARG 712[NE]	2.88	A:ALA 233[O]	
B:GLU 727[OE2]	3.03	A:LYS 239[NZ]	Conserved
B:GLU 727[O]	2.76	A:LYS 239[NZ]	
B:VAL 647[N]	2.87	A:SER 240[O]	Conserved
B:VAL 647[O]	2.85	A:GLU 242[N]	Conserved
B:LYS 648[NZ]	2.44	A:GLU 242[OE2]	
B:PHE 649[N]	3.46	A:GLU 242[O]	
B:GLU 375[N]	2.75	A:GLN 247[OE1]	Conserved
B:GLU 375[O]	2.75	A:GLN 247[NE2]	
B:GLU 727[OE1]	2.93	A:ARG 255[NH1]	Conserved
B:GLU 727[OE2]	2.88	A:ARG 255[NH2]	
B:GLU 727[OE2]	3.26	A:ARG 255[NH1]	
B:GLU 727[OE1]	2.93	A:ARG 255[NH1]	

```
SfACT      -MCDDDVAALVVDNGSGMCKAGFAGDDAPRAVFPSIVGRPRHQGVMVGMGQKDSYVGDEA 59
hACTB      --MDDDIAALVVDNGSGMCKAGFAGDDAPRAVFPSIVGRPRHQGVMVGMGQKDSYVGDEA 58
mACTB      --MDDDIAALVVDNGSGMCKAGFAGDDAPRAVFPSIVGRPRHQGVMVGMGQKDSYVGDEA 58
DdACT      -MDGEDVQALVIDNGSGMCKAGFAGDDAPRAVFPSIVGRPRHTGVMVGMGQKDSYVGDEA 59
aACTA      MCDEDETTALVCDNGSGLVKAGFAGDDAPRAVFPSIVGRPRHQGVMVGMGQKDSYVGDEA 60
               ::  *** *****: ********************** ****************

SfACT      QSKRGILTLKYPIEHGIITNWDDMEKIWHHTFYNELRVAPEEHPVLLTEAPLNPKANREK 119
hACTB      QSKRGILTLKYPIEHGIVTNWDDMEKIWHHTFYNELRVAPEEHPVLLTEAPLNPKANREK 118
mACTB      QSKRGILTLKYPIEHGIVTNWDDMEKIWHHTFYNELRVAPEEHPVLLTEAPLNPKANREK 118
DdACT      QSKRGILTLKYPIEHGIVTNWDDMEKIWHHTFYNELRVAPEEHPVLLTEAPLNPKANREK 119
aACTA      QSKRGILTLKYPIEHGIITNWDDMEKIWHHTFYNELRVAPEEHPTLLTEAPLNPKANREK 120
           ******************:**************************.***************

SfACT      MTQIMFETFNSPAMHVAIQAVLSLYASGRTTGIVLDSGDGVSHTVPIYEGYALPHAILRL 179
hACTB      MTQIMFETFNTPAMYVAIQAVLSLYASGRTTGIVMDSGDGVTHTVPIYEGYALPHAILRL 178
mACTB      MTQIMFETFNTPAMYVAIQAVLSLYASGRTTGIVMDSGDGVTHTVPIYEGYALPHAILRL 178
DdACT      MTQIMFETFNTPAMYVAIQAVLSLYASGRTTGIVMDSGDGVSHTVPIYEGYALPHAILRL 179
aACTA      MTQIMFETFNVPAMYVAIQAVLSLYASGRTTGIVLDSGDGVTHNVPIYEGYALPHAIMRL 180
           ********** ***:*******************:******:*.*************:**

                                    ▲
SfACT      DLAGRDLTDYLMKILTERGYSFTTTAEREIVRDIKEKLCYVALDFEQEMATAAASTSLEK 239
hACTB      DLAGRDLTDYLMKILTERGYSFTTTAEREIVRDIKEKLCYVALDFEQEMATAASSSSLEK 238
mACTB      DLAGRDLTDYLMKILTERGYSFTTTAEREIVRDIKEKLCYVALDFEQEMATAASSSSLEK 238
DdACT      DLAGRDLTDYMMKILTERGYSFTTTAEREIVRDIKEKLAYVALDFEAEMQTAASSSALEK 239
aACTA      DLAGRDLTDYLMKILTERGYSFVTTAEREIVRDIKEKLCYVALDFENEMATAASSSSLEK 240
           **********:***********.***************.******* ** ***:*::***

SfACT      SYELPDGQVIAIGNERFRCPEALFQPSFLGMESCGIHETVYNSIMKCDVDIRKDLYANTV 299
hACTB      SYELPDGQVITIGNERFRCPEALFQPSFLGMESCGIHETTFNSIMKCDVDIRKDLYANTV 298
mACTB      SYELPDGQVITIGNERFRCPEALFQPSFLGMESCGIHETTFNSIMKCDVDIRKDLYANTV 298
DdACT      SYELPDGQVITIGNERFRCPEALFQPSFLGMESAGIHETTYNSIMKCDVDIRKDLYGNVV 299
aACTA      SYELPDGQVITIGNERFRCPETLFQPSFIGMESAGIHETTYNSIMKCDIDIRKDLYANNV 300
           **********:**********:******:****.*****.:*******:*******.* *

SfACT      MSGGTTMYPGIADRMQKEITALAPSTIKTKIIAPPERKYSVWIGGSILASLSTFQQMWIS 359
hACTB      LSGGTTMYPGIADRMQKEITALAPSTMKIKIIAPPERKYSVWIGGSILASLSTFQQMWIS 358
mACTB      LSGGTTMYPGIADRMQKEITALAPSTMKIKIIAPPERKYSVWIGGSILASLSTFQQMWIS 358
DdACT      LSGGTTMFPGIADRMNKELTALAPSTMKIKIIAPPERKYSVWIGGSILASLSTFQQMWIS 359
aACTA      MSGGTTMYPGIADRMQKEITALAPSTMKIKIIAPPERKYSVWIGGSILASLSTFQQMWIT 360
           :******:*******:**:*******:* ******************************:

SfACT      KEEYDESGPGIVHRKCF    376
hACTB      KQEYDESGPSIVHRKCF    375
mACTB      KQEYDESGPSIVHRKCF    375
DdACT      KEEYDESGPSIVHRKCF    376
aACTA      KQEYDEAGPSIVHRKCF    377
           *:****:**.*******
```

Figure 3.21 Sequence alignment of actin protein sequences, including *S.frugiperda* actin (SfACT: accession: AEK82131), human β-actin (hATCB, accession: NP_001092.1), mouse β-actin (mACTB, accession: AAA37164), *D.discoideum* actin (DdACT, AAA33145) and rabbit α-actin (aACTA, accession: CAA43139.1). The corresponding position for Thr202 of *S.frugiperda* is marked with a black triangle. The alignment was performed using Clustal Omega.

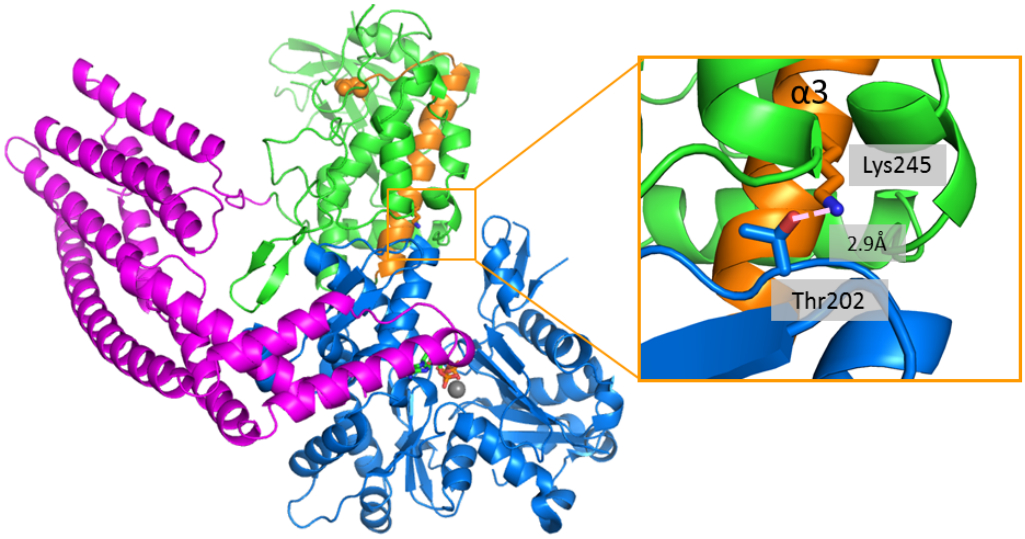


Figure 3.22 Structural basis of differential actin isoform preference of YopO. Thr202 forms a hydrogen bond with Lys245 of YopO with a bond length of 2.9 Å. Lys245 of YopO is on helix α3. Helix α3 and the loop leading to the catalytic Asp267 are shown in orange, with Asp267 shown as orange spheres. Actin is shown in marine, the GDI domain in magenta and the kinase domain in green.

To validate whether the hydrogen bond between Thr202 of actin with Lys245 of YopO confers differentiation between muscle and non-muscle actin isoforms, a mutant YopO K245M was designed, to abolish this hydrogen bond. YopO WT and K245M were tested for the ability to sequester actin in an actin polymerization assay. The sequestration activity of cytoplasmic actin and Sf9 actin of the K245M mutant is about two-fold weaker compared to YopO WT (**Fig. 3.23**). In contrast, rabbit α-actin does not differentiate between YopO WT and K245M. The ability of YopO WT and K245M to autophosphorylate in the presence of cytoplasmic actin, Sf9 actin and rabbit α-actin were then tested (**Fig. 3.24**), as described in **section 2.17.2**. Autophosphorylation is much weaker for K245M as compared to YopO WT at the same concentrations, for both cytoplasmic and Sf9 actin. For muscle actin, the levels of autophosphorylation for K245M and YopO WT are equal, if not better, with K245M.

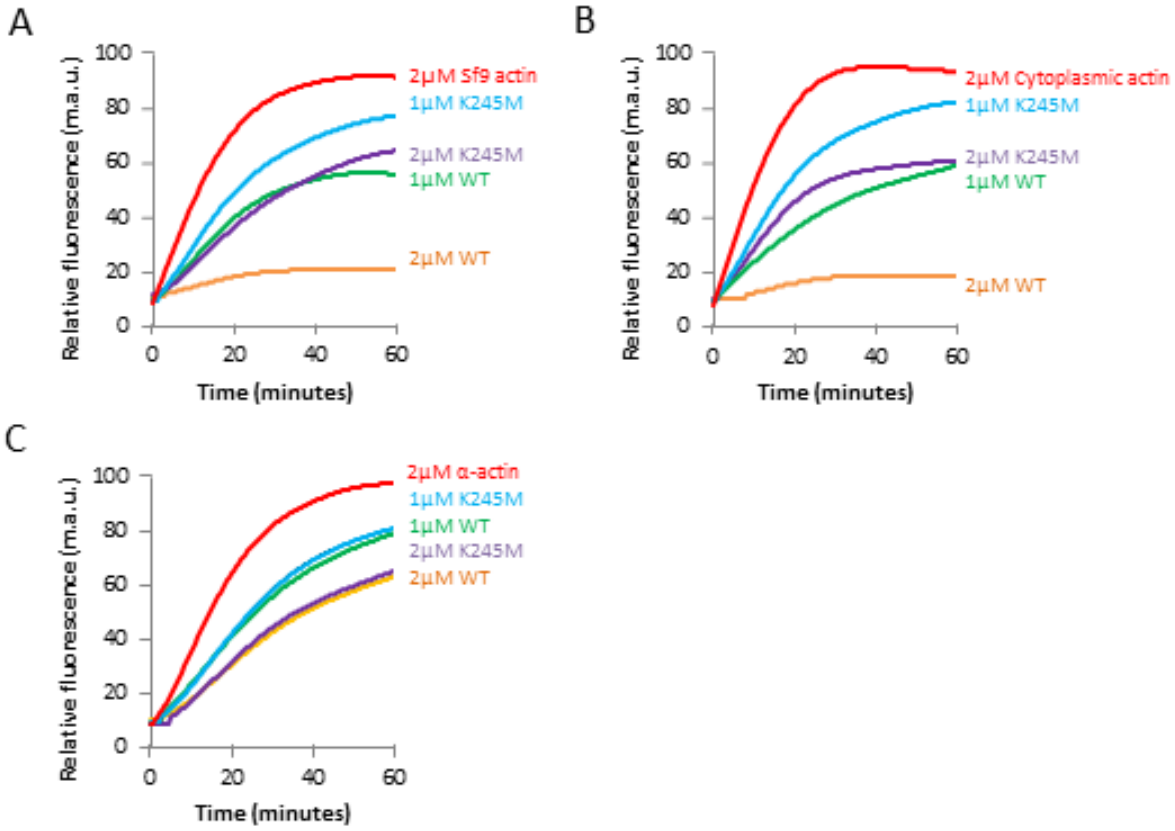


Figure 3.23 Actin monomer sequestration activities of YopO and the K245M mutant towards different actin isoforms. (A) 2 μM Sf9 actin. (B) 2 μM cytoplasmic actin (mixture of β and γ isoforms). (C) 2 μM α-actin.

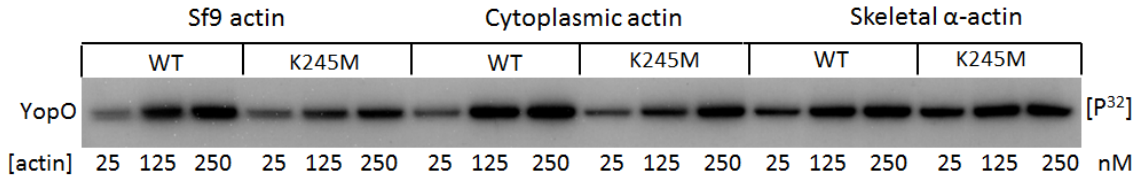


Figure 3.24 Autophosphorylation of YopO WT and YopO K245M in the presence of various ratios of Sf9, cytoplasmic and skeletal α-actin. YopO WT and YopO K245M are both at 125 nM and various actin isoforms are at 25, 125 or 250 nM. The ratios of YopO to actin are at 5:1, 1:1 and 1:2 respectively. The dried gel as exposed to X-ray film.

3.15 Discussion

3.15.1 Insights into the mechanism of actin sequestration by YopO

The structure reveals that YopO binds actin primarily on subdomain 4 with further contacts on subdomain 2. The binding of YopO on the pointed end of actin would inhibit actin nucleation and the YopO-bound actin monomer cannot be added to the barbed end of an actin filament due to steric hindrance of YopO. This corresponds with the pyrene actin assay, which showed that YopO retards actin polymerization, with near complete retardation when YopO is at an equimolar ratio to actin (**Fig. 3.25**).

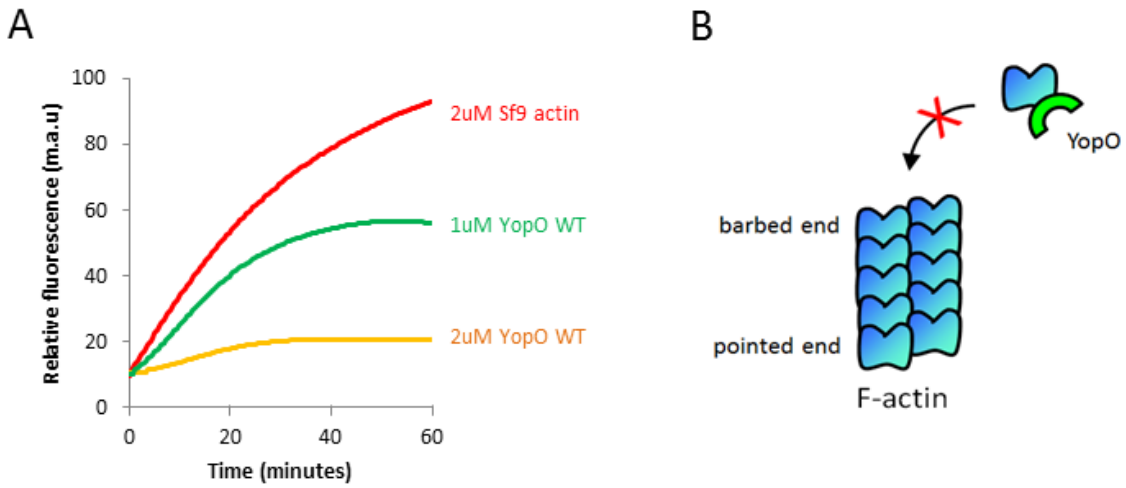


Figure 3.25 Actin monomer sequestration of YopO WT. (A) The retardation of actin polymerization by YopO WT. (B) Schematic representation of YopO WT sterically hindering its bound actin monomer from being added to the barbed end of an actin filament.

3.15.2 Insights into the kinase domain of YopO

From the crystal structure, the helices of the C-lobe of the kinase domain interact extensively with actin. These interactions appear to allosterically position the catalytic loop and the activation segment for kinase activity. It also appears that the kinase domain cannot maintain its active conformation if it is not bound to actin. The active site of the kinase domain lies above the bound actin and is flanked by the kinase domain and the GDI domain. The kinase domain is positioned such that it can only phosphorylate substrates that get inserted between the kinase domain and the GDI domain (**Fig. 3.26**). In the YopO-actin structure, these two domains lay only 31.5-33.0 Å and substrates have to insert into this gap for phosphorylation to take place.

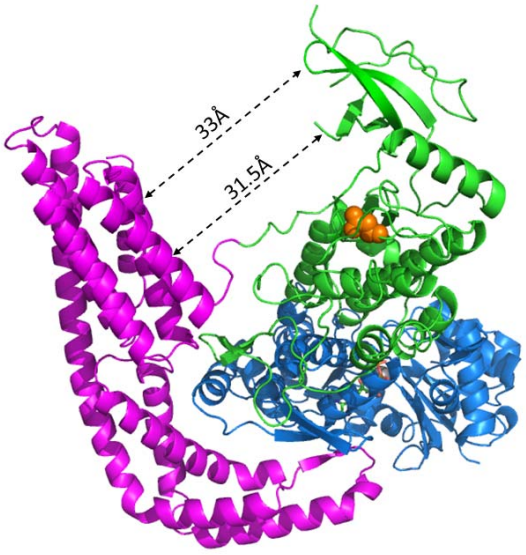


Figure 3.26 Kinase substrate binding groove on YopO. Substrates have to be accommodated in the space between the kinase and the GDI domain.

3.15.3 Interference of YopO with nucleotide-exchange of profilin-actin

The interaction of YopO with actin bridges subdomains 2 and 4 of actin and appears to stabilize the closed conformation of the nucleotide-binding cleft of actin (**Fig. 3.27**). Asp407 of YopO forms hydrogen bonds with Arg63 in subdomain 2 and Thr204 in subdomain 4 of actin, right at the top of the nucleotide-binding cleft. This mode of binding is reminiscent of thymosin-β (Tβ) proteins. The C-terminal half of Tβ binds between actin subdomains 2 and 4 preventing the dynamic opening and closing of the two halves of actin, inhibiting nucleotide exchange (Irobi et al. 2004). Similarly, the binding of YopO to actin stabilizes the closed conformation of the nucleotide-binding cleft, blocking the dissociation of the nucleotide, and may lead to the inhibition of nucleotide exchange (**Fig. 3.28**). YopO potentially interferes with the nucleotide exchange of profilin-actin. Polymerization of ADP-actin is less favourable than for ATP-actin, and the exchange of ADP- for ATP-bound monomeric actin constitutes an important control point in the assembly of the actin cytoskeleton (Goldschmidt-Clermont et al. 1992). Profilin, in part, regulates the pool of ADP-actin in cells by converting ADP-actin to ATP-actin. The binding of YopO to profilin-actin may prevent profilin-bound actin from nucleotide exchange (Goldschmidt-Clermont et al. 1992), thus hampering efficient actin turnover.

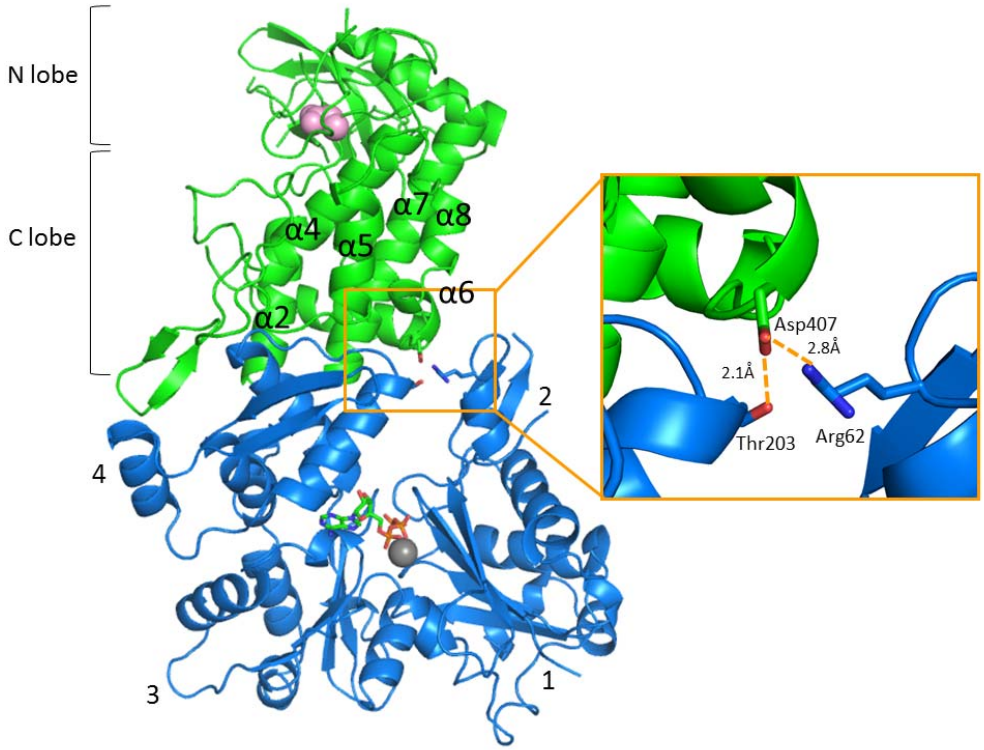


Figure 3.27 YopO stabilizes subdomains 2 and 4 of actin in the closed conformation. The GDI domain is not shown. The kinase domain is shown in green and actin is shown in marine. Selected helices within the kinase domain are labelled. The catalytic Asp267 is shown as pink spheres.

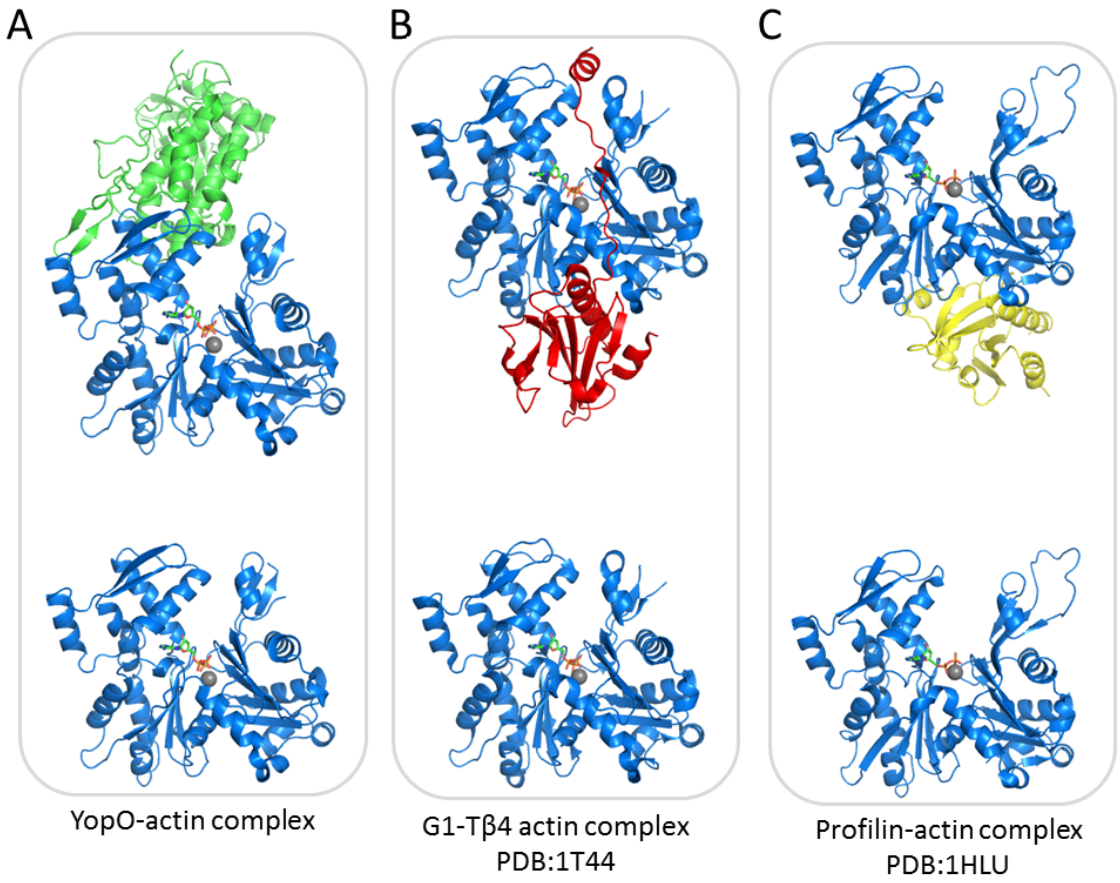


Figure 3.28 Conformations of the nucleotide-binding cleft of actin. (A) YopO-actin complex, with the GDI domain omitted for clarity. Actin in the YopO-actin structure adopts a closed nucleotide-binding cleft. (B) G1-Tβ4 actin complex. Actin in the G1-TB4:actin structure adopts a closed nucleotide-binding cleft (PDB: 1T44 (Irobi et al. 2004)). (C) Profilin-actin. Actin in the profilin-actin structure with an open nucleotide-binding cleft (PDB: 1HLU (Chik et al. 1996)).

3.16 Conclusions

In this chapter, the complex of YopO and actin was successfully crystallized. Initial crystals had poor crystal order, and after struggling with a multitude of methods for improving crystal diffraction, surface entropy reduction mutagenesis gave rise to YopO-actin crystals that diffracted to better than 3 Å. The crystal structure reveals that the GDI domain and the kinase domain of YopO sandwich subdomain 4 and part of subdomain 2 of actin. Mutations to the YopO-actin interface derived from the structure, abolished interaction with actin, confirming validity of the structure. The structure also agrees with reports that the penultimate 20 residues of YopO are involved in binding actin (Juris et al. 2000; Trasak et al. 2007).

The capping of the pointed end of actin by YopO provides the structural basis for the inhibition of actin polymerization by YopO (Trasak et al. 2007). Putative phosphorylation sites Ser90 and Ser95 are located outside of the catalytic centre of YopO, suggesting that YopO is auto-inhibited in the inactive state (Trasak et al. 2007). The kinase domain adopts the structure of a typical eukaryotic kinase in the active state but with extended loops for interaction with actin. The interaction of the kinase domain with actin allows allosteric stabilization of structural elements of the catalytic cleft, enabling kinase activity.

The substitution of valine in muscle actin isoforms (Val203 in rabbit α-actin) for threonine in non-muscle isforms (Thr201 in mouse and human β-actin; Thr202 in *S.frugipera* and *D.discoideum*), accounts for the weaker activation of YopO by non-muscle actin isoforms. Thr202 of *S.frugipera* actin forms a hydrogen bond with Lys245 of YopO, which appears to stabilize the catalytic loop within the kinase

domain. When this hydrogen bond is abolished with the YopO K245M mutant, weaker autophosphorylation is observed. Analysis of the crystal packing of YopO-actin reveals that one of the SER mutation clusters mediates crystal contact and may have helped to improve crystal order.

The interaction of YopO with actin bridges subdomain 2 and 4 of actin, and appears to stabilize the closed conformation of the nucleotide-binding cleft of actin. YopO might inhibit nucleotide exchange of the bound actin monomer and the actin-profilin complex. The binding of YopO to subdomain 4 and part of subdomain 2 of actin is unique in that no other actin-binding protein discovered so far binds to this interface. Most actin-binding proteins bind actin on the 'hotspot' between subdomains 1 and 3 and YopO has left this region on actin unobstructed. The catalytic cleft of the kinase domain is flanked between the kinase domain and the GDI domain and lies above the bound actin. These seem to suggest that YopO could be using actin as a scaffold for means of substrate selection and as bait for recruitment of substrates. In the next chapter, the interaction of YopO and actin in the presence of other actin-binding proteins is investigated via a proteomics approach, to shed light on the mechanism of interference of the actin cytoskeleton by YopO and to identify substrates of kinase activity of YopO.

Chapter 4

Identifying novel kinase substrates of YopO

4.1 Stable isotope labelling with amino acids in cell culture

To identify proteins that interact with YopO as well as potential kinase substrates of YopO, quantitative proteomics with SILAC (stable isotope labelling with amino acids in cell culture) was performed. SILAC is an *in vivo* labelling strategy that enables characterization of protein–protein interactions with the advantage of being able to distinguish between specific and non-specific interactions (Mann 2006; Blagoev & Mann 2006). Macrophages have been characterised as a key target of *Yersinia* pathogenesis, so the Raw264.7 mouse leukemic monocyte macrophage cell line was used for the pull downs. The cell culture is split and grown simultaneously in either heavy isotopic ^{13}C-arginine and ^{13}C-lysine or normal isotopic ^{12}C-arginine and ^{12}C-lysine and passaged for at least five cell doublings to allow complete isotope incorporation of the entire proteome. The substitution of lysine and arginine, in combination with trypsin digestion, which cleaves at the carboxyl side of amino acids lysine and arginine (except when either is bound to a C-terminal proline), results in the labelling of every peptide in the mixture (except for the c-terminal peptide of the protein). This labelling enables direct quantitative comparison between ‘heavy’ and ‘light’ states using mass spectrometry.

4.2 Identification of proteins that interact with YopO

To identify proteins that interact with YopO, His-tagged YopO was used to saturate Ni-NTA agarose beads and allowed to pull proteins out of the 'heavy' lysate (**Fig. 4.1**). In parallel, as the control, agarose beads with no bait were incubated with the 'light' lysate. Both agarose samples were subjected to extensive washes and thereafter subjected to elution with 3C protease as described in **section 2.18.2**. The eluted samples were combined and ran on SDS-PAGE and cut into five slices (**Fig. 4.2**), separating highly abundant bait, actin and 3C protease proteins from the low abundance targets and separately analyzed by tandem liquid chromatography mass spectrometry (LC-MS/MS). The mass spectrometry and data extraction were carried out by Sanford-Burnham Proteomics Facility as described in **section 2.18.3-5** and briefly as follows. Peptides and proteins are identified from the MS/MS peak list data, with the addition of modified masses of SILAC amino acids as criteria for the search engine SEQUEST. Light and heavy peptides in the SILAC pair are used to quantitate the isotopic distribution of the protein in the heavy and light state.

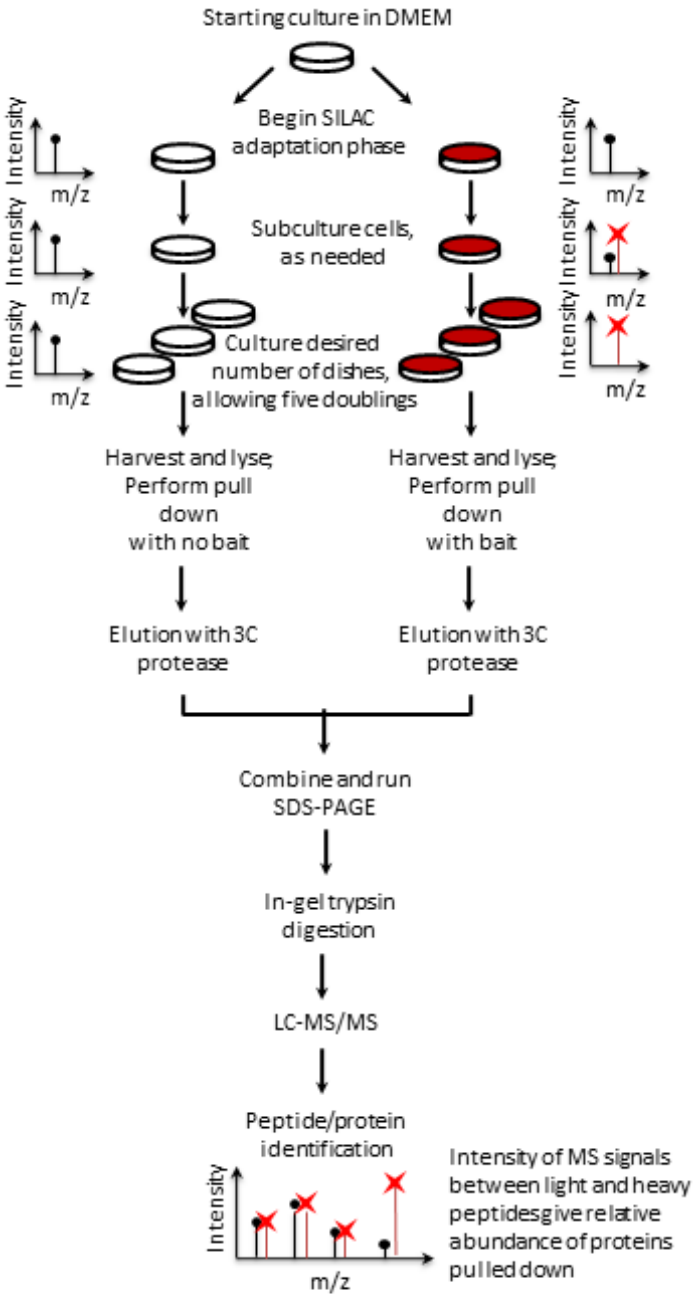


Figure 4.1 Flowchart describing the steps in the identification of proteins that interact with either YopO, profilin or YopO nRac mutant. The protein levels in the two samples are compared by quantifying the heavy and light peptides.

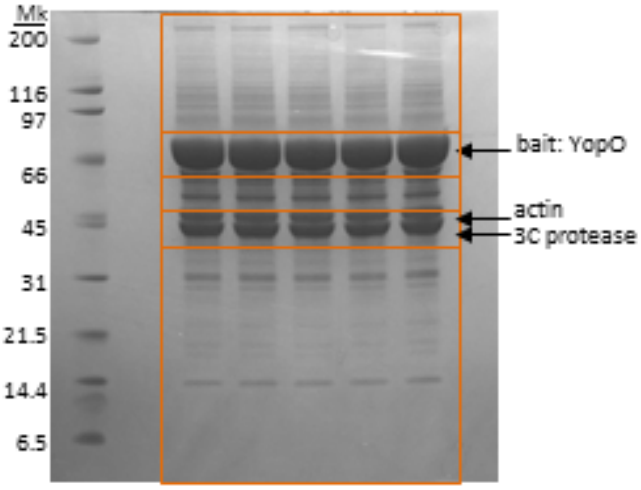


Figure 4.2 Gel of pull down with YopO as bait submitted for analysis by mass spectrometry. The gel was stained by Coomassie blue. The orange boxes demarcate the slices that were individually analyzed. Major proteins bands are indicated and BenchMark protein standards (Invitrogen) were used as molecular size markers (Mk).

The number of spectra identified for a given protein containing light amino acids is termed the light spectral count (Light Spec), and for heavy amino acids, as the heavy spectral count (Heavy Spec). The ratio of Heavy Spec over Light Spec (heavy/light) is calculated for all identified proteins, and used as a measure for identifying true interactions over background binding. For the proteins with no identified light spectra, they are given an empirical value of 0.5 instead of zero as the light spectral count, to allow for the calculation of the ratio of heavy spec over light spec. The entire dataset is plotted as a graph to show the distribution (**Fig. 4.3**). The median heavy/light ratio of proteins identified in the pull down with YopO is 0.4 with a standard deviation of 2.6. The cut off to demarcate putative interaction partners from background binding as determined based on median value plus one standard deviation, comes to 3.0. Details of proteins that make the cut off are listed in **Table 4.1**. The proteins are further filtered via sequence coverage criteria in which

proteins that have less than 10% of their sequence identified in the mass spectrometry are greyed out, leaving targets that are significantly enriched over background and have been confidently identified in the mass spectrometry.

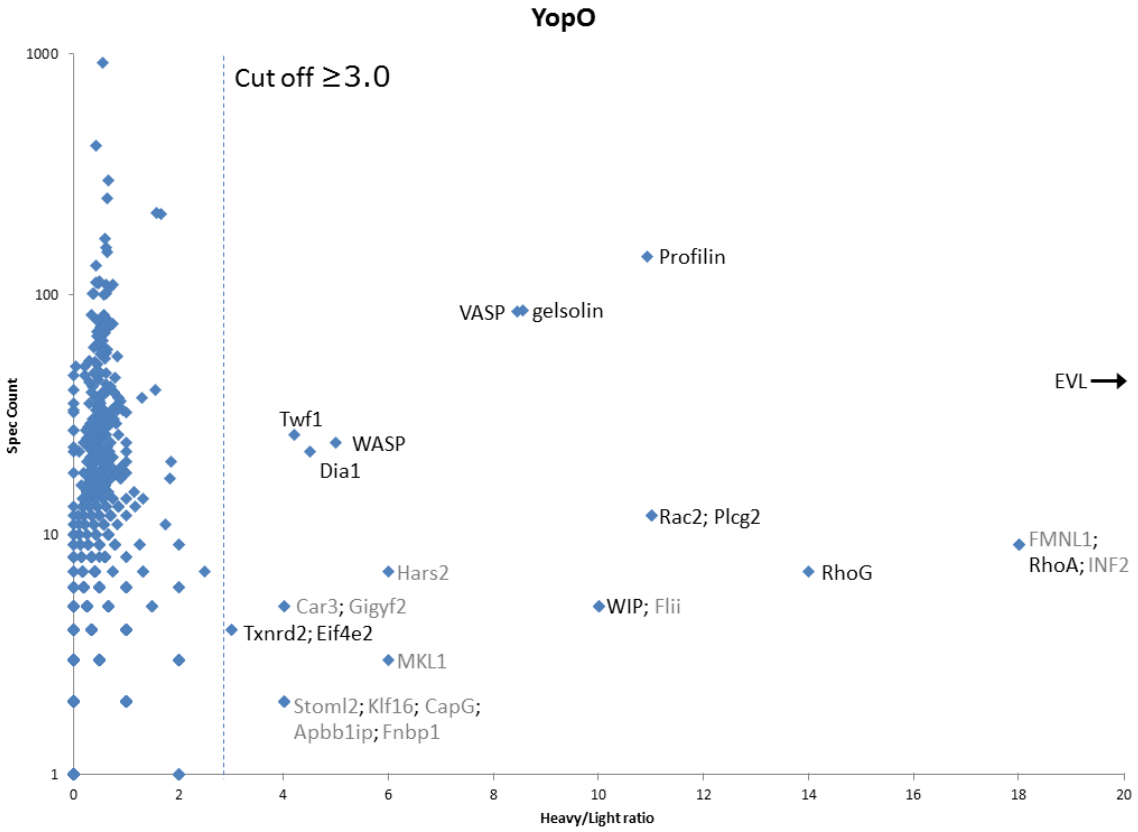


Figure 4.3 Chart showing the distribution of proteins identified by mass spectrometry upon pull down using His-tagged YopO as heavy to light ratio against spectrometry count (logarithmic scale). Labels are indicated for data points belonging to proteins above the cut off of heavy/light ratio of 3.0. Proteins with percentage sequence coverage of less than 10% are displayed in grey. Multiple protein labels per data point are due to overlapping data points. EVL is at a heavy to light ratio of 60 and is outside the range of this chart. Data points pertaining to actin have been removed from this chart.

Table 4.1 Proteins that were identified to be enriched via pull down with His-tagged YopO as bait in SILAC mass spectrometry. Table shows proteins that were enriched above heavy/light ratio of 3.0 or more. Data on proteins with percentage sequence coverage of less than 10% are displayed in grey. Actin has been removed from this table.

Sequence coverage (%)	Sequence count	Spec count	Symbol	Description	Heavy Spec	Light Spec	Heavy/ Light ratio
40.1	20	30	EVL	Ena/VASP-like protein	30	0.5*	60
5	5	9	FMNL1	formin-like protein 1	9	0.5*	18
26.9	6	9	RhoA	transforming protein RhoA	9	0.5*	18
8.2	9	9	INF2	Inverted formin-2	9	0.5*	18
35.6	5	7	RhoG	Rho-related GTP-binding protein RhoG	7	0.5*	14
32.8	8	12	Rac2	ras-related C3 botulinum toxin substrate 2	11	1	11
11.8	11	12	Plcg2	phosphatidylinositol-4,5-bisphosphate phosphodiesterase gamma-2	11	1	11
92.9	48	143	Profilin	profilin-1	131	12	10.9
32.6	5	5	RhoC	Rho-related GTP-binding protein RhoC	5	0.5*	10
15.4	4	5	WIP	WAS/WASL-interacting protein family member 1	5	0.5*	10
4.7	5	5	Flii	protein flightless-1	5	0.5*	10
42.4	45	86	gelsolin	gelsolin	77	9	8.6
60.3	52	85	VASP	vasodilator-stimulated phosphoprotein	76	9	8.4
6.3	2	7	Hars2	histidyl-tRNA synthetase	6	1	6
5;6.5	3	3	MKL1	MKL/myocardin-like protein 1	3	0.5*	6
23.3	16	24	WASP	Wiskott-Aldrich syndrome protein	20	4	5
14.5	19	22	Dia1	diaphanous1	18	4	4.5
28	14	26	Twf1	twinfilin1	21	5	4.2

5	5	5	Car3	carbonic anhydrase 3	4	1	4
6.7	5	5	Gigyf2	PERQ amino acid-rich with GYF domain-containing protein 2	4	1	4
8.8	2	2	Stoml2	stomatin-like protein 2	2	0.5*	4
7.6	2	2	Klf16	krueppel-like factor 16	2	0.5*	4
4	1	2	CapG	macrophage capping protein	2	0.5*	4
2.8	2	2	Apbb1ip	amyloid beta A4 precursor protein-binding family B member 1-interacting protein	2	0.5*	4
3.6	1	2	Fnbp1	formin-binding protein 1	2	0.5*	4
11.6	4	4	Txnrd2	thioredoxin reductase 2	3	1	3
12.3	4	4	Eif4e2	eukaryotic translation initiation factor 4E type 2	3	1	3

*the original light spec counts were zero, but have been modified to 0.5 in order to calculate a heavy/light ratio.

In the pull down with YopO as bait, proteins that were enriched (with heavy/light ratio of more than 3.0) include Rac and Rho family proteins (Rac2, RhoA and RhoG) and many actin-binding proteins including profilin, VASP, Ena/VASP-like (EVL), twinfilin1 (Twf1), gelsolin, formin diaphanous 1 (Dia1), ARP2/3 activator WASP, WASP binding protein WIP, and eukaryotic translation initiation factor 4E type 2. There were two proteins that did not fall into either category- phosphatidylinositol-4,5-bisphosphate phosphodiesterase gamma-2 and thioredoxin reductase 2. A number of actin-binding proteins were filtered out due to poor sequence coverage, including formins- formin-like protein 1 (FMNL1), inverted formin 2 (INF2); gelsolin-like proteins- flightless (Flii) and CapG; and

MKL/myocardin-like protein 1. Enrichment of Rac and Rho family proteins in the pull down agrees with literature that through its GDI domain, YopO interacts with Rho GTPases like Rac1 and RhoA but not Cdc42 (Barz et al. 2000; Dukuzumuremyi et al. 2000; Groves et al. 2010).

As with all pull down experiments, it is important to distinguish if the proteins enriched directly interact with YopO or interact indirectly through adapter proteins. The interaction of YopO with Rac and RhoA have been validated in literature (Barz et al. 2000; Dukuzumuremyi et al. 2000; Groves et al. 2010) and it is most likely that these proteins have been pulled down due to direct interaction with YopO. However, it is less likely that YopO has the ability to directly interact with the plethora of proteins that have been pulled down and it is more plausible that the actin-binding proteins were pulled down indirectly via actin and in the form of a ternary complex with YopO and actin.

To confirm this, available crystal structures of these identified proteins were superimposed on YopO-actin. The structure of profilin in complex with actin shows that profilin binds the barbed end of G-actin, between subdomains 1 and 3 on the underside of actin (Schutt et al. 1993). YopO binds actin, mostly on subdomain 4 and there is no steric clash with the binding of profilin to the same actin (**Fig. 4.4A**). VASP and EVL fall under the same family of Ena/VASP proteins and have similar domain structures. They bind to actin directly via the G-actin-binding site on EVH2 domain or indirectly through profilin via the proline-rich region. The structure of actin and profilin in complex with the G-actin-binding site of EVH2 and a section of the proline-rich region (Ferron et al. 2007) reveals that profilin binds as per the actin-

profilin complex and the G-actin-binding site of EVH2 binds actin on the hydrophobic cleft between subdomains 1 and 3 while a section of the proline-rich region binds profilin. There is no steric clash with the binding of YopO, profilin and G-actin-binding site of VASP on the same actin (**Fig. 4.4B**). Twinfilin consists of two ADF-H domains. The structure of ADF-H in complex with actin shows that ADF-H binds actin on the hydrophobic cleft between subdomains 1 and 3, presenting no steric clash with the binding of YopO on the same actin (Paavilainen et al. 2008) (**Fig. 4.4C**).

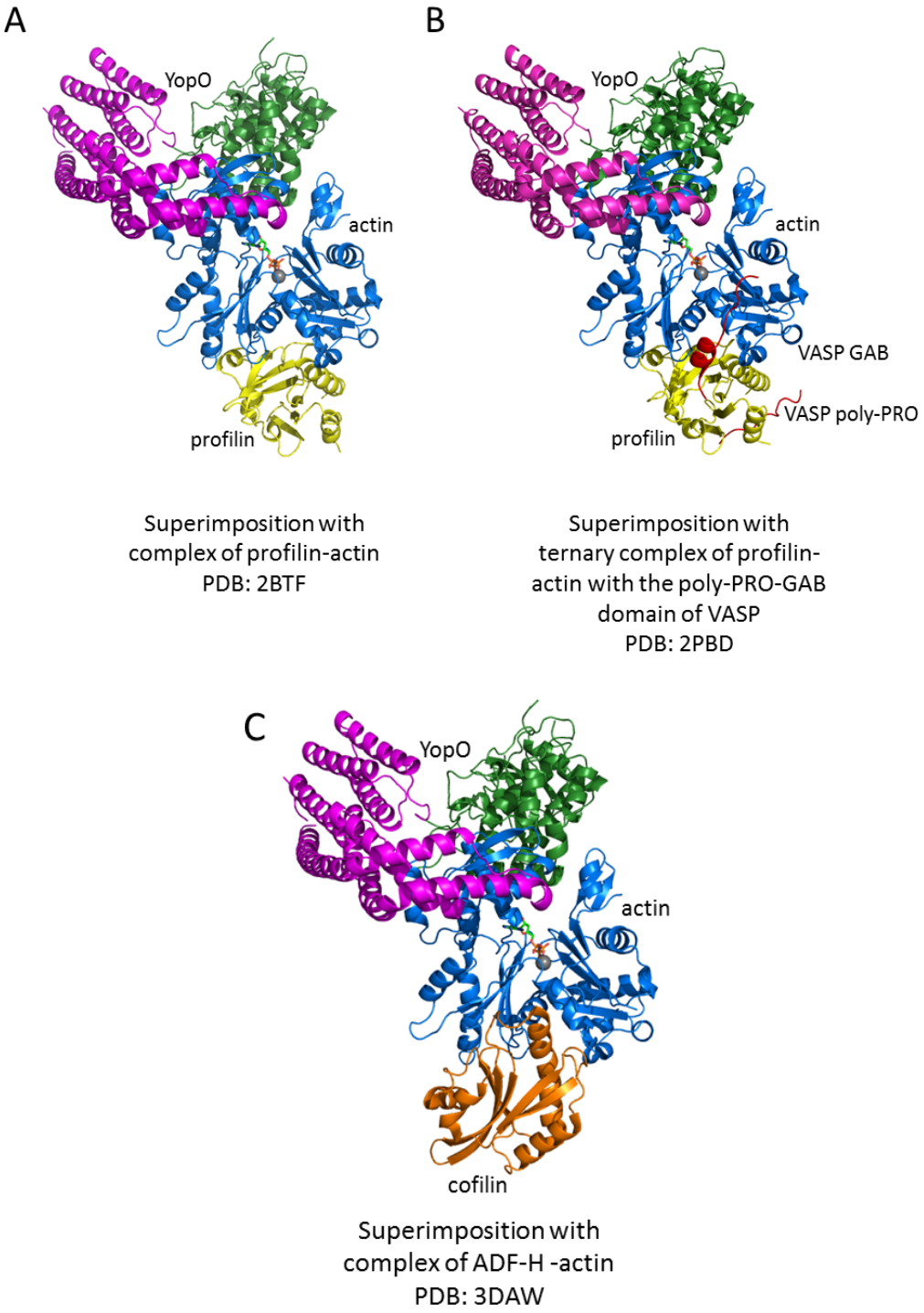


Figure 4.4 Superimposition of selected actin-binding proteins on YopO-actin. (A) Superimposition of profilin alone (PDB: 2BTF (Schutt et al. 1993)). (B) Superimposition of profilin and VASP construct containing part of proline-rich region and G-actin-binding site (PDB: 2PBD (Ferron et al. 2007)). (C) Superimposition of the ADF-H domain from twinfilin (PDB: 3DAW (Paavilainen et al. 2008).

Gelsolin is made up of six repeating homologous domains named G1-6. The interaction of gelsolin with actin has been solved in two parts- gelsolin domains 1-3 in complex with actin (Burtnick et al. 2004) and G4-6 in complex with actin (Choe et al. 2002). G1 binds at the hydrophobic cleft between subdomains 1 and 3, while G2 binds to subdomain 2, and G3 binds to subdomain 1. In the structure of G4-6 in complex with actin, G4 binds at the hydrophobic cleft between subdomains 1 and 3, G6 binds to subdomain 3 while G5 does not contact actin. YopO does not sterically hinder the binding of either half of gelsolin on the same G-actin (**Fig. 4.5**). WASP can bind to actin directly via the WH2 domain or indirect via profilin through its proline-rich regions. WIP contains a verprolin domain which consists of two WH2 domains. WIP can bind to actin indirectly via WASP, or directly via its own WH2 domains. All WH2-actin structures elucidated so far show that WH2 domains interact with actin on the hydrophobic cleft between subdomains 1 and 3 and likewise for the WH2 domain of WASP and WIP (Chereau et al. 2005). YopO does not sterically hinder the binding of the WH2 domain on the same G-actin (**Fig. 4.6**). Diaphanous can bind directly to actin via its FH2 domain or indirectly via profilin. The FH2 domain exists as a homodimer, binding around the short pitch of an actin filament (Otomo et al. 2005; Thompson et al. 2013). Since the binding of YopO is incompatible with actin in the filamentous state (**Fig. 4.7**), it cannot exist as a ternary complex with FH2-actin. As such, the pull down of formins by YopO is likely to take place via the recruitment of YopO-bound profilin-actin through the FH1 domain.

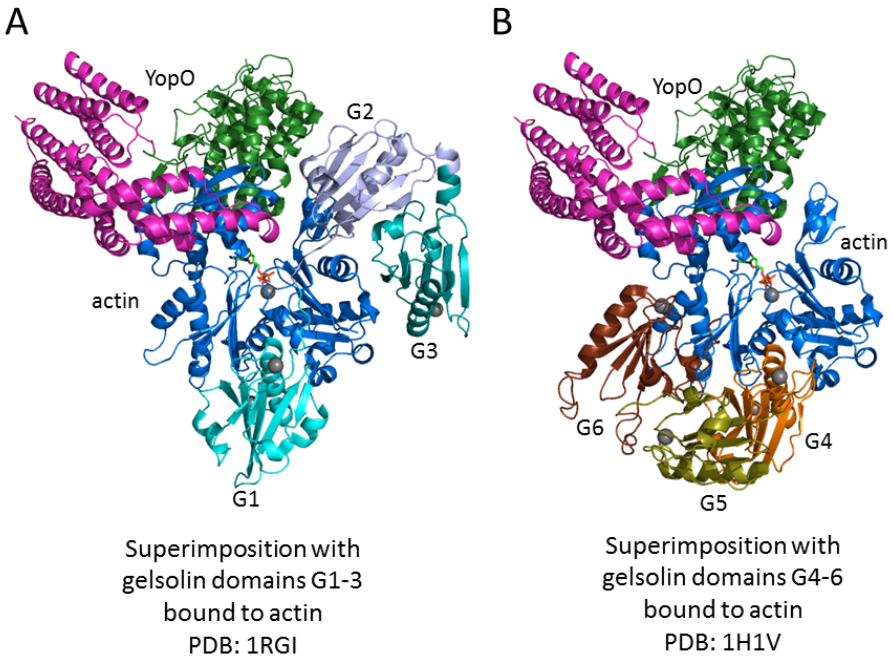


Figure 4.5 Superimposition of gelsolin-actin structures on YopO-actin. (A) Superimposition of gelsolin G1-3/actin complex (PDB: 1RGI (L D Burtnick et al. 2004)) (B) Superimposition of gelsolin G4-6/actin complex (PDB: 1H1V (H Choe et al. 2002)).

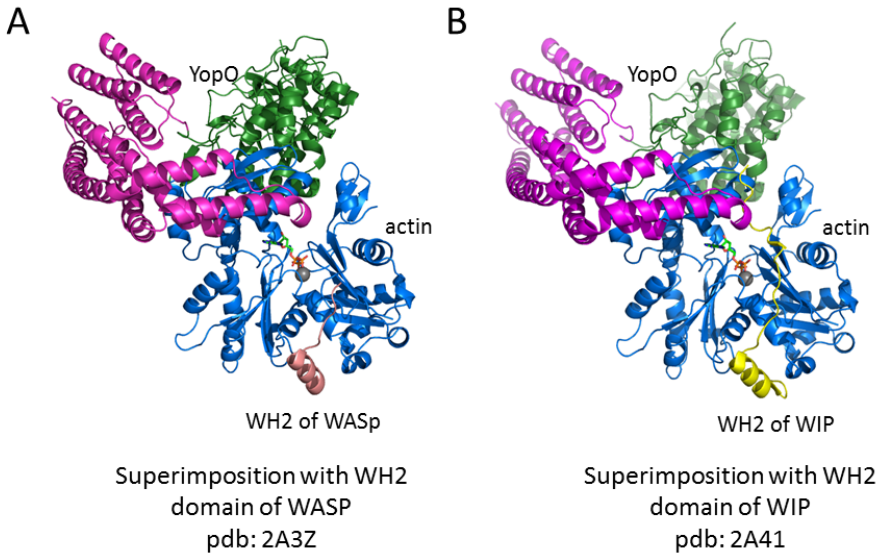


Figure 4.6 Superimposition of WH2 domains from WASP and WIP on YopO-actin. The structures of the WH2 domains were solved as a ternary complex with actin and DNase1. (A) Superimposition of WH2 from WASP (PDB: 2A3Z (Chereau et al. 2005). (B) Superimposition of WH2 from WIP (PDB: 2PBD (Ferron et al. 2007))

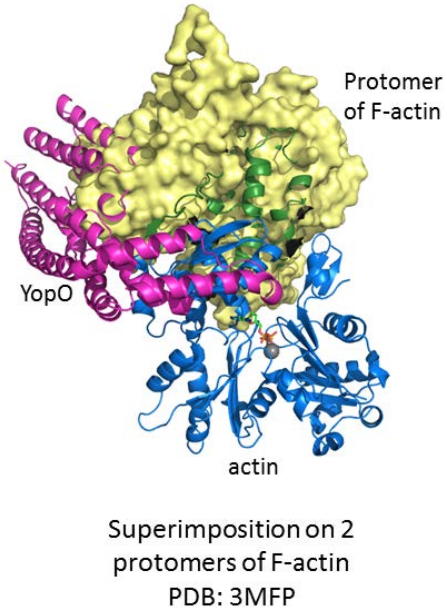


Figure 4.7 Superimposition of YopO-actin on two actin protomers in the F-actin conformation. One of the protomers is shown in yellow as surface representation.

In summary, of the proteins identified in the YopO pull down, Rho GTPases were directly bound by YopO, while the actin-binding proteins including formins, Ena/VASP family proteins, WH2 domain containing proteins, gelsolin family proteins and ADF-H containing proteins were pulled down indirectly via actin or by profilin-actin as complexes with YopO.

4.3 Identification of proteins that interact with profilin

We hypothesised that the actin-binding proteins which were pulled down with YopO were indirectly pulled down by actin. A pull down using profilin was performed to identify the profile of actin-binding proteins present in Raw264.7 cells. His-tagged profilin was used to saturate Ni-NTA agarose beads and allowed to pull proteins out of 'heavy' lysate. In parallel, agarose beads with no bait was incubated with 'light' lysate. The experimental setup is similar to that for identification of proteins that interact with YopO. Both agarose samples were subjected to extensive washes and thereafter subjected to elution with 3C protease. The eluted samples were combined and ran on SDS-PAGE and cut into three slices (**Fig. 4.8**), separating highly abundant bait, actin and 3C protease proteins from the low abundance targets and separately analyzed by tandem liquid chromatography mass spectrometry (LC-MS/MS).

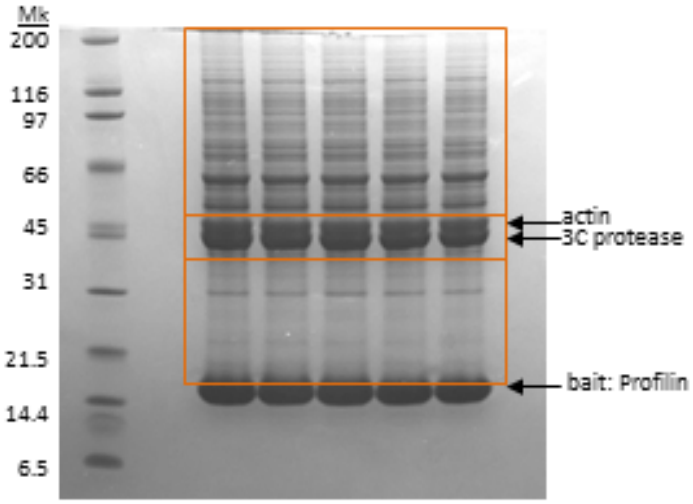


Figure 4.8 Gel of pull down with profilin as bait submitted for analysis by mass spectrometry. The gel was stained by Coomassie blue. Orange boxes demarcate the slices that were individually analyzed. Major proteins bands are indicated. BenchMark protein standards (Invitrogen) were used as molecular size markers (Mk).

Proteins identified in the pull down with profilin were plotted as a graph to show the distribution of spectral count (in logarithmic scale) against heavy over light ratio (**Fig. 4.9**). The median heavy/light ratio of proteins identified in the pull down with profilin was 0.1 with a standard deviation of 3.2 thus the cut off demarcating putative interaction partners from background binding was set at 3.3. Details of proteins that made the cut off were listed in **Table 4.2** where the proteins were further filtered via sequence coverage criteria. Proteins that had less than 10% of their sequence identified in the mass spectrometry were greyed out, while targets that were significantly enriched over background and confidently identified in the mass spectrometry were shown in black.

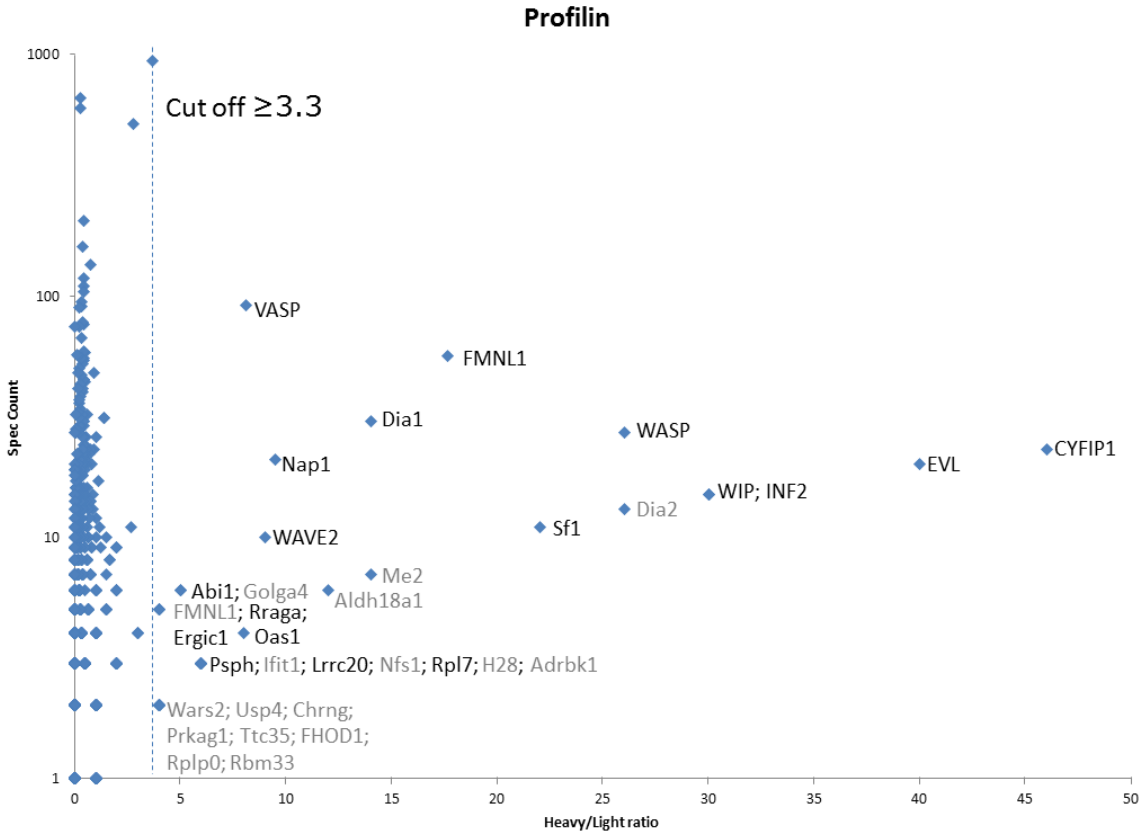


Figure 4.9 Chart showing distribution of proteins identified by mass spectrometry upon pull down using His-tagged profilin as heavy to light ratio against spectrometry count (logarithmic scale). Names are indicated for data points belonging to proteins above the cut off of heavy/light ratio of 3.3. Proteins with percentage sequence coverage of less than 10% are displayed in grey. Multiple protein labels per data point are due to overlapping data points.

Table 4.2 Proteins that were identified to be enriched via pull down with His-tagged profilin as bait in SILAC mass spectrometry. Table shows proteins that were enriched above heavy/light ratio of 3.3 or more. Data on proteins with percentage sequence coverage of less than 10% are displayed in grey. Actin has been removed from this table.

Sequence coverage (%)	Sequence count	Spec count	Symbol	Description	Heavy Spec	Light Spec	Heavy/ Light ratio
17.3	19	23	Cyfip1	cytoplasmic FMR1-interacting protein 1	23	0.5*	46
42.8	17	20	EVL	Ena/VASP-like protein	20	0.5*	40
37.7	10	15	WIP	WASP/WASL-interacting protein family member 1	15	0.5*	30
12.6	14	15	INF2	Inverted formin-2	15	0.5*	30
41.3	14	27	WASP	Wiskott-Aldrich syndrome protein	26	1	26
8.7	9	13	Dia2	diaphanous 2	13	0.5*	26
17	6	11	Sf1	splicing factor 1	11	0.5*	22
32.6	39	56	FMNL1	formin-like protein 1	53	3	17.7
14.7	21	30	Dia1	diaphanous 1	28	2	14
8.3	3	7	Me2	NAD-dependent malic enzyme	7	0.5*	14
9.7	5	6	Aldh18a1	delta-1-pyrroline-5-carboxylate synthase	6	0.5*	12
16.9	18	21	Nap1	NCK associated protein 1	19	2	9.5
13.3	9	10	WAVE2	Wiskott-Aldrich syndrome protein family member 2	9	1	9
44.5	60	91	VASP	vasodilator-stimulated phosphoprotein ;	81	10	8.1
13.1	4	4	Oas1	oligoadenylate synthetase 1	4	0.5*	8
16.9	3	3	Psph	phosphoserine phosphatase	3	0.5*	6
5.4	2	3	Ifit1	interferon-induced protein with tetratricopeptide repeats 1	3	0.5*	6
10.9	2	3	Lrrc20	leucine-rich repeat-containing protein 20	3	0.5*	6
5.4	1	3	Nfs1	cysteine desulfurase	3	0.5*	6

11.1	3	3	Rpl7	60S ribosomal protein L7	3	0.5*	6
8.8	3	3	H28	interferon-induced protein 44-like	3	0.5*	6
2.8	2	3	Adrbk1	beta-adrenergic receptor kinase 1	3	0.5*	6
2.1	3	6	Golga4	golgin subfamily A member 4	5	1	5
16.7	6	6	Abi1	abelson interactor 1	5	1	5
4.3	4	5	FMN1	formin-1	4	1	4
14.1	5	5	Rraga	ras-related GTP-binding protein A	4	1	4
16.6	4	5	Ergic1	endoplasmic reticulum-Golgi intermediate compartment protein 1	4	1	4
7.5	2	2	Wars2	tryptophanyl tRNA synthetase 2	2	0.5*	4
2.4	2	2	Usp4	ubiquitin carboxyl-terminal hydrolase 4	2	0.5*	4
4	1	2	Chrng	acetylcholine receptor subunit gamma	2	0.5*	4
8.5	2	2	Prkag1	AMP-activated protein kinase subunit gamma-1	2	0.5*	4
8.4	2	2	Ttc35	tetratricopeptide repeat protein 35	2	0.5*	4
2.6	2	2	FHOD1	FH1-FH2 domain-containing protein 1	2	0.5*	4
8.4	2	2	Rplp0	60S acidic ribosomal protein P0	2	0.5*	4
2	2	2	Rbm33	RNA-binding protein 33	2	0.5*	4

*the original light spec counts were zero, but have been modified to 0.5 in order to calculate a heavy/light ratio.

VASP, Ena/VASP-like (EVL), inverted formin 2 (INF2), diaphanous 1 (Dia1), formin-like 1 (FMNL1), ARP2/3 activator WASP and WAVE2 contain actin-binding sites as well as proline-rich regions which bind profilin for recruiting profilin-actin and could be pulled down directly by binding profilin and indirectly via actin. WIP could be pulled down indirectly via actin or while bound to WASP. Cyfip1 and Nap1 exist in the same complex as WAVE2. Unlike the pull down with YopO, twinfilin1 and gelsolin were not pulled down, due to competition for the same binding sites on actin and the absence of proline-rich regions for binding profilin. On the other hand, components of the WAVE complex were enriched in the pull down with profilin, but were absent in the pull down with YopO. As the WAVE complex is activated by Rac, the sequestration of Rac by YopO would result in the inactivation of the WAVE complex preventing it from being pulled down by YopO-actin. To test this hypothesis, a YopO non-Rac binding mutant (YopO nRac- Y588A, N592A, E596A) was constructed to be used as bait for a pull down experiment. These mutations abolish binding of Rac1 to YopO (Prehna et al. 2006). The mutations were verified to ensure that the YopO nRac mutant sequesters actin similarly to wild type YopO in an actin polymerization assay (**Fig. 4.10**).

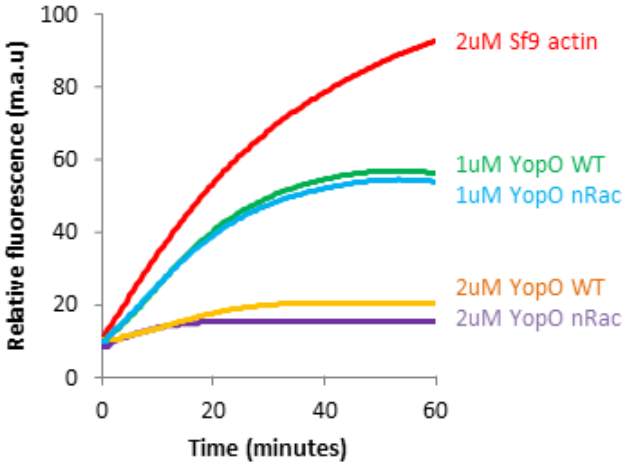


Figure 4.10 Actin monomer sequestration activity of YopO and YopO non-Rac mutant towards Sf9 actin. Red – 2 µM Sf9 actin. Green – 1 µM YopO WT added to 2 µM Sf9 actin. Orange – 2 µM YopO WT added to 2 µM Sf9 actin. Blue – 1 µM YopO nRac added to 2µM Sf9 actin. Magenta – 2 µM YopO nRac added to 2 µM Sf9 actin. Polymerization was initiated with the addition of KMEI buffer.

4.4 Identification of proteins that interact with the YopO nRac mutant

To identify proteins that interact with YopO nRac, the His-tagged YopO nRac mutant was used to saturate Ni-NTA agarose beads and allowed to pull proteins out of 'heavy' lysate. In parallel, as a control, agarose beads with no bait were incubated with 'light' lysate. The setup was identical to **section 4.2** using YopO (wild type). The eluted samples were combined and ran on SDS-PAGE and cut into five slices and analyzed by tandem liquid chromatography mass spectrometry (LC-MS/MS) (**Fig. 4.11**). Proteins identified in the pull down with YopO nRac were plotted into a graph to show the distribution of spectral count (in logarithmic scale) against heavy over light ratio (**Fig. 4.12**). The median heavy/light ratio of protein identified in the pull down with YopO nRac was 0.5 with a standard deviation of 4.0 and the cut off, set at median value plus one standard deviation, comes to 4.5. Details of proteins that made the cut off were listed in **Table 4.3** where the proteins were further filtered via sequence coverage criteria in which proteins that have less than 10% of their sequences identified in the mass spectrometry were shown in grey. The remaining targets which were shown in black have met criteria of significant enrichment over background and were identified with confidence in the mass spectrometry.

Proteins that were enriched were similar to that of YopO WT, however with YopO nRac, as expected, Rho GTPases like Rac2, RhoA and RhoG were not enriched (**Fig. 4.13**). However, components of the WAVE complex (WAVE2, Cyfip1, Nap1 and Abi1) were not detected. As such, in conclusion from our SILAC

data, YopO does not interact with the WAVE complex, either directly or indirectly. This also suggested that the binding of Rho GTPases and actin by YopO are independent events and do not affect each other.

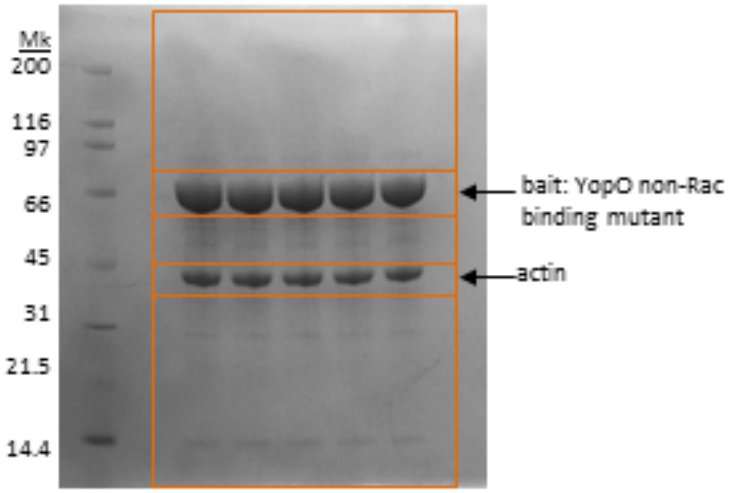


Figure 4.11 Gel of pull down with YopO nRac as bait submitted for analysis by mass spectrometry. The gel was stained by Coomassie blue. The orange boxes demarcate the slices that were individually analyzed. Major proteins bands are indicated. BenchMark protein standards (Invitrogen) were used as molecular size markers (Mk).

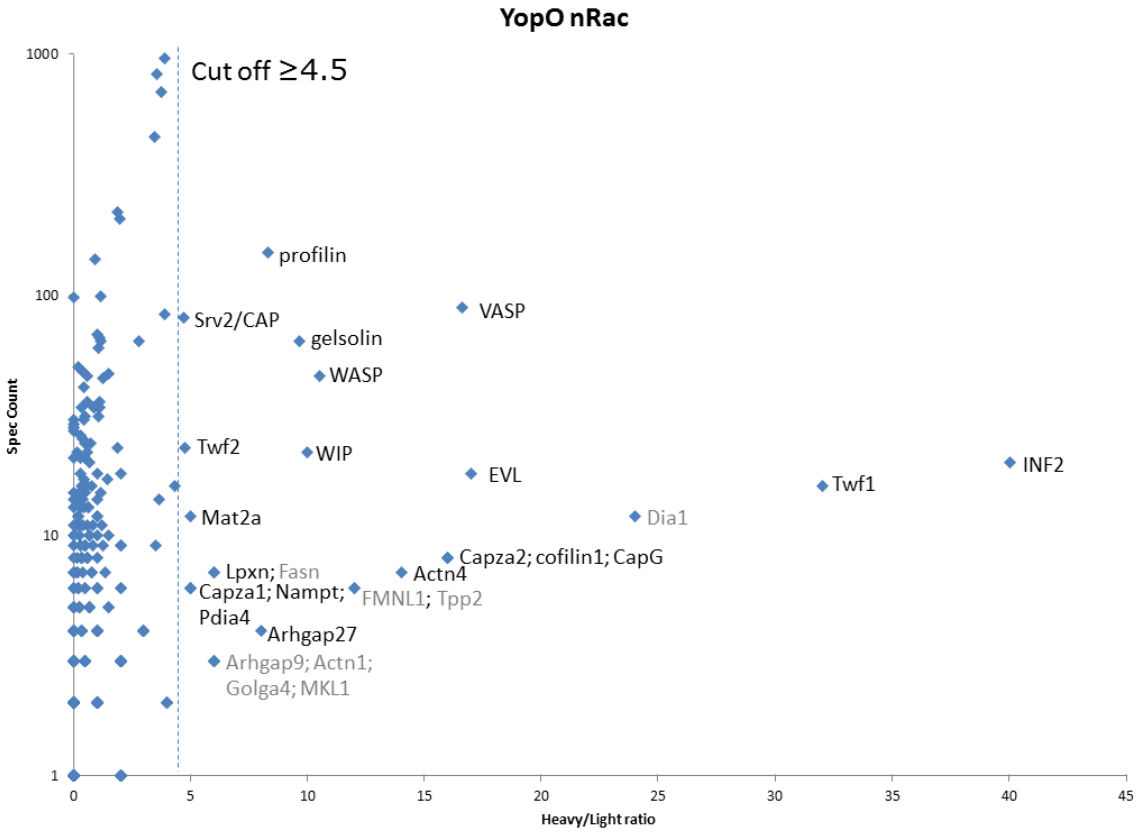


Figure 4.12 Chart showing distribution of proteins identified by mass spectrometry upon pull down using His-tagged YopO nRac as heavy to light ratio against spectrometry count (logarithmic scale). Names are indicated for data points belonging to proteins above the cut off of heavy/light ratio of 4.5. Proteins with percentage sequence coverage of less than 10% are displayed in grey. Multiple protein labels per data point are due to overlapping data points.

Table 4.3 Proteins that were identified to be enriched via pull down with His-tagged YopO nRac as bait in SILAC mass spectrometry. Table shows proteins that were enriched above heavy/light ratio of 4.5 or more. Data on proteins with percentage sequence coverage of less than 10% are displayed in grey. Actin has been removed from this table.

Sequence coverage (%)	Sequence count	Spec count	Symbol	Description	Heavy Spec	Light Spec	Heavy/ Light ratio
21.7	16	20	INF2	Inverted formin-2	20	0.5*	40
22.3	7	16	Twf1	twinfilin-1	16	0.5*	32
8.6	9	12	Dia1	diaphanous 1	12	0.5*	24
24.7	9	18	EVL	Ena/VASP-like protein	17	1	17
64.3	36	88	VASP	vasodilator-stimulated phosphoprotein	83	5	16.6
42.7	7	8	Capza2	F-actin-capping protein subunit alpha-2	8	0.5*	16
28.9	6	8	cofilin-1	cofilin-1	8	0.5*	16
28.4	7	8	CapG	macrophage capping protein	8	0.5*	16
10.1	6	7	Actn4	alpha-actinin-4	7	0.5*	14
7.6	5	6	FMNL1	formin-like protein 1	6	0.5*	12
6	4	6	Tpp2	tripeptidyl-peptidase 2	6	0.5*	12
31.3	12	46	WASP	Wiskott-Aldrich syndrome protein	42	4	10.5
31	8	22	WIP	WASP/WASL-interacting protein family member 1	20	2	10
35	28	64	gelsolin	gelsolin	58	6	9.7
82.1	26	149	profilin-1	profilin-1	133	16	8.3
13.6	3	4	Arhgap27	Rho GTPase-activating protein 27	4	0.5*	8
17.6	5	7	Lpxn	leupaxin	6	1	6
4.2	7	7	Fasn	fatty acid synthase	6	1	6
4.4	2	3	Arhgap9	Rho GTPase activating protein 9	3	0.5*	6
3.5	2	3	Actn1	alpha-actinin-1	3	0.5*	6
1.3	2	3	Golga4	golgin subfamily A member 4	3	0.5*	6

1.5	1	3	MKL1	MKL/myocardin-like protein 1	3	0.5*	6
28.7	5	6	Capza1	F-actin-capping protein subunit alpha-1	5	1	5
19	5	12	Mat2a	S-adenosylmethionine synthase isoform type-2	10	2	5
12.4	4	6	Nampt	nicotinamide phosphor-ribosyltransferase	5	1	5
10	4	6	Pdia4	protein disulfide-isomerase A4	5	1	5
37.1	10	23	Twf2	twinfilin 2	19	4	4.75
55.9	31	80	Srv2/CAP	adenylyl cyclase-associated protein	66	14	4.7

*the original light spec count is zero, but have been modified to 0.5 in order to calculate a heavy/light ratio.

4.5 Mechanism of recruitment of actin machinery of YopO

Proteins enriched in the respective datasets are compared in the form of Venn diagrams (**Fig. 4.13** & **4.14**). The majority of actin binding proteins pulled down are common between both YopO WT and YopO nRac datasets (**Fig. 4.13)**. All the proteins common between the YopO WT, YopO nRac and profilin datasets contain proline-rich regions. The accommodation of YopO-actin-profilin as ternary complexes allows YopO to be bound to these proteins via their proline-rich regions. YopO can also be recruited to profilin-incompatible actin complexes including gelsolin, CapG, twinfilin1 and MKL1 (**Fig. 4.14**). The identification of MKL1 and FMNL1 in both YopO WT and YopO nRac datasets improves confidence that MKL1 is a true binder despite poor sequence coverage.

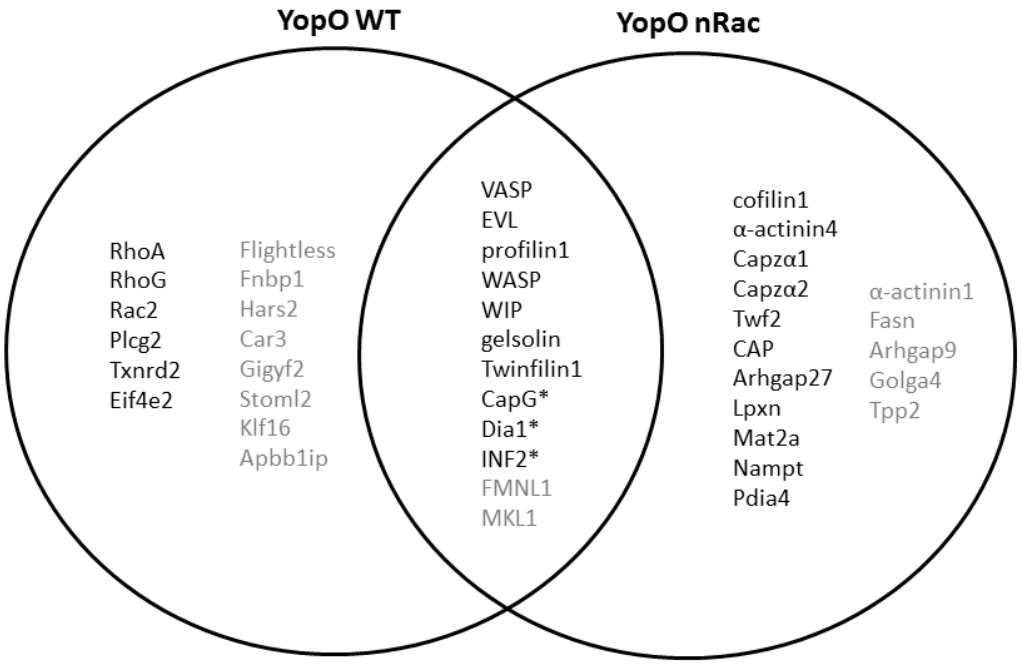


Figure 4.13 Venn diagram showing the overlap of and exclusive targets enriched within the datasets obtained with YopO WT and YopO nRac. In the centre quadrant showing the overlap of targets, protein names in grey indicate low sequence coverage in both of the datasets, and protein names with an asterisk indicate low sequence coverage in one of the datasets. In the side quadrants showing the exclusive targets, protein names displayed in grey indicate low sequence coverage in their respective datasets.

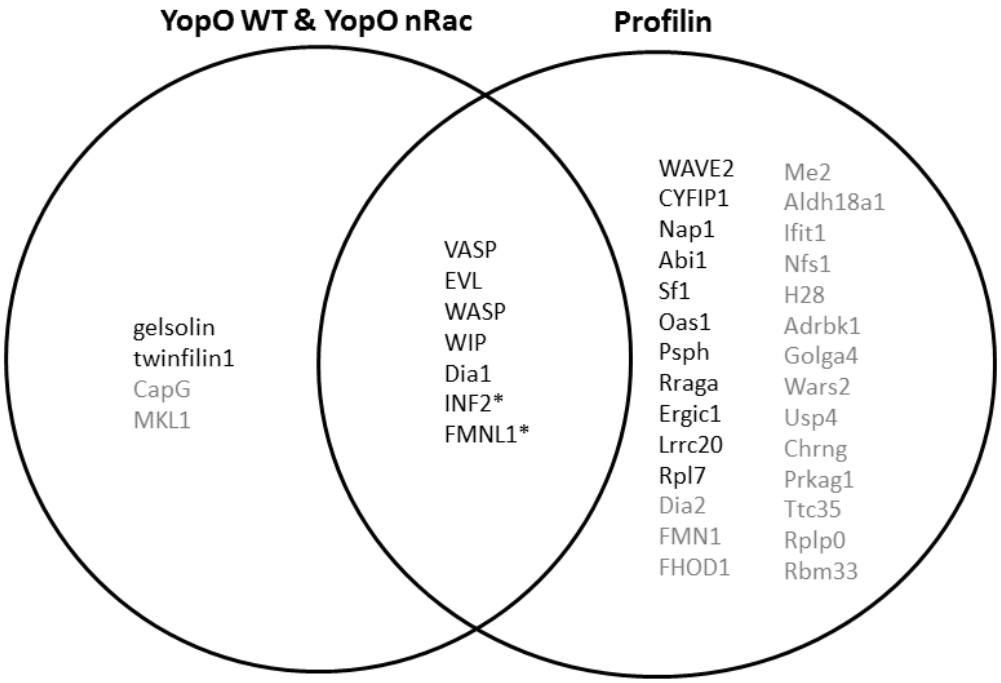


Figure 4.14 Venn diagram showing a comparison of common targets between YopO WT and YopO nRac against targets identified with profilin. In the centre quadrant showing the overlap of targets, protein names with an asterisk indicate low sequence coverage in one of the datasets. In the side quadrants showing exclusive targets, protein names displayed in grey indicate low sequence coverage in their respective datasets.

4.6 Implications of recruitment of actin-binding proteins by YopO

YopO binds actin primarily on subdomain 4 with further contacts on subdomain 2. In contrast, the most common binding surface on actin by host actin-binding proteins lies across subdomains 1 and 3. The majority of actin-binding proteins bind at the hydrophobic cleft between subdomains 1 and 3 and these include the Ena/VASP family of proteins, WH2 domains, RPEL domains, gelsolin (via G1 and G4) and ADF-H domains. YopO can exist in a ternary complex with these proteins. Profilin binds on the underside of subdomains 1 and 3, thus YopO can accommodate profilin in a ternary complex with actin. The recruitment of profilin-actin by proline-rich regions forms a common recruitment mode for most actin polymerization machineries, including formins, WASP family proteins and Ena/VASP family proteins. YopO has evolved to bind a surface on actin away from the 'hotspot' utilized by most other actin-binding proteins, putting it in prime spot to interfere with the plethora of actin reactions occurring in the cell, through steric hindrance and/or by phosphorylation.

YopO binds the pointed end of an actin monomer, a position which will inhibit nucleation and the addition of the bound actin monomer to a filament. The YopO-actin complex gets incorporated into actin nucleators that usually recruit profilin-actin. However, the YopO-bound actin monomer cannot be added to the barbed end of an actin filament due to steric hindrance of YopO, potentially stalling filament elongation of proteins by formins, ARP2/3 and the Ena/VASP family proteins. Sequestration of actin monomers requires YopO at a one to one ratio per actin monomer and the stalling of elongation of actin filaments theoretically requires one YopO per actin filament.

4.6.1 Implications of recruitment of MKL1 by YopO

MKL1, also known as MAL, is a transcriptional coactivator. It contains three actin-binding RPEL motifs that collectively bind three to five actins (Mouilleron et al. 2011). It binds actin as a means of sensing G-actin concentration such that increases in the cytosolic concentration of G-actin prevent nuclear import of MKL1 and thus prevents the activation of transcription of serum response factor (SRF) by MKL1 (Miralles et al. 2003). SRF regulates the transcription of a number of cytoskeletal components which include various actin isoforms and actin-binding proteins: profilin, gelsolin and cofilin (Sun et al. 2006). RPEL motifs bind between subdomains 1 and 3 spanning the hydrophobic cleft and reaching down to the underside of actin where profilin binds (Mouilleron et al. 2008). YopO-actin can accommodate being in a ternary complex with individual RPEL motifs (**Fig. 4.15**). In the macrophage, YopO is bound to the host membrane by the membrane localization domain. The binding of MKL1 by YopO would result in the retention of MKL1 in the cytoplasm, stopping signalling to the nucleus, to prevent the activation of the transcription of SRF.

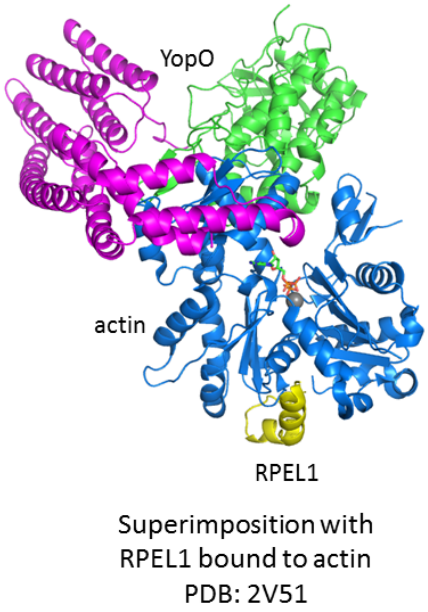


Figure 4.15 Superimposition of RPEL domain 1 from MKL1(PDB: 2V51 (Mouilleron et al. 2008)**) on YopO-actin.**

4.7 Determining the kinase activity of different YopO mutants

From the SILAC pull down data, we hypothesised that most of the enriched proteins can be accommodated in a ternary complex with YopO-actin and that actin serves as bait for the recruitment of kinase substrates for phosphorylation by YopO. Some of these enriched proteins might be phosphorylated by YopO. VASP was selected to be tested for phosphorylation by YopO via the *in vitro* kinase phosphorylation assay as described in **section 2.17.2** (**Fig. 4.16**).

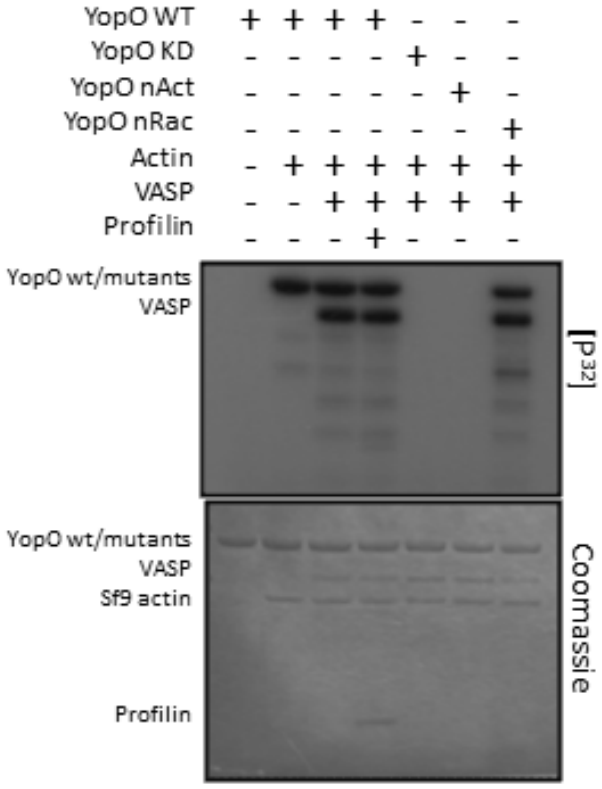


Figure 4.16 *In vitro* phosphorylation assay of YopO WT and mutants. YopO WT or mutants (4.7 μM) in the presence or absence of either Sf9 actin (4.7 μM), VASP as substrate (14 μM) or profilin (14 μM) as indicated, supplemented with [γ-32P]ATP. Proteins were separated by SDS-PAGE and visualized by Coomassie Blue staining (lower panel). Dried gels were exposed to X-ray film (upperpanel).

YopO autophosphorylates only in the presence of actin and phosphorylates VASP in the presence or absence of profilin. YopO non-actin-binding mutant (YopO nAct) does not autophosphorylate or phosphorylate the substrate VASP. These suggest that actin-binding is essential for autophosphorylation and kinase activity. The kinase dead mutant (YopO KD) does not autophosphorylate or phosphorylate VASP but retained the ability to sequester actin monomers in an actin polymerization assay, albeit with lower efficiency (**Fig. 4.17**). This suggests that catalytic activity of the kinase domain is not required for sequestration of actin, but might be required for stabilizing the active conformation of YopO for efficient actin sequestration. Autophosphorylation and substrate phosphorylation were unaffected by mutations to Rac binding site in YopO nRac mutant, suggesting that the ability to bind Rac is independent of kinase activity.

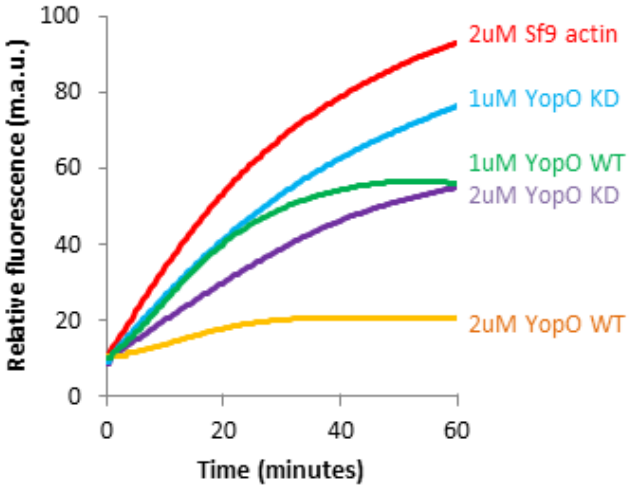


Figure 4.17 Actin monomer sequestration activity of YopO WT and YopO KD mutant towards Sf9 actin. Red – 2 µM Sf9 actin. Green – 1 µM YopO WT added to 2 µM Sf9 actin. Orange – 2 µM YopO WT added to 2 µM Sf9 actin. Blue – 1 µM YopO KD added to 2 µM Sf9 actin. Magenta – 2 µM YopO KD added to 2 µM Sf9 actin. Polymerization was initiated with the addition of KMEI buffer.

4.8 Validation of phosphorylation targets via *in vitro* autoradiography assays

Following the confirmation that VASP can be phosphorylated by YopO *in vitro*, more proteins were tested for phosphorylation by YopO via the *in vitro* kinase phosphorylation assay. These included EVL, Dia1, WASP, gelsolin, CapG and twinfilin1. A construct of Dia1 named Dia1 FH1-FH2 consisting of the FH1 and FH2 domains was used instead of the full length formin. A construct of WASP named WASP PWA which includes the proline-rich region up to the C-terminal end, including the VCA domain was used instead of the full length WASP. The GST and His tags were not cleaved from proteins Dia1 FH1-FH2 and WASP PWA as tag removal induced protein precipitation. All other proteins used were of the full length with their tags removed. As WASP PWA (with the GST and His tag) migrated at the same rate as YopO WT on SDS-PAGE, the GST tag of WASP PWA was cleaved with thrombin after the phosphorylation reaction to allow their differentiation on the SDS-PAGE and the X-ray film, as described in **section 2.17.2**.

To test the hypothesis that actin serves as bait for recruitment of kinase substrates for phosphorylation by YopO, three molar excess gelsolin domain 1 (G1) was added to compete with potential substrates for binding to actin, and as a second control, three molar excess profilin. G1 binds actin between subdomains 1 and 3, with an affinity of K_d = 5 pM (Nyakern-Meazza et al. 2002). G1 can accommodate being in a ternary complex with YopO-actin but will compete with other proteins for binding to the same region on actin. Profilin binds actin between subdomains 1 and 3 with an affinity of K_d = 0.7 μM (Gieselmann et al. 1995) but will not affect the

binding of proteins with proline-rich regions which bind profilin-actin and can be recruited into YopO-actin-profilin complexes.

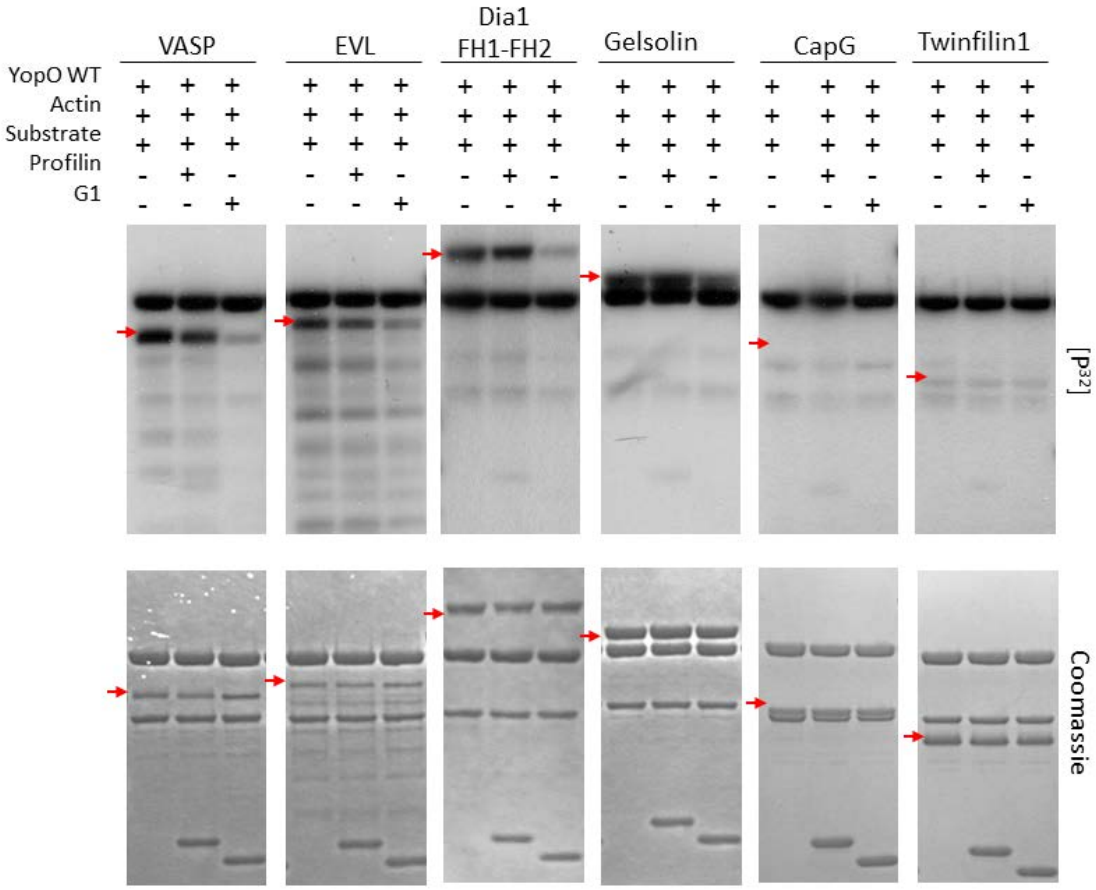


Figure 4.18 *In vitro* phosphorylation assays for potential substrates of YopO. YopO WT (4.7 μM) incubated with Sf9 actin (4.7 μM) and various substrates (4.7 μM), in the presence or absence of either profilin (14 μM) or gelsolin domain 1 (14 μM) as indicated, supplemented with [γ-^{32}P]ATP. Substrates are marked with red arrows. Dried gels were exposed to X-ray film (upper panel). Proteins were separated by SDS-PAGE and visualized by Coomassie Blue staining (lower panel).

In the presence of actin, YopO phosphorylates VASP, EVL, Dia1 FH1-FH2 and gelsolin, but not CapG and twinfilin1 (**Fig. 4.18**). VASP, EVL and Dia1 FH1-FH2 contain proline-rich regions and their phosphorylation by YopO was independent of the presence or absence of profilin. Their phosphorylation was

significantly reduced in the presence of G1, suggesting that the substrates were phosphorylated by YopO only if they could be recruited by actin, confirming the hypothesis that actin serves as bait for recruitment of kinase substrates for phosphorylation by YopO. Significantly reduced phosphorylation due to the competition of binding of G1 also suggested that the kinase predominantly phosphorylates in *cis*, the protein that is on the YopO-bound actin. Gelsolin is phosphorylated by YopO regardless of the presence of profilin, due to the higher affinity of gelsolin (K_d in pM range) for actin than profilin (K_d in μM range). Phosphorylation was only slightly reduced in the presence of G1, due to minor competition for the same binding site.

Thrombin cleaved WASP PWA gave rise to multiple protein bands with the major band corresponding to GST at 25 kDa, and other very faint bands (**Fig. 4.19**). YopO phosphorylates WASP PWA, as can be seen by the overlay of phosphorylated YopO WT on the phosphorylated uncleaved WASP PWA. Following cleavage with thrombin, while cleavage products were faint on the SDS-PAGE, they appeared to be phosphorylated on the X-ray film. The phosphorylation of WASP PWA cleavage fragments were slightly reduced in the presence of profilin, and strongly reduced in the presence of G1.

While ARP2/3 was not enriched in the pull down with YopO WT, ARP2/3 was tested whether it would interfere with the phosphorylation of WASP PWA or be phosphorylated in the presence of WASP PWA. There were no changes to the phosphorylation patterns of WASP PWA, suggesting that ARP2/3 was not phosphorylated by YopO and did not affect the phosphorylation of WASP PWA.

This could be due to two possibilities: the absence of a suitable phosphorylation site on ARP2/3 for YopO phosphorylation, or the inability of ARP2/3 at 220 kDa, to fit into the 31.5 – 33.0 Å kinase substrate binding groove flanked by the GDI and the kinase domain.

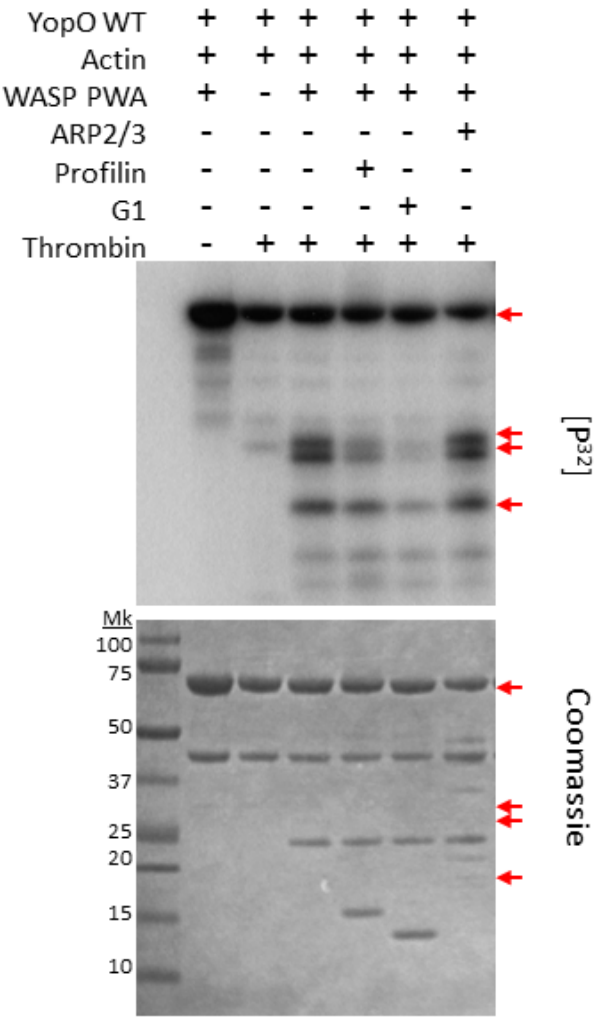


Figure 4.19 The phosphorylation of WASP PWA by YopO. YopO WT (4.7 μM) was mixed with Sf9 actin (4.7 μM) in the presence or absence of profilin (14 μM) or gelsolin domain 1 (G1) (14 μM), WASP PWA (4.7 μM) and/or ARP2/3 complex (4.7 μM) supplemented with [γ-32P]ATP. Selected samples as indicated, were subjected to cleavage with thrombin. Corresponding positions on SDS-PAGE and the X-ray film were marked by red arrows. Dried gels were exposed to X-ray film (upper panel). Proteins were separated by SDS-PAGE and visualized by Coomassie Blue staining (lower panel).

4.9 Effect of phosphorylation on the activity of VASP

To ascertain the effect of phosphorylation by YopO on the activity of VASP, VASP was phosphorylated by YopO in the presence of Sf9 actin and its ability to increase the rate of polymerization of α-actin was tested. α-actin was used for the polymerization as YopO has lower affinity for α-actin and the stalling of VASP by YopO would be minimal. As a control, VASP was subjected to the same phosphorylation conditions with the YopO kinase dead mutant (YopO KD), which has been shown to have no kinase activity. Phosphorylated VASP was observed to have attenuated ability to enhance the polymerization of actin, as compared to the unphosphorylated VASP and VASP in the presence of YopO KD (**Fig. 4.20**).

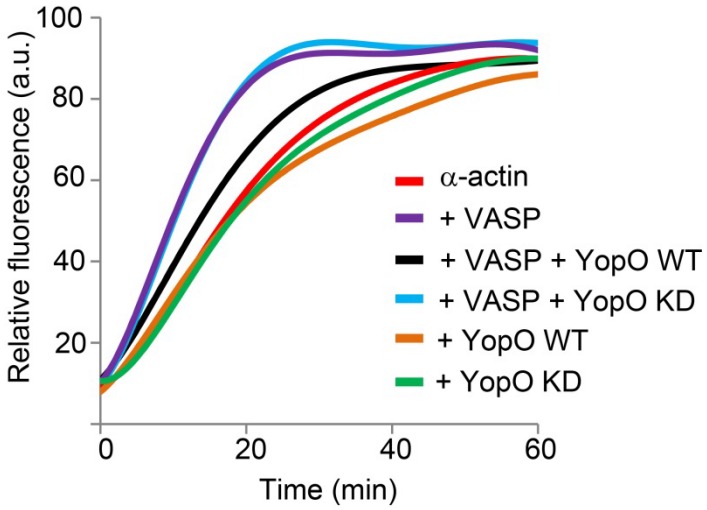


Figure 4.20 Effect of YopO-phosphorylated VASP on rate of actin polymerization. Red – 2 μM rabbit muscle α-actin. Magenta – 0.1 μM unphosphorylated VASP added to 2 μM rabbit muscle α-actin. Black – 0.1 μM VASP phosphorylated in the presence of 0.1 μM YopO WT and 0.1 μM Sf9 actin and added to 2 μM rabbit muscle α-actin. Blue- 0.1 μM VASP phosphorylated in the presence of 0.1 μM YopO KD and 0.1 μM Sf9 actin and then added to 2 μM rabbit muscle α-actin. Brown – 0.1 μM YopO WT added to 2 μM rabbit muscle α-actin. Green – 0.1 μM YopO KD added to 2μM rabbit muscle α-actin. Polymerization was initiated with the addition of KMEI buffer.

4.10 Discussion

4.10.1 Modulation of the actin cytoskeleton by steric hindrance

This work has identified proteins that are recruited by YopO-actin and YopO-actin-profilin. These include VASP family proteins (VASP and EVL); WASP and WASP binding protein WIP; gelsolin family proteins (gelsolin and CapG); formins Dia1, INF2 and FMNL1; twinfilin1; and MKL1. YopO uses actin as bait for recruitment of actin cytoskeletal components and these components are recruited by direct binding to actin, or by binding profilin-actin via their proline-rich regions. The YopO-actin complex gets incorporated into actin polymerization machinery like WASP, VASP family proteins and formins that usually recruit profilin-actin. However, the YopO-bound actin monomer cannot be added to the barbed end of actin filaments due to steric hindrance caused by YopO, potentially leading to the stalling of filament elongation. Schematic representations are shown in **Fig. 4.21**, illustrating how recruitment of YopO-bound actin monomers can lead to stalling of filament elongation.

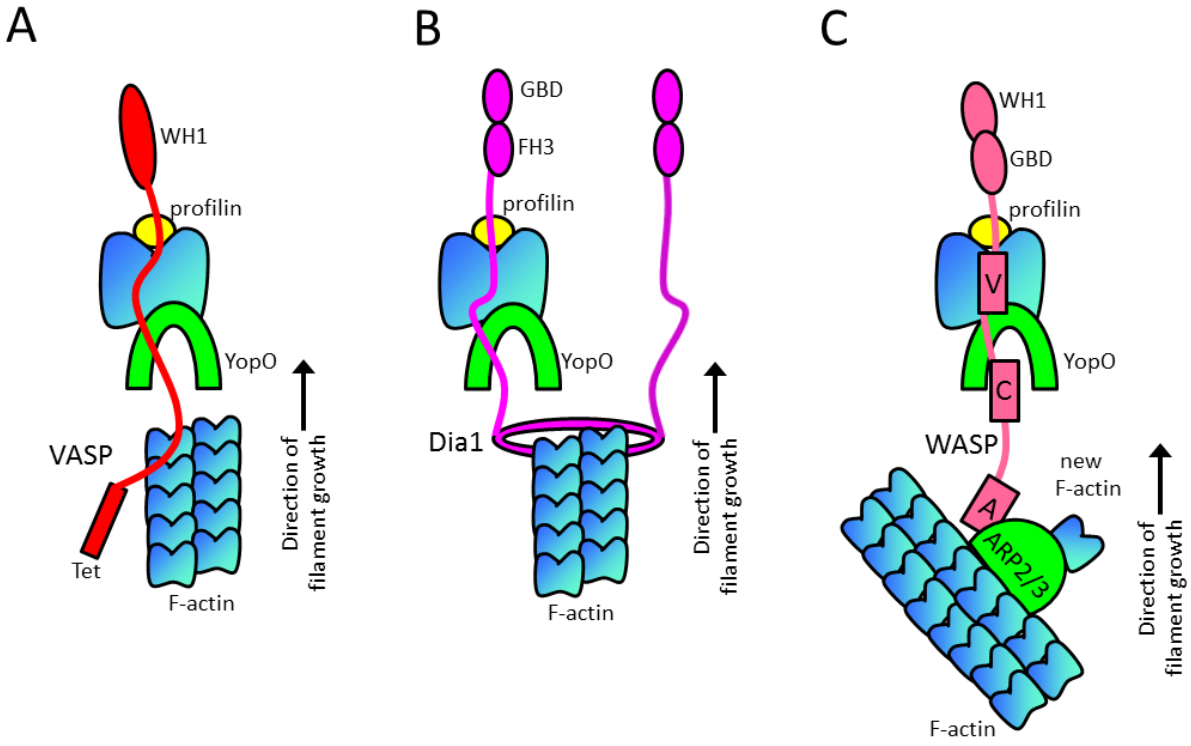


Figure 4.21 Schematics representations of steric hindrance of YopO towards filament elongation by various actin polymerization machineries. (A) VASP. For simplicity, only a subunit of the VASP tetramer is shown. The domain nomenclature denotes WASP homology domain 1 (WH1) and tetramerization domain (Tet). (B) Dia1 is shown as a homodimer. The domain nomenclature denotes Rho GTPase-binding domain (GBD) and formin homology domain 3 (FH3). (C) WASP. For simiplicity, only a WASP monomer is shown. The domain nomenclature denotes WASP homology domain 1 (WH1) and verprolin-central-acidic domain (VCA). Schematics are not drawn to scale.

4.10.2 Mechanism of kinase substrate selection of YopO

YopO phosphorylates only a subset of proteins that it recruits. YopO phosphorylates VASP, EVL, Dia1, gelsolin and WASP PWA, but not CapG, twinfilin1, profilin and G1. All of the phosphorylated proteins seem to have the ability to reach the catalytic cleft. Schematic representations of the binding of these actin-binding proteins to YopO-actin are shown in **Fig. 4.22**. While gelsolin and CapG are believed to bind to actin in a similar manner, gelsolin is phosphorylated but not CapG. This is possibly due to the inability of CapG to reach the catalytic cleft while bound to the same actin. Likewise, twinfilin1 seemed to be unable to reach the catalytic cleft. The unique positioning of the catalytic cleft, flanked between the kinase domain and the GDI domain, makes it such that substrates have to fit into the gap between the two domains for phosphorylation. As such, it seems that the criteria for phosphorylation appear to be the ability to access the kinase catalytic cleft and the presence of a phosphorylation site, while specificity for the recognition sequence on the substrate appears to play a minor role, if any. Thus the crystal structure and phosphorylation data suggest that YopO phosphorylates proteins that are bound to the same actin and can reach the catalytic cleft.

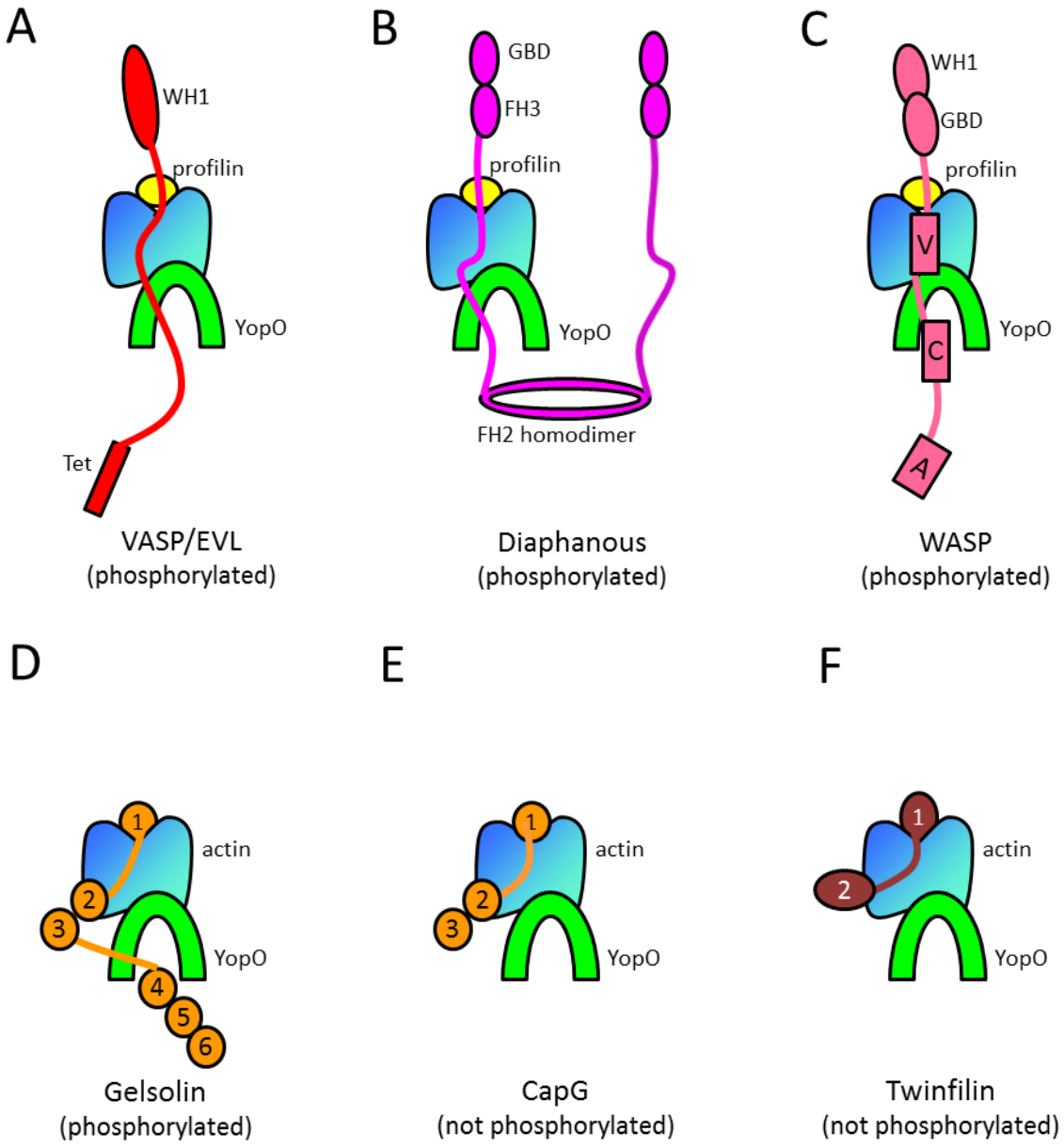


Figure 4.22 Schematic representation of binding of actin-binding proteins for phosphorylation by YopO. (A) The phosphorylation of VASP. For simplicity, only a subunit of the VASP tetramer is shown. The domain nomenclature denotes WASP homology domain 1 (WH1) and tetramerization domain (Tet). (B) The phosphorylation of diaphanous. Diaphanous is shown as a homodimer. The domain nomenclature denotes Rho GTPase-binding domain (GBD), formin homology domains 2 (FH2) and 3 (FH3). (C) The phosphorylation of WASP. The domain nomenclature denotes WASP homology domain 1 (WH1), Rho GTPase-binding domain (GBD) and verprolin-central-acidic domain (VCA). (D) The phosphorylation of gelsolin. The numbers present domains G1-6. (E) CapG is not phosphorylated. The numbers present domains G1-6. (F) Twinfilin is not phosphorylated. The numbers present domains ADF-H 1 and 2. The binding interface of the ADF-H 2 of twinfilin to actin is unknown. Schematics are not drawn to scale.

4.10.3 Modulation of the actin cytoskeleton by phosphorylation

Besides actin monomer sequestration and steric hindrance to filament elongation, YopO phosphorylates a subset of proteins that it recruits. Phosphorylation is a catalytic reaction that confers turnover, allowing YopO to exert productive effect beyond the number of YopO molecules. This work has shown that YopO phosphorylates VASP, EVL, Dia1, gelsolin and WASP and that the phosphorylation of VASP by YopO results in the loss of actin polymerization ability of VASP. Based on the similarity of domain structures, the phosphorylation should result in similar inhibition of the activity of EVL.

4.11 Conclusions

In this chapter, proteins recruited by YopO in RAW264.7 macrophages have been identified using SILAC. Rho GTPases including Rac2, RhoA and RhoG were pulled down as well as a number of actin-binding proteins. Rac2, RhoA and RhoG are important mediators in actin cytoskeletal dynamics. The superimposition of known structures of actin-binding proteins on the YopO-actin structure yielded no steric clashes, suggesting that the actin-binding proteins including formins, Ena/VASP family proteins, gelsolin family proteins, and WH2 domain, ADF-H domain and RPEL domain-containing proteins were pulled down indirectly via actin or by profilin-actin as complexes with YopO. A pull down with profilin was performed to identify the profile of actin-binding proteins present in Raw264.7 cells. Components of the WAVE complex were enriched in the pull down with profilin, but were absent in the pull down with YopO. The YopO nRac mutant with mutations to abolish Rho GTPase-binding was constructed to rule out that the WAVE complex

did not bind as they have been inactivated by the absence of Rac due to their sequestration by the GDI domain of YopO. Components of the WAVE complex were not pulled down with YopO nRac, confirming that YopO does not interact with the WAVE complex. The actin-binding proteins that were enriched with YopO nRac were similar to that of YopO WT, suggesting that the binding of Rho GTPases and actin by YopO are independent events and do not interfere with each other.

The YopO-actin crystal structure enabled interpretation of the SILAC pull down data to suggest that YopO uses actin as bait for recruitment of actin cytoskeletal components. A subset of the recruited proteins, as validated by the *in vitro* phosphorylation assays, has been identified to be phosphorylated by YopO and these include VASP, EVL, gelsolin, Dia1 and WASP. The abolishment of phosphorylation in the presence of competition by G1 suggests that substrates are phosphorylated only when they are bound to the same actin as YopO. CapG, twinfilin, profilin and G1 were not phosphorylated by YopO, suggesting that the ability to reach the catalytic cleft while bound to the YopO-bound actin is a prerequisite for phosphorylation. These reveal that YopO's substrate selection strategy involves the use of actin for recruitment and as a recognition scaffold for phosphorylation. VASP was shown to have had its actin polymerization activity curtailed upon phosphorylation by YopO. While the effect of phosphorylation on targets like WASP, gelsolin and formin have yet to be determined, these are important components in actin cytoskeletal dynamics. Phosphorylation of these components could wreak havoc on the temporal and spatial regulation of actin dynamics, upsetting the balance between actin polymerization and turnover.

Various YopO mutants were generated to shed light on the mechanism of activation of YopO. The inability of YopO non-actin-binding mutant (YopO nAct) to autophosphorylate or phosphorylate substrates suggests that actin-binding is essential for kinase activity. The YopO kinase dead mutant does not autophosphorylate or phosphorylate substrates but retained the ability to inhibit actin polymerization, albeit with a lower efficiency, suggesting that kinase activity is not required for binding actin, but might be required for stabilizing the active conformation of YopO for efficient actin sequestration. Autophosphorylation and substrate phosphorylation were unaffected in YopO nRac mutant, suggesting that the ability to bind Rac is independent of kinase activity. These would contribute to establishing a hypothetical mechanism for the activation of YopO and the generation of hypothetical models of inactive YopO, which would be discussed in the subsequent chapter.

Chapter 5

Establishing an integrated model for the mechanism of action of YopO

Kinase substrates of YopO have been identified and validated. The identification of kinase substrates of YopO has shed light on the specificity of YopO towards kinase substrates and this will be discussed in greater detail in this chapter. The structural, biochemical and proteomics work performed so far will be reconciled to provide an overview of the multi-faceted interference of the actin cytoskeleton by YopO and this includes: the inhibition of nucleotide-exchange by YopO; the sequestration of Rho GTPases; inhibition to actin filament formation; and phosphorylation of actin machineries by YopO. A couple of questions will also be addressed: how does the interference of the actin cytoskeleton by YopO contribute to the disruption of phagocytosis; and how does YopO complement the functions of other Yops in modulating host immune defense. Lastly, a mechanism for the activation of YopO and models of inactive YopO will be established from a compilation of structural and biochemical data with predictions from programs Hingeprot and Elnemo.

5.1 The proposed mechanism of substrate selection of YopO

The specificity of a kinase is determined by two main factors: the peptide specificity of the kinase for the substrate, and the frequency of encounter between the kinase and the substrate (Zhu et al. 2005). YopO has precise substrate selection strategies that enable it to cripple the actin cytoskeleton in a targeted manner. YopO has a membrane localization domain (Letzelter et al. 2006) and has been shown to be localized to the inner surface of the host cell membrane upon injection into the host cell (Håkansson et al. 1996). Membrane localization is extremely important for effective function of YopO. In the absence of the membrane localization domain, YopO loses its anti-phagocytosis function (Groves et al. 2010). YopO is localized at the cell membrane, allowing it to target the actin cortex where actin polymerization machineries and signals for actin remodelling in the form of Rho GTPases are located. The membrane localization of YopO increases its frequency of encounter with target substrates.

The kinase domain of YopO cannot maintain its active conformation if it is not bound to actin. YopO uses actin as a scaffold for means of substrate selection. YopO does not have a binding site for recognising the plethora of actin machineries, but by binding actin it can attract actin-binding proteins using the bound actin as bait. It then phosphorylates a subset of the proteins it recruits. In the active conformation, the catalytic cleft of the kinase domain is flanked between the kinase domain and the GDI domain. The kinase domain is positioned such that it can only phosphorylate substrates that come to be flanked between the kinase domain and the GDI domain (**Fig. 5.1**). In the YopO-actin structure, these two domains are only 31.5-33.0 Å apart. Such configuration restricts the phosphorylation to targets that can insert into

the gap between the kinase domain and the GDI domain.

In vitro, YopO has been found to phosphorylate VASP, EVL, diaphanous1, WASP and gelsolin. YopO does not phosphorylate profilin, G1, CapG and twinfilin. Structurally, it appears that these proteins are not phosphorylated as they were unable to reach the catalytic cleft of the YopO kinase domain upon binding to the YopO-bound actin. At the moment, the specificity of YopO for the recognition sequence on the substrate has yet to be worked out but it appears that the ability to access the kinase catalytic cleft seems to be a prerequisite for target phosphorylation. As such, it seems that frequency of encounter seems to be the major determinant in the substrate specificity of YopO and this is influenced by the membrane localization, the binding of actin as bait and scaffold, and the restrictive configuration of the kinase substrate binding groove.

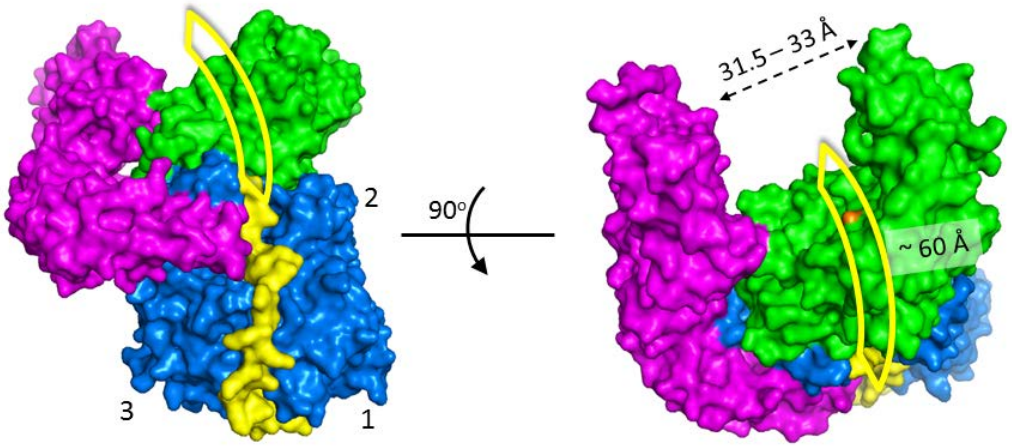


Figure 5.1 The mode of binding of substrates for phosphorylation. This model is obtained by the superimposition of the WH2 domain from WIP (PDB: 2A41(Chereau et al. 2005)) on the structure of YopO-actin. The model is shown in surface representation, in which actin is in blue, the GDI domain is in magenta, the kinase domain is in green, the catalytic Asp267 is in orange and WH2 domain of WIP is in yellow. Subdomains 1-3 of actin are labelled. The yellow box indicates the hypothetical path of the substrate for reaching the catalytic cleft (marked by Asp267) for phosphorylation.

5.1.1 Model of binding and phosphorylation of VASP by YopO

VASP was shown in **Section 4.9** to be phosphorylated by YopO. The model of substrate bound to YopO, built based on the superimposition of the WH2 domain from WIP (PDB: 2A41) (Chereau et al. 2005) on the structure of YopO-actin (**Fig. 5.1**), was used to predict YopO's phosphorylation site on VASP. Alignment of the primary sequence of the WH2 domain of WIP with the G-actin binding region of VASP suggests that YopO would be phosphorylating VASP C-terminal to the G-actin binding region (**Fig. 5.2**). The path length from the last ordered residue of the WH2 domain of WIP to the catalytic Asp267 of the kinase domain of YopO is approximately 60 Å. Given that in full extension, the distance between two amino acids is about 3.6 Å, a minimum of 17 residues would be required to span 60 Å. Thus Thr278 of VASP lies closest to the putative region of phosphorylation. In agreement, phosphorylation of VASP at Thr278 has been reported to reduce VASP's ability to enhance the rate of actin polymerization (Harbeck et al. 2000; Doeppler et al. 2013).

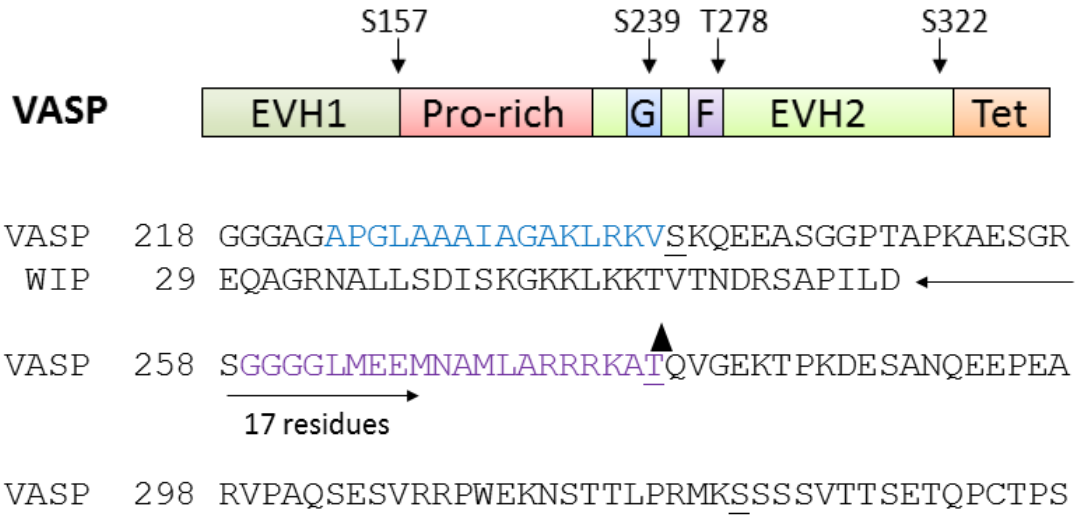


Figure 5.2 Approximation of putative phosphorylation sites on VASP by sequence alignment with WH2 from WIP. The sequence of a section of VASP is aligned with the sequence of the WH2 domain from WIP observed in PDB: 2A41(Chereau et al. 2005). The sequence of VASP shown in blue denotes the region involved in binding G-actin (PDB: 2PBD (Ferron et al. 2007)) and shown in magenta denotes the region known to bind F-actin. Reported serine and threonine phosphorylation sites are underlined. Thr278 is marked with a black triangle.

5.2 Multi-faceted interference of the actin polymerization machinery by YopO

YopO potentially interferes with actin polymerization in a number of ways: interference of YopO with nucleotide exchange kinetics of profilin-actin; sequestration of Rho GTPases; sequestration of actin monomers and inhibition to actin filament formation by steric hindrance; and phosphorylation of actin machinery. These aspects collectively lead to the disabling of actin cytoskeletal dynamics to result in the disruption of phagocytosis.

5.2.1 Interference with nucleotide exchange of profilin-actin

YopO stabilizes the closed conformation of the nucleotide-binding cleft of actin and potentially interferes with the nucleotide exchange of profilin-actin. ATP-actin is favoured for polymerization over ADP-actin and maintenance of a pool of ATP-bound monomeric actin is important for persistent cell migration (Goldschmidt-Clermont et al. 1992). Profilin regulates the pool of ADP-actin in cells by promoting the conversion of ADP-actin to ATP-actin. The binding of YopO to profilin-actin may prevent the profilin-bound actin from nucleotide exchange (Goldschmidt-Clermont et al. 1992), impeding efficient actin turnover (**Fig. 5.3**).

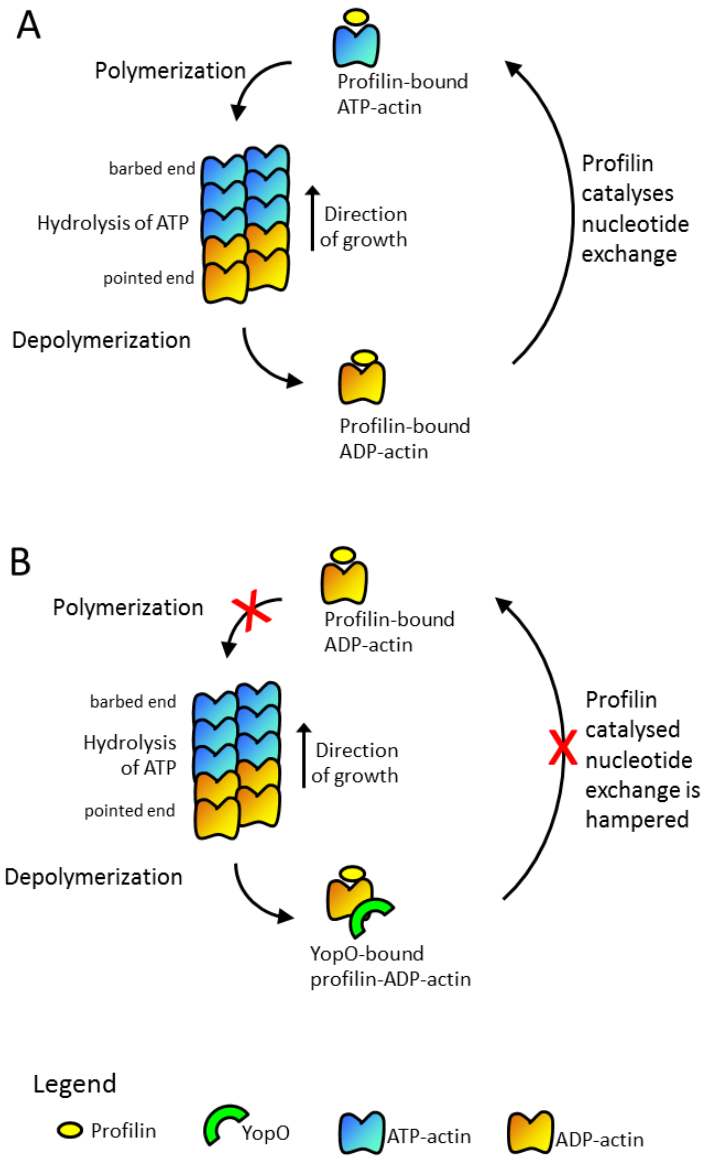


Figure 5.3 The interference of actin turnover by inhibition of nucleotide exchange of profilin-actin by YopO. Actin monomers from the depolymerization of actin filaments are ADP-bound. However, ATP-bound G-actin is preferentially incorporated into the actin filament over ADP-bound G-actin. Profilin binds to and catalyzes the exchange of ADP for ATP on actin monomers. (A) Actin turnover under normal circumstances. (B) Actin turnover hampered by YopO.

5.2.2 Implications of sequestration of Rho GTPases on actin dynamics

Rho GTPases Rac2, RhoA and RhoG were enriched in the pull down with YopO WT against macrophage cells. The binding of kinase substrates does not sterically hinder the binding of Rho GTPases, suggesting that phosphorylation by the kinase domain and Rho GTPase sequestration can occur concurrently.

RhoG is involved in the activation of Rac and Cdc42 and the sequestration of RhoG would lead to the inhibition of the activation of Rac and Cdc42 (**Fig. 5.4**). Rac and Cdc42 activate formins Dia2 and Dia3, leading to actin polymerization. Rac activates the WAVE complex and Cdc42 activates WASP, both leading to actin polymerization through the activation of ARP2/3 (Lammers et al. 2008). Rac and Cdc42 activate PAK, leading to the phosphorylation of LIMK which phosphorylates and inhibits cofilin (Edwards et al. 1999). Rac2 is also involved in the reactive oxygen species (ROS) production pathway. The binding of Rac to p67(Phox) is necessary for the assembly of NADPH oxidase, a multi-protein enzyme complex that produces ROS for killing bacteria. The sequestration of RhoG and Rac means that signals downstream of Rac and Cdc42 are switched off, translating to the inactivation of actin polymerization by Dia2, 3, the WAVE complex, and WASP; the inactivation of ROS production; and the activation of depolymerisation by cofilin.

RhoA activates the formin Dia1 and ROCK which in turn activates LIMK leading to phosphorylation and inhibition of cofilin (Maekawa 1999). ROCK is also involved in the phosphorylation of myosin light chain (MLC), which leads to the

formation of stress fibres and focal adhesions which are important for actin fibre contraction (Leung et al. 1996). The sequestration of RhoA by YopO would translate to the inactivation of actin polymerization by Dia1; the inactivation of the formation of actin stress fibres and focal adhesions; and the activation of depolymerisation by cofilin.

So collectively, sequestration of Rac2, RhoG and RhoA leads to the inhibition of actin polymerization machinery, inhibition of actin stress fibre formation and focal adhesions and the activation of depolymerisation.

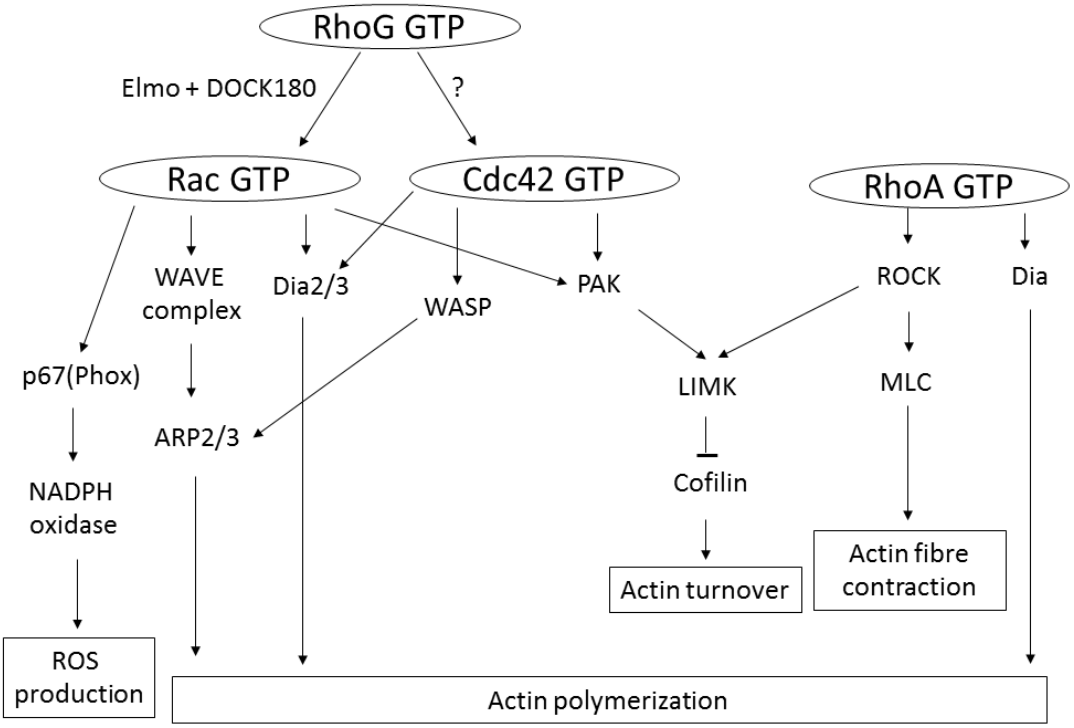


Figure 5.4 The effects of Rac, RhoA and RhoG sequestration. The inhibition of RhoG would result in the inactivation of Rac and Cdc42. The effect of RhoG on Cdc42 occurs by a unknown pathway. The sequestration of Rac results in the inactivation of the WAVE complex and dia2 and 3, switching off actin polymerization. Sequestration of Rac also turns off the reactive oxygen species (ROS) production pathway. Sequestration of Rho leads to inhibition of dia1, switching off actin polymerization. The inhibition of ROCK by sequestration of Rho turns off actin fibre contraction by MLC. The sequestration of Rac and Rho both contribute to turning off the inhibition of cofilin, leading to actin depolymerization by cofilin.

5.2.3 Actin monomer sequestration and inhibition to actin filament formation

YopO binds the pointed end of an actin monomer, sequestering the actin monomer and preventing their polymerization (**Fig. 5.5 A**). The YopO-bound actin-profilin cannot be added to the barbed end of an actin filament due to steric hindrance with YopO. This may interfere and stall actin polymerization machineries that have managed to recruit YopO-bound actin and YopO-bound actin-profilin. In the process of stalling the actin polymerization machinery, YopO will phosphorylate some of these machineries (**Fig. 5.5 B**).

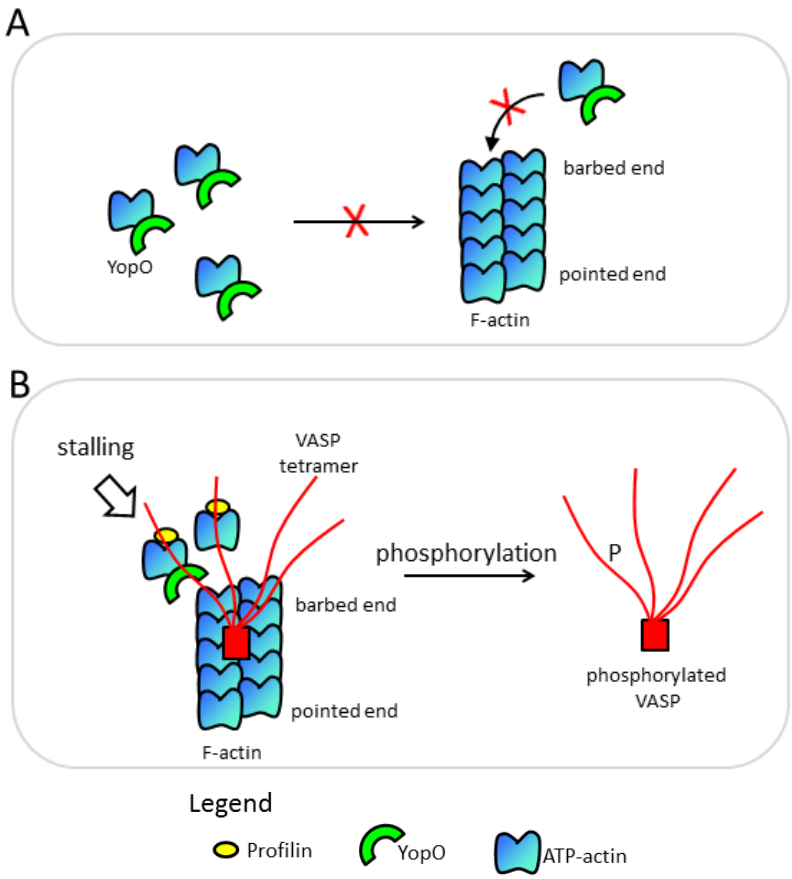


Figure 5.5 The effects of YopO on actin polymerization. (A) The sequestration of actin monomers and the inhibition to formation of F-actin. (B) The recruitment of YopO-bound actin monomers stalls actin polymerization machinery and YopO phosphorylates the actin machinery. VASP is shown here as an example, in the form of a tetramer.

5.2.4 Implications of phosphorylation of actin machinery by YopO

Many actin cytoskeletal components have been reported to be regulated by phosphorylation and these include WAVE2, WASP, VASP, WIP, CapG, gelsolin and diaphanous proteins. This work has shown that YopO phosphorylates WASP, VASP, gelsolin and Dia1, while WIP, MKL1, INF2 and FMNL1 have not been tested. This gives rise to the hypothesis that YopO hijacks native phosphorylation pathways that occur under non-pathogenic conditions to exert control over actin cytoskeletal dynamics.

5.3 Mechanism of disruption of phagocytosis by YopO

YopO contributes to the ability of *Yersinia* to resist phagocytosis (Navarro et al. 2007; Grosdent et al. 2002; Wiley et al. 2006; Groves et al. 2010). In both opsonin receptor-dependent and -independent pathways, *Yersinia* bacteria lacking YopO were phagocytosed significantly more by leukocytes and macrophages than wild type *Yersinia* (Grosdent et al. 2002). YopO inhibits phagocytosis of both IgG-opsonised and C3bi-opsonised particles, which take place via Fcγ-mediated and CR3-mediated pathways respectively, with a greater inhibitory effect on the FcγR pathway (Groves et al. 2010).

Particle internalization is an actin-based process (Aderem & Underhill 1999). YopO targets both the signals and effectors of the actin remodelling process, which is essential for phagocytosis. In macrophages, YopO sequesters Rac2, RhoG and RhoA. Cdc42 and Rac are necessary in FcγR-mediated phagocytosis (Cox et al. 1997) and RhoA is necessary in CR3-mediated phagocytosis (Caron & Hall 1998).

RhoG is required in both FcγR and CR3-mediated phagocytosis (Tzircotis et al. 2011).

Besides inhibiting the signalling molecules, YopO targets effectors of the remodelling process. WASP is important for the activation of ARP2/3, which is required for both FcγR- and CR3-mediated phagocytosis (Park & Cox 2009; May et al. 2000). While YopO does not seem to phosphorylate ARP2/3, it exerts effects on ARP2/3 via the phosphorylation of WASP. Besides WASP and ARP2/3, actin machineries implicated in phagocytosis include VASP, diaphanous, gelsolin and CapG. VASP and gelsolin are involved in FcγR-mediated phagocytosis (Coppolino & Matthias Krause 2001; Serrander et al. 2000), Diaphanous is involved in CR3-mediated phagocytosis (Colucci-Guyon et al. 2005), and CapG is involved in both phagocytosis pathways (Witke et al. 2001). VASP, diaphanous, gelsolin and CapG can be recruited by YopO, of which VASP, diaphanous and gelsolin are targeted for phosphorylation by YopO. It appears that YopO targets, if not most, all of the key players orchestrating actin dynamics in the phagocytosis process (**Fig. 5.6**).

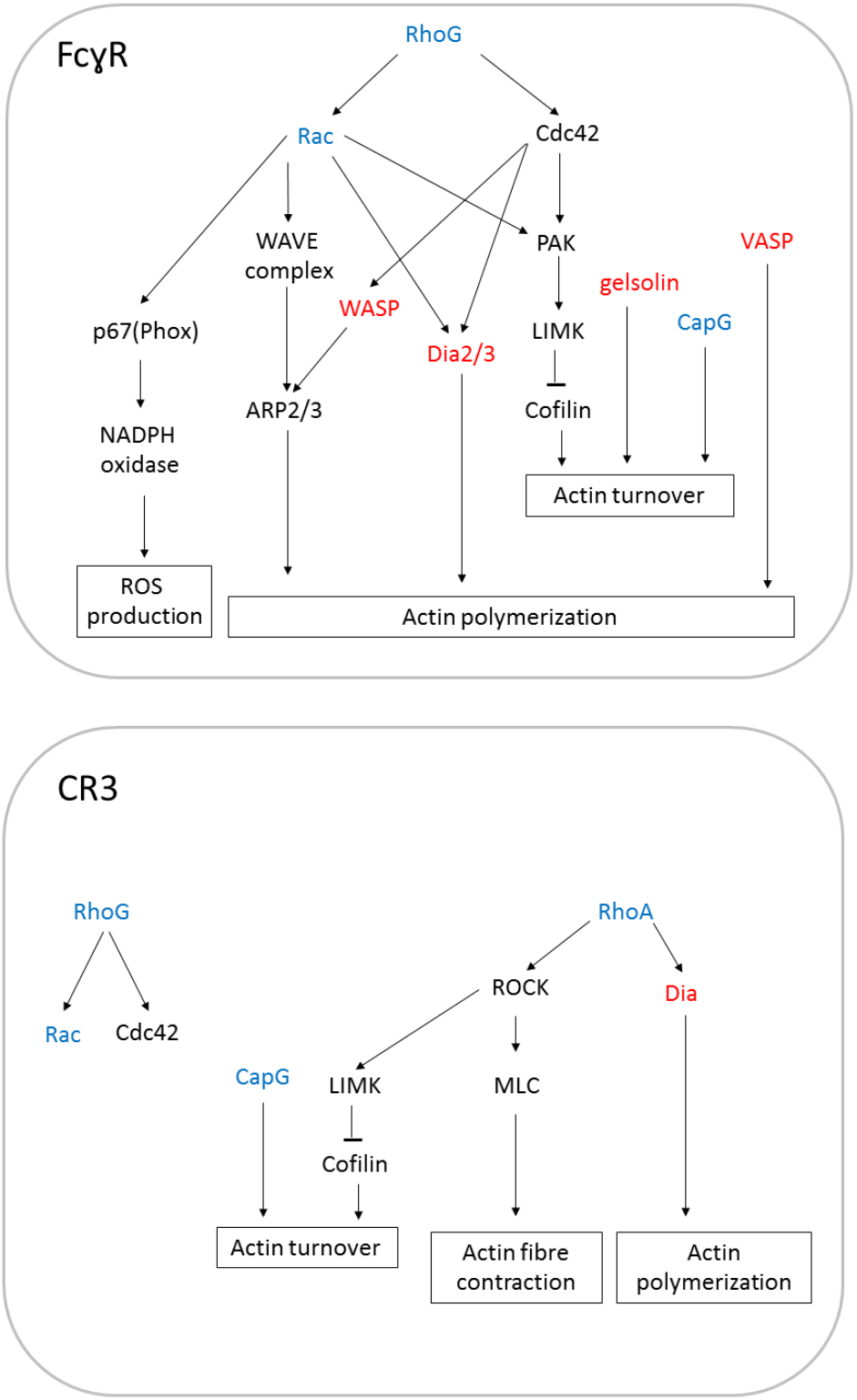


Figure 5.6 Effectors involved in FcγR- and CR3-mediated phagocytosis. In the schematic for CR3, pathways downstream of Rac and Cdc42 are the same for FcγR signalling and are not shown for clarity. Proteins that are sequestered in a ternary complex with YopO-actin are shown in blue. Proteins that are sequestered and phosphorylated by YopO are shown in red.

5.4 Overview of actin cytoskeletal disruption by YopO

As YopO is injected into the macrophage by the bacterium, it anchors itself into the plasma membrane via its membrane binding domain (residues 1-88). There it can sequester Rac2, RhoA and RhoG, turning off actin polymerization machinery including WASP, the WAVE complex, diaphanous; turning off actin stress fibre formation by myosin light chain; turning on actin depolymerisation by cofilin; and turning off ROS production.

At the same time, it sequesters a portion of profilin-actin, inhibiting their nucleotide exchange. YopO-bound actin-profilin will not be able to join free barbed ends, due to steric hindrance. YopO-bound actin monomers and YopO-bound actin-profilin get recruited into the remaining actin polymerization protein complexes that have retained activity despite the sequestration of Rac2, RhoA and RhoG by YopO. YopO stalls filament elongation of actin polymerization machinery like VASP, formins and ARP2/3 by preventing the addition of the bound monomer to the barbed end of the filament by steric hindrance. While stalling filament elongation, YopO phosphorylates some of these actin polymerization machineries, including VASP, diaphanous 1 and WASP (**Fig. 5.7**). YopO also binds and phosphorylates gelsolin, potentially exerting effect on actin turnover. PIP_2 is an important regulator of actin dynamics around nascent phagosomes (Scott et al. 2005). PIP_2 dissociates profilin, twinfilin, CapZ, CapG and gelsolin from actin, and also activates WASP, to give rise to a surge in localized actin polymerization. YopO sequesters and/or phosphorylates most of the effectors of PIP_2 signalling, including profilin, twinfilin, CapG, gelsolin and WASP, crippling its downstream effects. The sequestration of MKL1 by YopO stops nuclear translocation of MKL1, thus preventing SRF activity, so that new cytoskeletal components are not transcripted. So the collective effect of the

sequestration of actin, the kinase activity and sequestration of Rac, RhoA and RhoG results in a multifaceted subversion of the actin cytoskeleton, rendering macrophages incapable of performing actin remodeling for phagocytosis.

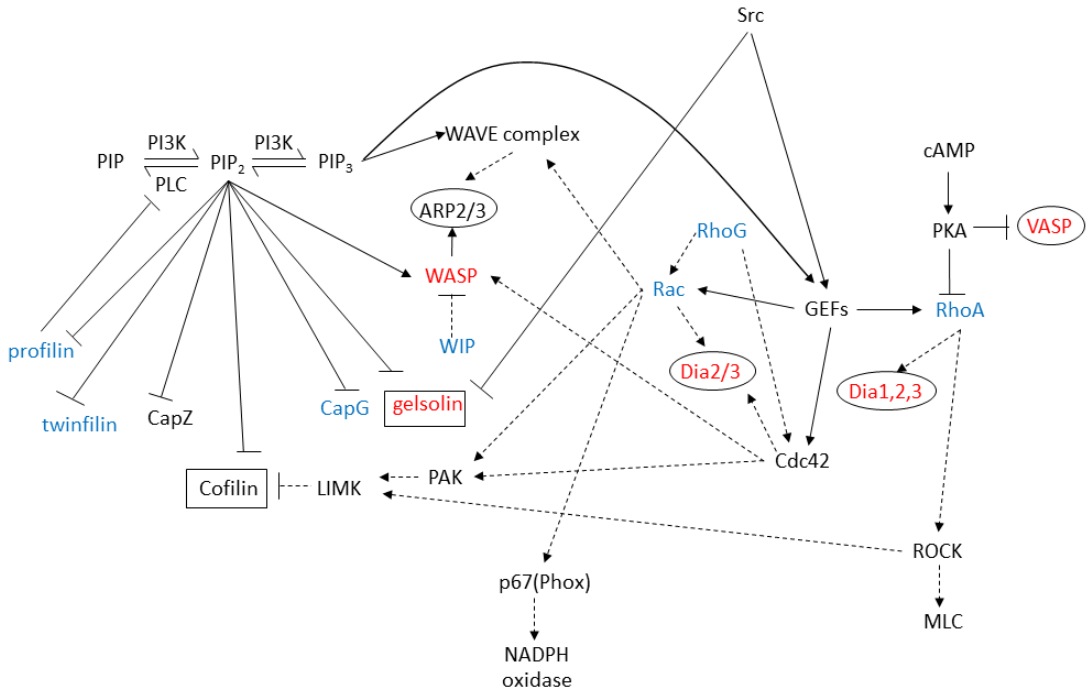


Figure 5.7 Actin cytoskeletal disruption by YopO. Proteins that are sequestered in a ternary complex with YopO-actin are shown in blue. These include proteins that have been proven to be not phosphorylated by YopO, and proteins which phosphorylation have not been tested. Proteins that are sequestered and phosphorylated by YopO are shown in red. Actin polymerization machineries are marked in circles, while actin turnover machineries are marked in rectangles. YopO sequesters Rac2, RhoA and RhoG, and pathways downstream of these Rho GTPases are marked by dashed lines.

5.5 Reconciling the activity of YopO with activities of other Yops

The innate immune system forms the first line of defence against pathogens. Major functions of innate immunity include the production of pro-inflammatory factors that recruit immune cells to sites of infection, recognition of foreign matter by the complement system, antigen presentation by dendritic cells and phagocytosis of foreign matter by macrophages and leukocytes. The Yops secreted by pathogenic strains of *Yersinia* include YpkA/YopO, YopH, YopM, YopT, YopP/J, and YopE which collectively attenuate these functions, allowing rapid proliferation and colonisation of the host.

Yersinia induces apoptosis of macrophages and dendritic cells via effector YopP/J (Monack et al. 1997; Mills et al. 1997). YopP/J inhibits the cellular activation of NF*k*B resulting in the attenuation of antigen presentation (Ruckdeschel et al. 1998). YopP/J also suppresses the release of pro-inflammatory factors TNF-α and IFN-γ by infected macrophages (Boland et al. 1998) via inactivation of the macrophage mitogen-activated protein kinases (MAPKs) pathway. YopM is involved in causing systemic depletion of natural killer (NK) cells in mouse infection models by interfering with cytokine expression essential for maintenance of NK cells (Kerschen et al. 2004).

YopH, YopT and YopO helped to confer resistance to phagocytosis in leukocytes and in macrophage cells (Grosdent et al. 2002). YopE significantly resists phagocytosis only in leukocytes and not in macrophage cells (Grosdent et al. 2002). While cytoskeletal disruption was observed, overexpression of YopE, YopH, YopT, or YopO alone did not confer resistance to phagocytosis, suggesting that collective

action by YopE, YopH, YopT and YopO is necessary to halt the phagocytic process (Grosdent et al. 2002).

YopH inhibits the activation of signal transduction in the early stages of the immune response. YopH is a tyrosine phosphatase that inhibits FcγR-mediated signal transduction in macrophages (Bliska & Black 1995); the β1 integrin phagocytic pathway, a non-opsonization phagocytic pathway (Black et al. 2000); and T cell antigen receptor signalling (De la Puerta et al. 2009). YopH also reduces the production of ROS (Charnetzky & Shuford 1985).

Unlike YopH which inhibits the activation of signal transduction for the onset of phagocytosis, YopE, YopT and YopO inhibit the actin remodelling process required for phagocytosis. YopO, YopE and YopT resist phagocytosis by targeting Rho GTPases (Fällman et al. 1995; Rosqvist et al. 1990; Rosqvist et al. 1988). YopE is a GTPase-activating protein. It binds Rac, RhoA and Cdc42, accelerating the hydrolysis of their bound GTP, thus inactivating the Rho GTPase signals (Black & Bliska 2000). YopT is a cysteine protease that cleaves and releases RhoA, Rac and Cdc42 from the plasma membrane (Shao et al. 2003). Rho GTPases orchestrate actin cytoskeletal dynamics at the cell leading edge and localization at the cell membrane is essential for function. Away from the leading edge, the effectiveness of the Rho GTPase signals is attenuated. YopO complements the activities of YopE and YopT in modulating Rho GTPase activity. YopO is a guanidine-nucleotide dissociation inhibitor that binds and inhibits Rho GTPases (Rac, RhoA and RhoG), preventing them from activating downstream targets. YopE, YopT and YopO have different specificities for Rho GTPases. YopE and YopT both target Rac, RhoA and Cdc42

while YopO targets Rac, RhoA and RhoG. Collectively, YopE, YopT and YopO disable actin remodelling required for phagocytosis by targeting Rho GTPases.

Besides targeting the Rho GTPases which are signalling molecules for the actin remodelling process, YopO has an additional function of directly targeting effectors required for the remodelling. YopO sequesters actin and actin-profilin, and by steric hindrance, prevents their addition to the barbed end of filaments. YopO gets recruited into actin polymerization machineries including formins, Ena/VASP family proteins and WH2 domain containing proteins whereby YopO stalls filament elongation. While stalling filament elongation, YopO phosphorylates a subset of the proteins which recruit it, and these include VASP, EVL, diaphanous, WASP and gelsolin. The binding of MKL1 by YopO prevents nuclear translocation of MKL1, preventing the activation of SRF and the transcription of new cytoskeletal components. YopO potentially inhibits nucleotide exchange YopO-bound profilin-actin, impeding actin turnover.

5.6 Mechanism of activation of YopO

In an attempt to achieve a model for the activation of YopO, the programs HingeProt (Emekli et al. 2007) and Elnemo (Suhre & Sanejouand 2004) were used to predict possible flexibility in YopO that might be involved in the conformational changes from the inactive to active state.

HingeProt (Emekli et al. 2007) enables the prediction of rigid protein 'domains' and flexible hinge regions to understand the cooperative motions of various conformational states in a protein. HingeProt predicts that YopO consists of two major rigid domains: the kinase domain and the GDI domain and that they have translational and rotational flexibility at the linker region between residues 425-438 (**Fig. 5.8**). Given the modular domain structure of YopO, this would be unsurprising. Hingeprot also predicts that the GDI domain can be considered as two subdomains composed of two bundles of helices connected by flexible backbone helix α14. The backbone helix α14 serves as a flexible hinge such that helices α9-α13 and half of helix α14 form a six-helix bundle while helices α15-α18 together with the other half of helix α14 form a five-helix bundle. Within the kinase domain, there are two minor rigid subdomains: loops 335-373 between helix α4 and α5 constitute one subdomain and the catalytic core of the kinase forms the other subdomain.

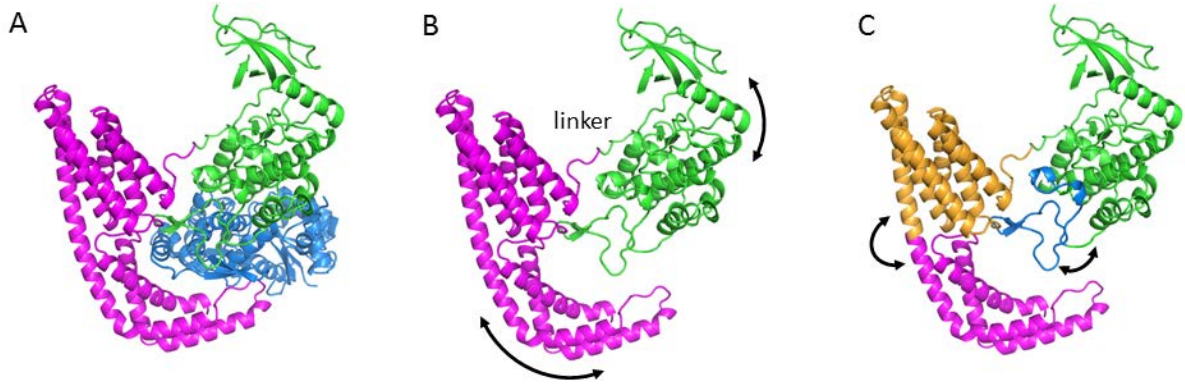


Figure 5.8 Domain movements of YopO as predicted by HingeProt. (A) The structure of the YopO-actin complex. (B) YopO consists of two major rigid domains (shown in green and magenta) with translational and rotational flexibility relative to each other around the linker region. (C) Each major domain consists of two minor rigid subdomains. The six-helix bundle consisting of α9-13 and half of α14 is shown in orange while the five-helix bundle α15-α18 and half of helix α14 is shown in magenta. The flexible loops of residues 335-373 between helices α4 and α5 are shown in blue. The catalytic core of the kinase domain is shown in green. Domain movements are depicted as arrows.

Elnemo (Suhre & Sanejouand 2004) was used to shed light on domain movements of YopO that are triggered by ligand binding. The actin molecule was removed from the PDB file of the structure of YopO-actin and loaded into the Elnemo server. The predictions from Elnemo agree with those suggested by HingeProt that domain movements occur between the kinase domain and the GDI domain, such that the kinase domain swings around linker region residues 425-438, bringing the kinase domain either closer to or further from the bundle of helices α15-18 (horizontal panel) (**Fig. 5.9**). There also seems to be rotational movement between the kinase and the GDI domain (vertical panel) around linker region residues 425-438. The normal modes predicted from Elnemo are overlaid and visualized in **Fig. 5.10**.

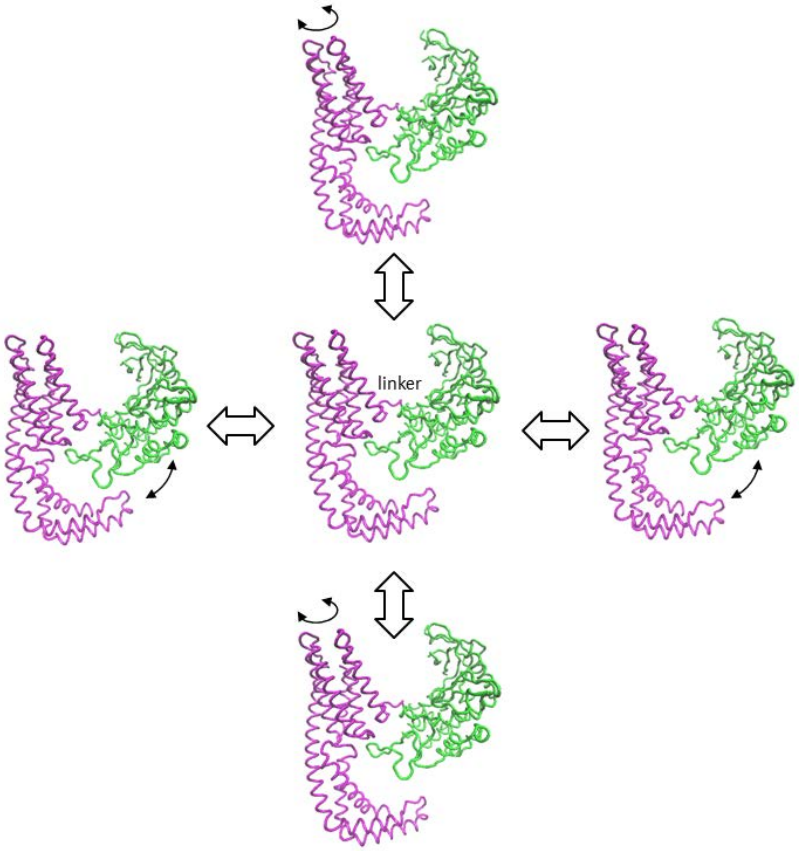


Figure 5.9 Normal mode analysis of YopO using Elnemo. Four of the lowest frequency modes are displayed. Figures were generated using the last frame of each trajectory using visualization software VMD. The centre diagram shows the structure of YopO from the YopO-actin structure. The vertical panel shows relative translational movement between the kinase (green) and GDI domain (magenta). The horizontal panel shows rotation of the kinase domain with respect to the GDI domain around the linker region (residues 425-438).

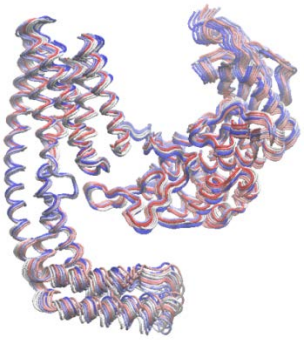


Figure 5.10 Overlay of all frames within the trajectories of four of the lowest frequency modes derived from Elnemo. Figure is generated using VMD.

5.7 Hypothetical models of inactive YopO

In the YopO-actin structure, Ser90 and Ser95 which contain the putative phosphorylation sites (Trasak et al. 2007) are disordered. The location of phosphorylation sites outside of the core kinase domain suggests that YopO is autoinhibited in the inactive state. Autoinhibition is a common feature across many kinase families (Ha et al. 2012; Lietha et al. 2007; Chen et al. 2009). In the inactive structure, residues 89-107 possibly fold back onto the catalytic cleft as an autoinhibitory sequence, also known as a pseudosubstrate sequence. The linear distance of 34 Å between the first ordered residue Lys108 and the catalytic Asp267 can easily be spanned by residues 89-107 (**Fig. 5.11**).

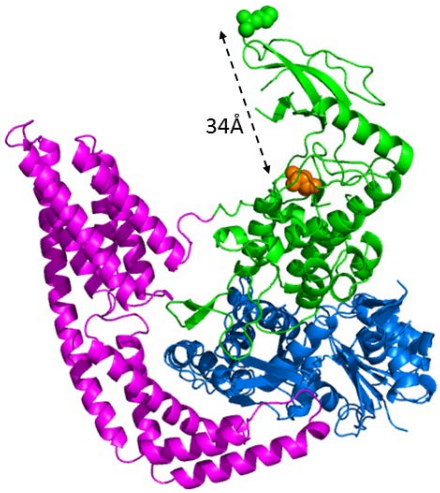


Figure 5.11 The distance between the catalytic cleft and the first ordered residue of YopO. The first ordered residue Lys108 (green spheres) and catalytic Asp267 (orange spheres) are 34 Å apart.

A comparison of the structure of the GDI domain on its own, with that within the YopO-actin structure reveals that the backbone helix α14 of YopO undergoes a 30^{o} bending upon binding actin (**Section 3.10)**. The analysis of conformational

flexibility of YopO by Elnemo and Hingeprot collectively point to domain movements between the kinase and the GDI domain around the linker (residues 425-438).

Prior to binding actin, in the inactive conformation of YopO, the autoinhibition sequence would be folded back onto the catalytic cleft. Rac1 binding is independent of the state of activation of YopO (Dukuzumuremyi et al. 2000). This, together with structural data, suggests that the Rac1 binding interface is conserved and accessible in both the active and the inactive conformations. In the inactive conformation, the backbone helix α14 of the GDI domain would be straight (**Fig. 5.12 A**). Large predicted domain movements between the kinase domain and the GDI domain around the linker, make it plausible that in the inactive conformation, the kinase substrate binding groove flanked between the kinase domain and the GDI domain is obscured. The binding of actin would induce a multistage activation process with a conformational change between the relative positions of the kinase domain and GDI domain to result in the kinase substrate binding groove being revealed.

The interaction of YopO with actin involves two interfaces: the interaction of the kinase domain, and the interaction of the GDI domain with actin. Most likely, either one of these interfaces binds to actin first. Both scenarios are illustrated in **Fig. 5.12 B** and **C**. As calculated by PDBePISA, the interaction of the kinase domain with actin yields a larger interface area at 1218.4 $Å^2$ than that of the GDI domain to actin at 811.8 $Å^2$. However, the formation of the interface of the GDI domain to actin yields a solvation free energy gain of -5.6 kcal/mol, which is larger than that of the

kinase domain to actin, at -3.2 kcal/mol. Thus most likely, actin binds to the GDI domain first. This brings about a bending of the GDI domain and further conformational changes that lead to the binding of the kinase domain to actin, sandwiching actin between the two domains (**Fig. 5.12 D**). The kinase dead mutant (YopO KD) does not autophosphorylate but retains the ability to sequester actin monomers in the actin polymerization assay, albeit with lower efficiency. This suggests that the sequestration of actin does not require the catalytic activity of the kinase domain and sequestration of actin precedes autophosphorylation. The proposed reorganisation of domains induced by actin-binding leads to the orientation of the catalytic elements within the kinase domain into the active state, leading to autophosphorylation of residues Ser90 and Ser95 and the release of the autoinhibition sequence. This stabilizes the active conformation, in which the kinase substrate binding groove is exposed and the kinase catalytic cleft is no longer obscured by the autoinhibition sequence.

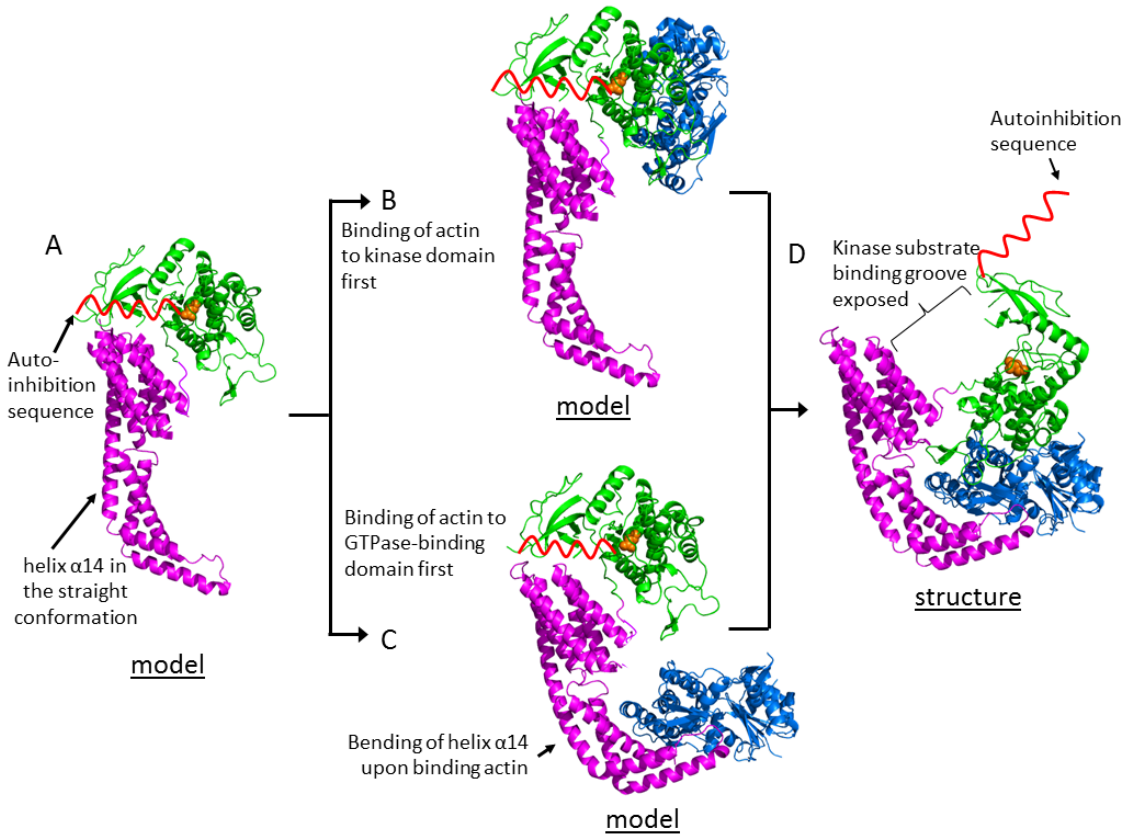


Figure 5.12 Hypothetical models of inactive YopO and conformational changes upon binding actin. The GDI domain is shown in magenta, the kinase domain is shown in green, the autoinhibition sequence is shown in red and actin is shown in marine. (A) In the model of the inactive structure, the kinase active site (catalytic Asp267 is shown in orange) would be inaccessible and the backbone helix α14 of the GDI domain would be straight. The autoinhibition sequence would be bound in the catalytic cleft. (B) In the model of the intermediate state, actin could bind to either the kinase domain or the (C) GDI domain first, though (C) the second model is more plausible due to a greater solvation free energy gain for the formation of this interface as compared to binding of actin to the kinase domain. (D) The kinase substrate binding groove is revealed in the active structure of the YopO-actin complex and the autoinhibition sequence hangs out of the kinase substrate binding groove.

Chapter 6

Conclusions and future research

6.1 Conclusions

More than 15 years after its discovery, understanding of the cellular function of YpkA/YopO remains incomplete. Reports on the contribution of the sequestration of Rho GTPase and the kinase activity of YopO to the disruption of the actin cytoskeleton have yielded variable findings (Juris et al. 2000; Prehna et al. 2006; Groves et al. 2010). Prior to the work in this thesis, little was known about the kinase activity of YopO except that it is activated by actin. To further our understanding of the cellular function of YopO, structural, biochemical and proteomics work were carried out to address how YopO forms a complex with actin, how actin activates the kinase activity of YopO, and which actin machineries interact with YopO and which proteins are phosphorylated by activated YopO.

The structure of YopO in complex with actin was solved by crystallography, with the use of surface entropy reduction mutagenesis. The structure showed that actin is sandwiched between the GDI domain and the kinase domain of YopO. The kinase domain has a catalytic core structurally similar to eukaryotic kinases in the active conformation. The Rac1 binding interface in the structure is unchanged compared with the published structure of the YpkA GDI domain (Prehna et al. 2006), however the backbone helix of the GDI domain undergoes a bending of 30^{o} to clamp around actin. The binding of YopO to actin bridges subdomains 2 and 4, stabilizing

the closed conformation of the nucleotide-binding cleft, suggesting that YopO may interfere with nucleotide-exchange of the bound actin. In addition, the binding of YopO to the pointed end of actin provides the structural basis for sequestration of actin polymerisation by YopO (Trasak et al. 2007). Putative phosphorylation sites Ser90 and Ser95 (Trasak et al. 2007) are found outside the catalytic core of the kinase, giving rise to the hypothesis that YopO is autoinhibited in the inactive state.

The crystal structure reveals how the kinase domain is activated upon binding actin. The N-lobe of the kinase domain of YopO interacts extensively with actin, allosterically positioning and stabilizing the catalytic loop and the activation segment for activation of kinase activity. The crystal structure also provided a structural basis for the differential ability of muscle and non-muscle actin isoforms to activate YopO. Muscle α-actin contains a valine at position 203 while non-muscle actin contains threonine in the corresponding position (202). Muscle actin is weaker at activating YopO due to the inability of the α-actin isoform to mediate a hydrogen bond with Lys245 of YopO and this interaction appears to be important for stabilizing the catalytic loop. This hypothesis is confirmed by the YopO K245M mutant, in which the Lys245-Thr202 hydrogen bond is abolished, where the ability of YopO K245M to autophosphorylate upon binding non-muscle actins is attenuated.

YopO binds to actin on subdomain 4 with minor contact on subdomain 2, leaving the hotspot between subdomains 1 and 3 available. The contact is unique in that most actin-binding proteins known to date bind between subdomains 1 and 3. SILAC was used to identify proteins that were bound to YopO via actin. Superimposition of available structures of actin-binding proteins on the YopO-actin

structure suggested that these proteins were pulled down indirectly via actin or by profilin-actin as complexes with YopO. Thus the YopO-actin structure enabled interpretation of the SILAC mass spectrometry data to suggest that actin is being used by YopO for recruitment into the actin machineries and that actin is used as a scaffold for the selection and binding of substrates for phosphorylation.

These data enabled the identification of a subset of the proteins recruited by YopO through actin, that are phosphorylated by YopO. These include WASP, VASP, EVL, Dia1 and gelsolin. These results were then validated via *in vitro* phosphorylation assays. *In vitro* phosphorylation experiments in the presence of competition by gelsolin domain 1 demonstrated that the YopO kinase phosphorylates these proteins as they were bound to the YopO-bound actin, suggesting that YopO hijacks actin as a bait to lure and inactivate actin regulators in a precise substrate selection strategy. CapG and twinfilin1 were not phosphorylated by YopO, suggesting that these proteins were not phosphorylated due to their inability to reach the catalytic cleft of the YopO kinase domain upon binding to the YopO-bound actin. In the SILAC pull downs, YopO was identified to interact with Rho GTPases Rac2, RhoA and RhoG within macrophage lysate. This is the first instance that identifies the interaction of RhoG with YopO.

The structure helps to clarify previous mutation and deletion studies that have been used to map out the relative contributions of the GDI domain and the kinase domain to actin cytoskeletal disruption. Constructs with just the GDI domain gave rise to an intermediate phenotype of cytoskeletal disruption compared to YopO WT (Prehna et al. 2006), while constructs with just the kinase domain no longer cause

cytoskeletal disruption (Groves et al. 2010). These data lead to the conclusion that the GDI domain is the dominant contributor to actin cytoskeletal disruption (Prehna et al. 2006; Groves et al. 2010). The YopO-actin structure reveals that this conclusion was only part of the mechanism, as phosphorylation requires actin sequestration which in turn requires an intact GDI domain for a functional actin-binding interface. The work in this thesis also clarifies why a low level of cytoskeletal disruption can still be observed despite mutations to both the catalytic residues of the kinase domain and the Rac1-binding interface of YpkA (Prehna et al. 2006). This is due to sequestration of actin and stalling of actin polymerization machinery by YopO, which is independent of kinase and Rho GDI activity.

In conclusion, the work in this thesis suggests that YopO adopts a six-pronged approach to handicapping the actin cytoskeleton: sequestration and inhibition of Rac, RhoA and RhoG, sequestration of actin monomers, inhibition of nucleotide-exchange of profilin-actin, stalling of actin polymerization by steric hindrance, modulation of actin polymerization machineries by phosphorylation, and turning off the transcription of actin cytoskeletal components by the sequestration of MKL1. Thus through this multi-faceted targeting to switch off actin dynamics, YopO stalls the engulfment machinery preventing macrophages from ingesting the bacteria. YopO is an essential virulence factor and as such, the actions of YopO were able to contribute to the deaths of hundreds of millions of people through the evasion of the immune system via ensuring the survival of the pathogen within the host.

Beyond understanding the mechanisms of pathogenicity of *Yersinia*, this work suggests that YopO hijacks native phosphorylation control pathways. A

number of key actin polymerization players have been reported to be regulated by phosphorylation, and YopO phosphorylates a number of them, including WASP, VASP, gelsolin and Dia1. Thus, this work helps shed light on native phosphorylation pathways regulating the actin cytoskeleton, which occur under non-pathogenic conditions.

6.2 Future work

6.2.1 Identification of other novel substrates

In this work, five novel substrates of YopO have been validated and these include VASP, EVL, gelsolin, Dia1 and WASP while twinfilin1 and CapG have been shown not to be phosphorylated by YopO. The phosphorylation of VASP, EVL, Dia1 and WASP and not twinfilin1 and CapG suggests that YopO phosphorylates proteins which can reach the catalytic cleft while bound to the same actin. Putative substrates WIP, MKL1, and formins INF2 and FMNL1 have not been tested due to the absence of working constructs but seem to meet the criteria and are likely to be phosphorylated by YopO. Future work would include the validation of phosphorylation of WIP, MKL1 and formins INF2 and FMNL1 by YopO.

6.2.2 Determining the effect of phosphorylation on substrate protein function

The phosphorylation of VASP by YopO resulted in the attenuation of the ability of VASP to enhance the polymerization of actin. The effect of phosphorylation on other validated substrates including WASP, Dia1 and gelsolin has yet to be determined. The analysis of proteins that were phosphorylated by YopO, and those not phosphorylated by YopO suggested that the ability to access the kinase catalytic cleft appears to be the determining factor on whether a protein is phosphorylated by YopO or not, while specificity for the recognition sequence on the substrate appears to play a minor role, if any. The identification of phosphorylation sites on substrates would contribute to the generation of a recognition consensus

sequence, that might, along with other criteria, be used to predict the site(s) of phosphorylation of kinase substrates of YopO. The identification of phosphorylation sites would be required for the generation of phosphomimetic mutants. Phosphomimetic mutants involve mutation of the serines or threonines at the phosphorylation sites to aspartic acid, to mimic the phosphorylated residue. This allows determination of the effect of phosphorylation at each site on the activity of the protein and this would shed light on the mechanism of regulation by phosphorylation, on the function of each protein.

6.2.3 Validation of the interaction between YopO and RhoG

The SILAC experiments suggest that YopO interacts with RhoG. The interaction of RhoG with YopO has not been reported and requires validation. Once validated to be of relevance *in vivo*, this would further improve the understanding of the effect of YopO on host systems.

6.2.4 Determining if YopO blocks pointed end depolymerisation

Tropomodulin binds to actin at the pointed end of the filaments, stabilizing the bound actin filaments, increasing their half-life and resulting in a reduction of actin turnover. While YopO binds to the pointed end of actin monomers, it remains to be determined if YopO, like tropomodulin, binds to the pointed end of filaments and physically blocks the dissociation of ADP-bound actin monomers from the pointed end of filaments (Weber et al. 1994).

6.2.5 Validation of the inhibition of nucleotide exchange of actin by YopO

YopO interacts with residues in both subdomains 2 and 4 of actin at the top of the nucleotide-binding cleft. This appears to stabilize the closed conformation of the nucleotide-binding cleft of actin in a similar manner to the binding of thymosin-β (Tβ) to actin. The C-terminal half of Tβ4 binds between actin subdomains 2 and 4, preventing the dynamic opening and closing of the two halves of actin, resulting in the inhibition of nucleotide exchange (Irobi et al. 2004). Profilin, on the other hand, stabilizes the open conformation of the nucleotide-binding cleft of actin, promoting nucleotide exchange (Mockrin & Korn 1980). The inhibition of nucleotide exchange of actin by YopO can be tested using etheno-ATP (1-N^6-ethenoadenosine 5'-triphosphate, also known as epsilon-ATP) (Wang & Taylor 1981; Secrist et al. 1972). The binding of etheno-ATP to actin results in an increase in fluorescence intensity, allowing a read out indicative of the rate of exchange of nucleotide in a solution of actin monomers. A comparison of kinetics of nucleotide exchange of actin on its own and in the presence of YopO, profilin or β-thymosins would determine if YopO hampers nucleotide exchange of actin, and contribute to the hampering of actin turnover.

6.2.6 Validation of the hypothesis of autoinhibition

In the YopO-actin structure, residues 89-107 which include Ser90 and Ser95, the putative phosphorylation sites, are disordered. The location of phosphorylation sites outside of the core kinase domain suggests that YopO is autoinhibited in the inactive state. Residues 89-107 possibly fold back onto the catalytic cleft as a pseudosubstrate sequence. The pseudosubstrate sequence possibly mimics the substrate recognition sequence for YopO in target proteins. The structure of inactive YopO would serve to validate this hypothesis. While not described in this thesis, substantial effort has been put into crystallization trials of YopO (89-729) (both WT and 1YY mutant), in the absence of actin, but no crystal hits have been obtained. Constructs encompassing the kinase domain and the putative pseudosubstrate sequence have also been made, in an attempt to determine the inactive structure of the kinase domain. However, despite extensive screening of expression conditions, proteins produced were insoluble. Full length YopO (1-729) has poor or no solubility and this is attributed to the membrane localization domain (1-88). SycO, a chaperone for YopO, binds and masks this domain, preventing this insolubility (Letzelter et al. 2006). The exclusion of the membrane localization domain results in a soluble YopO construct (89-729) in the absence of SycO. There is a possibility that the inactive structure of YopO (89-890) might require the presence of the membrane localization domain, and chaperone SycO for stabilization. As such, the determination of the inactive structure of YopO might require full length YopO (1-729) co-expressed with SycO and crystallized in the form of YopO-SycO complex.

REFERENCES

Aderem, A. & Underhill, D., 1999. Mechanisms of Phagocytosis in Macrophages. *Annual Review of Immunology*, 17(1), pp.593–623.

Aepfelbacher, M, Trasak, C. & Ruckdeschel, K., 2007. Effector functions of pathogenic Yersinia species. *Thromb Haemost*, (98), pp.521–529.

Afonine, P.V. et al., 2012. Towards automated crystallographic structure refinement with phenix.refine. *Acta crystallographica. Section D, Biological crystallography*, 68(Pt 4), pp.352–67.

Ahuja, R. et al., 2007. Cordon-bleu is an actin nucleation factor and controls neuronal morphology. *Cell*, 131(2), pp.337–350.

Aktories, K. et al., 2011. Actin as target for modification by bacterial protein toxins. *The FEBS journal*, 278(23), pp.4526–4543.

Alberts, A.S., 2001. Identification of a carboxyl-terminal diaphanous-related formin homology protein autoregulatory domain. *The Journal of Biological Chemistry*, 276(4), pp.2824–30.

Amatruda, J. & Cooper, J., 1992. Purification, characterization, and immunofluorescence localization of Saccharomyces cerevisiae capping protein. *The Journal of Cell Biology*, 117(5), pp.1067–1076.

Ambruso, D.R. et al., 2000. Human neutrophil immunodeficiency syndrome is associated with an inhibitory Rac2 mutation. *Proceedings of the National Academy of Sciences of the United States of America*, 97(9), pp.4654–9.

Applewhite, D.A. et al., 2007. Ena/VASP proteins have an anti-capping independent function in filopodia formation. *Molecular Biology of the Cell*, 18, pp.2579–2591.

Arber, S. et al., 1998. Regulation of actin dynamics through phosphorylation of cofilin by LIM-kinase. *Nature*, 393(6687), pp.805–9.

Ardern, H. et al., 2006. Src-dependent phosphorylation of Scar1 promotes its association with the Arp2/3 complex. *Cell motility and the cytoskeleton*, 63(1), pp.6–13.

Aslanidis, C. & De Jong, P.J., 1990. Ligation-independent cloning of PCR products (LIC-PCR). *Nucleic acids research*, 18(20), pp.6069–74.

Baarlink, C., Wang, H & Grosse, R., 2013. Nuclear actin network assembly by

formins regulates the SRF coactivator MAL. *Science*, 340(6134), pp.864–7.

Baba, Y. et al., 1999. Involvement of wiskott-aldrich syndrome protein in B-Cell cytoplasmic tyrosine kinase pathway. *Blood*, 93(6), pp.2003–12.

Bachmann, C. et al., 1999. The EVH2 Domain of the Vasodilator-stimulated Phosphoprotein Mediates Tetramerization, F-actin Binding, and Actin Bundle Formation. *Journal of Biological Chemistry*, 274(33), pp.23549–23557.

Balcer, H.I. et al., 2003. Coordinated regulation of actin filament turnover by a high-Molecular-weight Srv2/CAP complex, cofilin, profilin, and Aip1. *Current Biology*, 13(24), pp.2159–2169.

Bartolini, F. et al., 2008. The formin mDia2 stabilizes microtubules independently of its actin nucleation activity. *The Journal of Cell Biology*, 181(3), pp.523–36.

Barz, C. et al., 2000. The Yersinia Ser/Thr protein kinase YpkA/YopO directly interacts with the small GTPases RhoA and Rac-1. *FEBS Letters*, 482(1-2), pp.139–143.

Barzik, M. et al., 2005. Ena/VASP proteins enhance actin polymerization in the presence of barbed end capping proteins. *The Journal of Biological Chemistry*, 280(31), pp.28653–62.

Bashaw, G.J. et al., 2000. Repulsive axon guidance: Abelson and Enabled play opposing roles downstream of the roundabout receptor. *Cell*, 101(7), pp.703–15.

Bauman, J.D. et al., 2008. Crystal engineering of HIV-1 reverse transcriptase for structure-based drug design. *Nucleic Acids Research*, 36(15), pp.5083–5092.

Bayliss, R. et al., 2003. Structural basis of Aurora-A activation by TPX2 at the mitotic spindle. *Molecular Cell*, 12(4), pp.851–862.

Bear, J. E. et al., 2002. Antagonism between Ena/VASP proteins and actin filament capping regulates fibroblast motility. *Cell*, 109(4), pp.509–21.

Belmont, L.D. et al., 1999. A change in actin conformation associated with filament instability after Pi release. *Proceedings of the National Academy of Sciences of the United States of America*, 96(1), pp.29–34.

Benvenuti, M. & Mangani, S., 2007. Crystallization of soluble proteins in vapor diffusion for x-ray crystallography. *Nature Protocols*, 2(7), pp.1633–1651.

Benz, P.M. et al., 2008. Cytoskeleton assembly at endothelial Cell-Cell contacts is regulated by alphaII-spectrin-VASP complexes. *The Journal of Cell Biology*, 180(1), pp.205–19.

Berrow, N.S. et al., 2007. A versatile ligation-independent cloning method suitable for high-throughput expression screening applications. *Nucleic acids research*,

35(6), p.e45.

Bertling, E et al., 2004. Cyclase-associated Protein 1 (CAP1) promotes cofilin-induced actin dynamics in mammalian nonmuscle Cells. *Molecular Biology of the Cell*, 15(May), pp.2324–2334.

Bertling, E et al., 2007. Mechanism and Biological role of profilin-Srv2/CAP interaction. *Journal of Cell Science*, 120(Pt 7), pp.1225–1234.

Black, D.S. et al., 2000. The Yersinia tyrosine phosphatase YopH targets a novel adhesion-regulated signalling complex in macrophages. *Cellular MicroBiology*, 2(5), pp.401–414.

Black, D.S. & Bliska, J B, 2000. The RhoGAP activity of the Yersinia pseudotuberculosis cytotoxin YopE is required for antiphagocytic function and virulence. *Molecular microBiology*, 37(3), pp.515–27.

Blagoev, B. & Mann, M., 2006. Quantitative proteomics to study mitogen-activated protein kinases. *Methods*, 40(3), pp.243–250.

Blanchoin, L., 1999. Mechanism of interaction of acanthamoeba actophorin (adf/cofilin) with actin filaments. *Journal of Biological Chemistry*, 274(22), pp.15538–15546.

Blethrow, J.D. et al., 2008. Covalent capture of kinase-specific phosphopeptides reveals Cdk1-cyclin B substrates. *Proceedings of the National Academy of Sciences of the United States of America*, 105(5), pp.1442–7.

Bliska, J. & Black, D., 1995. Inhibition of the Fc receptor-mediated oxidative burst in macrophages by the Yersinia pseudotuberculosis tyrosine phosphatase. *Infection and immunity*, 63(2), pp.681–685.

Block, J. et al., 2012. FMNL2 drives actin-based protrusion and migration downstream of Cdc42. *Current Biology*, 22(11), pp.1005–12.

Blume, C. et al., 2007. AMP-activated protein kinase impairs endothelial actin cytoskeleton assembly by phosphorylating vasodilator-stimulated phosphoprotein. *The Journal of Biological Chemistry*, 282(7), pp.4601–12.

Bobkov, A. et al., 2006. Cooperative effects of cofilin (ADF) on actin structure suggest allosteric mechanism of cofilin function. *Journal of Molecular Biology*, 356(2), pp.325–34.

Boland, A. & Cornelis, G.R, 1998. Role of YopP in Suppression of Tumor Necrosis Factor Alpha Release by Macrophages during Yersinia Infection Role of YopP in Suppression of Tumor Necrosis Factor Alpha Release by Macrophages during Yersinia Infection. *Infection and Immunity*, 66(5), pp.1878–1884.

Borm, B. et al., 2005. Membrane ruffles in Cell migration: indicators of inefficient

lamellipodia adhesion and compartments of actin filament reorganization. *Experimental Cell research*, 302(1), pp.83–95.

Boujemaa-Paterski, R et al., 2001. Listeria protein ActA mimics WASp family proteins: it activates filament barbed end branching by Arp2/3 complex. *Biochemistry*, 40(38), pp.11390–404.

Brandt, D.T. et al., 2007. Dia1 and IQGAP1 interact in Cell migration and phagocytic cup formation. *The Journal of Cell Biology*, 178(2), pp.193–200.

Burtnick, L D et al., 2004. Structure of the N-terminal half of gelsolin bound to actin: roles in severing, apoptosis and FAF. *The European Molecular Biology Organization Journal*, 23(14), pp.2713–2722.

Burtnick, L.D. et al., 1997. The Crystal Structure of Plasma Gelsolin : Implications for Actin Severing , Capping , and Nucleation. *Cell*, 90, pp.661–670.

Butt, E. et al., 1994. cAMP- and cGMP-dependent protein kinase phosphorylation sites of the focal adhesion vasodilator-stimulated phosphoprotein (VASP) in vitro and in intact human platelets. *The Journal of Biological Chemistry*, 269(20), pp.14509–17.

Van Buul, J.D. et al., 2007. RhoG regulates endothelial apical cup assembly downstream from ICAM1 engagement and is involved in leukocyte trans-endothelial migration. *The Journal of Cell Biology*, 178(7), pp.1279–93.

Cai, L. et al., 2008. Coronin 1B antagonizes cortactin and remodels Arp2/3-containing actin branches in lamellipodia. *Cell*, 134(5), pp.828–42.

Carl, U.D. et al., 1999. Aromatic and basic residues within the EVH1 domain of VASP specify its interaction with proline-rich ligands. *Current Biology*, 9(13), pp.715–8.

Carlier, M.F. et al., 1997. Actin depolymerizing factor (ADF/cofilin) enhances the rate of filament turnover: implication in actin-based motility. *The Journal of Cell Biology*, 136(6), pp.1307–22.

Carlier, M.F. et al., 2000. GRB2 links signaling to actin assembly by enhancing interaction of neural Wiskott-Aldrich syndrome protein (N-WASp) with actin-related protein (ARP2/3) complex. *The Journal of Biological Chemistry*, 275(29), pp.21946–52.

Carlier, M.F. et al., 1993. Modulation of the interaction between G-actin and thymosin beta 4 by the ATP/ADP ratio: possible implication in the regulation of actin dynamics. *Proceedings of the National Academy of Sciences of the United States of America*, 90(11), pp.5034–5038.

Carlier, M.F. et al., 1996. Tbeta 4 is not a simple G-actin sequestering protein and interacts with F-actin at high concentration. *The Journal of Biological*

Chemistry, 271(16), pp.9231–9239.

Carlier, M.-F. et al., 2011. Control of Actin Assembly by the WH2 Domains and Their Multifunctional Tandem Repeats in Spire and Cordon-Bleu. *International Review of Cell and Molecular Biology*, 290, pp.55-85.

Caron, E & Hall, A, 1998. Identification of Two Distinct Mechanisms of Phagocytosis Controlled by Different Rho GTPases. *Science*, 282(5394), pp.1717–1721.

Charnetzky, W.T. & Shuford, W.W., 1985. Survival and growth of Yersinia pestis within macrophages and an effect of the loss of the 47-megadalton plasmid on growth in macrophages. *Infection and immunity*, 47(1), pp.234–41.

Chaudhry, F. et al., 2010. A central role for the WH2 domain of Srv2/CAP in recharging actin monomers to drive actin turnover in vitro and in vivo. *Cytoskeleton*, 67(2), pp.120–133.

Chaudhry, F. et al., 2013. Srv2/cyclase-associated protein forms hexameric shurikens that directly catalyze actin filament severing by cofilin. *Molecular Biology of the Cell*, 24(1), pp.31–41.

Chen, L et al., 2009. Structural insight into the autoinhibition mechanism of AMP-activated protein kinase. *Nature*, 459(7250), pp.1146–1149.

Chereau, D. et al., 2005. Actin-bound structures of Wiskott–Aldrich syndrome protein (WASP)-homology domain 2 and the implications for filament assembly. *Proceedings of the National Academy of Sciences of the United States of America*, 102(46), pp.16644–16649.

Chhabra, E.S. et al., 2009. INF2 is an endoplasmic reticulum-associated formin protein. *Journal of Cell Science*, 122(Pt 9), pp.1430–40.

Chhabra, E.S. & Higgs, H.N., 2007. The many faces of actin: matching assembly factors with Cellular structures. *Nature Cell Biology*, 9(10), pp.1110–1121.

Chhabra, E.S. & Higgs, Henry N, 2006. INF2 Is a WASP homology 2 motif-containing formin that severs actin filaments and accelerates both polymerization and depolymerization. *Journal of Biological Chemistry*, 281(36), pp.26754–26767.

Chik, J.K., Lindberg, Uno & Schutt, C.E., 1996. The Structure of an Open State of beta-Actin at 2.65Å resolution. *Journal of Molecular Biology*, 263(4), pp.607–623.

Choe, H. et al., 2002. The Calcium Activation of Gelsolin: Insights from the 3Å Structure of the G4–G6/Actin Complex. *Journal of Molecular Biology*, 324(4), pp.691–702.

Chou, H.C. et al., 2006. WIP regulates the stability and localization of WASP to podosomes in migrating dendritic Cells. *Current Biology : CB*, 16(23), pp.2337–44.

Colucci-Guyon, E. et al., 2005. A role for mammalian diaphanous-related formins in complement receptor (CR3)-mediated phagocytosis in macrophages. *Current Biology*, 15(22), pp.2007–12.

Condliffe, A.M. et al., 2006. RhoG regulates the neutrophil NADPH oxidase. *Journal of Immunology*, 176(9), pp.5314–20.

Cooper, D.R. et al., 2007. Protein crystallization by surface entropy reduction: optimization of the SER strategy. *Acta Crystallographica Section D Biological Crystallography*, 63(Pt 5), pp.636–645.

Coppolino, M. & Krause, M., 2001. Evidence for a Molecular complex consisting of Fyb/SLAP, SLP-76, Nck, VASP and WASP that links the actin cytoskeleton to Fcγ receptor signalling during phagocytosis. *Journal of Cell Science,* 114, pp.4307–4318.

Cornelis, G.R., 2006. The type III secretion injectisome. *Nature Reviews MicroBiology*, 4(11), pp.811–825.

Cornelis, G.R. et al., 1998. The virulence plasmid of Yersinia, an antihost genome. *Microbiol Mol Biol Rev*, 62(4), pp.1315–1352.

Cornelis, G.R. & Wolf-Watz, H, 1997. The Yersinia Yop virulon: a bacterial system for subverting eukaryotic Cells. *Molecular Microbiology*, 23(5), pp.861–7.

Cornelis, G.R, 2000. Molecular and Cell Biology aspects of plague. *Proceedings of the National Academy of Sciences of the United States of America*, 97(16), pp.8778–8783.

Cornelis, G.R, 2002. The Yersinia Ysc-Yop "type III" weaponry. *Nature Reviews Molecular Cell Biology*, 3(10), pp.742–752.

De Corte, V et al., 1999. Identification of Tyr438 as the major in vitro c-Src phosphorylation site in human gelsolin: a mass spectrometric approach. *Protein Science*, 8(1), pp.234–41.

De Corte, V, Gettemans, J & Vandekerckhove, J, 1997. Phosphatidylinositol 4,5-bisphosphate specifically stimulates PP60c-src catalyzed phosphorylation of gelsolin and related actin-binding proteins. *FEBS Letters*, 401(2-3), pp.191–196.

Cory, G.O.C. et al., 2003. Phosphorylation of the WASP-VCA domain increases its affinity for the Arp2/3 complex and enhances actin polymerization by WASP. *Molecular Cell*, 11(5), pp.1229–1239.

Cowtan, K., 2010. Recent developments in classical density modification. *Acta*

crystallographica. Section D, Biological crystallography, 66(Pt 4), pp.470–8.

Cox, B.D. et al., 1997. Requirements for Both Rac1 and Cdc42 in Membrane Ruffling and Phagocytosis in Leukocytes. *Journal of Experimental Medicine*, 186(9), pp.1487–1494.

Dabiri, G.A. et al., 1992. Molecular Cloning of Human Macrophage Capping Protein cDNA. *Journal of Biological Chemistry*, 267(23), pp.16545–16552.

Danson, C.M. et al., 2007. Phosphorylation of WAVE2 by MAP kinases regulates persistent Cell migration and polarity. *Journal of Cell Science*, 120(23), pp.4144–54.

DeBakker, C.D. et al., 2004. Phagocytosis of Apoptotic Cells Is Regulated by a UNC-73 / TRIO-MIG-2 / RhoG Signaling Module and Armadillo Repeats of CED-12 / ELMO. *Current Biology*, 14, pp.2208–2216.

Devriendt, K. et al., 2001. Constitutively activating mutation in WASP causes X-linked severe congenital neutropenia. *Nature genetics*, 27(3), pp.313–7.

Didsbury, J. et al., 1989. Rac, a Novel Ras-Related Family of Proteins That Are Botulinum Toxin Substrates. *The Journal of Biological Chemistry*, 264(28), pp.16378–82.

Doeppler, H.R. et al., 2013. Protein Kinase D1 mediated phosphorylations regulate vasodilator-stimulated phosphoprotein (VASP) localization and Cell migration. *The Journal of Biological Chemistry*, 288, pp.24382–24393.

Dominguez, R, 2004. Actin-binding proteins - a unifying hypothesis. *Trends in Biochemical Sciences*, 29(11), pp.572–578.

Dukuzumuremyi, J.M. et al., 2000. The Yersinia protein kinase A is a host factor inducible RhoA/Rac-binding virulence factor. *The Journal of Biological Chemistry*, 275(45), pp.35281–35290.

Duncan, M.C. et al., 2001. Yeast Eps15-like endocytic protein , Pan1p , activates the Arp2/3 complex. *Nature Cell Biology*, 3(July), pp.687–690.

Edwards, D.C. et al., 1999. Activation of LIM-kinase by Pak1 couples Rac/Cdc42 GTPase signalling to actin cytoskeletal dynamics. *Nature Cell Biology*, 1(5), pp.253–9.

Egile, C et al., 2005. Mechanism of filament nucleation and branch stability revealed by the structure of the Arp2/3 complex at actin branch junctions. *PLoS Biology*, 3(11), p.e383.

Ellerbroek, S.M. et al., 2004. SGEF , a RhoG Guanine Nucleotide Exchange Factor that Stimulates Macropinocytosis. *Molecular Biology of the Cell*, 15, pp.3309–3319.

Emekli, U. et al., 2007. HingeProt: Automated prediction of hinges in protein structures. *Proteins*, 70(4), pp.1219–1227.

Emsley, P. et al., 2010. Features and development of Coot. *Acta crystallographica. Section D, Biological crystallography*, 66(Pt 4), pp.486–501.

Endicott, J.A., Noble, M.E.M. & Johnson, L.N., 2012. The structural basis for control of eukaryotic protein kinases. *Annual review of Biochemistry*, 81, pp.587–613.

Esnouf, R.M., 1998. Continuous and discontinuous changes in the unit Cell of HIV-1 reverse transcriptase crystals on dehydration. *Acta crystallographica. Section D, Biological crystallography*, 54(Pt 5), pp.938–953.

Eswaran, J. et al., 2008. UnPAKing the class differences among p21-activated kinases. *Trends in Biochemical Sciences* , 33(8), pp.394–403.

Falck, S. et al., 2004. Biological role and structural mechanism of twinfilin-capping protein interaction. *The European Molecular Biology Organization Journal*, 23(15), pp.3010–9.

Fällman, M. et al., 1995. Yersinia pseudotuberculosis inhibits Fc receptor-mediated phagocytosis in J774 Cells . Yersinia pseudotuberculosis Inhibits Fc Receptor-Mediated Phagocytosis in J774 Cells. *Infection and Immunity*, 63(8), pp.3117–3124.

Fellouse, F.A., Wiesmann, C. & Sidhu, S.S., 2004. Synthetic antibodies from a four-amino-acid code: a dominant role for tyrosine in antigen recognition. *Proceedings of the National Academy of Sciences of the United States of America*, 101(34), pp.12467–72.

Ferron, F. et al., 2007. Structural basis for the recruitment of profilin-actin complexes during filament elongation by Ena/VASP. *The European Molecular Biology Organization Journal*, 26(21), pp.4597–606.

Frischknecht, F. et al., 1999. Actin-based motility of vaccinia virus mimics receptor tyrosine kinase signalling. *Nature*, 401(6756), pp.926–9.

Fujii, T. et al., 2010. Direct visualization of secondary structures of F-actin by electron cryomicroscopy. *Nature*, 467(7316), pp.724–728.

Galán, J.E., 1999. Type III Secretion Machines: Bacterial Devices for Protein Delivery into Host Cells. *Science*, 284(5418), pp.1322–1328.

Galimand, M., Carniel, E. & Courvalin, P., 2006. Resistance of Yersinia pestis to antimicrobial agents. *Antimicrobial agents and chemotherapy*, 50(10), pp.3233–6.

Galyov, E.E. et al., 1993. A secreted protein kinase of Yersinia pseudotuberculosis is

an indispensable virulence determinant. *Nature*, 361(6414), pp.730–2.

Gambaryan, S. et al., 2001. Distribution, Cellular localization, and postnatal development of VASP and Mena expression in mouse tissues. *Histochem Cell Biol*, 116(6), pp.535–43.

Geese, M., Loureiro, J.J. & Bear, J E, 2002. Contribution of Ena/VASP Proteins to IntraCellular Motility ofListeria Requires Phosphorylation and Proline-rich Core but Not F-Actin Binding or Multimerization. *Molecular Biology of the Cell*, 13, pp.2383–2396.

Gerst, J.E. et al., 1991. Saccharomyces cerevisiae adenylyl cyclase Bifunctional Component of the Saccharomyces cerevisiae Adenylyl Cyclase Complex. *Molecular and Cellular Biology*, 11(3), pp.1248–1257.

Gieselmann, R. et al., 1995. Distinct Biochemical characteristics of the two human profilin isoforms. *European Journal of Biochemistry*, 229(3), pp.621–8.

Ginocchio, C.C., Olmsted, S.B. & Wells, C.L., 1994. Contact with Epithelial Cells Induces the Formation of Surface Appendages on Salmonella typhimurium. *Cell*, 76, pp.717–724.

Gohla, A., Birkenfeld, J. & Bokoch, G M, 2005. Chronophin, a novel HAD-type serine protein phosphatase, regulates cofilin-dependent actin dynamics. *Nature Cell Biology*, 7(1), pp.21–9.

Goldschmidt, L. et al., 2007. Toward rational protein crystallization: A Web server for the design of crystallizable protein variants. *Protein Science*, 16(8), pp.1569–1576.

Goldschmidt-Clermont, P.J. et al., 1990. The actin-binding protein profilin binds to PIP2 and inhibits its hydrolysis by phospholipase C. *Science*, 247(4950), pp.1575–8.

Goldschmidt-Clermont, P.J. et al., 1992. The control of actin nucleotide exchange by thymosin beta 4 and profilin. A potential regulatory mechanism for actin polymerization in Cells. *Molecular Biology of the Cell*, 3(9), pp.1015–1024.

Goley, E.D. et al., 2004. Critical conformational changes in the Arp2/3 complex are induced by nucleotide and nucleation promoting factor. *Molecular Cell*, 16, pp.269–279.

Good, M., Zalatan, J. & Lim, W., 2011. Scaffold proteins: hubs for controlling the flow of Cellular information. *Science Signaling*, 332(6030), pp.680–686.

Goode, B.L. et al., 2001. Activation of the Arp2/3 Complex by the Actin Filament Binding Protein Abp1p. *Journal of Cell Biology*, 153(3), pp.627–634.

Goode, B.L., Drubin, D G & Lappalainen, P, 1998. Regulation of the cortical actin

cytoskeleton in budding yeast by twinfilin, a ubiquitous actin monomer-sequestering protein. *The Journal of Cell Biology*, 142(3), pp.723–33.

Gorbatyuk, V.Y. et al., 2006. Mapping the phosphoinositide-binding site on chick cofilin explains how PIP2 regulates the cofilin-actin interaction. *Molecular Cell*, 24(4), pp.511–522.

Gouin, E. et al., 2004. The RickA protein of Rickettsia conorii activates the Arp2/3 complex. *Nature*, 427(6973), pp.457–461.

Gournier, H., Goley, E. & Niederstrasser, H., 2001. Reconstitution of human Arp2/3 complex reveals critical roles of individual subunits in complex structure and activity. *Molecular Cell*, 8, pp.1041–1052.

Grosdent, N. et al., 2002. Role of Yops and Adhesins in Resistance of Yersinia enterocolitica to Phagocytosis Role of Yops and Adhesins in Resistance of Yersinia enterocolitica to Phagocytosis. *Infection and Immunity*, 70(8), pp.4165–4176.

Groves, E. et al., 2010. Sequestering of Rac by the Yersinia effector YopO blocks Fcgamma receptor-mediated phagocytosis. *The Journal of Biological Chemistry*, 285(6), pp.4087–4098.

Gruenheid, S. et al., 2001. Enteropathogenic E. coli Tir binds Nck to initiate actin pedestal formation in host Cells. *Nature Cell Biology*, 3(9), pp.856–9.

Ha, B.H. et al., 2012. Type II p21-activated kinases (PAKs) are regulated by an autoinhibitory pseudosubstrate. *Proceedings of the National Academy of Sciences of the United States of America*, 109(40), pp.16107–12.

Håkansson, S et al., 1996. The Yersinia YpkA Ser/Thr kinase is translocated and subsequently targeted to the inner surface of the HeLa Cell plasma membrane. *Molecular MicroBiology*, 20(3), pp.593–603.

Hamid, N. et al., 1999. YopH dephosphorylates Cas and Fyn-binding protein in macrophages. *Microbial Pathogenesis*, 27(4), pp.231–42.

Hanks, S.K. & Hunter, T., 1995. The eukaryotic protein kinase superfamily : kinase (catalytic) domain structure and classification. *FASEB J*, 9(8), pp.576–96.

Harbeck, B. et al., 2000. Phosphorylation of the vasodilator-stimulated phosphoprotein regulates its interaction with actin. *The Journal of Biological Chemistry*, 275(40), pp.30817–30825.

Heasman, S.J. & Ridley, A.J., 2008. Mammalian Rho GTPases: new insights into their functions from in vivo studies. *Nature Reviews Molecular Cell Biology*, 9(9), pp.690–701.

Heiss, S.G. & Cooper, J A, 1999. Regulation of CapZ, an actin capping protein of

chicken muscle, by anionic phospholipids. *Biochemistry*, 30(36), pp.8753–8.

Helfer, E. et al., 2006. Mammalian twinfilin sequesters ADP-G-actin and caps filament barbed ends: implications in motility. *The European Molecular Biology Organization Journal*, 25(6), pp.1184–95.

Heras, B. et al., 2003. Dehydration converts DsbG crystal diffraction from low to high resolution. *Structure London England 1993*, 11(2), pp.139–145.

Heras, B. & Martin, J.L., 2005. Post-crystallization treatments for improving diffraction quality of protein crystals. *Acta Crystallographica Section D Biological Crystallography*, 61(Pt 9), pp.1173–80.

Hertzog, M. et al., 2004. The beta-thymosin/WH2 domain; structural basis for the switch from inhibition to promotion of actin assembly. *Cell*, 117(5), pp.611–623.

Higgs, H. N., 1999. Regulation of Actin Polymerization by Arp2/3 Complex and WASp/Scar Proteins. *Journal of Biological Chemistry*, 274(46), pp.32531–32534.

Higuchi, R., Krummel, B. & Saiki, R.K., 1988. A general method of in vitro preparation and specific mutagenesis of DNA fragments: study of protein and DNA interactions. *Nucleic acids research*, 16(15), pp.7351–7368.

Ho, H.H. et al., 2001. CR16 forms a complex with N-WASP in brain and is a novel member of a conserved proline-rich actin- binding protein family. *Proceedings of the National Academy of Sciences of the United States of America*, 98(20), pp.11306–11311.

Ho, H.H. et al., 2004. Toca-1 Mediates Cdc42-Dependent Actin Nucleation by Activating the N-WASP-WIP Complex. *Cell*, 118, pp.203–216.

Holmes, K.C. et al., 1990. Atomic model of the actin filament. *Nature*, 347(6288), pp.44–49.

Hoppe, A.D. & Swanson, J.A., 2004. Cdc42, Rac1, and Rac2 display distinct patterns of activation during phagocytosis. *Molecular Biology of the Cell*, 15(August), pp.3509–3519.

Huse, M. & Kuriyan, J., 2002. The conformational plasticity of protein kinases. *Cell*, 109(3), pp.275–282.

Husson, C. et al., 2011. Cordon-Bleu Uses WH2 Domains as Multifunctional Dynamizers of Actin Filament Assembly. *Molecular Cell*, 43(3), pp.464–477.

Ichetovkin, I. et al., 2002. Actin Filaments that Are Preferred for Dendritic Nucleation by the Arp2 / 3 Complex Albert Einstein College of Medicine. , 12(01), pp.79–84.

Imai, Kohsuke et al., 2004. Clinical course of patients with WASP gene mutations. *Blood*, 103(2), pp.456–64.

Van Impe, K. et al., 2008. A new role for nuclear transport factor 2 and Ran: nuclear import of CapG. *Traffic (Copenhagen, Denmark)*, 9(5), pp.695–707.

Irobi, E et al., 2004. Structural basis of actin sequestration by thymosin-beta4: implications for WH2 proteins. *the The European Molecular Biology Organization Journal*, 23(18), pp.3599–3608.

Ismail, A.M. et al., 2009. The WAVE regulatory complex is inhibited. *Nature Structural & Molecular Biology*, 16(5), pp.561–563.

Janmey, P.A. et al., 1985. Interactions of gelsolin and gelsolin-actin complexes with actin. Effects of calcium on actin nucleation, filament severing, and end blocking. *Biochemistry*, 24(14), pp.3714–23.

Janmey, P.A. & Stossel, T.P., 1987. Modulation of gelsolin function by phosphatidylinositol 4,5-bisphosphate. *Nature*, 325, pp.362 – 364.

Jaroszewski, L. et al., 2011. FFAS server: novel features and applications. *Nucleic acids research*, 39(Web Server issue), pp.W38–44.

Johnson, L.N. & Barford, D., 1993. The effects of phosphorylation on the structure and function of proteins. *Annual Review of Biophysics and BioMolecular Structure*, 22, pp.199–232.

Jung, G. et al., 2001. The Dictyostelium CARMIL protein links capping protein and the Arp2/3 complex to type I myosins through their SH3 domains. *The Journal of Cell Biology*, 153(7), pp.1479–97.

Juris, S.J. et al., 2000. A distinctive role for the Yersinia protein kinase: Actin binding, kinase activation, and cytoskeleton disruption. *Proceedings of the National Academy of Sciences of the United States of America*, 97(17), pp.9431–9436.

Kabsch, W. et al., 1990. Atomic structure of the actin: DNase I complex. *Nature*, 347, pp.37–44.

Kabsch, W., 1993. Automatic processing of rotation diffraction data from crystals of initially unknown symmetry and Cell constants. *Journal of Applied Crystallography*, 26(6), pp.795–800.

Kaplan, G., 1977. Differences in the mode of phagocytosis with Fc and C3 receptors in macrophages. *Journal of Immunology*, 6(8), pp.797–807.

Katoh, H. et al., 2000. Small GTPase RhoG Is a Key Regulator for Neurite Outgrowth in PC12 Cells Small GTPase RhoG Is a Key Regulator for Neurite Outgrowth in PC12 Cells. *Molecular and Cellular Biology*, 20(19), pp.7378–

7387.

Katoh, H., Hiramoto, K. & Negishi, M., 2006. Activation of Rac1 by RhoG regulates Cell migration. *Journal of Cell Science*, 119(Pt 1), pp.56–65.

Katoh, H. & Negishi, M., 2003. RhoG activates Rac1 by direct interaction with the Dock180-binding protein Elmo. *Nature*, 5799(1997), pp.461–464.

Kerschen, E.J. et al., 2004. The plague virulence protein YopM targets the innate immune response by causing a global depletion of NK Cells. *Infection and Immunity*, 72(8), pp.4589–4602.

Kim, K. et al., 2004. Capping protein binding to actin in yeast: Biochemical mechanism and physiological relevance. *The Journal of Cell Biology*, 164(4), pp.567–80.

Kim, Y. et al., 2006. Phosphorylation of WAVE1 regulates actin polymerization and dendritic spine morphology. *Nature*, 442(7104), pp.814–7.

Kimura, K. et al., 2013. Proteomic identification of the macrophage-capping protein as a protein contributing to the malignant features of hepatoCellular carcinoma. *Journal of proteomics*, 78, pp.362–73.

Kinley, A.W. et al., 2003. Cortactin Interacts with WIP in Regulating Arp2 / 3 Activation and Membrane Protrusion. *Current Biology*, 13(03), pp.384–393.

Klostermann, A. et al., 2000. The orthologous human and murine semaphorin 6A-1 proteins (SEMA6A-1/Sema6A-1) bind to the enabled/vasodilator-stimulated phosphoprotein-like protein (EVL) via a novel carboxyl-terminal zyxin-like domain. *The Journal of Biological Chemistry*, 275(50), pp.39647–53.

Ko, T.P. et al., 2010. Structures of human MST3 kinase in complex with adenine, ADP and Mn2+. *Acta Crystallographica Section D Biological Crystallography*, 66(2), pp.145–54.

Kobayashi, K. et al., 1998. p140Sra-1 (Specifically Rac1-associated Protein) Is a Novel Specific Target for Rac1 Small GTPase. *Journal of Biological Chemistry*, 273(1), pp.291–295.

Kornev, A.P. et al., 2006. Surface comparison of active and inactive protein kinases identifies a conserved activation mechanism. *Proceedings of the National Academy of Sciences of the United States of America*, 103(47), pp.17783–8.

Kouyama, T. & Mihasi, K., 1981. Fluorimetry Study of. *European Journal of Biochemistry*, 114, pp.33–38.

Krause, M. et al., 2004. Lamellipodin, an Ena/VASP ligand, is implicated in the regulation of lamellipodial dynamics. *Developmental Cell*, 7(4), pp.571–83.

Ksiazek, D. et al., 2003. Structure of the N-terminal domain of the adenylyl cyclase-associated protein (CAP) from Dictyostelium discoideum. *Structure London England 1993*, 11(9), pp.1171–1178.

Kudryashov, D.S. et al., 2008. Connecting actin monomers by iso-peptide bond is a toxicity mechanism of the Vibrio cholerae MARTX toxin. *Proceedings of the National Academy of Sciences of the United States of America*, 105(47), pp.18537–18542.

Kühnel, K. et al., 2004. The VASP tetramerization domain is a right-handed coiled coil based on a 15-residue repeat. *Proceedings of the National Academy of Sciences of the United States of America*, 101(49), pp.17027–17032.

Kwiatkowski, D.J. et al., 1986. Plasma and cytoplasmic gelsolins are encoded by a single gene and contain a duplicated actin-binding domain. *Nature*, 323, pp.455–458.

Kwiatkowski, D.J., 1988. Predominant induction of gelsolin and actin-binding protein during myeloid differentiation. *The Journal of Biological Chemistry*, 263(27), pp.13857–62.

De La Cruz, E.M. et al., 2000. Thymosin-beta(4) changes the conformation and dynamics of actin monomers. *Biophysical Journal*, 78(5), pp.2516–27.

De la Fuente, M. a et al., 2007. WIP is a chaperone for Wiskott-Aldrich syndrome protein (WASP). *Proceedings of the National Academy of Sciences of the United States of America*, 104(3), pp.926–31.

De la Puerta, M.L. et al., 2009. Characterization of new substrates targeted by Yersinia tyrosine phosphatase YopH. *PloS one*, 4(2), p.e4431.

Lambrechts, A. et al., 2000. cAMP-dependent protein kinase phosphorylation of EVL, a Mena/VASP relative, regulates its interaction with actin and SH3 domains. *The Journal of Biological Chemistry*, 275(46), pp.36143–51.

Lammers, M. et al., 2008. Specificity of interactions between mDia isoforms and Rho proteins. *The Journal of Biological Chemistry*, 283(50), pp.35236–46.

Lang, A.E. et al., 2010. Photorhabdus luminescens toxins ADP-ribosylate actin and RhoA to force actin clustering. *Science*, 327(5969), pp.1139–42.

Lappalainen, P et al., 1997. Essential functions and actin-binding surfaces of yeast cofilin revealed by systematic mutagenesis. *The European Molecular Biology Organization Journal*, 16(18), pp.5520–30.

Lassing, I. & Lindberg, Uno, 1985. Specific interaction between phosphatidylinositol 4,5-bisphosphate and profilactin. *Nature*, 314(6010), pp.472–474.

Lebrand, C. et al., 2004. Critical role of Ena/VASP proteins for filopodia formation

in neurons and in function downstream of netrin-1. *Neuron*, 42(1), pp.37–49.

Leng, Y. et al., 2005. Abelson-interactor-1 promotes WAVE2 membrane translocation and Abelson-mediated tyrosine phosphorylation required for WAVE2 activation. *Proceedings of the National Academy of Sciences of the United States of America*, 102(4), pp.1098–1103.

Letzelter, M. et al., 2006. The discovery of SycO highlights a new function for type III secretion effector chaperones. *the The European Molecular Biology Organization Journal*, 25(13), pp.3223–3233.

Leung, T et al., 1996. The p160 RhoA-binding kinase ROK alpha is a member of a kinase family and is involved in the reorganization of the cytoskeleton . The p160 RhoA-Binding Kinase ROK Is a Member of a Kinase Family and Is Involved in the Reorganization of the Cytoskeleton. *Molecular and Cellular Biochemistry*, 16(10), pp.5313–5327.

Lewkowicz, E. et al., 2008. The microtubule-binding protein CLIP-170 coordinates mDia1 and actin reorganization during CR3-mediated phagocytosis. *The Journal of Cell Biology*, 183(7), pp.1287–98.

Li, D. et al., 2013. cAMP-stimulated phosphorylation of diaphanous 1 regulates protein stability and interaction with binding partners in adrenocortical Cells. *Molecular Biology of the Cell*, 24(6), pp.848–57.

Li, F. & Higgs, H N, 2005. Dissecting requirements for auto-inhibition of actin nucleation by the formin, mDia1. *The Journal of Biological Chemistry*, 280(8), pp.6986–92.

Lietha, D. et al., 2007. Structural basis for the autoinhibition of focal adhesion kinase. *Cell*, 129(6), pp.1177–1187.

Longenecker, K.L. et al., 2001. Protein crystallization by rational mutagenesis of surface residues: Lys to Ala mutations promote crystallization of RhoGDI. *Acta Crystallographica Section D Biological Crystallography*, 57(Pt 5), pp.679–688.

Lorenzi, R. et al., 2000. Wiskott-Aldrich syndrome protein is necessary for efficient IgG-mediated phagocytosis. , 95(9).

Luan, Q. & Nolen, B.J., 2013. Structural basis for regulation of Arp2/3 complex by GMF. *Nature structural & Molecular Biology*, (July).

Lueck, A., Brown, D. & Kwiatkowski, D.J., 1998. The actin-binding proteins adseverin and gelsolin are both highly expressed but differentially localized in kidney and intestine. *Journal of Cell Science*, 111 (Pt 2, pp.3633–43.

Machesky, L.M. et al., 1997. Mammalian actin-related protein 2/3 complex localizes to regions of lamellipodial protrusion and is composed of evolutionarily conserved proteins. *Journal of Biochemistry*, 328, pp.105–112.

Madrid, R. et al., 2010. The formin INF2 regulates basolateral-to-apical transcytosis and lumen formation in association with Cdc42 and MAL2. *Developmental Cell*, 18(5), pp.814–27.

Maekawa, M., 1999. Signaling from Rho to the Actin Cytoskeleton Through Protein Kinases ROCK and LIM-kinase. *Science*, 285(5429), pp.895–898.

Maiti, S. et al., 2012. Structure and activity of full-length formin mDia1. *Cytoskeleton*, 69(6), pp.393–405.

Mann, M., 2006. Functional and quantitative proteomics using SILAC. *Nature Reviews Molecular Cell Biology*, 7(12), pp.952–958.

Maritzen, T. et al., 2012. Gadkin negatively regulates Cell spreading and motility via sequestration of the actin-nucleating ARP2/3 complex. *Proceedings of the National Academy of Sciences of the United States of America*, 109(26), pp.10382–7.

Martinez-quiles, N. et al., 2001. WIP regulates N-WASP-mediated actin polymerization and filopodium formation. *Nature Cell Biology*, 3, pp.484-491.

Mattila, P.K. et al., 2004. A High-affinity Interaction with ADP-Actin Monomers Underlies the Mechanism and In Vivo Function of Srv2/cyclase-associated Protein. *Molecular Biology of the Cell* , 15, pp.5158–5171.

May, R.C. et al., 2000. Involvement of the Arp2 / 3 complex in phagocytosis mediated by FcγR or CR3. *Nature Cell Biology*, 2, pp.246–248.

McCoy, A.J., 2007. Solving structures of protein complexes by Molecular replacement with Phaser. *Acta Crystallographica Section D Biological Crystallography*, 63(Pt 1), pp.32–41.

McDonald, C. et al., 2003. The yersinia virulence factor YopM forms a novel protein complex with two Cellular kinases. *The Journal of Biological Chemistry*, 278(20), pp.18514–18523.

McGough, A. et al., 1997. Cofilin changes the twist of F-actin: implications for actin filament dynamics and Cellular function. *The Journal of Cell Biology*, 138(4), pp.771–81.

Meira, M. et al., 2009. Memo is a cofilin-interacting protein that influences PLCgamma1 and cofilin activities, and is essential for maintaining directionality during ErbB2-induced tumor-Cell migration. *Journal of Cell Science*, 122(Pt 6), pp.787–97.

Pellegrin, S. & Mellor, H., 2005. The Rho Family GTPase Rif Induces Filopodia through mDia2. *Current Biology*, 15, pp.129–133.

Miki, H. & Miura, K., 1996. N-WASP, a novel actin-depolymerizing protein,

regulates the cortical cytoskeletal rearrangement in a PIP2-dependent manner downstream of tyrosine kinases. *The European Molecular Biology Organization Journal*, 15(19), pp.5326–5335.

Mills, S.D. et al., 1997. Yersinia enterocolitica induces apoptosis in macrophages by a process requiring functional type III secretion and translocation mechanisms and involving YopP, presumably acting as an effector protein. *Proceedings of the National Academy of Sciences of the United States of America*, 94(23), pp.12638–43.

Miralles, F. et al., 2003. Actin dynamics control SRF activity by regulation of its coactivator MAL. *Cell*, 113, pp.329–342.

Mittal, R., Peak-Chew, S.-Y. & McMahon, H.T., 2006. Acetylation of MEK2 and I kappa B kinase (IKK) activation loop residues by YopJ inhibits signaling. *Proceedings of the National Academy of Sciences of the United States of America*, 103(49), pp.18574–9.

Mockrin, S.C. & Korn, E.D., 1980. Acanthamoeba profilin interacts with G-actin to increase the rate of exchange of actin-bound adenosine 5'-triphosphate. *Biochemistry*, 19(23), pp.5359–62.

Monack, D M et al., 1997. Yersinia signals macrophages to undergo apoptosis and YopJ is necessary for this Cell death. *Proceedings of the National Academy of Sciences of the United States of America*, 94(19), pp.10385–90.

Morofuji, N. et al., 2012. Macrophage-capping protein as a tissue biomarker for prediction of response to gemcitabine treatment and prognosis in cholangiocarcinoma. *Journal of proteomics*, 75(5), pp.1577–89.

Moseley, J B et al., 2006. Twinfilin is an actin-filament-severing protein and promotes rapid turnover of actin structures in vivo. *Journal of Cell Science*, 119(Pt 8), pp.1547–57.

Mouilleron, S. et al., 2008. Molecular basis for G-actin binding to RPEL motifs from the serum response factor coactivator MAL. *The European Molecular Biology Organization Journal*, 27(23), pp.3198–3208.

Mouilleron, S. et al., 2011. Structure of a pentavalent G-actin*MRTF-A complex reveals how G-actin controls nucleocytoplasmic shuttling of a transcriptional coactivator. *Science signaling*, 4(177), p.ra40.

Muhlrad, A. et al., 2006. Inorganic phosphate regulates the binding of cofilin to actin filaments. *The FEBS journal*, 273(7), pp.1488–96.

Mukherjee, S. et al., 2006. Yersinia YopJ acetylates and inhibits kinase activation by blocking phosphorylation. *Science*, 312(5777), pp.1211–1214.

Mullins, D., Heuser, J. & Pollard, T D, 1998. The interaction of Arp2¯3 complex

with actin : Nucleation , high affinity pointed end capping , and formation of branching. *Proceedings of the National Academy of Sciences of the United States of America*, 95(May), pp.6181–6186.

Murakami, K. et al., 2010. Structural basis for actin assembly, activation of ATP hydrolysis, and delayed phosphate release. *Cell*, 143(2), pp. 275-287.

Nag, S. et al., 2009. Ca2+ binding by domain 2 plays a critical role in the activation and stabilization of gelsolin. *Proceedings of the National Academy of Sciences of the United States of America*, 106(33), pp.13713–13718.

Nakanishi, O. et al., 2007. Effect of WAVE2 phosphorylation on activation of the Arp2/3 complex. *Journal of Biochemistry*, 141(3), pp.319–25.

Nakano, K. et al., 2010. GMF is an evolutionarily developed Adf/cofilin-super family protein involved in the Arp2/3 complex-mediated organization of the actin cytoskeleton. *Cytoskeleton Hoboken NJ*, 67(6), pp.373–382.

Namgoong, S. et al., 2011. Mechanism of actin filament nucleation by Vibrio VopL and implications for tandem W domain nucleation. *Nature Structural & Molecular Biology*, 18(9), pp.1060–1067.

Narayan, K. et al., 2003. Activation in isolation: exposure of the actin-binding site in the C-terminal half of gelsolin does not require actin. *FEBS Letters*, 552(2-3), pp.82–85.

Navarro, L. et al., 2007. Identification of a Molecular target for the Yersinia protein kinase A. *Molecular Cell*, 26(4), pp.465–477.

Nejedlik, L., Pierfelice, T. & Geiser, J.R., 2004. Actin distribution is disrupted upon expression of Yersinia YopO/YpkA in yeast. *Yeast Chichester England*, 21(9), pp.759–768.

Niebuhr, K. et al., 1997. A novel proline-rich motif present in ActA of Listeria monocytogenes and cytoskeletal proteins is the ligand for the EVH1 domain, a protein module present in the Ena/VASP family. *The European Molecular Biology Organization Journal*, 16(17), pp.5433–44.

Nyakern-Meazza, M. et al., 2002. Tropomyosin and gelsolin cooperate in controlling the microfilament system. *The Journal of Biological Chemistry*, 277(32), pp.28774–9.

Oda, T. et al., 2009. The nature of the globular- to fibrous-actin transition. *Nature*, 457(7228), pp.441–445.

Ohki, T. et al., 2009. Purification of cytoplasmic actin by affinity chromatography using the C-terminal half of gelsolin. *Biochemical and Biophysical Research Communications*, 383(1), pp.146–150.

Ohta, Y. et al., 2003. Differential activities, subCellular distribution and tissue expression patterns of three members of Slingshot family phosphatases that dephosphorylate cofilin. *Genes to Cells*, 8(10), pp.811–824.

Oikawa, T. et al., 2004. PtdIns(3,4,5)P3 binding is necessary for WAVE2-induced formation of lamellipodia. *Nature Cell Biology*, 6(5), pp.420–6.

Ojala, P J et al., 2002. The Two ADF-H Domains of Twinfilin Play Functionally Distinct Roles in Interactions with Actin Monomers. , 13(November), pp.3811–3821.

Oldenbourg, R., Katoh, K. & Danuser, G., 2000. Mechanism of lateral movement of filopodia and radial actin bundles across neuronal growth cones. *Biophysical journal*, 78(3), pp.1176–82.

Onoda, K. & Yin, Helen L, 1993. gCap39 Is Phosphorylated. *Journal of Biological Chemistry*, 268(6), pp.4106–4112.

Orlova, A. et al., 2004. Actin-destabilizing factors disrupt filaments by means of a time reversal of polymerization. *Proceedings of the National Academy of Sciences of the United States of America*, 101(51), pp.17664–8.

Oser, M. et al., 2009. Cortactin regulates cofilin and N-WASp activities to control the stages of invadopodium assembly and maturation. *The Journal of Cell Biology*, 186(4), pp.571–87.

Otomo, T. et al., 2005. Structural basis of actin filament nucleation and processive capping by a formin homology 2 domain. *Nature*, 433(7025), pp.488–494.

Otterbein, L.R., Graceffa, P & Dominguez, R, 2001. The crystal structure of uncomplexed actin in the ADP state. *Science*, 293(5530), pp.708–11.

Otwinowski, Z. & Minor, W., 1997. Processing of X-ray diffraction data collected in oscillation mode. *Macromol Crystallogr Methods Enzymol*, 276, pp.307–326.

Paavilainen, V.O. et al., 2004. Regulation of cytoskeletal dynamics by actin-monomer-binding proteins. *Trends in Cell Biology*, 14(7), pp.386–394.

Paavilainen, V.O. et al., 2007. Structural basis and evolutionary origin of actin filament capping by twinfilin. *Proceedings of the National Academy of Sciences of the United States of America*, 104(9), pp.3113–8.

Paavilainen, V.O. et al., 2008. Structure of the actin-depolymerizing factor homology domain in complex with actin. *The Journal of Cell Biology*, 182(1), pp.51–59.

Padrick, S.B. et al., 2011. Arp2/3 complex is bound and activated by two WASP proteins. *Proceedings of the National Academy of Sciences of the United States of America*, 108(33), pp.E472–9.

Padrick, S.B. et al., 2008. Hierarchical regulation of WASP/WAVE proteins. *Molecular Cell*, 32(3), pp.426–38.

Palazzo, A. F. et al., 2001. mDia mediates Rho-regulated formation and orientation of stable microtubules. *Nature Cell Biology*, 3(8), pp.723–9.

Palmgren, S. et al., 2001. Interactions with PIP2, ADP-actin monomers, and capping protein regulate the activity and localization of yeast twinfilin. *The Journal of Cell Biology*, 155(2), pp.251–60.

Pantaloni, D & Carlier, M.F., 1993. How profilin promotes actin filament assembly in the presence of thymosin beta 4. *Cell*, 75(5), pp.1007–1014.

Parikh, S.S. et al., 2003. CapG − / − Mice Have Specific Host Defense Defects That Render Them More Susceptible than CapG + / + Mice to Listeria monocytogenes Infection but Not to Salmonella enterica Serovar Typhimurium Infection CapG ⁒ / ⁒ Mice Have Specific Host Defense Defects T.

Park, H. & Cox, D., 2009. Cdc42 Regulates FcReceptor-mediated Phagocytosis through the Activation and Phosphorylation of Wiskott-Aldrich Syndrome Protein (WASP) and Neural-WASP. *Molecular Biology of the Cell*, 20, pp.4500–4508.

Patel, P.C. & Harrison, R.E., 2008. Membrane Ruffles Capture C3bi-opsonized Particles in Activated Macrophages. , 19(November), pp.4628–4639.

Pereira, S.F.F., Goss, L. & Dworkin, J., 2011. Eukaryote-like serine/threonine kinases and phosphatases in bacteria. *MicroBiology and Molecular Biology reviews MMBR*, 75(1), pp.192–212.

Perelroizen, I. et al., 1996. Role of Nucleotide Exchange and Hydrolysis in the Function of Profilin in Actin Assembly. *Journal of Biological Chemistry*, 271(21), pp.12302–12309.

Perrin, B.J. & Ervasti, J.M., 2010. The Actin Gene Family: Function Follows Isoform. *Cytoskeleton Hoboken NJ*, 67(10), pp.630–634.

Pike, A.C.W. et al., 2008. Activation segment dimerization: a mechanism for kinase autophosphorylation of non-consensus sites. *The European Molecular Biology Organization Journal*, 27(4), pp.704–714.

Pocha, S.M. & Cory, G.O., 2009. WAVE2 is regulated by multiple phosphorylation events within its VCA domain. *Cell motility and the cytoskeleton*, 66(1), pp.36–47.

Pohanka, M. & Skladal, P., 2009. Bacillus anthracis, Francisella tularensis and Yersinia pestis. The Most Important Bacterial Warfare Agents — review. *Folia Microbiol*, 54(4), pp.263–272.

Pollard, T.D., Borisy, G.G. & Haven, N., 2003. Cellular Motility Driven by Assembly and Disassembly of Actin Filaments. *Cell*, 112, pp.453–465.

Pollard, T.D. & Cooper, J A, 2009. Actin, a central player in Cell shape and movement. *Science*, 326(5957), pp.1208–1212.

Pollard, T.D. & Cooper, J.A., 1984. Quantitative analysis of the effect of Acanthamoeba profilin on actin filament nucleation and elongation. *Biochemistry*, 23(26), pp.6631–41.

Ponti, A. et al., 2004. Two distinct actin networks drive the protrusion of migrating Cells. *Science*, 305(5691), pp.1782–6.

Prehna, G. et al., 2006. Yersinia virulence depends on mimicry of host Rho-family nucleotide dissociation inhibitors. *Cell*, 126(5), pp.869–880.

Prehoda, K.E., 2000. Integration of Multiple Signals Through Cooperative Regulation of the N-WASP-Arp2/3 Complex. *Science*, 290(5492), pp.801–806.

Price, W.N. et al., 2009. Understanding the physical properties that control protein crystallization by analysis of large-scale Experimental data. *Nature Biotechnology*, 27(1), pp.51–57.

Pring, M. et al., 2003. Mechanism of formin-induced nucleation of actin filaments. *Biochemistry*, 42(2), pp.486–96.

Quinlan, M.E. et al., 2005. Drosophila Spire is an actin nucleation factor. *Nature*, 433(7024), pp.382–388.

Quinlan, M.E. et al., 2007. Regulatory interactions between two actin nucleators, Spire and Cappuccino. *The Journal of Cell Biology*, 179(1), pp.117–28.

Quintero-Monzon, Omar et al., 2009. Reconstitution and dissection of the 600-kDa Srv2/CAP complex: roles for oligomerization and cofilin-actin binding in driving actin turnover. *The Journal of Biological Chemistry*, 284(16), pp.10923–10934.

Ramesh, N et al., 1997. WIP, a protein associated with wiskott-aldrich syndrome protein, induces actin polymerization and redistribution in lymphoid Cells. *Proceedings of the National Academy of Sciences of the United States of America*, 94(26), pp.14671–6.

Reinhard, M et al., 1992. human platelets is a novel protein associated with actin filaments and focal contacts. *The European Molecular Biology Organization Journal,* 1(6), pp.2063–2070.

Dos Remedios, C.G. et al., 2003. Actin binding proteins: regulation of cytoskeletal microfilaments. *Physiological Reviews*, 83(2), pp.433–473.

Reményi, A., Good, M.C. & Lim, W. a, 2006. Docking interactions in protein kinase and phosphatase networks. *Current opinion in structural Biology*, 16(6), pp.676–85.

Renz, M. et al., 2008. Invasive breast cancer Cells exhibit increased mobility of the actin-binding protein CapG. *International journal of cancer. Journal international of cancer*, 122(7), pp.1476–82.

Ressad, F. et al., 1998. Kinetic Analysis of the Interaction of Actin-depolymerizing Factor (ADF)/Cofilin with G- and F-Actins. *Journal of Biological Chemistry*, 273(33), pp.20894–20902.

Robinson, R.C. et al., 2001. Crystal structure of Arp2/3 complex. *Science*, 294(5547), pp.1679–1684.

Robinson, R.C. et al., 1999. Domain movement in gelsolin: a calcium-activated switch. *Science*, 286(5446), pp.1939–1942.

Rocca, D.L. et al., 2008. Inhibition of Arp2/3-mediated actin polymerization by PICK1 regulates neuronal morphology and AMPA receptor endocytosis. *Nature Cell Biology*, 10(3), pp.259–71.

Rohatgi, R. et al., 2001. Nck and phosphatidylinositol 4,5-bisphosphate synergistically activate actin polymerization through the N-WASP-Arp2/3 pathway. *The Journal of Biological Chemistry*, 276(28), pp.26448–52.

Rohatgi, R, Ho, H.H. & Kirschner, M W, 2000. Mechanism of N-WASP Activation by CDC42 and Phosphatidylinositol 4 , 5-bisphosphate. , 150(6), pp.1299–1309.

Romero, S. et al., 2004. Formin is a processive motor that requires profilin to accelerate actin assembly and associated ATP hydrolysis. *Cell*, 119(3), pp.419–29.

Rosqvist, R. et al., 1990. The cytotoxic protein YopE of Yersinia obstructs the primary host defence. *Molecular microBiology*, 4(4), pp.657–67.

Rosqvist, R., Bolin, I. & Wolf-watz, H., 1988. Inhibition of phagocytosis in Yersinia pseudotuberculosis : a virulence plasmid-encoded ability involving the Yop2b protein. *Infection and Immunity*, 56(8), p.2139.

Rouiller, I. et al., 2008. The structural basis of actin filament branching by the Arp2/3 complex. *The Journal of Cell Biology*, 180(5), pp.887–95.

Ruckdeschel, K. et al., 1998. Yersinia enterocolitica impairs activation of transcription factor NF-kappaB: involvement in the induction of programmed Cell death and in the suppression of the macrophage tumor necrosis factor alpha production. *The Journal of Experimental Medicine*, 187(7), pp.1069–79.

Ruckdeschel, K. et al., 1997. Yersinia enterocolitica Promotes Deactivation of

Macrophage Mitogen-activated Protein Kinases ExtraCellular Signal-regulated Kinase-1/2, p38, and c-Jun NH2-terminal Kinase. *Journal of Biological Chemistry*, 272(25), pp.15920–15927.

Sablin, E.P. et al., 2002. How does ATP hydrolysis control actin's associations? *Proceedings of the National Academy of Sciences of the United States of America*, 99(17), pp.10945–10947.

Safer, D., Golla, R. & Nachmias, V.T., 1990. Isolation of a 5-kilodalton actin-sequestering peptide from human blood platelets. *Proceedings of the National Academy of Sciences of the United States of America*, 87(7), pp.2536–2540.

Sasahara, Y. et al., 2002. Mechanism of Recruitment of WASP to the Immunological Synapse and of Its Activation Following TCR Ligation. *Molecular Cell*, 10, pp.1269–1281.

Schafer, D.A., Jennings, P.B. & Cooper, J A, 1996. Dynamics of capping protein and actin assembly in vitro: uncapping barbed ends by polyphosphoinositides. *The Journal of Cell Biology*, 135(1), pp.169–79.

Schafer, D.A., Mooseker, M.S. & Cooper, J A, 1992. Localization of capping protein in chicken epithelial Cells by immunofluorescence and Biochemical fractionation. *The Journal of Cell Biology*, 118(2), pp.335–46.

Schleberger, C. et al., 2006. Structure and action of the binary C2 toxin from Clostridium botulinum. *Journal of Molecular Biology*, 364(4), pp.705–715.

Schönichen, A. & Geyer, M., 2010. Fifteen formins for an actin filament: a Molecular view on the regulation of human formins. *Biochimica et Biophysica Acta*, 1803(2), pp.152–163.

Schumacher, N. et al., 2004. Overlapping expression pattern of the actin organizers Spir-1 and formin-2 in the developing mouse nervous system and the adult brain. *Gene expression patterns*, 4(3), pp.249–55.

Schutt, C.E. et al., 1993. The structure of crystalline profilin-beta-actin. *Nature*, 365(6449), pp.810–816.

Scott, C.C. et al., 2005. Phosphatidylinositol-4,5-bisphosphate hydrolysis directs actin remodeling during phagocytosis. *The Journal of Cell Biology*, 169(1), pp.139–49.

Secrist, J.A. 3rd, Barrio, J.R. & Leonard, N.J., 1972. A fluorescent modification of adenosine triphosphate with activity in enzyme systems: 1,N 6 - ethenoadenosine triphosphate. *Science*, 175(4022), pp.646–7.

Selden, L.A., Gershman, L.C. & Estes, J.E., 1986. A kinetic comparison between Mg-actin and Ca-actin. *Journal of muscle research and Cell motility*, 7(3), pp.215–224.

Serrander, L. et al., 2000. Selective inhibition of IgG-mediated phagocytosis in gelsolin-deficient murine neutrophils. *Journal of Immunology*, 165(5), pp.2451–7.

Seth, A., Otomo, C. & Rosen, M.K, 2006. Autoinhibition regulates Cellular localization and actin assembly activity of the diaphanous-related formins FRLalpha and mDia1. *The Journal of Cell Biology*, 174(5), pp.701–13.

Shao, F. et al., 2003. Biochemical characterization of the Yersinia YopT protease: cleavage site and recognition elements in Rho GTPases. *Proceedings of the National Academy of Sciences of the United States of America*, 100(3), pp.904–9.

Sharrocks, A.D., Yang, S.H. & Galanis, A., 2000. Docking domains and substrate-specificity determination for MAP kinases. *Trends in Biochemical Sciences*, 25(9), pp.448–453.

Skoble, J. et al., 2001. Pivotal role of VASP in Arp2/3 complex-mediated actin nucleation, actin branch-formation, and Listeria monocytogenes motility. *The Journal of Cell Biology*, 155(1), pp.89–100.

Small, J.V. et al., 2002. The lamellipodium: where motility begins. *Trends in Cell Biology*, 12(3), pp.112–20.

Southwick, F., 1995. Gain-of-function mutations conferring actin-severing activity to human macrophage Cap G. *Journal of Biological Chemistry*, 270(1), pp.45–48.

Spudich, J.A. & Watt, S., 1971. The regulation of rabbit skeletal muscle contraction. Biochemical studies of the interaction of the tropomyosin-troponin complex with actin and the proteolytic fragments of myosin. *Journal of Biological Chemistry*, (246), pp.4866–4871.

Staus, D.P., Taylor, J.M. & Mack, C.P., 2011. Enhancement of mDia2 activity by Rho-kinase-dependent phosphorylation of the diaphanous autoregulatory domain. *The Biochemical journal*, 439(1), pp.57–65.

Stein, N., 2008. CHAINSAW: a program for mutating pdb files used as templates in Molecular replacement. *Journal of Applied Crystallography*, 41, pp.641–643.

Stevens, J.M., Galyov, Edouard E & Stevens, M.P., 2006. Actin-dependent movement of bacterial pathogens. *Nature Reviews MicroBiology*, 4(2), pp.91–101.

Stewart, D.M. et al., 1996. Studies of the Expression of the Wiskott-Aldrich Syndrome Protein. *The Journal of Clinical Investigation*, 97(11), pp.2627–2634.

Straley, S.C. & Bowmer, W.S., 1986. Virulence genes regulated at the transcriptional level by Ca2+ in Yersinia pestis include structural genes for outer membrane proteins. *Infection and immunity*, 51(2), pp.445–54.

Suarez, C. et al., 2011. Cofilin tunes the nucleotide state of actin filaments and severs at bare and decorated segment boundaries. *Current Biology*, 21(10), pp.862–8.

Suetsugu, S. et al., 2006. Optimization of WAVE2 complex-induced actin polymerization by membrane-bound IRSp53, PIP(3), and Rac. *The Journal of Cell Biology*, 173(4), pp.571–85.

Suetsugu, S., Miki, H. & Takenawa1, T., 1999. Identification of Two Human WAVE/SCAR Homologues as General Actin Regulatory Molecules Which Associate with the Arp2/3 Complex. *Biochemical and Biophysical Research Communications*, 260(1), pp.296–302.

Suhre, K. & Sanejouand, Y.H., 2004. ElNemo: a normal mode web server for protein movement analysis and the generation of templates for Molecular replacement. *Nucleic acids research*, 32, pp.610–614.

Sun, Q. et al., 2006. Defining the mammalian CArGome. *Genome research*, 16(2), pp.197–207.

Suraneni, P. et al., 2012. The Arp2/3 complex is required for lamellipodia extension and directional fibroblast Cell migration. *The Journal of Cell Biology*, 197(2), pp.239–51.

Svitkina, T.M. et al., 1997. Analysis of the actin-myosin II system in fish epidermal keratocytes: mechanism of Cell body translocation. *Journal of Cell Biology*, 139(2), pp.397–415.

Svitkina, T.M. & Borisy, Gary G, 1999. Arp2/3 complex and actin depolymerizing factor/cofilin in dendritic organization and treadmilling of actin filament array in lamellipodia. *Journal of Cell Biology*, 145(5), pp.1009–1026.

Sweet, C.R. et al., 2007. YopJ targets TRAF proteins to inhibit TLR-mediated NF-kappaB, MAPK and IRF3 signal transduction. *Cellular microBiology*, 9(11), pp.2700–15.

Takahashi, K. & Suzuki, K., 2010. WAVE2 targeting to phosphatidylinositol 3,4,5-triphosphate mediated by insulin receptor substrate p53 through a complex with WAVE2. *Cellular signalling*, 22(11), pp.1708–16.

Takeya, R. et al., 2008. The mammalian formin FHOD1 is activated through phosphorylation by ROCK and mediates thrombin-induced stress fibre formation in endothelial Cells. *The European Molecular Biology Organization Journal*, 27(4), pp.618–28.

Tanaka, M. et al., 1995. Gelsolin: a candidate for suppressor of human bladder cancer. *Cancer research*, 55, pp.3228–3232.

Taoka, M. et al., 2003. V-1, a protein expressed transiently during murine cerebellar development, regulates actin polymerization via interaction with capping

protein. *The Journal of Biological Chemistry*, 278(8), pp.5864–70.

Terwilliger, T.C. et al., 2012. phenix.mr_rosetta: Molecular replacement and model rebuilding with Phenix and Rosetta. *Journal of structural and functional genomics*, 13(2), pp.81–90.

Terwilliger, T.C. et al., 2008. Iterative-build OMIT maps: map improvement by iterative model building and refinement without model bias. *Acta crystallographica. Section D, Biological crystallography*, 64(Pt 5), pp.515–24.

Thompson, M.E. et al., 2013. FMNL3 FH2-actin structure gives insight into formin-mediated actin nucleation and elongation. *Nature structural & Molecular Biology*, 20(1), pp.111–8.

Toshima, J. et al., 2001. Cofilin phosphorylation by protein kinase testicular protein kinase 1 and its role in integrin-mediated actin reorganization and focal adhesion formation. *Molecular Biology of the Cell*, 12(4), pp.1131–45.

Trasak, C et al., 2007. Yersinia protein kinase YopO is activated by a novel G-actin binding process. *The Journal of Biological Chemistry*, 282(4), pp.2268–2277.

Trosky, J.E., Liverman, A.D.B. & Orth, K., 2008. Yersinia outer proteins: Yops. *Cellular MicroBiology*, 10(3), pp.557–565.

Tsuboi, S. & Meerloo, J., 2007. Wiskott-Aldrich syndrome protein is a key regulator of the phagocytic cup formation in macrophages. *The Journal of Biological Chemistry*, 282(47), pp.34194–203.

Tzircotis, G., Braga, V.M.M. & Caron, Emmanuelle, 2011. RhoG is required for both FcγR- and CR3-mediated phagocytosis. *Journal of Cell Science*, 124(Pt 17), pp.2897–902.

Ubersax, J.A. & Ferrell, J.E., 2007. Mechanisms of specificity in protein phosphorylation. *Nature reviews. Molecular Cell Biology*, 8(7), pp.530–41.

Uruno, T. et al., 2001. Activation of Arp2/3 complex-mediated actin polymerization by cortactin. *Nature Cell Biology*, 3(March), pp.259–266.

Vartiainen, M. et al., 2000. Mouse A6 / Twinfilin Is an Actin Monomer-Binding Protein That Localizes to the Regions of Rapid Actin Dynamics Mouse A6 / Twinfilin Is an Actin Monomer-Binding Protein That Localizes to the Regions of Rapid Actin Dynamics.

Vartiainen, M.K. et al., 2003. Mammals have two twinfilin isoforms whose subCellular localizations and tissue distributions are differentially regulated. *The Journal of Biological Chemistry*, 278(36), pp.34347–55.

Vasioukhin, V. et al., 2000. Directed Actin Polymerization Is the Driving Force for Epithelial Cell – Cell Adhesion. *Cell*, 100, pp.209–219.

Vetterkind, S. et al., 2002. The rat homologue of Wiskott-Aldrich syndrome protein (WASP)-interacting protein (WIP) associates with actin filaments, recruits N-WASP from the nucleus, and mediates mobilization of actin from stress fibers in favor of filopodia formation. *The Journal of Biological Chemistry*, 277(1), pp.87–95.

Viboud, G.I. & Bliska, James B, 2005. Yersinia outer proteins: role in modulation of host Cell signaling responses and pathogenesis. *Annual Review of MicroBiology*, (59), pp.69–89.

Vincent, S., Jeanteur, P. & Fort, P., 1992. Growth-Regulated Expression of rhoG , a New Member of the ras Homolog Gene Family. *Molecular and Cellular Biology*, 12(7), pp.3138–3148.

Vojtek, A et al., 1991. Evidence for a functional link between profilin and CAP in the yeast S. cerevisiae. *Cell*, 66(3), pp.497–505.

Walter, T.S. et al., 2005. A procedure for setting up high-throughput nanolitre crystallization experiments. Crystallization workflow for initial screening, automated storage, imaging and optimization. *Acta crystallographica. Section D, Biological crystallography*, 61(Pt 6), pp.651–7.

Walter, T.S. et al., 2006. Lysine methylation as a routine rescue strategy for protein crystallization. *Structure*, 14(11), pp.1617–1622.

Wang, H., Robinson, R.C & Burtnick, L.D, 2010. The structure of native G-actin. *Cytoskeleton*, 67(7), pp.456–65.

Wang, Q. et al., 2003. Regulation of the formation of osteoclastic actin rings by proline-rich tyrosine kinase 2 interacting with gelsolin. *The Journal of Cell Biology*, 160(4), pp.565–75.

Wang, Y. & Taylor, D.L., 1981. Exchange of 1 , N-etheno-ATP with actin-bound nucleotides as a tool for studying the steady-state exchange of subunits in F-actin solutions. *Proceedings of the National Academy of Sciences of the United States of America*, 78(9), pp.5503–5507.

Watanabe, N. et al., 1997. p140mDia, a mammalian homolog of Drosophila diaphanous, is a target protein for Rho small GTPase and is a ligand for profilin. *The European Molecular Biology Organization Journal*, 16(11), pp.3044–56.

Wear, M.A. et al., 2003. How Capping Protein Binds the Barbed End of the Actin Filament. *Current Biology*, 13, pp.1531–1537.

Wear, M.A. & Cooper, J.A., 2004. Capping protein: new insights into mechanism and regulation. *Trends in Biochemical Sciences*, 29(8), pp.418–28.

Weber, a et al., 1994. Tropomodulin caps the pointed ends of actin filaments. *The Journal of Cell Biology*, 127(6), pp.1627–35.

Weber, A. et al., 1992. Interaction of thymosin beta 4 with muscle and platelet actin: implications for actin sequestration in resting platelets. *Biochemistry*, 31(27), pp.6179–85.

Wentworth, J.K.T., Pula, G. & Poole, A.W., 2006. Vasodilator-stimulated phosphoprotein (VASP) is phosphorylated on Ser157 by protein kinase C-dependent and -independent mechanisms in thrombin-stimulated human platelets. *The Biochemical journal*, 393(Pt 2), pp.555–64.

Wiley, D.J. et al., 2006. The Ser/Thr kinase activity of the Yersinia protein kinase A (YpkA) is necessary for full virulence in the mouse, mollifying phagocytes, and disrupting the eukaryotic cytoskeleton. *Microbial Pathogenesis*, 40(5), pp.234–243.

Williams, D. et al., 2000. Dominant negative mutation of the hematopoietic-specific Rho GTPase, Rac2, is associated with a human phagocyte immunodeficiency. *Blood*, 96(5), pp.1646–1654.

Winter, G., Lobley, C.M.C. & Prince, S.M., 2013. Decision making in xia2. *Acta crystallographica. Section D, Biological crystallography*, 69(7), pp.1260–73.

Witke, W. et al., 2001. Comparisons of CapG and gelsolin-null macrophages: demonstration of a unique role for CapG in receptor-mediated ruffling, phagocytosis, and vesicle rocketing. *The Journal of Cell Biology*, 154(4), pp.775–84.

Witke, W. et al., 1995. Hemostatic, inflammatory, and fibroblast responses are blunted in mice lacking gelsolin. *Cell*, 81(1), pp.41–51.

Wu, X. et al., 2004. Focal adhesion kinase regulation of N-WASP subCellular localization and function. *The Journal of Biological Chemistry*, 279(10), pp.9565–76.

Yamashita, A., Maeda, K. & Maeda, Y., 2003. Crystal structure of CapZ : structural basis for actin filament barbed end capping. *The European Molecular Biology Organization Journal*, 22(7), pp.1529–1538.

Yang, S. et al., 2013. Molecular mechanism of fascin function in filopodial formation. *Journal of Biological Chemistry*, 288(1), pp.274–84.

Yarmola, E.G. et al., 2000. Actin-latrunculin A structure and function. Differential modulation of actin-binding protein function by latrunculin A. *The Journal of Biological Chemistry*, 275(36), pp.28120–7.

Yayoshi-Yamamoto, S., Taniuchi, I. & Watanabe, T, 2000. FRL, a novel formin-related protein, binds to Rac and regulates Cell motility and survival of macrophages. *Molecular and Cellular Biology*, 20(18), pp.6872–81.

Yin, H L, Albrecht, J.H. & Fattoum, A., 1981. Identification of gelsolin, a Ca2+-

dependent regulatory protein of actin gel-sol transformation, and its intraCellular distribution in a variety of Cells and tissues. *The Journal of Cell Biology*, 91(3), pp.901–906.

Yip, C.K. et al., 2005. Structural characterization of the Molecular platform for type III secretion system assembly. *Nature*, 435(7042), pp.702–707.

Yokoyama, N., Lougheed, J. & Miller, W.T., 2005. Phosphorylation of WASP by the Cdc42-associated kinase ACK1: dual hydroxyamino acid specificity in a tyrosine kinase. *The Journal of Biological Chemistry*, 280(51), pp.42219–26.

Young, T.A. et al., 2003. Structure of Mycobacterium tuberculosis PknB supports a universal activation mechanism for Ser/Thr protein kinases. *Nature structural Biology*, 10(3), pp.168–174.

Yu, F.X. et al., 1990. gCap39, a calcium ion- and polyphosphoinositide-regulated actin capping protein. *Science*, 250(4986), pp.1413–1415.

Zhang, Y. et al., 2013. Rapid Apoptosis in Macrophages Infected with Yersinia 1. *The Journal of Immunology*, 174, pp7939-7949.

Zhou, H. et al., 2005. Yersinia virulence factor YopJ acts as a deubiquitinase to inhibit NF-kappa B activation. *The Journal of Experimental Medicine*, 202(10), pp.1327–32.

Zhu, G., Liu, Y. & Shaw, S., 2005. Protein kinase specificity: A strategic collaboration between kinase peptide specificity and substrate recruitment. *Cell Cycle*, 4(1), pp.52–56.

Zhuang, C. et al., 2011. CDK1-mediated phosphorylation of Abi1 attenuates Bcr-Abl-induced F-actin assembly and tyrosine phosphorylation of WAVE complex during mitosis. *The Journal of Biological Chemistry*, 286(44), pp.38614–26.

Zigmond, S.H. et al., 2003. Formin leaky cap allows elongation in the presence of tight capping proteins. *Current Biology*, 13, pp.1820–1823.

Zoudilova, M. et al., 2007. Beta-arrestin-dependent regulation of the cofilin pathway downstream of protease-activated receptor-2. *The Journal of Biological Chemistry*, 282(28), pp.20634–46.

Zuchero, J.B. et al., 2009. p53-cofactor JMY is a multifunctional actin nucleation factor. *Nature Cell Biology*, 11(4), pp.451–9.

Zwart, P.H., Afonine, P.V. & Grosse-Kunstleve, R.W., 2008. Automated structure solution with the PHENIX suite. *Methods Mol Biol*, 426, pp.419–35.

APPENDIX

A1. Vectors

A range of different purification and solubility tags have been used in this work. Specific details on these vectors could be found in **Table A.1**.

pSY5 vector

The pSY5 vector, as reported (Nag et al. 2009), was modified from pET-21d (Novagen) and contains an N-terminal octa-histidine (eight histidines) sequence, followed by a human rhinovirus (HRV) 3C protease cleavage site, followed by the multi-cloning site (MCS). It is a T7/*lac*O driven expression vector for use with (DE3) *E. coli* strains.

pOPINF and pOPINE vectors

pOPINF and pOPINE vectors, as reported (Berrow et al. 2007), are modified from the pTriEx2 vector. They contain the T7/*lac*O operator for use with (DE3) *E. coli* strains; but also contain a hybrid cytomegalovirus (CMV) enhancer and ß-actin promoter for mammalian expression; and the baculoviral p10 promoter and the lef-2 and 1629 baculo-recombination elements for insect cell expression. pOPINF contains an N-terminal hexa-histidine sequence, followed by a human rhinovirus (HRV) 3C protease cleavage site, followed by the multi-cloning site (MCS). pOPINE contains a non-cleavable C-terminal hexa-His-tag but was used for the expression of non-tagged proteins. A stop codon is inserted at the end of the coding sequence for the protein of interest so that the hexa-histidine tag is not translated.

pToomy vector

The pToomy vector, as reported (Narayan et al. 2003), was modified from pGEX-6P1 (GE Healthcare). It contains the T7/*lac*O operator for use with (DE3) *E. coli* strains. It contains an N-terminal GST tag, followed by a human rhinovirus (HRV) 3C protease cleavage site, a octa-histidine sequence, a thrombin protease cleavage site, followed by the multi-cloning site (MCS).

Modified pGEX-4T1

The pGEX-4T1 originally contains an N-terminal GST tag, followed by a thrombin cleavage site. It has been modified to include a C-terminal non-cleavable hexa-His tag, as reported (Maiti et al. 2012). It is a T7/*lac*O driven expression vector for use with (DE3) *E. coli* strains.

Table A.1 Vectors used in protein production.

Vector	Fusion tag	Product	Parent vector	Antibiotic resistance
pSY5	MAEEHHHHHHHH LEVLFQ|GP-POI	N-8xHis-3C-POI	pET-21d	Ampicillin
pOPINF	MAHHHHHHS SGLEVLFQ|GP-POI	N-6xHis-3C-POI	pTriEx2	Ampicillin
pOPINE	POI-*-KHHHHHH	No tag	pTriEx2	Ampicillin
pToomy	GST- LEVLFQ|GP-HHHHHHHH-LVPR|GS-POI	N-GST-3C-8xHis-thrombin-POI	pGEX-6P1	Ampicillin
modified pGEX-4T1	GST- LVPR|GS – POI-HHHHHH	N-GST-3C-POI-6xHIS-C	pGEX-4T1	Ampicillin

* denotes stop codon.
| denotes protease cleavage site.
POI denotes protein of interest.